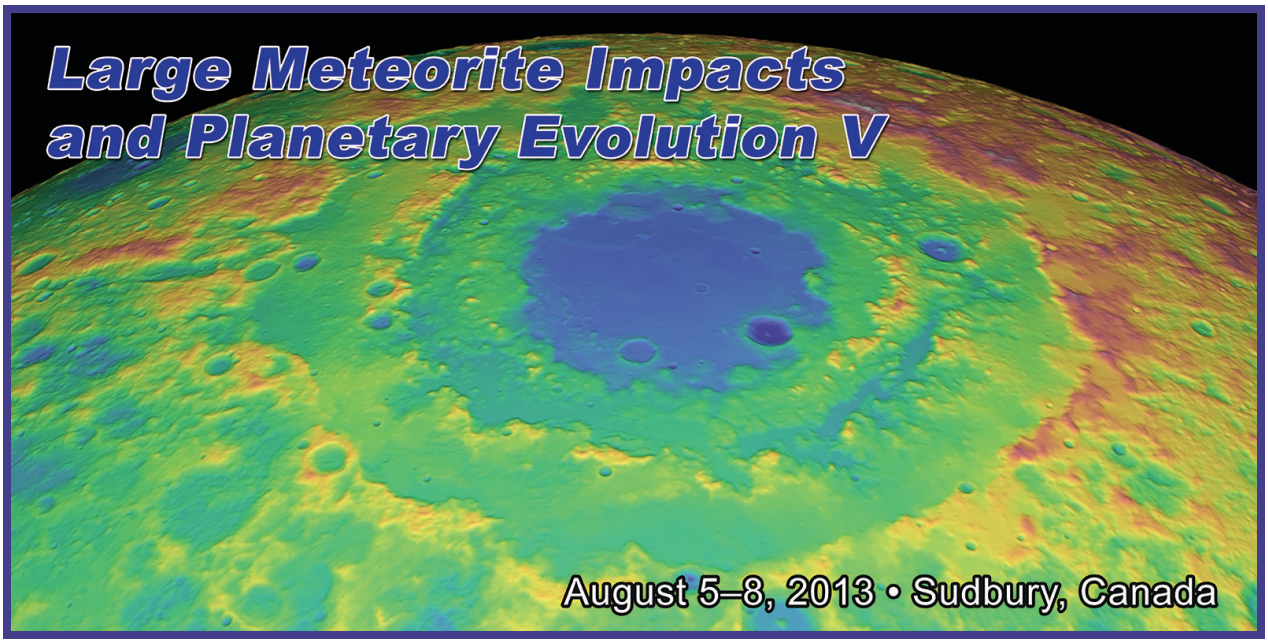

Program and Abstract Volume

LPI Contribution No. 1737

LUNAR AND PLANETARY INSTITUTE

USRA

ORGANIZER

Universities Space Research Association (USRA)

INSTITUTIONAL SUPPORT

Canadian Lunar Research Network
Centre for Excellence in Mining Innovation (CEMI)
Geological Association of Canada Planetary Sciences Division
Laurentian University
University of Western Ontario

CONVENERS

Gordon R. Osinski, *University of Western Ontario*
David A. Kring, *USRA-Lunar and Planetary Institute*

SCIENTIFIC ORGANIZING COMMITTEE

Ulrich Riller, *Universität Hamburg*
James E. Mungall, *University of Toronto*
C. Michael Lesher, *Laurentian University*
Joe Petrus, *Laurentian University*
Peter Lightfoot*, Vale, Copper Cliff*
Livio Tornabene, University of Western Ontario
Kai Wünnemann, Museum für Naturkunde-Leibniz Institute

Lunar and Planetary Institute 3600 Bay Area Boulevard Houston TX 77058-1113

LPI Contribution No. 1737

Compiled in 2013 by

Meeting and Publication Services
Lunar and Planetary Institute
USRA Houston
3600 Bay Area Boulevard, Houston TX 77058-1113

This material is based upon work supported by NASA under Award No. NNX08AC28A. Any opinions, findings, and conclusions or recommendations expressed in this volume are those of the author(s) and do not necessarily reflect the views of the National Aeronautics and Space Administration.

The Lunar and Planetary Institute is operated by the Universities Space Research Association under a cooperative agreement with the Science Mission Directorate of the National Aeronautics and Space Administration.

Abstracts in this volume may be cited as

Author A. B. (2012) Title of abstract. In *Large Meteorite Impacts and Planetary Evolution V,* p. XX. LPI Contribution No. 1737, Lunar and Planetary Institute, Houston.

ISSN No. 0161-5297

Preface

This volume contains abstracts that have been accepted for presentation at the Large Meteorite Impacts and Planetary Evolution V, August 5–8, 2013, Sudbury, Canada.

Administration and publications support for this meeting were provided by the staff of the Meeting and Publication Services Department at the Lunar and Planetary Institute.

Sponsors

The organizers gratefully acknowledge support from

Laurentian University
Université Laurentienne

GOODMAN SCHOOL OF MINES
ÉCOLE DES MINES

Lunch and Coffee Break Sponsor

The organizers gratefully acknowledge support from

CEMI
Centre for Excellence in Mining Innovation

Opening Reception Sponsor

Technical Guide to Sessions

Monday, August 5, 2013

8:30 a.m.	Fraser Auditorium	Large Impact Basins: Their Formation, Structure, and Environmental Effects I
1:30 p.m.	Fraser Auditorium	Large Impact Basins: Their Formation, Structure, and Environmental Effects II

Tuesday, August 6, 2013

8:30 a.m.	Fraser Auditorium	Model and Experimental Insights into Cratering Processes
1:30 p.m.	Fraser Auditorium	Geochronology of Impact Events
4:00 p.m.	Alumni Hall	Poster Session
		Early Solar System Collisions
		Extraterrestrial Cratering
		Impact Vapor, Melt, and Ejecta
		Planet-Size Collisions
		Case Study of the Sudbury Structure I
		Geologic Measures of Impact Cratering

Wednesday, August 7, 2013

8:30 a.m.	Fraser Auditorium	Case Study of the Sudbury Structure II
1:30 p.m.	Fraser Auditorium	Complex Impact Craters: Their Formation and Structure

Thursday, August 8, 2013

8:30 a.m.	Fraser Auditorium	Impact Cratering on Mars
1:30 p.m.	Fraser Auditorium	Impactites: From Proximal to Distal

Travel Award Recipients

The organizers gratefully acknowledge support from the

Barringer Crater Company

which was used to provide travel support for the following students:

Sheridan Ackiss
Johns Hopkins University/Applied Physics Laboratory
Mineralogic Mapping of Huygens Crater, Mars: A Transect of the Highlands Crust and Hellas Basin Rim

Michael Bierhaus
Museum für Naturkunde, Berlin
Affect of Core Rheology on Shock Wave Propagation in Planetary Scale Impacts

Timothy Bowling
Purdue University
Antipodal Terrains Created by the Rheasilvia Impact on Asteroid 4 Vesta

Yu Chang
University of Tokyo
Characteristics and Vertical Profile of Shocked Quartz Grains in the YAX-1 Core: Constraints on Transient Crater Size and Ejecta Deposition Process of the Chicxulub Impact

Adam Coulter
University of Western Ontario
The Nature and Origin of the Enigmatic Garson Member of the Sudbury Impact Structure, Canada

Carmela-Lisa Cupelli
University of Western Ontario
Discovery of Mafic Impact Melt in the Central Uplift of the Vredefort Basin

Deepak Dhingra
Brown University
Mineralogy of Impact Melt at Copernicus Crater: Insights into Melt Evolution and Diversity

Ning Ding
University of Arizona
Mapping the Ritchey Crater Central Uplift, Mars

Daniel Moriarty
Brown University
Moon Mineralogy Mapper Observations of South Pole — Aitken: Constraints on Basin Formation

William Vaughan
Brown University
Impact Melt Differentiation in South Pole-Aitken Basin

Matthew Wielicki
University of California, LA
Terrestrial Impact Zircon Textures: Implications to Impact Geochronology

Opening Reception

The Centre for Excellence in Mining Innovation (CEMI) welcomes delegates of the Large Meteorite Impacts and Planetary Evolution V Conference to an opening reception on Sunday, August 4, at Sudbury's Dynamic Earth. The guest of honor at the reception will be Apollo 17 astronaut Harrison "Jack" Schmitt, the last person to walk on the Moon! Please join us for cocktails and appetizers beginning at 6:00 PM, and enjoy live entertainment, underground tours, and more while enjoying a unique setting that is home to the Big Nickel. Start off the conference with a bang by networking with colleagues, conference organizers, and speakers. Transportation to and from the event will be provided from the two conference hotels and the student residence beginning at 5:15 PM. Don't miss out on a spectacular evening. Space is limited, so register early.

CEMI
Centre for Excellence
in Mining Innovation

The Centre for Excellence in Mining Innovation (CEMI) directs and coordinates step-change innovation in the areas of exploration, deep mining, integrated mine engineering, environment and sustainability for the metal mining industry. With a seasoned team of program directors, CEMI identifies, assesses and manages industry-focused applied research and development projects that extend from geology and engineering to the natural sciences. CEMI recognizes innovation is a three-phase process: research, development and implementation (R & D, I). With implementation, CEMI turns innovative ideas into best practices.

CEMI
Centre for Excellence
in Mining Innovation

935 Ramsey Lake Road | Willet Green Miller Centre | Sudbury, Ontario, Canada P3E 2C6
T. 705.673.6568 | F. 705.671.3878 | info@miningexcellence.ca | www.miningexcellence.ca

Institutional Support

Contents

Program

Monday, August 5, 2013
LARGE IMPACT BASINS:
THEIR FORMATION, STRUCTURE, AND ENVIRONMENTAL EFFECTS I
8:30 a.m. Fraser Auditorium

New data, models, and mapping are used to study the formation, structure, and environmental effects of large impact basins on the Moon, Earth and Mercury.

Chairs: **David Kring**
Kai Wünnemann

8:30 a.m. Zuber M. T. * GRAIL Science Team
Gravity Recovery and Interior Laboratory (GRAIL): Analysis Status and Implications for Understanding the Role of Impacts in Lunar and Planetary Evolution **[#3048]**
High-resolution models of the lunar gravity field from GRAIL are enabling geophysical analyses that elucidate the role of large impacts on the evolution of the Moon, and by extension, other terrestrial planets.

9:00 a.m. Collins G. S. * Wieczorek M. A. Miljković K.
Large Impact Crater Formation on the Moon: Comparing Numerical Models with GRAIL-Derived Crustal Thickness Profiles **[#3072]**
We use gravity and crustal thickness anomalies measured by GRAIL, which provide new constraints on crustal deformation beneath large lunar craters, as a test of models of crater formation.

9:20 a.m. Potter R. W. K. * Kring D. A. Collins G. S. Kiefer W. S. McGovern P. J.
Orientale Basin: Formation Processes and Structure Inferred from Hydrocode Modeling **[#3026]**
By constraining hydrocode models to, primarily, gravity-inferred crustal structure, we present best-fit formation scenarios for the Orientale impact basin.

9:40 a.m. Blair D. M. * Johnson B. C. Freed A. M. Melosh H. J.
Gravity Anomalies of the Lunar Orientale Basin and the Mercurian Caloris Basin **[#3041]**
We model the formation and evolution of the lunar Orientale and mercurian Caloris basin gravity anomalies using a combination of hydrocode and finite-element methods, constrained by free-air and Bouguer gravity anomalies and basin topography.

10:00 a.m. *Coffee Break*

10:15 a.m. Miljkovic K. * Wieczorek M. A.
Tracing Lower Crust and Upper Mantle on the Surface on the Moon **[#3018]**
GRAIL-derived crustal thickness map shows that the lunar crust is thinner than previously thought. We investigate whether these crustal thicknesses could have caused the excavation of the lower crust and upper mantle during impact basin formation.

10:35 a.m. Baker D. M. H. * Head J. W. Phillips R. J. Neumann G. A. Smith D. E. Zuber M. T.
Grail Gravity Observations of the Transition from Complex Craters to Peak-Ring Basins on the Moon: Implications for Crustal Structure and Impact Basin Formation **[#3077]**
GRAIL gravity observations are combined with morphometric measurements to investigate the evolution of crust/mantle structure in the transition from complex craters to peak-ring basins on the Moon.

10:55 a.m. Kiefer W. S. * Potter R. W. K. McGovern P. J. Collins G. S. Kring D. A.
Thermal Evolution of Lunar Impact Basins and Implications for Mascon Formation **[#3009]**
In a basin-forming impact, the impact melt pool and surrounding mantle may deform as a rising gravity current, modifying the distribution of melt and its cooling time, and affecting the possible creation of super-isostatic mantle uplift.

11:15 a.m. Kring D. A. * Kramer G. Y. Potter R. W. K.
Interpreting the Depth of Origin of the Schrodinger Peak Ring and Implications for Other Impact Basins **[#3069]**
We propose a model for the formation of the Schrodinger peak ring that uplifts material from beneath the transient crater, but only exposes material from a fraction of the transient crater depth.

11:35 a.m. Schultz P. H. * Crawford D. A. Donaldson K. L.
New Contraints on Multi-Ring Basin Formation **[#3109]**
New near-infrared studies of the Moon reveal that the inner rings of large basins are composed of pure anorthosite derived from the crust (not the mantle) while retaining signatures of the impactor trajectory and size.

Monday, August 5, 2013
LARGE IMPACT BASINS:
THEIR FORMATION, STRUCTURE, AND ENVIRONMENTAL EFFECTS II
1:30 p.m. Fraser Auditorium

New data, models, and mapping are used to study the formation, structure, and environmental effects of large impact basins on the Moon, Earth and Mercury.

Chairs: **Gordon Osinski**
William McKinnon

1:30 p.m. Schmitt H. H. *
Large Meteor and Comet Impacts and Origin of Life **[#3119]**
Sample, photo-geological, and mineralogical analyses related to the Moon and Mars provide the foundation for understanding the environment in which early life evolved in our solar system.

2:00 p.m. Sapers H. M. * Osinski G. R. Banerjee N. R.
Microbial Trace Fossils Preserved in Impact Materials **[#3097]**
Meteorite impact events create unique microbial niches that may have been significant habitats on early Earth and astrobiological targets on other rocky bodies. Here we critique studies reporting evidence of biological activity in impact systems.

2:20 p.m. Cousineau M. L. * Therrien F. Maruoka T. Fortin D. Wing B. A.
New Insights into the Relative Timing and Contribution of the Chicxulub Impact and Deccan Volcanism in the Cretaceous-Paleogene Boundary Extinctions **[#3027]**
Using sulfur content and sulfur stable isotope measurements at two well-preserved KPg sections, we propose an environmental scenario for the KPg boundary that places the onset of the main Deccan eruptive phase after the Chicxulub impact.

2:40 p.m. Moriarty D. P. III * Pieters C. M.
Moon Mineralogy Mapper Observations of South Pole — Aitken: Constraints on Basin Formation **[#3108]**
Several impact scenarios (vertical, oblique, low-velocity) and melt behaviors (clast-rich flow, differentiation) are compared to Moon Mineralogy Mapper compositional observations of the lunar South Pole — Aitken basin to constrain formation models.

3:00 p.m. *Coffee Break*

3:15 p.m. Vaughan W. M. * Head J. W.
Impact Melt Differentiation in South Pole-Aitken Basin **[#3017]**
South Pole-Aitken basin (SPA) interior stratigraphy is consistent with that of a differentiated impact melt sheet. The noritic and Th-rich SPA floor may be melt differentiate, not primary crust.

3:35 p.m. Cupelli C. L. * Moser D. E. Barker I. R. Darling J. R. Bowman J. R. Wooden J. Dhuime B.
Discovery of Mafic Impact Melt in the Central Uplift of the Vredefort Basin **[#3096]**
Testing the impact origin of a gabbronorite dyke at Vredefort, evidence includes; contact relationships, shock microstructural state of major and accessory phases, U-Pb and Hf isotopic analysis of zircons, and Ti-in-zircon thermometry.

3:55 p.m. Schenk P. * O'Brien D. McSween H. Buczkowski D. Gaskell R. Preusker F. Marchi S. Yingst A. Mest S. Raymond C. Russell C.
Megascale Impacts into Vesta's South Pole **[#3100]**
Dawn orbital mapping and observations of the giant impacts into asteroid Vesta's South Polar region are described. Unusual features include a large central mound, extended ejecta deposits, and distinctive arcuate and spiral floor fracture patterns.

4:15 p.m. Bowling T. J. * Johnson B. C. Melosh H. J. Ivanov B. A. O'Brien D. P. Gaskell R. Marchi S.
Antipodal Terrains Created by the Rheasilvia Impact on Asteroid 4 Vesta **[#3083]**
The Rheasilvia Impact on 4 Vesta was sufficiently large to have caused terrain disruption at the impact antipode. We simulate this event, investigate which internal parameters of the target body control deformation, and compare to Dawn observations.

4:35 p.m. Buczkowski D. L. * Edrich S. Ackiss S. Seelos K. D.
Geomorphic Mapping of the Caloris Basin, Mercury **[#3089]**
We outline our mapping project of the Caloris basin and its associated intra-ejecta plains, intended to improve our knowledge of the geology and geologic history of the basin.

Tuesday, August 6, 2013
MODEL AND EXPERIMENTAL INSIGHTS INTO CRATERING PROCESSES
8:30 a.m. Fraser Auditorium

Hydrocode models and experimental impacts provide new insights into cratering processes.

Chairs: **Gareth Collins**
Debra Hurwitz

8:30 a.m. Elbeshausen D. * Wünnemann K. Collins G. S.
Crater Formation After Shallow Impacts — How do Elliptical Craters form? **[#3082]**
Why do some impacts result in a circular crater whereas others form elliptical shapes? How does the formation of elliptical craters differ from those of circular craters? We addressed these questions by conducting 3D numerical simulations.

8:50 a.m. Wünnemann K. * Ivanov B. A. Streb del Toro E.
Advanced Crater Size Scaling Laws Through Hydrocode Simulations **[#3023]**
Based on hydrocode simulations we propose improved scaling laws for the relation between impact energy and crater size in targets with varying properties including layered targets.

9:10 a.m. Crawford D. A. * Schultz P. H.
A Model of Localized Shear Heating with Implications for the Morphology and Paleomagnetism of Complex Craters **[#3047]**
A numerical model of localized shear heating using fault spacing estimates, frictional heating and conductive cooling can yield high fault temperatures with sufficient duration to influence complex crater morphology and paleomagnetism.

9:30 a.m. Vasconcelos M. A. R. * Wünnemann K. Reimold W. U. Elbeshausen D. Crósta A. P.
Numerical Modelling of the Vargeão Impact Structure, Southern Brazil **[#3039]**
Vargeão impact crater is a circular feature of ~12 km diameter, formed in basalts of the Southern Brazil. Here, we review the results of numerical simulations of Vargão carried out with the iSALE code, which explains its non-clear central uplift.

9:50 a.m. Poelchau M. H. * Kenkmann T. Hoerth T. Deutsch A. Thoma K. Schäfer F.
Experimental Cratering in Quartzite, Tuff and Sandstone: Final and Transient Crater Volumes **[#3054]**
Cratering experiments show the effects of porosity and pore space saturation on crater volume. The experiments also show the importance of constraining the effects of spallation on crater morphology.

10:10 a.m. *Coffee Break*

10:25 a.m. Güldemeister N. * Moser D. Wünnemann K. Hoerth T. Schäfer F.
Numerical Modeling of Seismic Signals Generated by Hypervelocity Impacts in Comparison to Experimental Observations **[#3019]**
We record and investigate seismic signals generated by hypervelocity impact experiments and compare experimental and numerical data to validate numerical material models and to quantify the seismic efficiency of hypervelocity impacts.

10:45 a.m. Johnson B. C. * Melosh H. J.
Jetting During the Vertical Impact of a Spherical Projectile **[#3014]**
Here we use the axisymmetric iSALE hydrocode at the unprecedented resolution of 800 cells per projectile radius to resolve jetting during the vertical impact of a spherical projectile.

11:05 a.m. Matsui T. * Kurosawa K. Ohno S. Kadono T. Sugita S.
Laser Gun Shock Experiments on Impact Vapor Plumes and its Implication for Origin and Evolution of Planetary Atmosphere **[#3066]**
We present the results of laser gun shock experiments, including the Hugoniot curve for forsterite and the chemical composition in the impact vapor plumes. We applied the results to the atmospheric blow-off on the Earth and the K/Pg impact event.

11:25 a.m. Bierhaus M. * Wünnemann K. Ivanov B. A.
Affect of Core Rheology on Shock Wave Propagation in Planetary Scale Impacts **[#3022]**
We use the iSALE hydrocode to investigate the effect of the thermal conditions and rheology of the target on the propagation of shock waves. In particular we focus on the effect of a liquid or solidified core on shock wave decay.

11:45 a.m. Kowitz A. * Güldemeister N. Reimold W. U. Schmitt R. T. Wünnemann K.
Porosity: The Reason for SiO_2 Melt Formation at even 5 GPa Shock Pressure. Experiments with Targets of 3 Different Porosities VS Mesoscale Modeling **[#3020]**
The influence of porosity on shock metamorphism was investigated with impact experiments (2.5–17.5 GPa) with sandstones and a quartzite. The results are compared to mesoscale numerical models quantifying the processes upon single-pore collapse.

12:05 p.m. Cox R. * Bauer A. W.
Through the Ice, Exposing the Ocean: Impact Breakthrough Parameters for Europa **[#3091]**
Hydrocode modeling shows that impacts penetrate to water if transient depth exceeds 0.8× ice thickness. For likely ice thicknesses, impact breaching at Europa is feasible on geologically short timescales, which may permit surface-ocean exchange.

Tuesday, August 6, 2013
GEOCHRONOLOGY OF IMPACT EVENTS
1:30 p.m. Fraser Auditorium

Several dating techniques are used to determine the timing of impact events throughout the solar system.

Chairs: **John Weirich**
Matthew Wielicki

1:30 p.m. Moser D. E. * Barker I. R. Tait K. T. Darling J. R. Chamberlain K. R. Schmitt A. K. Cupelli C. L. Reinhard D. A. Olson D. Clifton P. H. Larson D. J. Gault B. Bugnet M. Shaulis M. B. Lapen T. J. Irving A. J.
Atomic Records of Inner Solar System Impact Processes from U-Pb Dating Phases **[#3104]**
Nano- to atomic-scale records of impact processes on Earth, Moon, Asteroids and Mars; integration of microstructure and isotope geochronology of inner solar system minerals such as zircon and baddeleyite.

1:50 p.m. Wielicki M. M. * Harrison T. M.
Terrestrial Impact Zircon Textures: Implications to Impact Geochronology **[#3052]**
We report SIMS U-Pb analysis on the first terrestrial sieve textured zircons isolated from Vredefort impactites to investigate the use of such grains as probes of planetary impact history.

2:10 p.m. Crow C. A. * McKeegan K. D. Gilmour J. D. Crowther S. A. Taylor D. J.
Zircons as a Probe of Early Lunar Impact History **[#3059]**
Zircons are ideal for investigating the early lunar bombardment because we can measure both U-Pb crystallization ages and fissiongenic Xe degassing ages for the same crystal. We report U-Pb, Pb-Pb and U-Xe ages for two lunar zircons.

2:30 p.m. Bouvier A. *
Pb-Pb Chronometry of the Dark Melt Lithology of the Chelyabinsk LL Chondrite **[#3087]**
I will present results of the Pb-Pb radiochronometry of the dark melt lithology of the Chelyabinsk LL chondrite and discuss the impact history of the chondrite parent bodies.

2:50 p.m. *Coffee Break*

3:05 p.m. Weirich J. R. * Wittmann A. Isachsen C. E. Rumble D. Swindle T. D. Kring D. A.
Miller Range 05029: Evidence for a Large Impact on the L Chondrite Parent Body >4.5 Ga **[#3062]**
MIL 05029 is a slowly cooled, clast-free L impact melt rock with an ^{40}Ar-^{39}Ar age of ~4.52 Ga. Slow cooling implies deep burial and a crater diameter of 25–60 km. This impact may have shattered the parent body and disrupted the onion shell structure.

3:25 p.m. Biren M. B. * van Soest M. C. Wartho J-A. Hodges K. V. Dence M. R. Spray J. G.
(U-Th)/He Zircon Dating of the Clearwater West Impact Structure, Quebec, Canada **[#3117]**
Our (U-Th)/He dating results from the Clearwater West impact structure, Quebec, Canada are in good agreement with recent Ar-Ar dating and provides us with continued confidence for using the (U-Th)/He in the dating of terrestrial impacts structures.

Tuesday, August 6, 2013
POSTER SESSION: EARLY SOLAR SYSTEM COLLISIONS
4:00 p.m. Alumni Hall

Davison T. M. O'Brien D. P. Collins G. S. Ciesla F. J.
The Early Impact Histories of Meteorite Parent Bodies **[#3045]**
We have developed a Monte Carlo model to quantify impact histories for meteorite parent bodies in the early solar system. We evaluate proposed scenarios for the formation and evolution the CV, CB and H chondrite parent bodies and the IAB/winonaite body.

Abdulmyanov T. R.
Evolution of the Orbits of Bodies Formed Within the Proto-Planetary Rings **[#3011]**
Accumulation of dust particles in the proto-planetary rings and determination of the orbital elements of formed bodies are considered in this work.

Tuesday, August 6, 2013
POSTER SESSION: EXTRATERRESTRIAL CRATERING
4:00 p.m. Alumni Hall

Milbury C. Johnson B. C. Melosh H. J.
Hydrocode Simulation of the Transition from Central Peak to Peak-Ring Crater Morphology for the Moon **[#3013]**
We present results from impact simulations for complex and peak-ring craters for the Moon.

Nussbaumer J. W.
Evidence for Impact into Ice Rich Terrain and Melting to Produce Glaciation and Valley Networks in the Aeolis/Zephyria Region, Mars **[#3065]**
The spatial association between a 30 km crater in the Aeolis/Zephyria Region, Mars and paleochannels suggest that the impact was responsible for their formation.

Ackiss S. E. Seelos K. D. Buczkowski D. L.
Mineralogic Mapping of Huygens Crater, Mars: A Transect of the Highlands Crust and Hellas Basin Rim **[#3095]**
Huygens Crater, intersected by the Hellas rim, is a well preserved peak ring crater on Mars. By mapping the distribution of different mineral types, we hope to offer unique insight into the emplacement and alteration history of the highlands crust.

Kring D. A. Burns J. O. Hopkins J. B. Norris S. Lazio T. J. W.
Exploration of the Schrodinger Peak-Ring Basin on the Lunar Farside **[#3105]**
A close look at the geology of the Schrödinger basin for mission opportunities.

Otto K. Jaumann R. Krohn K. Matz K.-D. Preusker F. Roatsch T. Scholten F. Simon I. Stephan K. Raymond C. A. Russell C. T.
Spiral Features and the Coriolis Effect on Vesta's Basin Rheasilvia **[#3029]**
We investigated the spiral features associated with Vesta's south polar basin Rheasilvia and analysed the contribution of the Coriolis effect.

Barlow N. G. Boyce J. M. Wilson L.
The Role of Base Surge in the Formation of Martian Low-Aspect-Ratio Layered Ejecta (LARLE) Craters **[#3058]**
Martian Low-Aspect-Ratio Layered Ejecta (LARLE) craters are characterized by an extensive but thin layer extending beyond the normal layered ejecta blankets. We propose that base surge is responsible for producing the LARLE layer.

Calla O. P. N. Mathur S. Jangid M.
Comparision of Dielectric Constant of Apollo 17 Samples with MINI-RF and TALS **[#3007]**
DC of Apollo 17 samples have been compared with the Campbell's model DC using Mini-RF data and results are compared with the DC of TALS measured at laboratory. Results from above three sources are almost equal and model can be applied over equatorial region.

Calla O. P. N. Mathur S. Jangid M.
Water Ice Detected at Secondary Craters on Peary Floor Using Mini-SAR and Mini-RF **[#3008]**
PSR shows large variation in CPR range for Mini-SAR when compared with Mini-RF data. High CPR values together with low degree of polarization(m) and relative phase LH-LV (δ) signify presence of water ice in the secondary craters of Peary.

Wright S. P. Farrand W. H.
Spectral, Chemical, and Petrographic Comparisons of Hydrovolcanic Tephras with Basaltic Impactites: Relevance for Mars **[#3071]**
The origin of glasses and subsequent alteration products is not easily interpreted by planetary rovers. Basaltic hydrovolcanic tephras collected worldwide and impact melts from Lonar Crater have been examined using Mars Rover-like instrumentation.

Buhlmann E.
Searching for a Giant Impact Structure in the Flin Flon-Snow Lake Area, Manitoba **[#3103]**
Symmetric clusters of Early Proterozoic VMS deposits in the Flin Flon-Snow Lake mining district of Manitoba, centre on a 3.8 km circular structure. High Fe, Ti, P basalts and a 2.3 ppb Ir anomaly link the 140 km district to a possible impact event.

Tuesday, August 6, 2013
POSTER SESSION: IMPACT VAPOR, MELT, AND EJECTA
4:00 p.m. Alumni Hall

Hecht L. Hamann C. Schultze D. Ebert M. Reimold W. U. Wirth R.
Liquid Immiscibility and Disequilibrium Textures in Quenched Impact Melt of the Wabar and Tenoumer Craters **[#3115]**
Liquid immiscibility in impact melt from Tenoumer and Wabar Craters is induced by either rapid disequilibrium crystallization or addition of meteoritic iron from the projectile respectively.

Deutsch A. Metzler K. Berndt J. Langenhorst F.
LA-ICP-MS and Textural Analyses of Impact Spherules from the 2.54 Ga Bee Gorge Spherule Layer, Western Australia **[#3053]**
We have analyzed spherules in thin sections from the 2.54 Bee Gorge ejecta layer with special emphasize on the origin of textural features. We try to constrain the geochemical composition of the target using trace element analysis with LA-ICP-MS.

Swartz N. G. Davatzes A. E. K. Hassler S. W.
Size Distribution of Spherules in the Paraburdoo Spherule Layer **[#3070]**
The size distribution of spherules in the Paraburdoo spherule layer based on textural and compositional differences.

Hoffmann V. H. Kaliwoda M. Hochleitner R. Cornec J. H. Funaki M.
New Data on the Belize Tektites **[#3086]**
Belize tektites have been analyzed by magnetic means and LASER Micro Raman Spectroscopy.

King D. T. Jr. Petruny L. W.
Accretionary Lapilli (Carbonate Spherules) at the Cretaceous-Paleogene ('KT') Boundary in Belize (Central America) **[#3102]**
The Chicxulub impact event produced accretionary lapilli (or carbonate spherules) that fell across a wide area. This paper compares Chicxulub ('KT') accretionary lapilli from two sites in Belize: Albion Island and Armenia.

Tuesday, August 6, 2013
POSTER SESSION: PLANET-SIZE COLLISIONS
4:00 p.m. Alumni Hall

Fujita T. Genda H. Kobayashi H. Tanaka H. Abe Y.
Revised Fragmentation Model of Planet-Sized Collisions **[#3067]**
We re-estimate QD* and examine the relation between the ejecta mass and impact energy by the impact high-resolution SPH simulation. Then, the newly obtained QD* is smaller than that of previous works. That relation is described by two regimes.

Tuesday, August 6, 2013
POSTER SESSION: CASE STUDY OF THE SUDBURY STRUCTURE I
4:00 p.m. Alumni Hall

Lenauer I. Riller U.
Importance of Trishear Deformation for Mineral Exploration in the Southern Sudbury Basin, Ontario, Canada **[#3081]**
Post-impact deformation has changed the shape of the southern Sudbury Basin, marked by steeply dipping to overturned layer contacts in the Sudbury Igneous Complex. We discuss trishear deformation as a potential mechanism.

Salge T. Hecht L. Hansen B. Patzschke M.
Classification of Sulfides, Arsenides and Tellurides from the Sudbury Igneous Complex (SIC) Using Feature Analysis and Spectrum Imaging with Advanced EDS **[#3106]**
Developments in energy dispersive X-ray spectrometry offer advanced element analysis at high spatial resolution. Technological advances are demonstrated in representative samples for quantitative mineralogy and ore characterization.

Naumov M. V.
Sulfides in Impact Craters **[#3010]**
Data on sulfide mineralization in impact craters are generalized to show principal features of distribution and composition of sulfides within impact structures and to simulate impact-derived processes leading to the sulfide concentration.

Marion C. L. Osinski G. R. Grieve R. A. F. Bailey J. Péntek A. Smith D. Clayton J.
Mapping Sudbury Breccia in the North Range of the Sudbury Impact Structure, Canada **[#3093]**
Systematic mapping of the extent of Sudbury breccia in the North Range Footwall in collaboration with Wallbridge Mining Company Ltd. Preliminary results from small-scale mapping in summer 2012.

Osinski G. R. Ferrière L. Kring D. A. Anders D. Armstrong K. Baker D. Bamberg M. Beddingfield C. Gaither T. Harrison T. Huber M. S. Hurwitz D. Jaret S. Kramer G. Kuriyama Y. Lucas M. Marion C. L. Mercer C. Mount C. Neish C. Nuhn A. Ostrach L. Pickersgill A. Pilles E. Potter R. W. K. Ryan A. Sharp M. Swartz N. Thomson O. Veto M. Wielicki M. M. Wright S. Zanetti M.
Revisiting the Distribution and Properties of Shatter Cones at the Sudbury Impact Structure, Canada **[#3061]**
Here, we present the first results of a new multi-year research program that aims to systematically map the distribution of shatter cones and their physical properties around the Sudbury structure.

Hurwitz D. M. Zanetti M. Lucas M. P. Anders D. Kramer G. Thomson O. Kring D. A. Osinski G. R.
A Nested or Composite Shatter Cone Structure in the South Range of Sudbury **[#3111]**
In a recent survey of Sudbury shatter cones, we identified an outcrop of stacked, curvilinear foliations with well-developed, nested shatter cones that trend toward the apex of the foliations. We interpret this structure as a composite cone.

Anderson J. L. B. Beatty W. L. Kairies Beatty C. L.
Microstratigraphy of two Outcrops Within the Sudbury Impact Layer in Northern Minnesota **[#3034]**
The Sudbury Impact Layer (SIL) preserves ejecta deposited during the Sudbury impact. Two SIL outcrops in northern Minnesota were studied to create detailed micro-stratigraphic cross-sections. Implications for ejecta emplacement are discussed.

Fedorowich J. S. O'Connor C.
Modelling Cu-Ni-PGE Vein Arrays Within an Offset Dyke Environment of the Sudbury Igneous Complex **[#3094]**
Arrays of Cu-Ni-PGE veins are found in Offset Dykes and within the Footwall to the Sudbury Igneous Complex, and represent an important resource for mining over the last century. UDEC mechanical-hydraulic simulations of vein patterns are presented.

Beswick A. E.
SiO_2/Al_2O_3 Variations and Cross-Cutting Relationships in the Sudbury Igneous Complex: Evidence for Mixing of Multiple Endogenic Magmas **[#3016]**
Log Al_2O_3/Zr vs. log SiO_2/Zr diagrams demonstrate granophyres and norites of SIC have separate fractionation trends and transitional quartz gabbros lie along hybridization lines. This and cross-cutting relations indicate multiple magmas involved.

Tuesday, August 6, 2013
POSTER SESSION: GEOLOGIC MEASURES OF IMPACT CRATERING
4:00 p.m. Alumni Hall

Singleton A C. Osinski G. R.
Microscopic Effects of Shock Metamorphism in Zircon from the Haughton Impact Structure **[#3116]**
Zircon grains from the Haughton impact structure were studied to examine the correlation between microscopic features and the shock levels at which they occur. This includes a previously unreported microporous texture.

Vishnevsky S. A.
The Popigai: Unusual Features of Large Scale Impact Cratering **[#3005]**
The unique Popigai astrobleme exhibits a number of unusual impact formations, structures and features which are still unknown in other terrestrial impact sites. Some of these unusual properties and interpretation of their origin are presented.

Chanou A. Osinski G. R. Grieve R. A. F. Ames D. E.
Petrographic Characterization of Popigai Impact Melt-Bearing Breccias **[#3055]**
A set of impact melt-bearing breccias from Popigai impact structure was analyzed using optical microscopy, scanning electron microscopy, electron microprobe and digital image analysis. Here, we present their petrographic and textural characterization.

Misra S. Ray D. Androli M. A. G.
Carbonate-Rich Impact-Melt from Morokweng Impact Structure, South Africa **[#3063]**
The abstract first time reports carbonate impact-melt from Morokweng impact crater, South Africa. The observation comes from a bore hole study drilled by De Bears Company at ~15 km SW of Morokweng town.

Pati J. K. Reimold W. U. Greshake A. Koeberl C. K. Pati P.
Pseudotachylite Breccia Veins from Dhala Impact Structure, North Central India: Texture, Mineralogy and Geochemical Characterization **[#3064]**
This is the first report of pseudotachylitic breccia veins (PTB)in basement granitoids from the Dhala structure, north central India. The host granitoids and PTB show similar REE pattern despite extensive alteration and major element concentration.

Nakamura N. Meyer C.
Deciphering Lithological Contact of Granophyre Dikes with Bedrock Granites at Vredefort Dome, South Africa **[#3057]**
We report a petrological and rock magnetic study of the lithological contact of Vredefort Granophyre with bedrock granite.

Chang Y. Goto K. Sekine Y. Tajika E.
Characteristics and Vertical Profile of Shocked Quartz Grains in the YAX-1 Core: Constraints on Transient Crater Size and Ejecta Deposition Process of the Chicxulub Impact **[#3046]**
Characteristics and vertical profiles of PDFs on shocked quartz grains contained in the YAX-1 core derived from the Chicxulub Crater suggest that the core was located outside the transient crater, and that water had invaded into the crater.

Kerrigan M. C. Osinski G. R. Tornabene L. L.
Revisiting the Diameter of the West Clearwater Lake Impact Structure, Quebec, Canada **[#3085]**
We focus on West Clearwater Lake using remote sensing data to examine the surrounding terrain for structural features associated with an impact crater rim morphology outside of the lake area.

Suttak P. A. Boyce J. I. Hrvoic D.
Geophysical Mapping and Modelling of the Charity Shoal Structure, Lake Ontario, Canada **[#3032]**
The Charity Shoal structure is an enigmatic, crater-like depression in Lake Ontario. Magnetic, seismic and bathymetric data were collected over the shoal. Data analysis and forward modeling indicate an impact event or a diatreme as the likely origin.

Gottwald M. Fritz T. Breit H. Schättler B. Harris A.
Mapping Terrestrial Impact Craters with the TanDEM-X Digital Elevation Model **[#3001]**
We use the global digital elevation model (DEM) generated in the TanDEM-X mission for mapping terrestrial impact craters. This mission generates a global DEM with unprecedented properties permitting very detailed investigations of impact structures.

Khoury H. N. Salameh E. M. Reimold W. U.
Mineralogy and Geochemistry of Post-Impact Sedimentary Infill of the Crater Moat and Carbonates of the Crater Floor, Waqf As Suwwan Impact Structure **[#3030]**
Results of a shallow drilling program into the moat and central uplift of the Waqf as Suwwan impact structure, Jordan are presented. Stratigraphic evidence suggests a deep level of erosion.

Chaabout S. Chennaoui Aoudjehane H. Reimold W. U. Aboulahris M. Aoudjehane M.
Evidence of Non-Impact Cratering Origin of Imilchil (Morocco) Lakes (Isli and Tislit) **[#3074]**
Isli and Tislit lakes (High Atlas Mountains, Morocco) were recently proposed as impact structures, related to the Agoudal iron meteorite found about twenty km from the lakes. Our study did not provide any evidence for such an origin.

Pourkhorsandi H.
Search for Impact Craters in Iran: Citizen Science as a Useful Method **[#3038]**
To recognition probable impact craters in Iran, we use Google Earth data in the first step. Some probable structures identified and studies suggest non-impact origin for them. Studies on other craters in Iran are in progress.

Xie Z. Zuo S.
Airburst Impact Origin Hypothesis of Taihu Lake Basin in Southeast of China in Around 7000 Years ago **[#3076]**
The paper is to report investigation on unique morphology, occurrence, distribution, and mineralogy of siderite concretions found in Taihu Lake, Southeast of China, and discuss airburst impact origin hypothesis of Taihu Lake basin in ~7000 years ago.

Sisodia M. S.
Large Meteorite Impacts and Genesis of Precambrian Granites **[#3006]**
The earth scientists have been in pursuit for long to resolve granite genesis enigma. The Precambrian Dhala granites and Malani Rhyolites of India have their origin due to impact. It is thus proposed to find relation of impact and silicic provinces.

Wednesday, August 7, 2013
CASE STUDY OF THE SUDBURY STRUCTURE II
8:30 a.m. Fraser Auditorium

A close look at the Sudbury Structure precedes tomorrow's field trip.

Chairs: **Ulrich Riller**
Joshua Bailey

8:30 a.m. Bleeker W. * Kamo S. Ames D.
New Field Observations and U-Pb Age Data for Footwall (Target) Rocks at Sudbury: Towards a Detailed Cross-Section Through the Sudbury Structure **[#3112]**
To help constrain a detailed field-based cross-section through the entire Sudbury area we present new field observations and preliminary U-Pb age data on six rocks units in the footwall to the Sudbury impact structure.

8:50 a.m. Petrus J. A. * Ayer J. A. Long D. G. F. Lightfoot P. C. Kamber B. S.
Contributions to the Sudbury Igneous Complex and the Depth of Excavation: Evidence from Onaping Formation Zircon **[#3056]**
U-Pb data for zircon preserved in the crater-fill sequence (Onaping Formation) of the Sudbury impact structure reveal a previously unrecognized but significant contributor to the Sudbury Igneous Complex.

9:10 a.m. Riller U. * Clark M. Lenauer I. Santimano T.
Recent Advances in Understanding Tectonically Induced Crater Floor Modification at Sudbury: Importance for the Identification of Cu-Ni Sulphide Exploration Targets **[#3037]**
Individual segments of the Sudbury Igneous Complex and its respective host rocks deformed by different mechanisms. These mechanisms are delineated, along with their implications for occurrence of specific mineral deposits.

9:30 a.m. Smith D. A. * Bailey J. M. Pattison E. F.
Discovery of New Offset Dykes and Insights into the Sudbury Impact Structure **[#3090]**
Wallbridge Mining Company Limited has identified significant new Offset dykes related to the Sudbury impact structure which provide insight into its formation.

9:50 a.m. Lafrance B. * Kamber B. S. Ames D. E.
Formation of Sudbury Breccia by Shock Compression and Cataclasis **[#3080]**
The chemical compositions of Sudbury breccia suggest that it formed by shock compression and cataclasis during propagation of the shock wave. Additional brecciation and cataclasis occurred during modification and collapse of the transient crater.

10:10 a.m. *Coffee Break*

10:25 a.m. Pilles E. A. * Osinski G. R. Grieve R. A. F. Smith D. Bailey J.
Timing Relation Between Radial and Concentric Offset Dykes at Sudbury, Ontario: A Case Study of the Foy and Hess Offset Dykes **[#3043]**
The Offset Dykes at Sudbury are host to some of the largest Ni-Cu-PGE deposits in the world. This research focuses on understanding better their origin, the timing of emplacement, and how the different phases relate to one another.

10:45 a.m. Ames D E. * Hanley J. J. Tuba G. Bleeker W. Kamo S.
Primitive Source Revealed in the Sudbury Impact Structure: Implications for Cratering and Metal Sources **[#3099]**
New U-Pb zircon geochronology places constraints on As-rich target strata incorporated into the melt sheet upon initial impact and melting. Epidote Sr isotope results yields a primitive non-radiogenic source not recognized previously.

11:05 a.m. Anders D. * Osinski G. R. Grieve R. A. F.
The Onaping Intrusion, Sudbury, Canada — Impact Melt and Roof Rocks of the Sudbury Igneous Complex? **[#3092]**
In this study we investigated petrology and geochemistry of the Onaping Intrusion to further evaluate its origin and its relationship to the SIC.

11:25 a.m. Coulter A. B. * Osinski G. R. Grieve R. A. F.
The Nature and Origin of the Enigmatic Garson Member of the Sudbury Impact Structure, Canada **[#3035]**
New insight into the nature and origin of the Garson Member of the Onaping Formation within the Sudbury impact structure in central Ontario, Canada.

11:40 a.m. Ferrière L. * Osinski G. R.
Shatter Cones and Associated Shock-Metamorphic Microdeformations in Minerals — The Case of the Sudbury Impact Structure, Canada **[#3088]**
Shatter cones are the only diagnostic evidence of hypervelocity impact that develop on a macro- to megascopic scale. We report here on new macroscopic and petrographic investigations of shatter cone samples from the Sudbuy impact structure (Canada).

Wednesday, August 7, 2013
COMPLEX IMPACT CRATERS: THEIR FORMATION AND STRUCTURE
1:30 p.m. Fraser Auditorium

Insights into complex crater formation are gleaned from the Earth, Moon, and icy bodies.

Chairs: **David Kring**
Cassandra Marion

1:30 p.m. Shankar B. * Osinski G. R. Antonenko I.
Multispectral Assessment of Impact Melt Deposits Within Complex Lunar Craters **[#3068]**
This study summarizes the results of data fusion using multispectral datasets in the identification and characterization of impact melt deposits around complex craters on the Moon.

1:50 p.m. Dhingra D. * Pieters C. M.
Mineralogy of Impact Melt at Copernicus Crater: Insights into Melt Evolution and Diversity **[#3036]**
Mineralogy of impact melt is deciphered by remote spectral analysis to determine its implication on crustal diversity. The observed variation in composition and crystallinity is assessed in context of the melt morphology and target lithology.

2:10 p.m. Zanetti M. * Hiesinger H. Jolliff B. L.
Mapping Aristarchus Crater: Geology, Geomorphology, and Pre-Impact Stratigraphy **[#3114]**
Using available remote-sensing datasets we have geologically and geomorphologically mapped the Copernican-aged lunar impact in order to understand the distribution of impact melt and reconstruct the pre-impact stratigraphy of the target lithologies.

2:30 p.m. Clayton J. C. * Osinski G. R. Tornabene L. L. Kalynn J. D. Johnson C. L.
Effect of Target Lithology on the Simple to Complex Transition Diameter for Lunar Impact Craters **[#3110]**
We compare the number of terraces and crater depth for transitional and complex craters formed in different target types to gauge the possible effects of the target lithology on crater diameter and morphology.

2:50 p.m. *Coffee Break*

3:05 p.m. McKinnon W. B. * Singer K. N.
Secondary Craters of Large Craters and Basins on Europa and Ganymede: Ejecta Size-Velocity Distributions on Icy Bodies **[#3098]**
Mapped fields of secondary craters on two major icy worlds are converted to fragment size-velocity distributions. Maximum fragment sizes decrease with ejection velocity more gradually than on the terrestrial planets, and are larger than predicted.

3:25 p.m. Mader M. M. Marion C. L. Osinski G. R. Pickersgill A. E. Singleton A. C. Tornabene L. L.
A Systematic Multi-Year Field Campaign at the Mistastin Lake Impact Structure, Labrador, Canada **[#3113]**
In this report we summarize the results of an ongoing multi-year study of the 28 km diameter Mistastin Lake impact structure, focusing on the central uplift, crater rim, and impactites.

3:45 p.m. Kenkmann T. * Poelchau M. H.
The Central Uplift of Spider Crater, Western Australia **[#3025]**
We present micro- and macrostructural field data along with a simple kinematic model that explains the peculiar structure of the central uplift of Spider Crater. The structural inventory of mid-sized craters that formed by oblique impacts is reviewed.

4:05 p.m. Osinski G. R. * Francis R. Hansen J. Marion C. L. Pickersgill A. E. Tornabene L. L.
Structural Mapping of the Tunnunik Impact Structure, NWT, Canada: Insights in to Central Uplift Formation **[#3060]**
We report on structural mapping of the newly discovered Tunnunik impact structure, a 28 km diameter structure in the Canadian Arctic. The central uplift is exposed in a 2 km long canyon and features thrust-faulted blocks and outwards dipping strata.

Thursday, August 8, 2013
IMPACT CRATERING ON MARS
8:30 a.m. Fraser Auditorium

Impact cratering on Mars.

Chairs: **Nadine Barlow**
Livio Tornabene

8:30 a.m. Roberts J. H. * Arkani-Hamed J.
Impact Heating and Coupled Core Cooling and Mantle Dynamics on Mars **[#3042]**
Impact shock heats Mars / Drives large mantle upwelling / Halts core dynamo.

8:50 a.m. Ding N. * Bray V. J. McEwen A. S. Mattson S. S. Chojnacki M.
Tornabene L. L. Okubo C. H.
Mapping the Ritchey Crater Central Uplift, Mars **[#3021]**
To map the 3-dimensional geology of the central uplift of Ritchey and reconstruct the pre-impact stratigraphy, to better understand the Noachian stratigraphy of Mars.

9:10 a.m. Barlow N. G. *
Insights into the Formation of Martian Central Pit Craters and Implications for These Craters on Other Solar System Bodies **[#3051]**
Characteristics of martian central pit craters provide constraints on the possible formation mechanism for these features on other solar system bodies.

9:30 a.m. Tornabene L. L. * Osinski G. R. McEwen A. S.
Meter- to Decameter-Scale Morphology of Melt Rocks, Breccias, Bedrock and Structures in Central Uplifts Revealed by the Mars Reconnaissance Orbiter **[#3107]**
MRO observations elucidating various aspects of the impact process, particularly with respect to impact melt deposits and various impactites associated with central uplifts (CUs) in complex craters are summarized and presented here.

9:50 a.m. *Coffee Break*

10:05 a.m. Nuhn A. M. Tornabene L. L. Osinski G. R. McEwen A. S.
Mapping of Layered Bedrock in Martian Craters: Insights in to Central Uplift Formation **[#3079]**
We will present comparative morphologic and structural mapping of uplifts within three 30-km complex craters on Mars.

10:25 a.m. Jones E. * Osinski G. R.
The Links Between Target Properties and Layered Ejecta Craters in Acidalia and Utopia Planitiae Mars **[#3040]**
Layered ejecta craters on Mars may form from excavation into subsurface volatiles. We examine a new catalogue of martian craters to decipher differences between the single- and double-layered ejecta populations in Acidalia and Utopia.

10:45 a.m. Michalski J. R. * Bleacher J. E. Wright S. P.
A Holey Conundrum: Distinguishing Between Ancient Calderas and Degraded Impact Craters on Mars **[#3078]**
We present evidence that some of the most ancient, degraded basins on Mars are not actually impact basins but instead represent ancient calderas that formed in an early phase of explosive volcanism.

11:05 a.m. Montgomery J. * McDonald J.
Crater Profile Analysis Using High Resolution Laser Altimetry Data Sets **[#3118]**
Current methods for building crater profiles are unable to use recent NASA altimetry data. We present software that generates crater profiles dynamically and supports interactive crater morphometry using high-resolution altimetry data.

Thursday, August 8, 2013
IMPACTITES: FROM PROXIMAL TO DISTAL
1:30 p.m. Fraser Auditorium

A look at the properties and emplacement mechanism(s) of impactites, from proximal to distal.

Chairs: **Livio Tornabene**
Ludovic Ferrière

1:30 p.m. Grieve R. A. F. * Osinski G. R. Chanou A.
Onaping Formation, Ries Suevite and Melt-Fuel-Coolant-Interaction (MFCI) **[#3028]**
The Sudbury Onaping Formation and the Ries suevite Ries have been postulated to form as the result of melt-fuel-coolant-interaction (MFCI), i.e., by the explosive interaction between impact melt and water. Both interpretations cannot be correct.

1:50 p.m. Välja R. * Kirsimäe K. Boamah D. K. Somelar P.
Inverted Structure of Melt-Rich Impact Breccias at Bosumtwi Crater: Implications to Mixing and Cooling History of Fallout Suevites **[#3033]**
Fallout suevites at Bosumtwi Crater reveal gradual mineral and chemical changes that indicate mixing between suevites and underlying clastic breccia at the lower contact of suevite bed, and slow cooling of initially much thicker suevite blanket.

2:10 p.m. Salge T. * Goran D. Schulte P. Deutsch A.
The Distinct Behavior of Sedimentary Target Rocks During the Chicxulub Impact Event: Observations at Proximal and Distal Ejecta Deposits at K-Pg Sites El Guayal, La Lajilla, and Drill Cores UNAM-7 and ODP 207 **[#3101]**
EDS/EBSD analysis indicate melting and dissociation of carbonates and sulfates. Reformation of calcite would cause a prolonged release of thermal energy that may have initiated a delayed vapor release. It could force the gas driven ejecta transport.

2:30 p.m. *Coffee Break*

2:50 p.m. Davatzes A. E. K. * Enos M.
Spherule size Distribution and Lithology in the Dales Gorge Spherule Bed **[#3050]**
Size distribution of spherules in the Dales Gorge spherule layer and comparison to other Archean spherule beds.

3:05 p.m. Giuli G. * Cicconi M. R. Trapananti A. Eeckhout S. G. Pratesi G. Paris E. Koeberl C.
Iron Redox Variations in Australasian Muong Nong-Type Tektites **[#3084]**
The Fe oxidation state along few profile across dark/light layers of two Australasian Muong Nong tektite sample have been studied by Fe K-edge XANES. The dark layer results to be slightly but reproducibly more oxidized respect to the light layers.

3:25 p.m. Ebert M. * Hecht L. Deutsch A. Kenkmann T.
Element Partitioning Processes between Iron-Rich Projectiles and Silica-Rich Targets in Hypervelocity Impact Experiments **[#3044]**
This study addresses fundamental topics in impact cratering: 1) projectile partitioning into ejecta material, 2) element-fractionation processes during projectile-target interaction.

3:45 p.m. Wright S. P. *
Decompression Cracks in Altered Basalt Under Solid-State Shock Pressures: A New Macroscopic Shock Texture **[#3049]**
In Class 2 (~20–40 GPa) shocked basalts, which are solid-state (no melting), decompression cracks form in altered protoliths at Lonar Crater, India. This feature can be used to identify impact melt-bearing breccia and altered protoliths.

4:05 p.m. Huber M. S. * Plado J. Ferrière L.
Oldest Impact Structures on Earth — The Case Study of the Suavjärvi Structure (Russia) **[#3073]**
Suavjärvi (Russia) is considered to be the oldest confirmed impact structure on Earth. However, our recent field expedition and observations do not support the conclusion that the Suavjärvi structure was generated by a hypervelocity impact.

EVOLUTION OF THE ORBITS OF BODIES FORMED WITHIN THE PROTO-PLANETARY RINGS. T. R. Abdulmyanov, Kazan State Power Engineering University, Kazan, Russia (abdulmyanov.tagir@yandex.ru).

Introduction: Formation of the solar system, according to recent research [4], could start with the fragmentation of the proto-planetary disk and the formation of proto-planetary rings. The rings with a critical density, by gravitational instability will collapse [2]. The compression will not be local, if and only if the critical density will support by influx of particles from the outer regions of the ring. If the collapse is not local, then in the ring will be formed single planetesimal. Accumulation of dust particles in the protoplanetary rings and determination of the orbital elements of formed bodies are considered in this work.

Accumulation of dust particles in the proto-planetary rings: When the gravitational instability condition is satisfied, dust particles will combine to form the body of various mass and sizes. We assume that the dust particles of mass m_i are moved by the Kepler orbits around the central body of mass M ($M >> m_i$). Elliptical orbits of the particles in the polar coordinate system can be expressed as the following: $s = 1 / r = [1 + e\cdot\cos(v)]/p + G(M + m_i)/h^2$, where $p = a(1 - e^2)$, a, e, v - semi-major axis, eccentricity and the true anomaly of the particle orbits, h - the arbitrary constant. With the accumulation of dust particles orbit of new particles with mass $m = m_1 + +m_2 + ... + m_i$, will be changed. The equations of motion for new particles can be presented in the following form [3]: $ds_i /dv_i + + k_i^2 s_i = G(M + m_1 + ... + m_i)/h^2$, $dv_i/dv = k_i$, (1) $i = 1, 2, ..., n$. The solutions of these equations are as follows: $s_i = (e/p)\cdot\cos(k_i v) + G(M + m_1 + ... + m_i)/(h^2 k_i^2)$. New particles will have the following orbital elements: $p_i = h^2 k_i^2 /[G(M + m_1 + m_2 + ... + m_i)]$, $e_i = e\cdot p_i /p$. Since the mass of the dust particles and the newly formed particles is small compared with the central body, the changes in the orbital elements will also be small ($e_i \approx e$, $p_i \approx p$). However, the accumulation of orbital bodies will have a revolving of apsidal line [1]. As a result, the process of accumulation will occur in a short period of time, which is comparable with the period of rotation of the apsidal line.

Determination of the orbital elements of formed bodies: Suppose that at time t rectangular coordinates of the celestial body m are equal x, y, z, and coordinates of velocity are equal: x', y', z'. Initial speed φ' of the angle of perihelion φ also will be considered known. Using formulas: $c_1 = xz' - zx'$, $c_2 = yz' - zy'$, $c_3 = yx' - xy'$ the coordinates of the vector $\vec{r}\times\vec{V}$, orthogonal to the plane of the orbit are defined. Hence find the constants: $h_2^2 = c_1^2 + c_2^2 + c_3^2$, $h_1 = h_2 - r^2\varphi'$, $k = h_2 / h_1$ and $p = h_2^2 / \alpha^2$, where $r^2 = x^2 + y^2 + z^2$, $h_1 = r^2 dv/dt$, $h_2 = r^2 d(v + \varphi)/dt$. Then the eccentricity of the orbit can be determined by the formula: $r' = (V^2 - h_2^2 / r^2)^{1/2}$, $e^2 = (p/r - 1)^2 + (r' p/h_2)^2$. Define the inclination of the orbit and the longitude: $\cos i = c_3 / h_2$, $tg\Omega = -c_1 / c_2$. The angle $v + \varphi + \omega$ can be defined from the equations of the elliptic motion:

$$\sin(v + \varphi + \omega) = z/(r\sin i),$$

$$\cos(v + \varphi + \omega) = (x\cos\Omega + y\sin\Omega)/r .$$

To determine the true anomaly can be used the formulas: $\sin kv = r' p/(eh_2)$, $\cos kv = (p/r - 1)/e$. From the two laws (4) it follows what the partial $d\varphi/dv$ of differentials is a constant equal to k -1. Hence find the angle of perihelion, because the true anomaly is already known. As for as the angles $v + \varphi + \omega, v, \varphi$ are known can be find also the argument of perihelion - ω. Then the time of perihelion will define the known formula:

$$tg(E/2) = tg(v/2)\sqrt{(1-e)/(1+e)},\ t - \tau = M/n,$$

$$M = E - e\sin E,\ n = \alpha / a^{3/2},\ \alpha^2 = G(M + m).$$

Thus, orbital elements can be defined from the initial conditions of motion for the case rotation of the perihelion. According to the solution of the equations (1) the coefficient k indicated the absence or presence of spin-orbit perihelion. When k is equal to 1 the rotation will be absent, in other cases, the perihelion would rotate. It is known what the anomalies of the rotation of perihelion by Mercury, Venus, Earth and Mars are respectively 43,03''; 8,62''; 3,83''; 1,35''. Then the constant values k - 1 for these orbits of the planets will be respectively $3{,}3202\cdot10^{-5}$; $6{,}6512\cdot10^{-6}$; $2{,}9552\cdot10^{-6}$; $1{,}0416\cdot10^{-6}$.

The work is supported by the RFBR grant No 13-02-00792.

References: [1] Abdulmyanov T. R. (2012) 43rd *LPSC*, 19-23 March. Texas. USA. [2] Abdulmyanov T. R. (2013) *EPSC*, Abstract Vol. 8, EPSC2013-720. [3] Abdulmyanov T. R. (2013) *EPSC*, Abstract Vol. 8, EPSC2013-722. [4] Zabrodin A. V. et al. (2006) Preprint. Keldysh Institute. RAS. 43p.

MINERALOGIC MAPPING OF HUYGENS CRATER, MARS: A TRANSECT OF THE HIGHLANDS CRUST AND HELLAS BASIN RIM. S. E. Ackiss, K. D. Seelos, and D. L. Buczkowski, Johns Hopkins University Applied Physics Laboratory, Laurel, MD 20723 (Sheridan.Ackiss@jhuapl.edu).

Introduction: Huygens crater is a well preserved peak ring structure on Mars centered at 13.5°S, 55.5°E in the Noachian highlands between Terras Tyrrhena and Sabaea. With a diameter of ~450 km, it uplifted and exhumed Noachian crustal materials from depths greater than 30 km, likely including Hellas rim material (Figure 1).

In neighboring terrains, numerous small outcrops of aqueously altered minerals, such as phyllosilicates, have been identified [1-2] as well as frequent expanses of mafic-bearing plains [3-6]. By mapping the distribution of these different mineral types in and around Huygens, we hope to offer unique insight into emplacement and alteration history of the highlands crust.

Methods: We utilize data from the Compact Reconnaissaince Imaging Spectrometer for Mars (CRISM) which acquires visible and near infrared (0.36-3.9 µm) data [7]. Twelve CRISM multispectral maptiles (mosaicked at ~230 meters/pixel and corrected to Lambert Albedo) were used to understand regional mineralogic trends and define unit contacts.

Preliminary Mapping Results: Four mineralogy-based units have been defined for the Huygens region so far: olivine-, high calcium pyroxene (HCP)-, low calcium pyroxene (LCP)-, and Fe/Mg phyllosilicate-bearing material.

The olivine-bearing unit is associated with topographically lower, generally flat-lying plains, including the floor of Huygens and the infilled floors of smaller surrounding craters. It is also observed on intercrater plains consistent with high thermal interia, olivine-bearing "bedrock" units described by Rogers et al. [5] in the east of our study region. We have yet to confirm whether the olivine throughout the region is primary bedrock or transported material. Mapped occurrances of HCP-bearing material appear associated with similar plains morphology, also occurring in areas on the floor of Huygens as well as gradational with olivine-bearing plains within smaller, unnamed craters in the southwest part of the study region.

Exposures of LCP occur in distinct outcrops concentrated in the southern portion of the map area, interior to the Hellas rim boundary [6], and perhaps representing uplifted Hellas impact material. LCP is associated with a more erosionally-resistant material, usually forming knobs.

Fe/Mg phyllosilicate-bearing materials are localized and have been exposed by impact cratering, with signatures observed on crater rims, walls, and in ejecta blankets. Phyllosilicates are identified both inside (on the floor of) and outside Huygens.

Acknowledgements: This work was supported by the NASA Mars Data Analysis Program (grant number NNX10AO25G) and in part by an appointment at the JHU Applied Physics Lab (APL) administered by the Oak Ridge Institute for Science and Education through an agreement between the U.S. DOE and APL.

References: [1] Bibring, J.-P., et al. (2005) Sci., 307, 1576-1581. [2] Loizeau, D., et al. (2012) Icarus, 219, 476-497 [3] Koeppen, W. C., et al. (2008) JGR, 113, E05001. [4] Mustard, J. F., et al. (2005) Sci., 307, 1594-1597. [5] Rogers, D., et al. (2011) JGR, 116, E08005. [6] Rogers, D. et al. (in press) JGR. [7] Murchie, S. L., et al. (2007) JGR, 112, E05S03. [8] Frey, H. (2008) GRL, 35, L13203.

Figure 1. (Below) MOLA regional topography showing impacts and associated rings >1000 km (black circles) [8]. Huygens study region in large black box. (Bottom Left) Zoomed in preliminary map showing units over THEMIS daytime IR.

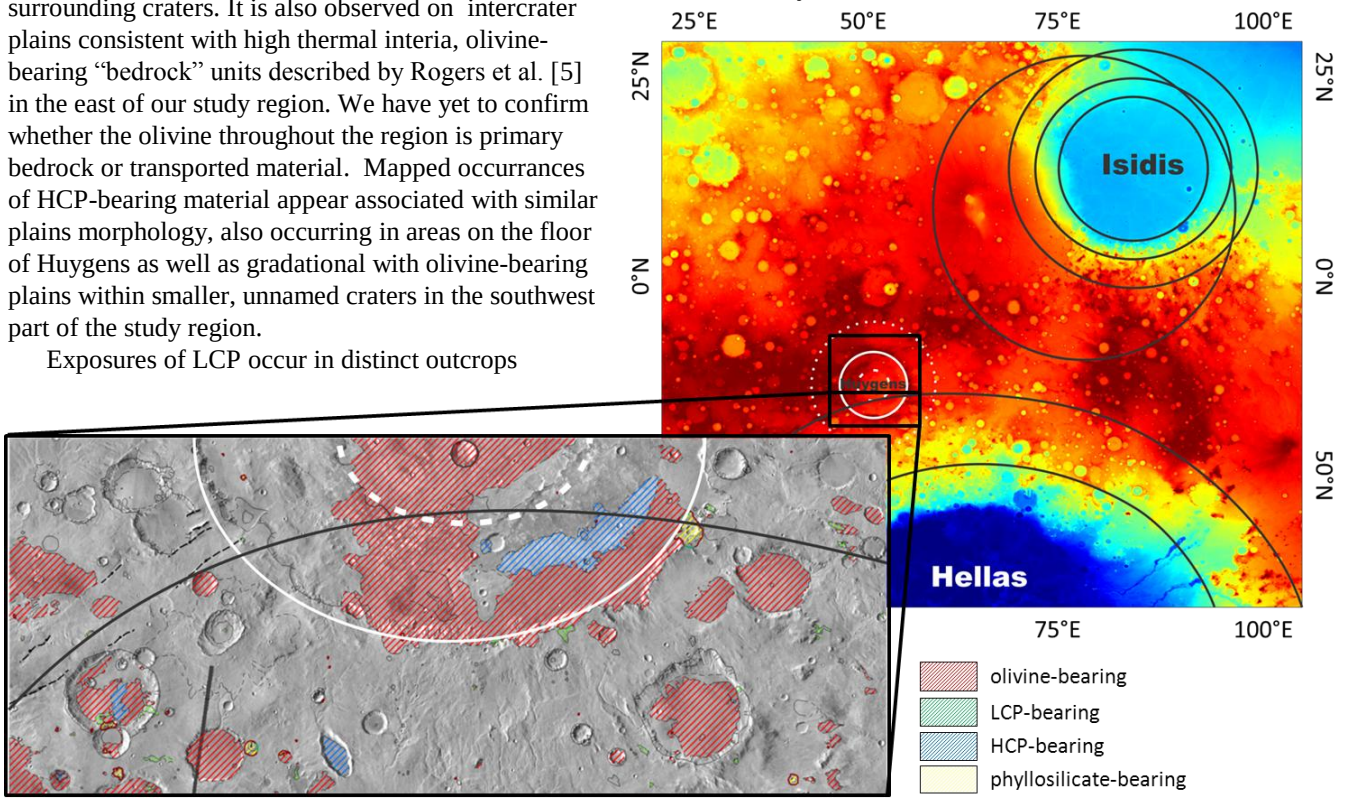

Primitive Source Revealed in the Sudbury Impact Structure: Implications for Cratering and Metal Sources.

D E. Ames[1] , J.J. Hanley[2], G. Tuba[1] W. Bleeker,[1] and S. Kamo[3], [1]Geological Survey of Canada, 601 Booth St Ottawa Canada dames@nrcan.gc.ca, [2] Saint Mary's University, Halifax, Canada. [3]University of Toronto, Canada.

Introduction: The Sudbury Structure is the eroded remnant of a large 150-200 km multi-ring impact crater and uniquely reveals on present-day surface the crustal impact structures in the crater floor below the igneous complex [1,2]. Large terrestrial impact structures had transient craters that penetrated 30-40 km depth and collapsed to form ~200 km impact craters with perturbations of the Moho [2,3]. The footwall environment to the Sudbury Igneous Complex contains permeable pseudotachylite zones that act as conduits for magmas, fluids and gases.

An extensive array of concentric and radial structures below the interpreted melt sheet crosscut the earlier pseudotachylite zones and may be filled with mafic igneous melt as at the Copper Cliff and Worthington offset dykes or partial melts of the footwall (meta/footwall breccia), discontinuous igneous pods and breccias (ie. Whistle, Trill). Recently unearthed concentric offset structures in the NW quadrant now extend over 45 km subparallel to and ~12 km below the base of the melt sheet.

North Range isotopic results: The Broken Hammer deposit is a Paleoproterozoic zone of Cu-Ni-PGE mineralization within brecciated Neoarchean gneiss and granites in the northern footwall of the Sudbury Igneous Complex. It is hosted, by impact-induced pseudotachylitic breccias 1 to 1.5 km below the crater floor. The Joe Lake mafic intrusion that extends 1.5 km from Broken Hammer to the SIC and over 10 km along the SIC contact was previously thought to be part of a Paleoproterozoic suite of mafic intrusions [2].

U-Pb geochronology. Preliminary zircon U-Pb geochronology and field observations of a penetrative fabric compatible with that of adjacent Levack gneisses indicate it must be older. Our initial results suggest the Joe Lake gabbro was metamorphosed at 2657±9 Ma, based on near concordant metamorphic zircons, and was intruded by relatively undeformed late Archean pegmatite dykes shortly after.

These mafic rocks in the impact target rocks have been proposed as a source of arsenic incorporated early into the impact melt during initial impact [5].

Low sulphide-PGE zone. An unusual hydrothermal occurrence of low-sulphide, silicate-rich, PGE-rich high-grade zone with a Pt: Pd ratio of 2:1 is situated in epidote-quartz extensional veins and pods on the edge of the Broken Hammer open pit. This spectacular high-grade PGE zone is dominated by coarse epidote, quartz and sperrylite ($PtAs_2$) crystals up to 13 mm (Fig 1).

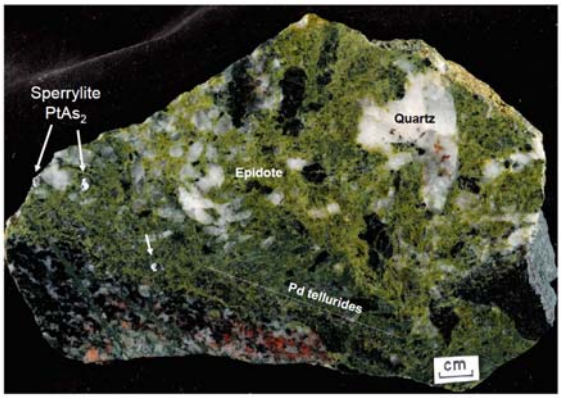

Figure 1. Polished rock slab of coarse epidote-quartz-sperrylite, minor merenskyite and Ni chlorite hydrothermal assemblage in contact with gabbro.

The dominant palladium mineral is merenskyite ($PdTe_2$) and not michenerite that formed in most North Range sulphide dominated ore systems. Isolated sperrylite grains in quartz-epidote have inclusions of gold, Au-Ag tellurides whereas complex intergrowths of Pd-, Bi- and Ag-tellurdes are associated with specular hematite and cassiterite reflecting oxidizing conditions.

Sr isotopes. Early formed epidote that hosts coarse sperrylite was analyzed by TIMS yielding a narrow range of low age-corrected $^{86}Sr/^{86}Sr$ ratios from 0.705948 to 0.706457 with a primitive non-radiogenic source. This reveals a source not recognized previously in the crustally dominated radiogenic Sr in the SIC, carbonates and other epidote in the SIC and Onaping Formation [6].

Implications and future work: In-situ LA-MC-ICP-MS Sr isotope analysis of epidote and calcite in a variety of paragenetic suites in the structures below the melt sheet will be used to identify potential sources and trace the evolution of fluids in the Sudbury crater.

References: [1] Milkereit et al. (2010), Large Meteorite Impacts and Planetary Evolution IV: GSA Special Paper 465, 115-131. [2] Ames et al. (2008), Econ. Geol. 103, 1057-1077. [3] Christenson et al. (2009), EPSL 284, 249-257. [4] Pentek et al. (2008), Econ. Geol. 103, 1005-1028. [5] Ames et al. (2010), SEG Keystone. [6] Hanley and Ames (2012) *PACROFI-XI*, **11**, 39-40.

THE ONAPING INTRUSION, SUDBURY, CANADA – IMPACT MELT AND ROOF ROCKS OF THE SUDBURY IGNEOUS COMPLEX? D. Anders[1], G. R. Osinski[1] and R. A. F. Grieve[1,2], [1]Dept. of Earth Sciences/Centre for Planetary Science and Exploration, University of Western Ontario, Canada (dander53@uwo.ca, gosinski@uwo.ca), [2]Earth Sciences Sector, Natural Resources Canada, (rgrieve@nrcan.gc.ca).

Introduction: The 1.85 Ga [1] Sudbury impact structure is one of the largest impact structures on Earth. The impact basin contains the Sudbury Igneous Complex (SIC); overlain by rocks of the Onaping Formation and post-impact sediments. Igneous bodies – the so called "Onaping Intrusion" (OI) – form sheets and sills at the contact between the SIC and the Sandcherry Member of the overlying Onaping Formation and occupies ~50% of this contact zone [2]. Based on a preliminary recent study, the OI has been interpreted as the roof rocks of the SIC [3]. The present study focuses on two drill cores to further examine the impact melt origin and the relationship to the SIC by a comparison of geochemical data of the OI and the SIC [4].

Core 70011: The 70011 drill core was taken from the North Range of the SIC and is composed of OI from 50' and underlying Granophyre of the SIC starting at 298'. The matrix of the OI is characterized by a skeletal intergrowth of quartz and feldspar indicating a rapid and simultaneous cooling of those minerals within the melt. Microprobe analyses of alkali feldspars and plagioclase revealed only Ca-depleted sanidine and albite compositions which correlates with Pearce Element Ratio plots that show a plagioclase-controlled crystallization of the OI. Secondary minerals, such as chlorite and epidote, distributed within the groundmass, have been formed by alteration of hornblende, pyroxene and biotite due to post-impact hydrothermal activity. Whole rock major element analyses reveal a high amount of SiO_2: 63.63 to 70.44 for the OI and 52.15 to 70.5 for the SIC [4]. Samples of both, the SIC and the OI, plot in the TAS diagram within the subalkalic area. For the SIC the amount of alkalis tends to increase with increasing amount of SIO_2 pointing to a typical differentiation and fractionation trend following Bowen's reaction series. This trend is not as clear for the OI which might be related to rapid cooling of the OI melt. Grain size tends to increase with increasing depth, while the number of target rock clasts encountered within the matrix decrease with increasing depth. This points to the existence of a temperature gradient within the melt assemblage with slower cooling close to the SIC, leading to longer crystallization times and assimilation of more clasts. The clasts are characterized by a rim as a result of interaction processes between liquid melt and clasts. Planar deformation features (PDFs), indicators of shock metamorphsim, occur in clasts and are typically decorated. The contact between Granophyre and OI is abruptly gradational with the first isolated patches of micrographic intergrowth at a depth of 282' within the OI and an increase of graphic intergrowth with increasing depth, becoming the dominant texture at 298'. This implies an interaction between OI and SIC during formation and suggests that they might have originated from the same melt pool.

Core 52847: Core 52847, also drilled from the North Range of the impact structure, consists of the lowest unit of the Onaping Formation, the Sandcherry Member, followed by OI and underlying Granophyre. While the Sandcherry Member occupies ~1000', the OI is only ~50' thick and transition gradational into Granophyre. Investigations show that the contact zone between Sandcherry Member and OI is more or less sharp, no gradational transition has been observed, which implies that Onaping Formation and OI are not genetically related.

Conclusions: The igneous groundmass and shocked clasts clearly demonstrated impact melt origin for the OI. Increasing grain size and decreasing amounts of clasts with increasing depth are general features of roof rocks leading to the hypothesis that the OI is, in fact, the roof rock complex of the SIC. The abruptly transitional contact between Grannophyre and OI suggests a relationship between OI and SIC and a formation from the same melt pool; however, the OI did not undergo a differentiation, as seen in the SIC. A suggested water-rich environment at the time of, and after, the impact might have influenced the formation of both units [2]. In this model, water flowing into the crater interacts with the hot, undifferentiated and highly viscous melt sheet of the SIC, the roof rocks (OI), and the early fallback breccias leading to explosive reactions and the blasting away of the roof rocks in certain regions.

References: [1] Krogh T. E. et al. (1996) In: Earth processes: Reading the isotopic code, edited by Hart S. and Basu A. Monograph 95, American Geophysical Union, pp. 343-353. [2] Grieve R. A. F. et al. (2010) Meteoritics & Planetary Science 45, Nr 5, pp. 759-782. [3] Brillinger D. T. M. et al. (2011) abstract #5405, 74th Annual Meeting of the Meteoritical Society. [4] Therriault A. M. et al. (2002) Economic Geology 97, pp. 1521-1540. [5] Stöffler D. and Langenhorst F. (1994) Meteoritics, 29, pp. 155-181.

Acknowledgements: Peter Lightfoot, Vale, is thanked for providing the core samples. Funding from NSERC is gratefully acknowledged.

Microstratigraphy of Two Outcrops within the Sudbury Impact Layer in Northern Minnesota. J.L.B. Anderson, W.L. Beatty, and C.L. Kairies Beatty, Winona State University; Winona, MN (JLAnderson @winona.edu).

Introduction: The Sudbury Impact Layer (SIL) was deposited 1.85 Ga as ejecta from the Sudbury impact in Sudbury, Ontario, fell over southern Ontario [1] and the upper Midwest [1,2,3,4,5]. Following the general description of [2], a typical SIL sequence includes a shocked mega- and meso-scale breccia at its base composed of deformed country rock, a gritstone boundary layer, and a thinner ejecta-bearing layer with larger lapilli stones beneath smaller spherules. The SIL is unique in that the unit (up to 30 m thick in some places) formed in less than one day and preserved an incredibly detailed record of distal ejecta emplacement from one of the largest known impact events on Earth.

Microstratigraphy and Methods: Two outcrops located 1.7 km apart in northern Minnesota (Stops 3 and 5 from [2]) showing the transition from ejecta-absent to ejecta-bearing layers within the SIL were selected for this study. Our goals were to (1) correlate two closely spaced SIL outcrops, (2) search for evidence of processes acting during SIL emplacement, and (3) assess whether the lapilli and/or spherules were warm or cold when deposited. Each outcrop was carefully measured, described in detail and sampled. A high-resolution panorama of each outcrop was captured using a GigaPan Epic robotic camera mount. In the lab, hand samples were cut and scanned at high resolution and thin sections were prepared.

Results: *Correlating the outcrops.* While all of the major units described in [2] were present between the two outcrops, each outcrop was missing one of the major units, although not the same one. Despite being so close to one another, the two outcrops were more diverse than expected. The microstratigraphy will be discussed in more detail in the presentation.

Evidence of emplacement processes. At both outcrops the deposition of ejecta, especially that of the spherules, appears less orderly than might be expected from ballistic emplacement but more orderly than might be expected from a ground-surge or debris cloud [e.g., 6]. At Stop 3, the spherules form centimeter-scale lenses or thin beds within the surrounding finer-grained ash matrix (Fig. 1) that repeat for at least 10 cm. This suggests a cyclical or pulsating mechanism that separated the spherules from the rest of the ejecta-bearing material as they were deposited.

Lapilli temperature when deposited. We initially set out to determine whether the lapilli were cold or warm when deposited by looking for cracks or softening features in hand sample and thin section. We instead observed pressure solution features in the lapilli-bearing layers, including stylolites, volume loss within lapilli (Fig. 2), and concave-convex grain contacts. We suggest that these are the result of intrusion of the Logan Sill at 1.115 Ga which thermally metamorphosed the SIL in northern Minnesota. SIL deposits observed in Thunder Bay, Ontario, do not show comparable evidence of pressure solution and are stratigraphically further away from the Logan intrusion than the SIL in northern Minnesota.

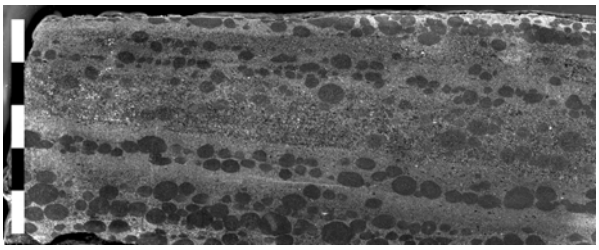

Figure 1. Cross-section of spherule layers outcrop interbedded with fine-grained ash matrix at Stop 3. Scale is 5 cm.

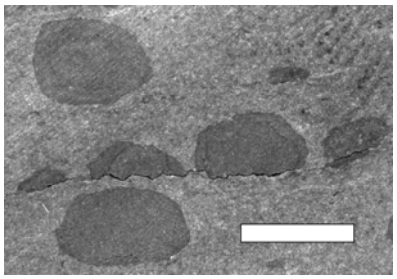

Figure 2. Pressure solution features including stylolites and volume loss in Gunflint Trail lapilli found at Stop 3. Scale is 5 mm.

Conclusions: Deposition of the ejecta-bearing units within the Sudbury Impact Layer in northern Minnesota shows moderate lateral variation on a kilometer scale. At the same time, the spherule-rich layers show centimeter-scale vertical bedding. Models for the emplacement of this deposit may predict the lateral variation but must also explain the small-scale layering of ejecta. Lastly, the lapilli in northern Minnesota have been modified after deposition, potentially by thermal metamorphism from the overlying Logan Intrusion, and cannot be used to infer the immediate post-impact condition of the ejecta in this region.

References: [1] Addision, WD, *et al.* (2005) *Geology, v. 33*, doi:10.1130/G21048.1. [2] Jirsa, MA, *et al.* (2011) GSA Field Guide 24, p. 147-169. [3] Jirsa, MA (2010) *Inst. of Lake Superior Geology, v. 56.* [4] Pufahl, PK, *et al.* (2007) *Geology, v.35*, p. 827-830. [5] Cannon, WF, *et al.* (2010 *GSA Bull., v. 122*, doi:10.1130B26517.1. [6] Branney, MJ & Brown, RJ (2011) *J. Geology, v119*, p. 275-292.

Acknowledgements: We thank our undergraduate research team: James Reed, Thomas Stromback, Melissa Maslowski, Christina Slowinski and Mallery Navis. We also thank Luke Zwiefelhofer (WSU), Dr. Mark Jirsa and Dr. Paul Wieblen (MN Geological Survey), and Dr. Phil Frahlick (Lakehead Univ., Thunder Bay).

GRAIL GRAVITY OBSERVATIONS OF THE TRANSITION FROM COMPLEX CRATERS TO PEAK-RING BASINS ON THE MOON: IMPLICATIONS FOR CRUSTAL STRUCTURE AND IMPACT BASIN FORMATION. David M.H. Baker[1], James W. Head[1], Roger J. Phillips[2], Gregory A. Neumann[3], David E. Smith[3,4], and Maria T. Zuber[3,4]. [1]Department of Geological Sciences, Brown University, Providence, RI 02912 USA, Email: David_Baker@brown.edu; [2]Planetary Science Directorate, Southwest Research Institute, Boulder, CO 80302 USA; [3]Solar System Exploration Division, NASA Goddard Space Flight Center, Greenbelt, MD 20771 USA; [4]Department of Earth, Atmospheric and Planetary Sciences, MIT, Cambridge, MA 02139 USA.

Introduction: The onset of impact basins on the Moon and other planetary bodies occurs with the appearance of two concentric topographic rings, forming peak-ring basins [1]. Recent lunar gravity measurements by the Gravity Recovery and Interior Laboratory (GRAIL) mission [2] now provide the opportunity to analyze the gravity and crustal structure of craters near the onset of impact basins in greater detail. We use these gravity measurements, combined with our morphometric observations [3-5] to investigate the evolution of the crust/mantle structure in the transition from complex craters to peak-ring basins on the Moon.

Methods: We measured the topography (LOLA), free-air and Bouguer gravity anomalies (GRAIL JGGRAIL_660C6A), and Moho relief (Model 1 of [6]) for peak-ring basins, protobasins, and complex craters ≥100 km in the catalogs of [3,5]. Datasets were expanded from spherical harmonic degrees 16 to 310 and in 4ppd grids. For each dataset, azimuthally averaged radial profiles were measured from the basin center to three crater/basin radii. The gravitational effects of mare fill were not removed here; however, our estimates indicate that mare does not substantially affect the overall trends.

Free-air gravity anomalies (FAAs): Lunar mascon basins [7] are characterized by positive central FAAs. Eleven peak-ring basins (250-580 km in diameter) show positive central FAAs. Positive central FAAs are generally absent in complex craters and protobasins, suggesting that the mascon-forming processes begin to dominate over lithospherically-supported topographic effects following the onset of peak-ring basins (~200 km).

Bouguer gravity anomalies (BAs): All peak-ring basins show a positive, central BA that is ringed by an annulus of negative BAs. The radius of the positive BA correlates well with the radius of the interior peak ring. The negative BA annulus reaches a minimum midway between the peak ring and rim crest and extends outward to near the rim crest. Protobasins and most complex craters do not exhibit this regular BA pattern. Instead, BAs are more irregular and not clearly tied to surface morphology [8]. The absolute magnitudes of the maximum central BA and minimum annular BA increase proportionally for peak-ring basins, with complex craters and protobasins following a different trend (Fig. 1)

Moho relief and crustal thickness: From the models of [6], we interpret the central positive BAs in peak-ring basins to represent central uplifts of the crust-mantle boundary and thinned crust confined within the peak ring. This mantle uplift is bounded by an annulus of thickened crust, producing the observed ring of negative BAs. Since strongly circular, central, positive BAs are generally absent in complex craters and protobasins, we suggest that mantle uplift is relatively minor or absent at these crater sizes.

Implications for the crater to basin transition: Our observations show that the formation of central positive Bouguer anomalies and associated negative BA annuli are fundamental characteristics of all basins (peak-ring basin to multi-ring basin [9]) on the Moon. Further, mascons occur down to diameters of at least 250 km, indicating that mascon-forming processes [10,11] are effective for small basins. The transition from complex craters to peak-ring basins not only involves a change in interior landforms (central peak to peak ring) but also a strong change in character of crustal and mantle structure. The coincidence of the onset of substantial mantle uplifts and crustal thickening with the onset of peak rings and the correlation of the radius of the central mantle uplift with the radius of the peak ring is highly suggestive that these features are intimately linked. These gravity observations and recent morphometric observations have important implications for models of the formation of peak rings and should together act as an observational framework for understanding impact basin formation on the Moon and other planetary bodies.

References: [1] Hartmann, W.K., Kuiper, G.P. (1962) *Commun. Lunar Planet. Lab, Univ. Arizona 1*, 51–66. [2] Zuber, M.T. et al. (2013) *Science, 339*, 668–671. [3] Baker, D.M.H. et al. (2011) *Icarus 214*, 377–393. [4] Baker, D.M.H. et al. (2012) *J. Geophys. Res. 117*, E00H16. [5] Baker et al. (2013) *Planet Space Sci., in review*. [6] Wieczorek et al. (2013) *Science 339*, 671–675. [7] Muller, P.M., Sjogren, W.L. (1968) *Science 161*, 680–684. [8] Phillips, R.J. et al. (2012) *AGU Fall Meeting*, no. G32A-07. [9] Neumann, G.A. et al. (1996) *J. Geophy. Res. 101(E7)*, 16,841–16,843. [10] Andrews-Hanna, J.C. (2013) *Icarus 222*, 159–168. [11] Freed et al. (2013) *Lunar Planet Sci. 44*, no. 2037.

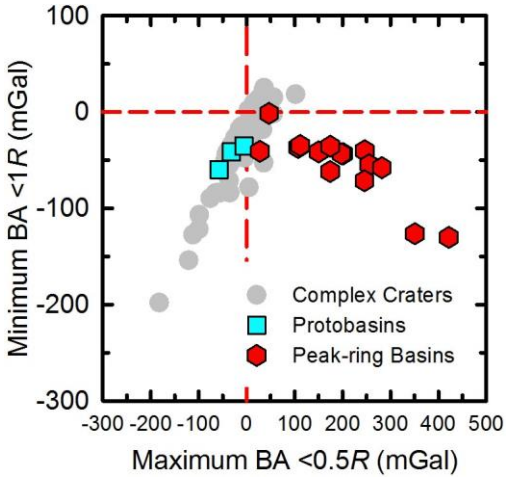

Fig. 1. Trends of the minimum Bouguer gravity anomaly (BA) within 1*R* (where *R* is crater/basin radius) versus the maximum BA within 0.5*R* for peak-ring basins, protobasins, and complex craters. For peak-ring basins, this plot shows the trend in the minimum value of the negative BA annulus versus the central BA maximum (both have linear trends with rim-crest diameter for peak-ring basins).

INSIGHTS INTO THE FORMATION OF MARTIAN CENTRAL PIT CRATERS AND IMPLICATIONS FOR THESE CRATERS ON OTHER SOLAR SYSTEM BODIES. Nadine G. Barlow, Dept. Physics and Astronomy, Northern Arizona University, Flagstaff, AZ 86011-6010 USA. Nadine.Barlow@nau.edu.

Introduction: Central pit craters display a depression either on the crater floor or atop a central rise (Fig. 1). A pit is classified as a floor pit when the pit floor lies below the crater floor and as a summit pit when the pit floor lies above that of the crater. Central pit craters are abundant on Mars, Ganymede, and Callisto, which led to the proposal that target volatiles are involved in the formation of these features [1, 2]. However, central pits also have been reported on Mercury and the Moon, although they are much less abundant on these more volatile-poor bodies [3-5], leading to the question of whether volatiles are required for central pit formation.

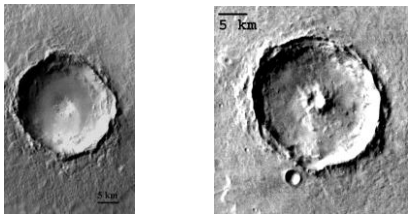

Figure 1: Examples of Floor Pit (left) and Summit Pit (right) craters. Floor pit crater is 24.8 km in diameter and located at 0.77°N 356.06°E (THEMIS image I11284045). Summit pit crater is 22.2 km in diameter and centered at 5.73°N 304.64°E (THEMIS image I03218002).

Four models have been proposed to explain the formation of central pit craters but here we only focus on the two leading models. Central peak collapse involves the inability of weak target materials to retain a central peak and thus the peak collapses to form a pit [2, 6]. The melt drainage model proposes that temperatures reached under the center of the transient cavity create a liquid "plug" which later drains away through subsurface fractures to leave a pit [6-8]. We are conducting a detailed study of central pit craters on Mars in an effort to better understand the conditions leading to the formation of these structures both on Mars and elsewhere in the solar system. Here we report on results for central pit craters in the northern hemisphere of Mars.

Central Pit Characteristics: The revised *Catalog of Large Martian Impact Craters* [9] lists 14,239 impact craters in the Martian northern hemisphere and includes 566 floor pit craters and 333 summit pit craters. Thus ~6% of all impact craters in the northern hemisphere of Mars are classified as central pit craters. Floor pit craters range in diameter from the lower-diameter cut-off of the *Catalog* at 5 km to 114.0 km. The pits range in diameter from 0.3 km to 17.8 km with a median of 2.4 km. The ratio of the pit diameter (D_p) to the crater diameter (D_c) ranges from 0.02 to 0.48 with a median of 0.15. Summit pit craters range in diameter from 5.5 to 125.4 km and their pits range from 0.3 to 13.9 km in diameter (median 1.9 km). Summit pit D_p/D_c ranges from 0.03 to 0.29 with a median of 0.12. Thus although summit pits are seen in craters of similar size and within a similar latitude range as floor pits, summit pits tend to be smaller relative to their parent crater than floor pits.

Floor pits sometimes display a raised rim along the edge of the pit while other times a rim is absent. We are currently dividing floor pits into three categories (rimmed (R), partially rimmed (PR), and non-rimmed (NR)) for a more detailed analysis of differences between these subclasses. A preliminary analysis [10] suggests that the difference between R, PR, and NR floor pits is a function of pit diameter and terrain.

Implications for Formation Models: The presence of floor pits, summit pits, and central peak craters in the same geographic regions on Mars suggests that pit formation is not simply the result of a transition to material too weak to support a central peak. Melt drainage model predictions are consistent with D_p/D_c ratios and the presence of central pits in craters of only a certain diameter range, and are in the direction expected as target volatile content changes (i.e., larger D_c and D_p/D_c for higher ice concentrations [8]). Although the original description of the melt drainage model for lunar central pit craters suggested weaker core material which did not require volatiles [7], recent numerical modeling finds that this mechanism does not work for silicate melts [11]. A detailed comparison study of central pits on volatile-richer bodies and volatile-poorer bodies is needed to determine whether the same formation mechanism can be applied everywhere.

Acknowledgements: This research is supported by NASA MDAP Awards NNX08AL11G and NNX12AJ31G.

References: [1] Wood C.A. et al. (1978) *PLPSC 9*, 3691-3709. [2] Passey Q.R. and Shoemaker E.M. (1982) *Satellites of Jupiter*, UAz Press, 379-434. [3] Allen C. C. (1975) *Moon, 12*, 463-474. [4] Xiao Z. and Komatsu G. (2013) *Planet. Space Sci.* in press. [5] Xiao Z. et al. (2013), submitted. [6] Bray V.J. et al. (2012) *Icarus, 217*, 115-129. [7] Croft S.M. (1981) *LPS XII*, 196-198. [8] Senft L.E. and Stewart S.T. (2011) *Icarus, 214*, 67-81. [9] Barlow N.G. (2006) *LPS XXXVII*, Abstract #1337. [10] Garner K.M.L. and Barlow N.G. (2012) *LPS XLII*, Abstract #1256. [11] Elder C.M. et al. (2012) *Icarus, 221*, 831-843.

THE ROLE OF BASE SURGE IN THE FORMATION OF MARTIAN LOW-ASPECT-RATIO LAYERED EJECTA (LARLE) CRATERS. N. G. Barlow[1], J. M. Boyce[2], and L. Wilson[3]. [1]Dept. Physics and Astronomy, Northern Arizona Univ., Flagstaff, AZ USA 86011-6010 (Nadine.Barlow@nau.edu). [2]HIGP, Univ. Hawaii, Honolulu, HI 96822 USA (jboyce@higp.hawaii.edu). [3]Lancaster Environment Centre, Lancaster Univ., Lancaster LA1 4YQ, UK (l.wilson@lancaster.ac.uk).

Introduction: Low-Aspect-Ratio Layered Ejecta (LARLE) craters are an unusual feature characterized by a thin but radially extensive deposit surrounding some Martian impact craters. LARLE craters are typically fresh enough to be surrounded by a normal layered ejecta morphology in addition to the extensive outer deposit (henceforth called the LARLE layer) (Fig. 1). LARLE deposits are characterized by extending much further than a normal layered ejecta blanket (up to ~20 crater radii (R_c)) but being extremely thin (typically less than 10 m). We propose that LARLE layers are primarily base surge deposits, like those developed in near-surface nuclear and high-explosion crater experiments conducted on land [1-4].

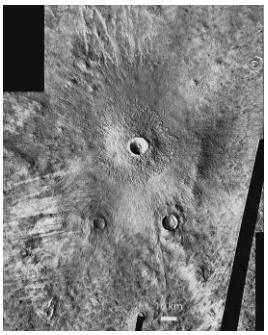

Figure 1. 10.3-km-diameter Lonar crater (72.99°N 38.30°E) is one of the largest and youngest LARLE craters.

Characteristics of LARLE Craters: We have conducted a survey to identify all Martian LARLE craters ≥1-km-diameter in the ±75° latitude zone [5]. Our survey reveals 139 craters which satisfy the LARLE criteria of maximum deposit extent of ≥6.0 R_c, sinuous "flame-like" terminus, and inability to be classified as any other Martian ejecta morphology [6]. LARLE craters range in diameter from the cut-off limit of 1.0 km to 12.2 km, with a median of 2.8 km. Most (97%) are found poleward of 35°N and 40°S, with the remainder concentrated in the equatorial Medusae Fossae Formation deposits. All LARLE craters form in regions covered by relatively thick fine-grained mantles. The average radius of the LARLE deposit (R_d) shows a linear relationship with R_c and the median R_d is 7.44R_c. The outer perimeter of the LARLE deposit has a sinuosity about twice as high as normal layered ejecta deposits. The surfaces of the freshest LARLE layers commonly exhibit radial, curvilinear ridges and dune-like landforms and a few fresh LARLE craters exhibit long, narrow, ray-like deposits of ejecta that extend outward for over 20 R_c. The LARLE deposit typically drapes over pre-existing terrain.

Formation of LARLE Craters: The thinness, large radial extent, sinuous perimeter, and morphologic characteristics of the LARLE deposit indicate that this layer is deposited in a different manner from the normal Martian layered ejecta blankets. We propose that impact into the relatively-thick fine-grained mantles results in production of a base surge that is deposited after formation of the inner layered ejecta blankets. This base surge is similar to the density-driven, turbulent cloud of suspended fine-grained particles produced by impact erosion and mobilization of the surrounding surface material by ejecta from shallow-depth-of-burst nuclear and high-explosion craters (Fig. 2). We have used the model of [7, 8], adjusted to Martian conditions, to predict the runout distances of a base surge deposit for two LARLE craters (10.3 km Lonar and 4.2 km Farim) and find the predicted runout distances are within 99% of the observed values [9, 10]. We suggest that while nearly all Martian impact craters should produce base surges, the reason for the production of the obvious LARLE layers is due to their formation in relatively thick fine-grained sedimentary deposits which are the source of the extra particulate debris.

Figure 2. Image of the Sedan nuclear explosion. Note the secondary impacts producing the base surge cloud along the surface.

References: [1] Nordyke M. and Wry, G., (1964), *JGR, 69*, 675-689. [2] Nordyke M. and Williamson M. (1965) *PNE-242F*, 103 pp. [3] Oberbeck (1975) Rev. Geophys. Space Phy., 13, 337-362. [4] Knauth et al. (2005) *Nature, 20*, 1123-1128. [5] Barlow N. G. and Boyce J. M. (2013) LPS XLIV, Abstract #1196. [6] Barlow N.G. et al. (2000) JGR, 105, 26733-26738. [7] Dade W. and Huppert H. (1995) *Nature, 381*, 509-510. [8] Dade W. (2003) *JGR, 108*, B4, 2211. [9] Boyce J.M. et al. (2012) LPS XLIII, Abstract #1081. [10] Boyce J.M. et al. (2013) *LPS XLIV*, Abstract #1004.

SiO_2/Al_2O_3 VARIATIONS AND CROSS-CUTTING RELATIONSHIPS IN THE SUDBURY IGNEOUS COMPLEX: EVIDENCE FOR MIXING OF MULTIPLE ENDOGENIC MAGMAS. A. E. Beswick, Center for Excellence in Mining Innovation, Laurentian University, 933 Ramsey Lake Road, Sudbury, Ontario, P3E 2C6, Canada. tonybeswick@sympatico.ca

Abstract: The genesis of the Sudbury Igneous Complex (SIC) has been controversial for most of the past century. Historically, debate focused on whether or not the norites and the more voluminous granophyres originated by fractionation of a single parent magma [1], [2], [3], [4], [5] and more recently on whether that magma was a meteorite impact melt sheet [6], [7], [8].

Major support for the impact melt sheet hypothesis was afforded by Therriault et al., [9] who purported to show that, on a diagram of Al_2O_3/Zr versus SiO_2/Zr, all rocks from across the North and South Ranges of the SIC fell along a single fractionation trend, interpreted as evidence for their co-magmatic origin.

This communication examines SiO_2:Al_2O_3 variations across the North and South Ranges of the SIC and, using simple component ratio diagrams such as Al_2O_3/Zr versus SiO_2/Zr, demonstrates that Therriault et al., [9] misinterpreted their data. Logarithmic scaled versions of these diagrams indicate that granophyres and norites lie along distinctly separate fractionation trends and that the transitional quartz gabbros lie along hybridization lines between them.

Similar examinations of Sublayer, Offest dikes, and 'melt rocks' in the Onaping Formation, suggest that many of these rocks are also of hybrid origin.

It is further noted that the granophyre compositions cluster around the minimum melting composition in the experimental system Quartz-Albite-Orthoclase [10] at water vapor pressures < 2 Kbars suggesting that they represent endogenic partial melts of the continental crust.

Additionally, a number of researchers have described cross-cutting relationships within the SIC, in the Upper Zone [11], the Middle Zone [5], and the Lower Zone [12], [13], [14], and based on high precision U-Pb age dating it has been claimed that the South Range norite is 400,000 yrs younger than the felsic norite on the North Range [15].

Finally, it should be noted that computer modeling attempts [16], [17] have proved incapable of matching the compositional profiles for either the North or South Ranges of the SIC or of explaining their differences, despite claims to the contrary [17].

Taken together with the SiO_2:Al_2O_3 variations presented above, these observations represent overwhelming and irrefutable evidence that multiple endogenic magmas and hybridization were involved in the genesis of the SIC and that it was not produced by differentiation of a single parent magma whether endogenic or exogenic in origin.

References: [1] Coleman A. P. (1913) Canada Dept. Mines, Mines Branch 170, 206 pp. [2] Harker A. (1916) J. Geol. 24, 554-558. [3] Bain G. W. (1925) J. Geol. 33, 509-525. [4] Bowen N. L (1925) J. Geol. 33, 825-829. [5] Phemister T. C. (1925) J. Geol. 33, 819-824. [6] Golightly J. P. (1994) Ont. Geol. Surv. Spec. Vol. 5, 105-118**.** [7] Grieve R. A. F. (1994) Ont. Geol. Surv. Spec. Vol. 5, 245-270. [8] Norman M. D. (1994) Geol. Soc. Amer. Spec. Paper 293, 331-341. [9] Therriault et al. (1996) Meteoritical Soc. Suppl. 32, A141-142. [10] Tuttle O.F. and Bowen N. L. (1958) Geol. Soc. Amer. Mem. 74. [11] Perederey W. V. (1972) Ph.D. Thesis, U. of Toronto. [12] Coats C. J. A. and Snajdr P. (1984) Ont. Geol. Surv. Spec. Vol. 1, 327-346. [13] Davis G. (1984) Ont. Geol. Surv. Spec. Vol. 1, 361-370. [14] Clayton-Capes P. (2001) M.Sc. Thesis, U. of Toronto. [15] Davis D. W. (2008) Geology 36, 5, 383-386. [16] Ariskin A. A. et al. (1999) Geol. Soc. Amer. Spec. Paper 339, 373-388. [17] Lavrenchuk A. et al. (2010) 11th International Planitum Symposium, Abstract.

AFFECT OF CORE RHEOLOGY ON SHOCK WAVE PROPAGATION IN PLANETARY SCALE IMPACTS. M. Bierhaus[1], K. Wünnemann[1], B. A. Ivanov[2], [1]Museum für Naturkunde Leibniz-Institut für Evolutions- und Biodiversitätsforschung, Invalidenstr. 43, 10115 Berlin Germany (Michael.Bierhaus@mfn-berlin.de) [2]Institute for Dynamics of Geospheres, RAS, 119334 Moscow, Russia

Introduction: Large impacts forming basin-sized structures on planetary surfaces generate shock waves that may be strong enough to deliver a significant amount of heat to the planetary interior. Planets and moons as well as large asteroids such as Vesta or Lutetia are thought to be differentiated into a silicate mantle and an iron core. How the heat budget of the interior of these bodies was affected by impact processes may depend on the thermodynamic state and, thus, the internal rheology during their thermal evolution.

We conduct a suite of iSALE [1-3] hydrocode models of large impacts on planetary-size target to investigate the effect of the thermal conditions and rheology of the target on the propagation of shock waves. In particular we focus on the effect of a liquid or solidified core on shock wave decay.

Shock decay in a planetary core: Figure 1 shows the shock decay in the target body after an impact of a 184 km-radius dunitic projectile at 10 km/s. The target planet has a radius of 3450 km and consists of a dunitic mantle and an iron core with a radius of 1725 km. Comparing the three different cases there are almost no differences in the shock pressure decay in the mantle up to a depth of 0.5 target planet radii which corresponds to the depth of the core mantle boundary (CMB) in the given model. Small deviations between the three different cases are due to small differences of the thermal gradients in the mantle. Below the CMB the three cases show significant differences. If an iron core is present (green and blue) there is a kink in the pressure decay caused by the impedance contrast between the core and the mantle. Inside the core the shock pressure decays much faster in case of the solid core (green) that has some strength Y in comparison to the liquid core (blue) that behaves hydrodynamically with no mechanical resistance against deformation. In the latter case the shock pressure is up to 3 times higher than for the solid core.

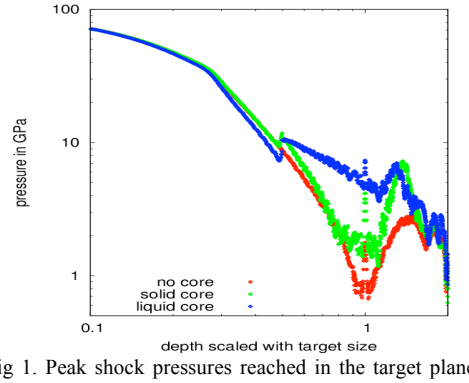

Fig 1. Peak shock pressures reached in the target planet, measured along the symmetry axis. Impactor radius of 184 km and velocity of 10 km/s. The target is a spherical dunitic body with a radius of 3450 km with no core (red), a solid core (green) and a liquid core (blue).

Planar impact models: To investigate the principle reason for the effect of strength on pressure decay we conducted planar shock wave propagation models assuming the rheology of liquid (strengthless) and solid (strength) material. For simplicity we use a constant strength of Y=1 GPa and neglect thermal softening or the dependency of strength on confining pressure and the deformation history (damage). The results (fig. 2) confirm that the shock pressure decays faster in the case with strength compared to the hydrodynamic case (strengthless). In our models the hydrodynamic material is unloaded to zero pressure while the material with strength maintains a pressure of the order of the given strength of 1 GPa. Complete unloading takes place at some later time. The incomplete unloading after shock wave release results in a slightly increased density and speed of sound of the material giving rise to a faster propagation of the rarefaction wave and, thus, faster attenuation of the shock wave.

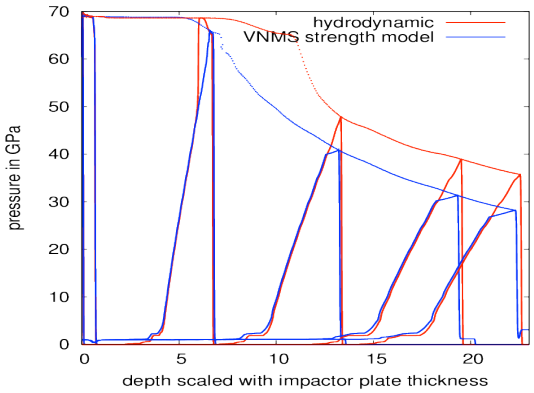

Fig 2. Shape of the shock wave in a planar impact model with an impact velocity of 5 km/s at different times. The dotted lines represent the peak pressure for each time step.

Conclusion: The rheology of the target body significantly affects the propagation and decay of a shock wave. If the target material has some strength the shock wave decays more rapidly than in the hydrodynamic case where no strength is present. This holds true even if the material is significantly weakend due to the accumulation of damage and its rheology is more like the one of granular matter. Consequently, a completely solidified iron core experiences significantly lower shock pressures than a liquid core after impact of an equally sized body.

Acknowledgements: We thank B.A: Ivanov and H.J. Melosh for contributing to the development of iSALE. This work was funded by Helmholtz-Alliance "Planetary Evolution and Life"(WP3200).

References: [1]Amsden A.A. et al. *Los Alamos National Laboratories Report*, LA-8095:101p, (1980). [2] Ivanov B.A. et al., (1997), *Int. J. Impact Eng.* 17, 375–386. [3]Wünnemann K. et. al. (2006), *Icarus*180

(U-Th)/He ZIRCON DATING OF THE CLEARWATER WEST IMPACT STRUCTURE, QUEBEC, CANADA. M.B. Biren[1], M.C. van Soest[1], J-A.Wartho[1], K.V. Hodges[1], M.R. Dence[2] and J.G. Spray[3]. [1]Noble Gas Geochemistry and Geochronology Laboratories, SESE, ASU, PO Box 876004, Tempe, AZ 85287, USA. Contact: marc.biren@asu.edu. [2]Suite 2602, 38 Metropole Private, Ottawa, Ontario, K1Z 1E9, Canada. [3]Planetary and Space Science Centre, University of New Brunswick, 2 Bailey Drive, Fredericton, New Brunswick E3B 5A3, Canada.

Introduction: The ~36 km diameter Clearwater West impact structure, along with its smaller twin (the ~26 km Clearwater East impact structure), forms one of the few known impact doublets on Earth. This study dates zircons from the impact melt sheet at Clearwater West using the (U-Th)/He technique, to compare with the impact ages from previous studies, to further our (U-Th)/He dating studies of terrestrial impact structures [e.g. 1, 2].

Geologic Background: The Clearwater West and Clearwater East structures located in Quebec, Canada (ca. 56°5'N; 74°7'W) were first linked to probable meteorite impacts by Dence et al. in 1965 [3]. An impact origin was later confirmed by way of petrographic, geochemical and structural evidence [4, 5, 6].

The target basement rocks associated with both structures are predominantly Precambrian granite gneisses, granodiorite, and quartz monzonite with lesser occurrences of more mafic rocks (i.e., granulite and metagabbro). Metamorphic grade varies from amphibolite to granulite facies in the basement rocks, and blocks of Ordovician limestone are all that remain of the sedimentary cover that once existed prior to impact [7].

Previous Age Estimates: Clearwater West has been previously dated with a variety of techniques. K-Ar and Rb-Sr methods yielded ages of 285 ± 30, 300 ± 30 and 266 ± 15 Ma [8, 7 and references therein]. Fission track dating of a melt glass yielded an age of ca. 34 Ma [9]. Initial $^{40}Ar/^{39}Ar$ dating of clast-bearing impact melt produced a partially reset age of 445 ± 2 Ma [10]. More recently, Buchner et al. applied the $^{40}Ar/^{39}Ar$ method to optically fresh samples of impact melt rock (drill core chips) to obtain a refined impact age of 283.9 ± 1.2 Ma (2σ, combined weighted mean age from 2 concordant samples; [11]).

Samples, Analytical Procedure, and Results: A ~2.5 kg sample of dark red fine-grained clast-bearing impact melt was originally retrieved from the ring of central islands at Clearwater West during the mid-to-late 1970's [4, 5]. For this (U-Th)/He dating study, the sample was crushed and a heavy mineral concentrate was prepared using standard magnetic and heavy liquid methods. A Leica MZ16 binocular microscope was used to select and accurately measure the dimensions of 10 mostly euhedral zircon grains, ranging in average width from ~55 to 117 µm respectively.

An ASI Alphachron helium extraction system was used to measure ^{4}He concentrations released from each grain by infra-red diode laser heating. U and Th concentrations were subsequently measured on a Thermo iCap Q inductively-coupled-plasma mass-spectrometer following zircon dissolution. Detailed analytical procedures are described in [1].

(U-Th)/He ages were calculated with an iterative process using blank corrected ^{4}He, ^{232}Th, and ^{238}U values (while using the natural abundance to account for ^{235}U). The ages were corrected for alpha-ejection [12], which is the loss of a fraction of the ^{4}He nuclei that are produced from their parent nuclei within the average stopping distance (~18 µm for zircon) from the edge of the crystal and results in anomalously young ages if not corrected for. The resulting corrected (U-Th)/He ages ranged from 156.3 ± 6.8 to 323.8 ± 9.5 Ma (2σ).

Discussion and conclusions: 3 of the (U-Th)/He ages have been interpreted as outliers (i.e., 156.3 ± 6.8; 233.5 ± 6.1; and 323.8 ± 9.5 Ma) and omitted from calculations of the mean impact ages. The remaining 7 ages give an unweighted mean of 284 ± 29 Ma (2σ), and a weighted mean age of 280 ± 12 Ma (95% confidence, MSWD=11.4) using Isoplot v. 3.71 [13]. These new ages clearly overlap with the most recent $^{40}Ar/^{39}Ar$ impact age of 283.9 ± 1.2 Ma [11] and provide us with continued confidence in using the (U-Th)/He technique for dating terrestrial impact structures.

References: [1] van Soest M. C. et al. (2011) *Geochem. Geophys. Geosys.* 12, 1-8. [2] Wartho J-A. et al. (2012) *Meteorit. & Planet. Sci.* 47, 1243-1255. [3] Dence, M. R. (1964) *Meteoritics* 2, 249–270. [4] Phinney, W.C. et al. (1978) *LPSC IX*, 2659–2694. [5] Simonds, C.H. et al. (1978) *LPSC IX*, 2633–2693. [6] Grieve, R.a.F., (1978) *Geochim. Cosmochim. Acta* 42, 429–431. [7] Reimold, W. U., et al. (1981) *Contr. Min. Petr.* 76, 73–76. [8] Wanless, R. K., et al. (1966) *Geol. Surv. Can. Paper* 17, 77-78. [9] Fleischer, R. L. et al. (1969) *Geochim. Cosmochim. Acta* 33, 523–527. [10] Bottomley, R.J. et al. (1990) *LPSC XX*, 421–431. [11] Buchner, E. et al. (2013) *76th MetSoc, Edmonton, Canada* (submitted abstract). [12] Farley, K. A., et al. (1996) *Geochim. Cosmochim. Acta* 60, 4223-4229. [13] Ludwig K. R., (2008) *BGC Spec. Pub.* 4.

GRAVITY ANOMALIES OF THE LUNAR ORIENTALE BASIN AND THE MERCURIAN CALORIS BASIN. D. M. Blair[1,*], B. C. Johnson[1], A. M. Freed[1], and H. J. Melosh[1]; [1]Department of Earth, Atmospheric, and Planetary Sciences, Purdue University, *dblair@purdue.edu.

Introduction: Gravitational anomalies of large impact basins [e.g. 1] expose structure deep inside of a planetary body, and provide a window to its past. Recent work [2] has shown that these anomalies form via a combination of syn- and post-impact processes, but this work focuses on just two basins, both on the Moon and both having an annulus of negative Bouguer gravity anomaly ~ 400 km in diameter (D_{masdef}). How might gravity anomaly formation differ for a larger impact, with a larger melt pool and non-negligible surface curvature, or an impact into a body other than the Moon?

Here we attempt to model the formation and evolution of the lunar Orientale (D_{masdef} ~ 600 km) and mercurian Caloris (D_{masdef} > 1000 km) basins to explore how gravity anomaly patterns form following very large bolide impacts. Our goal is to match the basins' observed free-air and Bouguer gravity anomalies, as well as their final topographies.

Methods: Our modeling effort occurs in two stages, allowing us to create a self-consistent representation of a basin's formation and evolution. First, we simulate bolide impact using the iSALE hydrocode, with the goal being to reproduce a basin where the annulus of thickened crust matches that suggested by gravity measurements. This model treats impactor kinetic energy, pre-impact crustal thickness, and subsurface thermal gradient as free parameters, and models the first few hours after impact. We then take the output state of the hydrocode model—its geometry, temperature, and density structure—and use that as the basis for a finite element model (FEM) using the Abaqus software suite [e.g. 2, 3], which simulates the basin's linked thermal and viscoelastic evolution over subsequent geologic time.

At the Moon, our models are constrained by gravity observations from NASA's dual GRAIL spacecraft [4] and topography from LRO/LOLA data [5]. At Mercury, the MESSENGER spacecraft provides both gravity [6] and topography [7, 8].

Results: Modeling is ongoing for both basins; in this abstract, we show preliminary results for Orientale (Fig. 1). Current models accurately predict the basin's present-day topography while slightly under-predicting both free-air and Bouguer gravity anomalies at the basin center. These models do not yet include mare basalt, however, which could alter our results; the presence of several major faults in Orientale could also explain some portion of the misfit.

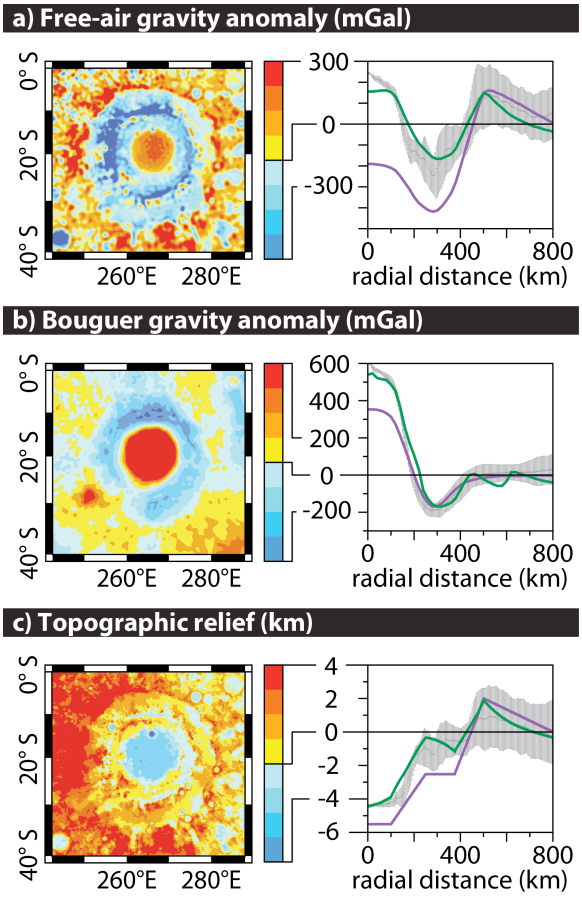

Figure 1: Observations and current model results for Orientale basin, showing a) free-air and, b) Bouguer gravity anomaly, and c) topographic relief. Purple lines represent the model results at the end of the hydrocode simulation, and green lines show results from after finite element simulations. Gray lines with error bars represent azimuthally-averaged data from [7] (a & b) and [8] (c), with topography observations uniformly shifted to match our model result of 0 km elevation at 800 km radius.

Acknowledgements: We gratefully acknowledge the developers of iSALE, including Gareth Collins, Kai Wünnemann, Boris Ivanov, Jay Melosh, and Dirk Elbeshausen.

References: [1] Muller, P. M., and Sjogren, W. L. (1968) *Science* 161, 680. [2] Melosh, H. J. et al. (2013) *Science*, in press. [3] Blair, D. M. et al. (2013) *JGR-Planets* 118, 47. [4] Zuber, M. T. et al. (2013) *Science* 339, 668. [5] Neumann, G.A. (2010), NASA PDS. [6] Smith, D. E. et al. (2012) *Science* 336, 214. [7] Zuber, M. T. et al. (2012) *Science* 336, 217. [8] Preusker, F. et al. (2011) *Planet. & Space Sci.* 59, 1910.

NEW FIELD OBSERVATIONS AND U-PB AGE DATA FOR FOOTWALL (TARGET) ROCKS AT SUDBURY: TOWARDS A DETAILED CROSS-SECTION THROUGH THE SUDBURY STRUCTURE.

Wouter Bleeker[1], Sandra Kamo[2], and Doreen Ames[1], [1]Geological Survey of Canada, 601 Booth Street, Ottawa, Canada, wbleeker@nrcan.gc.ca, [2]Jack Satterly Geochronology Laboratory, University of Toronto

Introduction: Despite much progress in the understanding of the 1850 Ma Sudbury impact structure, numerous questions on the evolution of this structure, its igneous complex and fill, its target rocks and their deformation history persist. A more detailed understanding of the polyphase deformational history of the Sudbury area would help constrain the "unfolding" of the structure. As preserved today, the Sudbury structure and its igneous complex (SIC) merely represent a down-folded (and faulted) erosional remnant of an initially much larger structure, with a centre and original extent that can only be speculated upon. A detailed cross-section across the deformed erosional remnant, incorporating all field observations, would help inform the overall interpretation. Obtaining precise ages on some of the target rocks has proven difficult due to most zircons having seen substantial Pb loss at multiple times, notably at 1850 Ma or shortly thereafter (during or after the impact event and associated shock metamorphism), but also at other times (e.g., multiple Proterozoic events). Discordance patterns are further complicated by variable degrees of recent Pb loss, making upper intercept age interpretations uncertain and non-unique. The only definitive answer on some of the key ages will come from more concordant data. The ability to analyse smaller and smaller single grain fragments, and to pre-treat these with "chemical abrasion", may finally resolve some of the key ages.

Creighton Granite: One major rock unit in target area (along the South Range) that has not been precisely dated is the "Creighton Granite". Field evidence suggests that this intrusion may be a shallow subvolcanic granodiorite sill that was the magma chamber for the Copper Cliff Rhyolite Formation, a multi-facies rhyolite and volcaniclastic formation further south within the folded Huronian stratigraphy. It is likely that the Creighton granodiorite, some smaller porphyry bodies higher in the stratigraphy, and the Copper Cliff Rhyolite form a single magmatic system, compositionally distinct from the Murray Granite. The overall map pattern of the Creighton granodiorite, as well as reversals in younging directions in lower Huronian strata near its inferred base, indicate that the Creighton intrusion is a sill-like body that was tightly folded in a fold-thrust belt that predates the Sudbury impact and the cross-cutting basal contact of the SIC. Mafic rocks along the northern contact of the granodiorite sill are not "inclusions" but more likely simply represent the hot base of the folded sill. Along its base, the granodiorite sill intruded into plagioclase megacrystic gabbro sills of the Matachewan event, with evidence for magma hybridization, thus indicating that felsic magmatism immediately followed a major pulse of the Matachewan event. Although Matachewan dykes are numerous north of Sudbury, we know of no Matachewan dykes that cut the Creighton granodiorite sill or Copper Cliff Rhyolite.

Preliminary U-Pb results: So far we have preliminary data on six samples that help constrain relationships both along the North Range and the South Range. All zircon analyses were on small, most translucent fragments of single zircon grains, and all were treated by chemical abrasion. A brief summary of results follows:

Joe Lake (meta)gabbro, North Range. Field observations suggest this body was penetratively deformed as part of the Levack gneiss basement complex. Three initial zircons, probably metamorphic in origin, indicate a minimum age of 2657±9 Ma, corroborating our field observations for a late Archean origin.

Cross-cutting pegmatite dyke, North Range. Undeformed, shallowly dipping, granitic pegmatites cut through the deformed Joe Lake metagabbro. Initial analyses indicate an upper intercept age of ca. 2660 Ma, in agreement with the field relationships.

Murray Granite, South Range. Although our least discordant result, indicating a minimum crystallization age to 2429±2 Ma, is less discordant than previous data in the literature, substantial uncertainty remains on the crystallization age of this granite body. Our data are consistent with those of Krogh et al. (1996), suggesting crystallization at 2477±9 Ma.

Creighton Granite, South Range. Our data indicate a minimum crystallization age of 2437±2 Ma, thus eliminating any possible suggestions of a much younger age (e.g., see thesis by Smith, 2002).

Copper Cliff Rhyolite, South Range. Again our initial results are more concordant than any previous data, indicating a minimum crystallization age of 2455±3 Ma. The data are compatible with the Creighton Granite and Copper Cliff forming a single magmatic system. Regressing the best data from both the Creighton and Copper Cliff together yields an upper intercept age of 2465±15 Ma. A tentative age of ca. 2455-2460 Ma would be in agreement with all analytical data and field relationships and would mark the end of the magmatic phase of the Huronian rift in the area.

PB-PB CHRONOMETRY OF THE DARK MELT LITHOLOGY OF THE CHELYABINSK LL CHONDRITE. A. Bouvier, University of Minnesota, Department of Earth Sciences, Minneapolis, MN 55455, USA (abouvier@umn.edu).

Introduction: On February, 15th 2013, a meteor fireball was witnessed in the Ural region, exploding at an altitude of 25-30 km, and generating a shockwave that injured more than 1,500 people in the city of Chelyabinsk in Russia. On February 19th, scientists of the Vernadsky Institute started recovering meteorites nearby the towns of Deputatsky, Pervomaysky and Emanjelinka, about 40 km south-west of Chelyabinsk. Hundreds of meteorite fragments from <1g to 1.8kg (most of them <20g) were found, often in patches, in the snow. The Chelyabinsk meteorite is an LL5 ordinary chondrite, with shock stage S4 [1]. About a third of the stones consist of a dark, fine-grained impact melt containing mineral and chondrule fragments [1]. This abundant dark melt is of particular interest for understanding impact processes within the asteroid belt and, because of its rapid recovery, is particularly suitable for Pb-Pb chronometry.

Study: A fragment from an individual stone representative of the dark melt lithology (10-134, 3.9g out of 5.9g) was recovered from the patch #10 and donated by the Vernadsky Institute to conduct chemical and isotopic studies at UMN. A ~1g interior piece of the fine grained dark melt lithology (chondrules and clasts were not observed in 10-134) was crushed as a bulk-rock powder. Two fractions of this powder were subsequently acid washed during a 5 to 6 steps leaching protocol (using Aristar Ultra HBr, HCl and HF, and double distilled HNO_3 acids) to progressively dissolve the recrystallized dark melt. Pb extraction and isotopic analysis using Tl-doping method followed similar protocols as described in [2] except that the Pb isotopic analyses were carried out by Neptune Plus MC-ICPMS techniques hooked up to a 50µl/mn ESI nebulizer and Cetac Aridus dessolvator giving together a sensitivity of 1800V/ppm.

Results: The $^{206}Pb/^{204}Pb$ ratios corrected from chemistry blank contribution for the leachates (L) and residues (R) of the two bulk rock samples of the dark melt lithology range from 70 to 81 for L1 to L4, and 142, 420, and 275 (identical for the two whole-rock residues) for L5, L6, and R respectively. Taken together, the Pb isotopic compositions of L5, L6 and R give an isochron Pb-Pb age of 4538.3 ± 2.1 Ma, MSWD = 0.17 (Fig. 1), using the $^{238}U/^{235}U$ ratio of 137.79 which was suggested to be homogeneous among bulk chondrites [3].

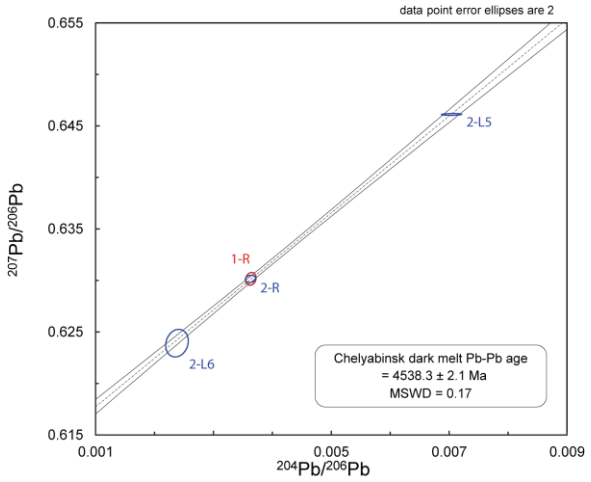

Figure 1: $^{207}Pb/^{206}Pb$ vs. $^{204}Pb/^{206}Pb$ of leachates and residues of the Chelyabinsk dark melt lithology.

Discussion: The Pb-Pb age of the dark melt of Chelyabinsk is ~30 My after the birth of the Solar System [2]. It is significantly older than Ar-Ar ages measured in other shocked LL chondrites (0.2-4.4 Ga) [4], but similar to Pb-Pb ages measured previously in relatively unshocked (S1-S2) type 5 L chondrites [5]. The Pb-Pb dates of L and LL chondrites were interpreted as cooling ages during thermal metamorphism on the respective parent bodies as well as secondary disturbances for L chondrites [5]. The ~4.54 Ga Pb-Pb age of the dark melt indicates that the LL parent body has been affected by at least one major impact event producing abundant shock melt following the main period of accretion of the parent body within the first 10 Ma of Solar System history [5]. The association of the light chondritic lithology with the dark melt brings new insight on the evolution of the LL chondrite parent body. Comparison of Pb-Pb dating with other radiometric methods in both lithologies will bring further constraints on the impact and thermal evolution of the LL parent asteroid [4].

Acknowledgements to M. Nazarov, N. Bezaeva, and the Vernadsky Institute for recovering and generously donating samples of the Chelyabinsk meteorite.

References: [1] Meteoritical Bulletin, MAPS 48, in prep. [2] Bouvier A. & Wadhwa M. 2010. Nature Geosc. 3:637-641 [3] Connelly J. N. et al. 2012. Science 338:651-655 [4] Swindle T. D. et al. 2013. Geological Society, London, v. 378, doi:10.1144/SP378.6 [5] Bouvier A. et al. 2007. GCA 71:1583-1604.

ANTIPODAL TERRAINS CREATED BY THE RHEASILVIA IMPACT ON ASTEROID 4 VESTA T. Bowling[1], B. Johnson[1], H. J. Melosh[1], B. Ivanov[2], D. O'Brien[3], R. Gaskell[3], and S. Marchi[4], [1]Purdue University (tbowling@purdue.edu), [2]Russian Academy of Sciences, [3]Planetary Science Institute, [4]NASA Lunar Science Institute.

Introduction: The Rheasilvia impact on asteroid 4 Vesta was large enough to have disrupted the terrain at the impact antipode in a manner similar to that which produced the hilly and lineated terrains opposite the Caloris basin on Mercury [1]. We utilize the iSALE shock physics hydrocodes [2-4] to simulate the impact event that formed the Rheasilvia basin and determine the amount of deformation expected at the impact antipode. In many of our models the amount of antipodal deformation is larger that the simulation resolution (400 m), and we are able to directly resolve displacements. When the amount of deformation is smaller than the simulation resolution, we rely on peak surface velocity to quantify the amount of deformation expected at the antipode. We test the dependence of antipodal deformation on three parameters: the porosity and sound speed of Vesta's mantle, and the strength of Vesta's iron core.

Results: Porosity plays a critical role in reducing the amount of impact energy that reaches the antipode. As the impact shockwave moves through the mantle, pore space is crushed out and energy is sapped from the wave. In simulations with 0% porosity, the impact antipode is significantly disrupted, to the point that a topographic feature several kilometers in height is formed. The introduction of mantle porosity quickly dampens this deformation. At 5% porosity (the expected value based on Dawn observations) no uplift can be resolved [5].

The strength of Vesta's iron core determines well the impact shockwave is transmitted through to the antipode. When a weak core is used, the core itself deforms considerably, and peak surface velocities at the antipode are small. When a strong core is used, stresses are more easily transmitted, core deformation is diminished, and velocities at the antipode are considerably higher.

As the impact shockwave passes through Vesta, the core acts like a convex lens, focusing stresses to the antipode. The amount of focusing that occurs is dependent on the sound speed difference between the core and the mantle. Raising or lowering the sound speed of the mantle changes the breadth and magnitude of surface velocities near the antipode.

Comparison to Observations: The antipodal point of the Rheasilvia impact lies on the edge of a morphologically fresh 63 kilometer diameter impact crater [6]. Any topographic uplift produced by the Rheasilvia impact would have been largely erased by the formation of the younger crater. The most convincing evidence that deformation did occur at the antipode comes from crater densities. At large crater sizes (D>9 km), densities resemble those of the ancient Vestan terrains that predate the Rheasilvia basin. At small crater sizes (D<3 km), densities resemble those of the Rheasilvia ejecta blanket. This suggests that the Rheasilvia impact induced enough deformation at its antipode to significantly degrade or erase craters several kilometers in diameter.

References: [1] Bowling T. J. et al. (2013) *JGR Planets, accepted*. [2] Wünnemann K. et al. (2006) *Icarus, 180,* 514. [3] Amsden A. et al. (1980) *Los Alamos National Laboratory Report, LA-8095*. [4] Ivanov B. A. et al. (1997) *International Journal of Impact Engineering, 20*, 411. [5] Jaumann R. et al. (2012) *Science, 336,* 687. [6] Blewett, D. T. et al. (2013) *JGR Planets*, *submitted*.

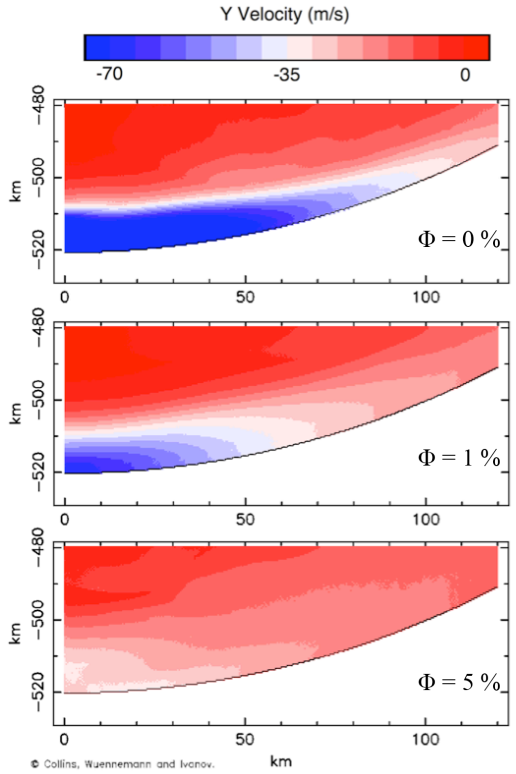

Figure 1: Peak surface velocity at the Rheasilvian antipode following the arrival of the impact shock wave, for mantle porosities of 0%, 1%, and 5%. The impact occurs at the origin.

GEOMORPHIC MAPPING OF THE CALORIS BASIN, MERCURY. D.L. Buczkowski, S. Edrich, S. Ackiss and K.D. Seelos, JHU/APL, Laurel, MD 20723, Debra.Buczkowski@jhuapl.edu.

Introduction: Two Mercury quadrangles based on Mariner 10 data cover the eastern third of the Caloris basin: H-8 Tolstoj [1] and H-3 Shakespeare [2]. This abstract outlines the progress associated with a mapping project of the entire Caloris basin and its associated intra-ejecta plains (Fig. 1), intended to improve our knowledge of the geology and geologic history of the basin, and thus facilitate an understanding of the thermal evolution of this region of Mercury.

Previous Caloris basin mapping: The dark annulus identified in MESSENGER data corresponds well to the mapped location of certain formations [3], primarily the Odin Formation. The Odin Formation is described in the quadrangle maps as a unit of low, closely spaced knobs separated by a smooth, plains-like material and was interpreted as ejecta from the Caloris impact. [1] observed that the intra-ejecta plains in the Odin Formation resemble the Smooth Plains unit that was also prevalent in the H-8 and H-3 quadrangles outside of Caloris. They state that these plains were included as part of the Odin Formation for mapping convenience, not because they necessarily shared the same formation mechanism.

A detailed analysis of the Odin Formation performed by [5] noted that the unit is easily recognizable circum-Caloris in the MESSENGER data and concluded that the Odin Formation knobs are Caloris ejecta blocks that have been mostly embayed and buried by younger volcanic deposits. They found that MDIS color data supported this hypothesis and divided the formation into two sub-units: knobby plains and smooth plains. However, recent work by [6] suggests that there is still no definitive proof that the Odin-style plains have either an impact or volcanic origin.

High-resolution mapping of the intra-ejecta dark plains: We use high resolution imaging data from the MDIS instrument to create our geomorphic map of the Caloris basin. We utilize a principle component map [3] to distinguish subtle differences in the color data. In the principle component map green represents the second principle component (PC2), which reflects variations between light and dark materials. Meanwhile, red is the inverted PC2 and blue is the ratio of normalized reflectance at 480/1000 nm, which highlights fresh ejecta.

We map all contacts between bright and dark materials within the intra-ejecta plains, as determined in the principle component map, as sub-units of the Odin Formation. All knobs are mapped individually and their color (either dark or bright) is noted. Ejecta blankets from local craters (both extent and color) are mapped separately.

The crater classification used in the H-3 and H-8 quadrangles [1,2] and formalized in 1981 [7] was based on degree of crater degradation. Our classification scheme includes both degradation state and level and type of infilling. Current classifications include: 1) blue and pristine, 2) fresh but not blue, 3) intact rim and superposed, 4) intact rim and embayed, 5) degraded rim and superposed, 6) degraded rim and embayed, 7) very degraded and superposed, 8) very degraded and embayed and 9) little to no rim.

Observations: The Odin Formation shows two distinct sub-units: a dark sub-unit and a (relatively) bright sub-unit. The dark sub-unit has a higher concentration of knobs, knobs that are both bright and dark and craters that are both embayed and superposed. Meanwhile, the bright sub-unit has a lower concentration of knobs, knobs that are predominantly bright and craters that are fresh and/or superposed. Outcrops of the bright material can be associated with crater ejecta blankets, but are not always.

References: [1] Schaber and McCauley (1980) USGS Map I-1199 [2] Guest and Greeley (1983) USGS Map I-1408 [3] Murchie et al (2008) *Science 321*, 73-76 [5] Fasset et al (2009) *Earth Planet. Sci Lett 285*, 297-308 [6] Denevi et al (2013) *JGR* doi:10.1002/ jgre.20075 [7] McCauley et al (1981) *Icarus 47*, 184-202

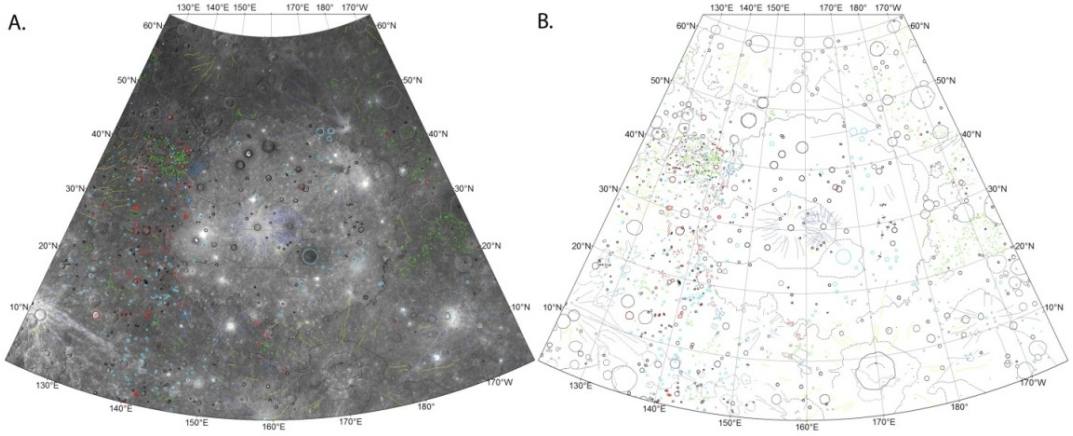

Figure 1. Geomorphic map of the Caloris basin, over the MESSENGER mosaic (A) and with no background image (B).

Searching for a giant impact structure in the Flin Flon ï Snow Lake area, Manitoba

E. Buhlmann, UCN Northern Manitoba Mining Academy

A 140 x 100 km ellipsoidal area centered on Elbow Lake, 65 km northeast of Flin Flon, Manitoba, comprises the Flin Flon ï Snow Lake VMS mining district including 29 past and currently producing mines. The deposits are arranged in two major clusters near Flin Flon and Snow Lake and two smaller óclustersô near Sherridon and Reed Lake.

The district is unique by reason of its mineral wealth in tonnage and grade of the copper ï zinc ï gold ores (past production and present resources 200 million tonnes). An ore-generating natural process would have had to process close to 300 tonnes of country rock with an average crustal copper abundance of 70 g/tonne to produce one tonne of ore. The gigantic amounts of focused energy to accomplish this can readily be supplied by an impact event, singular or clustered. To identify such an event would be a very challenging task because the impact would have been in offshore volcanic terrain. Up to the present no such events have been identified. But there are indirect pointers that leave much room for an impact event in the district. A specific volcanic rock type like icelandite tends to be spatially associated with VMS deposits. It is not clear if the icelandite formed in upper crustal magma chambers or from an impact melt.

A reconnaissance of numerous locations east and northeast of Flin Flon, around Sherridon and Elbow Lake was carried out. At Elbow Lake a circular area was defined on topographic maps and aerial photographs. It has a diameter of 3.8 km and encompasses the main Elbow shear zone under Elbow Lake. A microbreccia of granodioritic rock on Elbow Lake shows granophyric quartz feldspar intergrowth and a microbreccia sample returned a 2.5 ppb iridium anomaly. Near Flin Flon, several gabbroic breccias show a possible melt rock matrix. Hematization is common along the Missi/Amisk contact. Injections of melt or microbreccia into volcanic sediments were observed in at least two areas. Numerous volcanic sediments show intense striations, reminiscent of shatter cones but not definite enough.

The Flin Flon ï Sherridon ï Snow Lake ï Reed Lake area is well suited to show if and how normal volcanic processes can be separated from impact related processes. It can show if the immense energy of a major impact can result in ore-forming processes, how such processes work and how impact related ore bodies can be located.

E. Bu

COMPARISION OF DIELECTRIC CONSTANT OF APOLLO 17 SAMPLES WITH MINI-RF & TALS.

OPN Calla[1],Shubhra Mathur[1,2] and Monika Jangid[1,3] ,[1] International Center for Radio Science, Ranoji Ka Baag, Nayapura, Mandore, Jodhpur Rajasthan India [1]opnc06@gmail.com; [2]shubhra.icrs@gmail.com; [3]monika.jangid.icrs@gmail.com

Introduction: NASA's Lunar Reconnaissance Orbiter (LRO) has returned its first RADAR (Mini-RF) imagery of the Apollo moon landing sites. In this paper the Dielectric Constant of Apollo 17 samples [1] have been calculated using SAR data with suitable model and these results are compared with the DC of the re-tuned Apollo 17 samples and the Terristrial Analogue of Lunar Soil (TALS) [2] to check the applicability of DC model over lunar surface.

Electrical parameter: Microwaves can be used for measurement of dielectric constant in laboratory which can be further used to estimate emmisivity. Natural surfaces emit radiations in the microwave region of the EM spectrum as a function of their material properties and surface roughness. DC is one of the important electrical parameter of the lunar surface and provides basic data necessary for further exploration. Here Campbell inversion model [3] is used for estimating dielectric constant from the vertical and horizontal backscattering coefficient given by Mini-RF (LH and LV hybrid polarized backscattered data). This model works for rock-poor dust surface and when radar measurements are made in linear horizontal and vertical polarizations.

$$\varepsilon_{\min} = \left(\sin\varphi \Big/ \sin\left[\cos^{-1}\left(\frac{\sigma^0_{HH}}{\sigma^0_{VV}} \right)^{0.25} - \varphi \right] \right)^2 \qquad \text{----1}$$

Where, φ is the angle of incidence.
σ◦HH= Horizontal backscattering coefficient
σ◦VV = Vertical backscattering coefficient

The equation 1 shows Campbell Model's applicability to the fully polarimetric mode. Since Mini-RF is working in the hybrid polarimetric mode and in the literature no such models are available which can be used for estimating DC from Mini-RF data. Here authors have tried to validate the model for hybrid polarimetric data.

Results: The Dielectric Constant of the Apollo 17 samples which has been measured in laboratory and also has been calculated using eq.1 from the model has been summarized in the table 1.

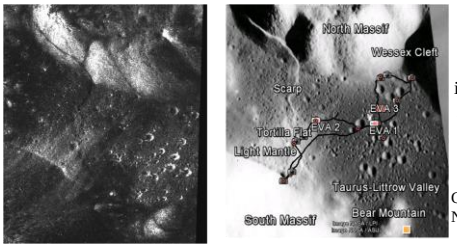

Fig. 1(i) Mini-RF image & (ii) Optical image of Apollo 17 Landing Site

Courtsey: Image NASA/LPI

From the results it can be concluded that Campbell model can be applied over some portion over lunar equitorial region since the dielectric constant values are almost equal to the DC values of the Apollo 17 samples and the DC values of TALS as shown in Table 2. Generation of appropriate model for dielectric constant estimation is important since it will help in identifying landing sites for future explorers, locate potential resources, describe the moon's radiation environment and demonstrate new technologies. For future work this model can be applied over other Apollo sites and results will be validated and also compared with measured DC of TALS.

Apollo 17 traversed path	**Ground based Apollo Results**		**DC from Campbell**
	Sample no.	DC	
Boulder	72441	3.12	3.158173
Camelot Crater	75080	2.40	2.461078
Near to Trident crater	75080	3.50	3.317966
Shorty crater	74220	2.60	2.112405
Shorty crater	74241	2.20	2.103984

Table 1. Comparion of DC from Campbell Model and Apollo 17 Ground based Results

Temp. (°C)	**DC from Apollo 17 Returned Samples (avg.)**	**DC from Campbell model using Mini-RF data (avg.)**	**Data obtained from our measurement 23 °C**
23° C	2.764	2.629	3.61–4.22

Table 2. In this table the measured DC of Terristrial Analogue of Lunar Soil (TALS) that was measured at room temperature at ICRS is given for comparision with the estimated values of DC using Campbelland Apollo 17 samples that were brought from the landing site.

References: [1] G.R. Olhoeft, D.W. Strangway "Dielectric Properties of First 100 meters of Moon" Earth & Planetary Science letters,24(1975) 394-404 [2]OPN Calla, Inder Singh Rathore "Study of complex dielectric properties of lunar simulants and comparison with Apollo samples at microwave frequencies" Advances in Space Research 50 (2012) 1607–1614 [3] B.A. Campbell, J.A. Grant, and T. Maxwell "Radar Penetration In Mars Analog Environments", Lunar and Planetary Science XXXIII (2002) 1616.

WATER ICE DETECTED AT SECONDARY CRATERS ON PEARY FLOOR USING MINI-SAR & MINI-RF. OPN Calla[1],Shubhra Mathur[1,2] and Monika Jangid[1,3] ,[1] International Center for Radio Science, Ranoji Ka Baag, Nayapura, Mandore, Jodhpur Rajasthan India [1]opnc06@gmail.com; [2]shubhra.icrs@gmail.com; [3]monika.jangid.icrs@gmail.com

Introduction: Images of the lunar poles obtained from Mini-SAR and Mini-RF, guide researchers to understand water ice detection phenomenon in better manner. In this paper shadowed and non-shadowed region of Peary crater has been studied using Mini-SAR of Chandrayaan-1 and Mini-RF of LRO.

Peary[1] is an irregularly-shaped impact crater centered at 88.5°N, 30°E having areas along its crater floor cast in permanent shadow, but it also has areas along its rim that are illuminated by the Sun.

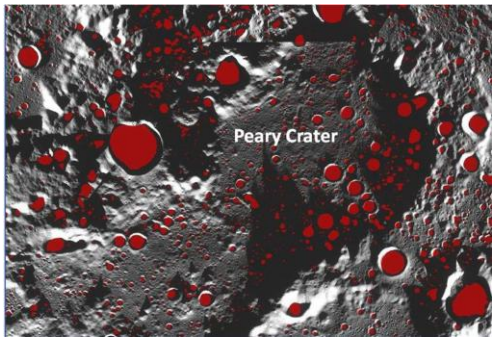

Fig. 1 This image is centered on the north pole of the Moon The red dots represent permanent shadow in Peary crater

Circular polarization ratio: The CPR is the most important derived parameter of Stokes vector, as it provides the indications for wavelength-scale complexity of the surface. The CPR, defined as the ratio between power reflected in the same sense of circular polarization (SC) as that transmitted and the echo in the opposite sense (OC) of circular polarization, is strongly modulated by roughness induced changes in scattering on or beneath a target surface[2]. Rough, rocky surface causes incident radar beams to bounce more than once, leading to more same sence signals and thus providing high CPR; therefore, rougher surfaces show higher mean CPR. Depending on the radar wavelength and the composition of the regolith, it is possible to observe features below the surface.CPR is used in study to find the evidence of subsurface scattering due to dielectric inhomogenity like water-ice. In the figure 1 we can see the peary crater on which the permanent shadowed data is overlaid.

Analysis: The analysis shows the variation in CPR values for inside and outside region of Peary crater. For inside crater permanantly shadowed secondary crater and for outside region non-shadowed secondary crater have been selected. From the graph shown in fig 2 and 3, CPR values are found to be high inside the crater but outside crater shows low CPR values. These higher values can be obtained from very rough surface like rock, lava deposits etc or due to scattering from volumetric ice particles.

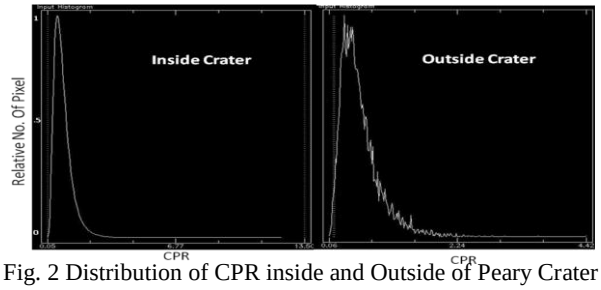

Fig. 2 Distribution of CPR inside and Outside of Peary Crater using Mini-RF Data

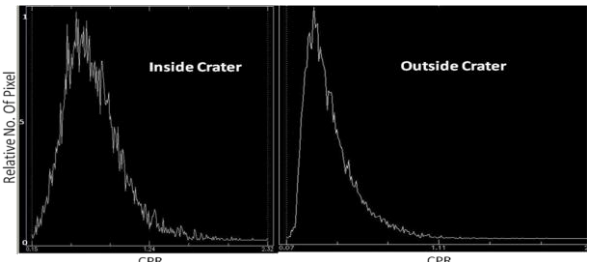

Fig. 3 Distribution of CPR inside and Outside of Peary Crater using Mini-SAR Data

	Mini-SAR		**Mini-RF**	
	Inside crater	Outside crater	Inside crater	Outside crater
CPR	.15-2.35	.07-1.6	.05-1.5	.06-2.27
DoP(m)	.3671	.6395	.4007	.4746
Delta	68.24°	73.97°	34.26°	60.160°

Table. 1 CPR,DoP & Delta (Relative phase LH-LV) range for inside and Outside of Peary Crater using Mini-SAR and Mini-RF data

Conclusion: From the table 1 high values of DoP and delta with high CPR range indicates the surface roughness on outside crater floor. While contrary results are obtained for inside region. It can observed that inside region of crater shows large variation in CPR range for Mini-SAR when compared with Mini-RF data. High CPR values together with low values of degree of Polarization (m) and relative phase of LH-LV (δ) signify presence of water ice in the secondary craters of Peary.

References:[1]http://www.nasa.gov/mission_pages/LRO/multimedia/lroimages/lroc-20091224pearycrater.html [2]BruceA. Campbell" High circular polarization ratios in radar scattering from geologic targets" JGR, VOL. 117, E06008, doi:10.1029/2012JE004061, 2012

EVIDENCE OF NON IMPACT CRATERING ORIGINE OF IMILCHIL (MOROCCO) LAKES (ISLI AND TISLIT). S. Chaabout[1], H. Chennaoui Aoudjehane[1], W.U. Reimold[2,3], M. Aboulahris[1], M. Aoudjehane[4], [1]Hassan II University Casablanca, Faculty of Sciences Aïn Chock, GAIA Laboratory, BP 5366 Maarif, Casablanca 20000 Morocco, [2]Museum für Naturkunde Berlin, Invalidenstrasse 43, 10115, Berlin Germany, [3]Humboldt – Universität zu berlin, Unter den Linden 6, 10099 Berlin, Germany, [4]302 Boulevard Panoramique, 20150 Casablanca, Morocco. (chaabout_souad@hotmail.com), (chennaoui_h@yahoo.fr).

Introduction: Isli and Tislit in the Imilchil region are two widely known lakes in Morocco. Local legend tells that these lakes were formed from the tears of separated lovers. The origin of these depressions has been discussed by some researchers [1,2] in terms of three processes: formation of a karstic depression, syncline formation, or meteorite impact. The most widely considered mode of origin is due to tectonic effects related to syncline formation.

In 2012, newspapers in Morocco reported the presence of two impact craters (Isli and Tislit) related to the Agoudal iron meteorite find. These meteorites have been found about 20 km from these lakes though [3,4]. In order to investigate this impact hypothesis, we organized a field mission to Imilchil area during May 2013.

Geographic localisation: Isli is one of the largest and deepest natural lakes in North Africa with 2.55 km^2 surface area and 95 m depth. It is located in the central part of the Moroccan High Atlas, 9 km NE of Imilchil town. Tislit is located about 8 km to the W of Isli and is a smaller lake, with a surface area of 1.3 km^2 and a comparatively reduced depth of about 16 m [1].

Geological setting: The Imilchil area is a part of the Moroccan High Atlas, the most elevated part of the intracontinental belt of Northern Africa. The Isli and Tislit lakes are located on the "Plateau des lacs" that is an Upper Paleocene / Lower Eocene perched syncline, developed in between Mesozoic elongated and narrow anticlinal ridges (Tassent Ridge and Msadrid Ridge) trending SW-NE. The lakes occur in the core of these syncline-topped anticlinal ridges (STARs) [2,5]. The core of the syncline is formed by the Bathonian (Middle Jurassic) Anemzi Red Bed Series made up of sandstone and shales, superposed onto Bajocian marly limestones that, in turn, cover Reef limestones of the Agoudim Series [5].

Field observation: The "Plateau des lacs" syncline is trapped between two important faults trending N70°, related to the Tassent and Msadrid ridges, with a sinestral movement. Numerous smaller faults essentially perpendicular to N70° were found at many places around Isli lake. The Isli lake is located within alternating bars of biodetrital limestone rich in corals, brachiopods and green marl increasingly thickening upward, of the middle and upper Bajocian [4]. Tislit lake is more recent than these rocks and likely its formation was initiated with the development of an angular unconformity between the Bajocian and Bathonian stages, with alternating calcareous sandstone, red sandstone, silt and clay deposition. Both lakes have dolerite intrusions crossing all layers that likely relate to a post Jurassic regional magmatism.

Our observations include:

- There is no elevated crater rim at either structure.
- The layers surrounding the lakes are not overturned.
- Pre-lake strata dip inward towards the lake center.
- The lake shores are sites of thick sub-horizontally, often cross-bedded lake terraces. In other places, the shallowly inward dipping beds forming the base of the syncline can be followed right into the shoals.
- No radial or concentric fault trends have been observed; all fault structures measured are related to the main faults surrounding the syncline,
- We observed perfectly preserved ripple marks in recent and older sedimentary deposits around the lake.
- No meteorite samples have been found around or close to the lakes.
- No shatter cones were noted.

Conclusion: This recent expedition showed that

- There are no shatter cones in evidence; the lithologies are currently being thin sectioned to investigate the alleged presence of shock microdeformation.
- No samples of the Agoudal iron meteorite (or any other meteorite) have been found close to the lakes.
- Results of our mapping around the lakes proved that there is no significant rock deformation surrounding the lakes that could be linked with a cataclysmic origin of these two structures.

Our results do not favor an impact origin of Isli and Tislit lakes. The local geology is consistent with a formation of the lakes within a synclinal basin as a result of tectonics, as already published [1,2,5].

Acknowledgments: The field work has been supported by the Barringer Crater company, the program CMIFMP Volubilis (MA/11/252), and CNRST-Morocco and CNRS-France, PICS (SDU 01/10). WUR's research is supported by the DFG (Deutsche Forschungsgemeinschaft).

References : [1] Zeroual E. (1995), Ph.D. Thesis, Neuchâatel University, Switzerland 191 p. [2] Ibouh H. (2004), Ph.D. Thesis, Cadi Ayyad University, Morocco. [3] Garvie L. et al. (2013), Meteoritics & Planetary Science 48. [4] Chennaoui H. et al. (2013), Meteoritics & Planetary Science 48, Abs. [5] Michard A. et al. (2011), Terra Nova, 23, 314–323.

CHARACTERISTICS AND VERTICAL PROFILE OF SHOCKED QUARTZ GRAINS IN THE YAX-1 CORE : CONSTRAINTS ON TRANSIENT CRATER SIZE AND EJECTA DEPOSITION PROCESS OF THE CHICXULUB IMPACT. Yu Chang[1*] , Kazuhisa Goto[2] , Yasuhito Sekine[3] , Eiichi Tajika[3], [1]Department of Eerth and Planetary Science, University of Tokyo. (joh@astrobio.k.u-tokyo.ac.jp) [2]IRIDeS.,Tohoku University, [3]Department of Complexity Science & Engineering, University of Tokyo.

Introduction: The Chicxulub crater, located in the Yucatan Peninsula in Mexico, is one of the largest impact structures on Earth (diameter of 180-200 km) [1]. Because the Chicxulub impact is considered to have caused a mass extinction at the Cretaceous-Paleogene (K-Pg) boundary [2], knowledge on the cratering process of the Chicxulub impact will be important not only for understanding a large-scale impact but also the environmental perturbations at the K-Pg boundary.

Despite such an importance, the detailed cratering process of the Chicxulub has been poorly constrained by geological evidence. First, the size of the transient crater has been largely unknown. Previous hydrodynamic simulations suggest that the diameter of the transient crater would have been 100 km to illustrate the size of the final crater [3], implying the Yaxcopoil-1 (YAX-1) drilling core located at 60 km from the center of the crater would have been outside the transient crater. However, no geological evidence has been reported to support the results of numerical calculations.

Second, it is still controversial whether water invation into the crater occurred associated with the impact. Some groups suggest that the upper parts of the impactites of the YAX-1 core are impact-induced tsunami deposits based on the observation of rock strata and geochemical analyses [4,5]. Nevertheless, others interpret that the same units of the YAX-1 core are ejecta deposits that fell in the air [6,7].

In this study, we analyzed both the size distribution and planar deformation features (PDFs) on shocked quartz grains contained in the YAX-1 core derived from the Chicxulub crater. Because the crystallographic orientation of PDFs preserves information of shock pressure achieved by impacts, characteristics and vertical profiles of PDFs along with the YAX-1 core will provide unique information on the excavation, transport, and deposition processes of each impactite unit of the YAX-1 core.

Method: Quartz grains were extracted from the YAX-1 drillcore samples by treating with hydrochloric acid (HCl), hydrogen peroxide (H_2O_2), and hydrofluosilicic (H_2SiF_6) [8]. After the acid treatment, resident quartz grains were mounted on glass plates with pedropoxy basin. Orientation of PDFs were measured and indexed using a four-axis universal stage (U-stage) microscope [9]. The obtained data was indexed following the method summarized in Nakano et al. [8].

Results & Discussions: We found 525 shocked quartz grains throughout the impactite sequences in the YAX-1 core (from Units 6 to 1 in ascending stratigraphic order). In the present study, 574 sets of PDFs were measured from fifteen vertical levels.

We found that all the shocked quartz grains contained in the impact melt layer (Unit 5) were predominantly undergone high shock pressures (> 25 GPa). Whereas, shocked quartz found in other impactite sequences are mixtures of quartz grains that were experienced various shock pressures. These results suggest that Unit 5 is likely to have been formed by an outward flow of impact melt-sheet from the transient crater cavity during the collapse of the central uplift and transient crater [6,7]. Shocked quartz in Unit 5 would have been originally located at the bottom of the transient crater and then transported by the outward flow of melt-sheet. Because impact ejecta are expected to contain mixtures of quartz with various shock pressures, they cannot explain the obtained PDFs pattern.

Given our interpretation of melt-sheet origin of Unit 5 together with the order of deposition of impact ejecta and melts suggested by numerical simulations [10], Unit 6 is considered to have be ejecta curtain deposits. The presence of ejecta curtain deposits in the YAX-1 core means that the core was located outside the transient crater, which support the results of hydrodynamic simulations [10].

In Unit 1, i.e., the uppermost impactite unit, we found an inverse correlation between shocked quartz grains undergone high shock pressures (> 25 GPa) and those undergone medium degree of shock pressures (12-25 GPa) associated with upward grain fining in the sequences. Such cyclic variations in PDFs pattern and grain size would be difficult to be explained by ejecta deposits. These results support the idea that Unit 1 was repeated impact-induced tsunami deposits [4], which suggest water invasions into the crater.

References: [1] Gulick et al. (2013) *Reviws of Geophysics, 51*, 31-52. [2] Schulte et al. (2010) *Science, 327,* 1214-1218. [3] Morgan et al. (2002) *EPSL, 183*, 347-354. [4] Goto et al. (2004) *Meteoritics & Planet. Sci., 39,* 1233-1247. [5] Tuchscherer et al. (2004) *Meteoritics & Planet. Sci., 39,* 899-930. [6] Stoffler et al. (2004), *39,* 1035-1067. [7] Bahlburg et al. (2010) *EPSL, 295*, 170-176. [8] Nakano et al. (2008) *Meteoritics & Planet. Sci., 43*, 745-760. [9] Ferriere et al. (2009) *Meteoritics & Planet. Sci., 44,* 925-940. [10] Collins et al. (2008) *EPSL, 270,* 221-230.

PETROGRAPHIC CHARACTERIZATION OF POPIGAI IMPACT MELT-BEARING BRECCIAS A. Chanou[1], G. R. Osinski[1,2], R. A. F. Grieve[1], and D. E. Ames[3] [1]Dept. of Earth Sciences/Centre for Planetary Science and Exploration and [2]Dept. Physics and Astronomy, University of Western Ontario, 1151 Richmond St., London, Ontario, Canada N6A5B7, [3]Geological Survey of Canada, 601 Booth St., Ottawa, ON, Canada K1A 0E8 *achanou@uwo.ca

Introduction: The Popigai impact structure located in Northern Siberia, Russia (71.38° N, 111.11° E) is a 100 km in diameter structure formed 35.7 ± 0.2 Ma. The mixed target lithologies of the Popigai impact resulted in a variety of impact products. Target lithologies comprise Archaean and Lower Proterozoic gneisses, schists, igneous and sedimentary rocks [1].

This study presents the preliminary petrographic results of a suite of impact melt-bearing breccias from Popigai. The samples are brecciated impactites found beneath the coherent impact melt sheet (tagamite). These melt-bearing breccias are widely cited in the literature as 'suevites'. This petrographic characterization is part of a broader comparative study of impact-generated breccias. As a result, all melt-bearing impact breccias are examined as a single "group" with the intention of comparing and contrasting their physical and petrographic caracteristics. The ultimate goal of this comparative study is to elucidate the formation and deposition mechanisms of a variety melt-bearing breccias from different geologic contexts within impact structures.

Methods: Petrographic investigation was conducted at both the micro- and macroscopic scales. Macroscopic textural analysis (hand sample) were done with the use of digital image processing [2]. Microscopic investigation was performed using traditional optical microscopy, Scanning Electron Microscopy (SEM), and Electron Microprobe Analysis (EMPA).

Textural characterization: Popigai melt-bearing breccias display a wide array of textural characteristics. Glass particles (commonly devitrified) vary in shape, complexity and appearance. The glass fragments vary from strongly vesiculated to almost non-vesicular and from "light-coloured" to "dark-coloured". In addition, these glass fragments occasionally exhibit an internal fabric, with preferentially oriented mineral clast inclusions, and stretched vesicles that appear to have deformed along with the glass fragment. Glass particles typically contain mineral fragments of various sizes. Occasionally, mineral clasts appear to have a coating of impact-melt glass. In addition, present are lithic particles that appear as angular to subrounded fragments. The clastic content varies in size range from sample to sample.

Of interest are ~100 μm wide features of recrystallized melt that appear to be mantled by clinopyroxene rims (Fig.1). Ballen quartz crystals with fractured zircon inclusions were also observed (Fig.2).

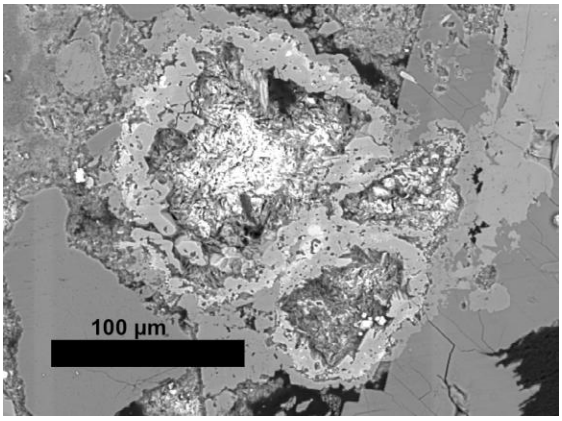

Figure 1. Backscatter image of the 100 μm wide features of mantled recrystallized melt that appears in the form of sheaf-like laths, "coated" with clinopyroxene rims.

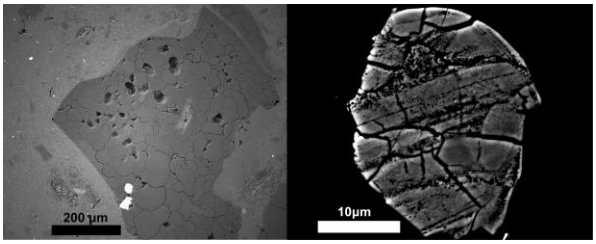

Figure 2. Ballen quartz with two zircon inclusions (left). Zircon crystal inclusion showing fracturing (right).

Preliminary chemical results suggest a mostly anhydrous aluminosilicate melt. The compositions are mainly quartzofeldspathic with the presence of Ca-rich pyroxenes. It has been observed that the clinopyroxenes have an extensively more Ca-rich composition compared to that of the impact melt rocks [3]. In addition, pyroxene aluminum content varies greatly; an observation that may reflect crystallization temperature. Generally, however, both impact melt rock and impact-melt clasts have a similar chemical composition [3]. Finally, the groundmass contains generally similar (but finer) phases as the clastic population of the breccia. It is composed mainly of comminuted plagioclase, quartz, pyroxene and some carbonate.

References: [1] Masaitis V. L. et al., (2004) *Popigai Impact Crater: Guide of geological excursions, VSEGEI Press*. [2] Chanou A. et al. (2011) LPS XLII Abstract #2164. [3] Whitehead J. et al., (2002) Mineralogy and petrology of melt rocks from the Popigai impact structure, Siberia, *Meteoritics & Planet. Sci., 37*.

EFFECT OF TARGET LITHOLOGY ON THE SIMPLE TO COMPLEX TRANSITION DIAMETER FOR LUNAR IMPACT CRATERS. J. C. Clayton[1], G. R. Osinski[1], L. L. Tornabene[1, 2], J. D. Kalynn[3], and C. L. Johnson[3,4], [1]Centre for Planetary Science and Exploration/Dept. Earth Sciences, University of Western Ontario, London, ON, Canada, [2]SETI Institute, Mountain View, CA, USA, [3]Dept. of Earth, Ocean and Atmospheric Sciences, University of British Columbia, BC V6T 1Z4, Canada, [4]Planetary Science Institute, Tucson, AZ, USA (jclayto6@uwo.ca).

Introduction: Impact craters are divided into two subgroups, based on morphology: simple and complex. The progression from simple to complex morphology is not abrupt and is represented by a "transitional" crater morphology. Due to target effects, the transition diameter, D_t, is best represented as the geometric mean of several crater diameter values that characterize this simple-to-complex morphologic transition [1]. For lunar impact craters, the average D_t has previously been estimated to be ~19 km [1], with D_t for maria and highlands occuring at 16 km and 21 km, respectively [1]. In this study, we revisit the simple-to-complex transition diameter and the characteristics of transitional craters with modern datasets with an emphasis on the effects of target lithology. Here we compare the number of terraces and crater depth for transitional and complex craters formed in different target types to gauge the possible effects of the target lithology on crater diameter and morphology.

Methodology: We constructed a database emphasizing transitional craters, but including some complex craters, based on a database of 111 'fresh' craters of Eratosthenian (3.2-1.1 Ga) age or younger [2, 3]. We define a transitional crater as a flat-floored crater that does not display the bowl-shaped form of a simple crater, has formed terraces or slumps, but lacks a central uplift. Lunar Reconnaissance Orbiter Camera (LROC) images, visualized within the Java Mission and Remote Sensing (JMARS) for Earth's Moon program [4], were used to map out the number of terraces for craters in Mare, Highlands or "Border" (i.e. in or near a Mare-Highland contact) targets. In addition, this mapping was also done for selected fresh, complex craters with well-defined central uplifts, to observe trends well into the complex crater diameter range.

Results and Discussions: *Target Effect on Terracing:* When comparing the number of terraces present to the diameter of the crater (Fig. 1), there is an evident trend in both target types where terracing generally increases with crater diameter. However, Figure 1 shows that the formation of terraces occurs at lower diameters in mare targets, rather than the highlands. It is hypothesized that this could be due to the layered nature of the mare target, not present in highlands, which aids in crater collapse. This is consistent with interpretations for terrestrial craters, whereby layering in sedimentary target results in a lower transition diameter compared to crystalline rock [5]. Thus, layering appears to be one of the most important properties in controlling the simple-to-complex transition.

Target Effect on Depth: Figure 2 shows that the depth of mare craters, both transitional and complex, plot consistently lower than the values for those of the highlands. This trend may be a result of the increased amount of terracing or slumping within the mare target, as explained above, further supporting the idea of collapse being enhanced in the mare basalt targets.

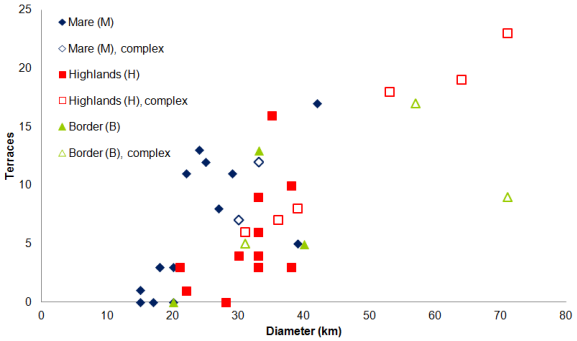

Figure 1: Plot of number of terraces versus diameter (km) for transitional and complex craters in mare, highlands and border target.

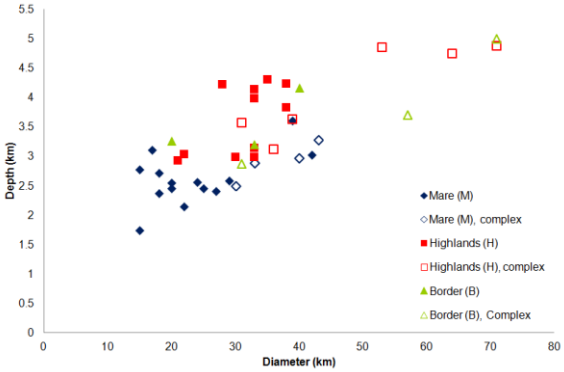

Figure 2: Depth-Diameter relationship for transitional and complex craters in various targets.

Conclusions: This work provides new and important insights into the nature of transitional impact craters on the Moon with evidence that target lithology plays an important role in changes in morphology, depth and transition diameter.

References: [1] Pike R. J. (1980) Proc. Lunar Planet. Sci. Conf. 11th, 2159-2189. [2] Kalynn J. et al. (2013) Geophys. Res. Lett., 40, 38–42. [3] Kalynn J. et al. (2013) LPS XLIV. [4] Christensen P.R. et al. (2009) AGU Fall, Abstract #IN22A-06. [5] Dence M.R. (1972) Int. Geol. Cong. Proc. 24th:77-89.

LARGE IMPACT CRATER FORMATION ON THE MOON: COMPARING NUMERICAL MODELS WITH GRAIL-DERIVED CRUSTAL THICKNESS PROFILES G. S. Collins[1], M. A. Wieczorek[2] and K. Miljković[2], [1]Impact and Astromaterials Research Centre, Dept. Earth Science & Eng., Imperial College, London, UK (g.collins@imperial.ac.uk), [2]Univ Paris Diderot, Sorbonne Paris Cité, Institut de Physique du Globe de Paris, France.

Introduction: The well-imaged record of impact craters on the Moon provides arguably the best test for numerical models of crater formation. However, previous numerical modeling studies have shown that the Moon's crater size-morphology progression can be matched with different model assumptions about target rheology [1,2]. In an effort to resolve this ambiguity, here we use gravity and crustal thickness anomalies measured by GRAIL [3], which provide new constraints on crustal deformation beneath large lunar craters, as an additional test of models of crater formation.

Methods: Numerical impact simulations, using the iSALE shock physics code [4-6], were performed for typical impact conditions on the Moon. Simulations assumed an impact velocity of 15 km/s, and a surface gravity of 1.63 m/s^2, a simplified two-layer target with a crustal thickness of 30-60 km and a range in impactor diameter from 0.1-50 km. The 2D, axial symmetry of the numerical models enforced an assumption of vertical impact. In all simulations the impactor and target mantle were modeled using a material model for dunite; the crust was modelled using a material model for grantite. Equation of state tables generated using ANEOS were used to describe the thermodynamic state of both materials, while material strength was modeled using the approach described in [5]. In some simulations, dilatancy (porosity increase during shear failure) was accounted for using a recently developed algorithm [7]. To facilitate late stage collapse of the craters, the block-oscillation model was used [e.g., 1]. A single choice of block model scaling constants was sought to produce a simulated crater morphology and crustal thickness structure for each impactor diameter that best matched observations (e.g., [8]; see Fig. 1).

For comparison with numerical models, azimuthal averages of surface topography, crust-mantle interface, and Bouguer gravity were calculated as a function of distance from the center of ~50 of the largest lunar craters. The crustal thickness profiles were derived from recent crustal thickness models [3], which take into account lateral variations in crustal density as constrained by orbital remote sensing data. The crustal thickness models were constructed by removing the gravity contribution of the surface topography (as mapped by the laser altimeter LOLA onboard LRO) from the observed GRAIL free-air gravity; the remaining signal was then interpreted as relief along the crust-mantle interface and inverted using standard techniques [9].

Results: Numerical impact simulations with consistent block-model scaling constants are able to reproduce several key observations, including: (a) the simple-to-complex transition diameter; (b) the central peak to peak-ring crater transition diameter; (c) the depth-to-diameter trend up to a crater diameter of ~300 km; (d) the peak-ring vs. rim diameter ratio [8]. Crater depth is over-estimated in the models for craters larger than 300 km diameter, which may be explained by post-impact visco-elastic modification of large basins [10]. The numerical simulations predict a central region of thinned crust, overlying mantle uplift, surrounded by a ring of thickened crust and depressed mantle, in qualitative agreement with crustal thickness models derived from GRAIL gravity. However, the crustal thickness in the basin centre and the mantle uplift diameter in the simulations tends to be less than is observed (Fig. 1).

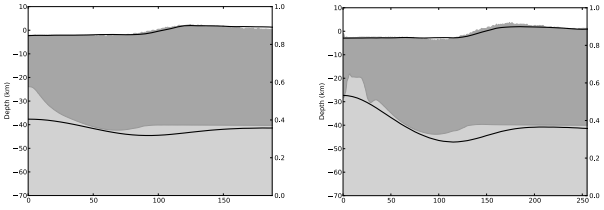

Figure 1 Comparison of simulated final crater profiles for a 17.5-km (left) and 25-km (right) diameter impactor with azimuthally averaged topography and crustal thickness profiles across d'Alembert (left) and Mendeleev (right) basins.

Acknowledgements We thank Boris Ivanov, Kai Wünnemann and Dirk Elbeshausen for their help developing iSALE.

References: [1] Wünnemann K and Ivanov BA (2003) Solar System Research, 51(13): 831-845 [2] Bray VJ, et al., (2008) *Meteoritics & Planet. Sci*., 43, 1979-1992 [3] Wieczorek M et al. (2012) *Science,* doi: 10.1126/science.1231530. [4] Amsden AA, et al. (1980) Los Alamos National Laboratory. LA-8095. [5] Collins GS, et al. (2004) *Meteoritics & Planet. Sci*., 39, 217-231. [6] Wünnemann K, et al. (2006) *Icarus*, 180, 514-527. [7] Collins GS (2013) *44th LPSC,* Abs. 2917 [8] Baker D et al. (2011) *Icarus*, 214(2): 377-393. [9] Wieczorek MA and Phillips RJ (1999) *Icarus* 139, 246–259. [10] Freed A, et al. (2013) *44th LPSC*, Abs. 2037.

THE NATURE AND ORIGIN OF THE ENIGMATIC GARSON MEMBER OF THE SUDBURY IMPACT STRUCTURE, CANADA. A. B. Coulter[1], G. R. Osinski[1] and R.A.F. Grieve[1], [1]Centre for Planetary Science and Exploration/Dept. Earth Sciences, University of Western Ontario, 1151 Richmond Street, London, ON Canada N6A 5B7 (acoulte6@uwo.ca, gosinski@uwo.ca).

Introduction: The 1.85 Ga, ~200 km diameter Sudbury impact structure is a tectonically altered impact basin located in central Ontario, Canada [1]. The structure is composed of three major constituents, from the centre of the crater outwards they are: the Whitewater Group, the Sudbury Igneous Complex (SIC) and the country rocks [2]. From youngest to oldest, the Whitewater group consists of four Formations: Onaping, Vermillion, Onwatin and Chelmsford [3]. The Onaping Formation is a 1.4-1.6 km thick complex series of breccias and melt bodies which is subdivided into three Members, from bottom to top: Garson, Sandcherry and Dowling Members [4].

The Garson Member is up to 500 m thick and is restricted to a 25 km strike length in the SE lobe of the impact structure [4]. The Garson Member has been previously described as comprising thickly bedded to massive fragmental rocks dominated by >20 to 85% Huronian quartzite fragments (<6 cm) and blocks (>6 cm to 50 m), and contains up to 15% vitric andesite lapilli, and <5% vitric andesite bombs and blocks [3]. These properties set it apart from any other member of the Onaping Formation. Furthermore, the reason(s) as to why the Garson Member is restricted to the SE of the Sudbury structure remains unanswered, providing motivation for this study.

Methods: Detailed mapping and sampling of the Garson Member took place during summer 2012. Laboratory analyses at the University of Western Ontario included optical microscopy, powder X-ray diffraction (XRD), micro X-ray diffraction (μXRD), X-ray fluorescence (XRF), inductively coupled plasma atomic emission spectroscopy (ICP-AES), and backscattered electron (BSE) imaging coupled with energy dispersive X-ray (EDX) spectroscopy on a scanning electron microscope (SEM).

Results: Massive quartzite clasts (~75%) set in an aphanitic groundmass (~25%) accounts for the entirety of the Garson Member. The clast size and shape in the Garson Member displays extensive variation from 10's of m's to only cm's. There was a general decrease in clast size moving upwards through the Garson Member towards the Sancherry Member. In addition, there was an apparent increase in deformation of the clasts, as they showed signs of east to west elongation. Along with the elongated quartzite clasts, many Quartz veins were found following the same east to west trend.

Petrology. Clasts were confirmed to be consistently dominated by quartz (≥95%). The remaining ≤5% contained variable amounts of K-feldspar, plagioclase, muscovite and chlorite. Chlorite overprints both the clasts and groundmass. Planar deformation features (PDFs) were noted within the quartzite clasts. The major phases in the igneous-textured groundmass included: ~40-55% quartz, 10-25% K-feldspar, 5-20% chlorite, <5% plagioclase, <5% muscovite and <5% opaques.

Geochemistry. XRF and ICP-AES analyses of the least altered groundmass samples suggests a close relationship to the Onaping Intrusion, while the Sandcherry Member and the Granophyre do not seem to be as closely related.

Discussions: The presence of shocked clasts and an aphanitic groundmass of igneous origin provides justification for the reclassification of the Garson Member as a clast-rich impact melt rock. The geochemical similarities between the Garson Member and the Onaping Intrusion and their similar stratigraphic context – i.e., between the SIC and the Sandcherry Member of the Onaping Formation – potentially suggest a similar origin.

Recent research has suggested the Onaping Intrusion actually represents the roof rocks of the SIC, as this melt sheet lacks a clast rich upper phase [5, 6 – Anders et al. this conference]. As such, it is proposed that the Garson Member, like the Onaping Intrusion, represent the roof rocks of the SIC. There are, however, several differences between the Garson Member and the Onaping Intrusion, including different clast size and shape, clast lithology and groundmass texture. A new model of the Garson Member has been developed to account for these differences, in addition to supporting the roof rock theory.

Acknowledgements: This study was supported by the NSERC CREATE project "Technologies and Techniques for Earth and Space Exploration".

References: [1] Spray, J.G. et al. (2004) Meteoritics & Planetary Science, v. 39, i. 2, p. 287-301. [2] Ames, D.E. and Farrow, C.E.G. (2007) GAC, Mineral Deposits Division Special Publication No. 5, p. 329-350. [3] Ames, D.E. et al. (2009) OGS Survey, Open File Report 6243, p. 14-30. [4] Grieve, R.A.F. (2010) Meteorics & Planetary Science, v. 45, p. 759-782. [5] Anders, et al. (2013) 44th LPSC, abstract #1637. [6] Anders, et al. (2013) Large Meteorite Impacts and Planetary Evolution V.

NEW INSIGHTS INTO THE RELATIVE TIMING AND CONTRIBUTION OF THE CHICXULUB IMPACT AND DECCAN VOLCANISM IN THE CRETACEOUS-PALEOGENE BOUNDARY EXTINCTIONS. M. L. Cousineau[1], F. Therrien[2], T. Maruoka[3], D. Fortin[1] and B. A. Wing[4], [1]University of Ottawa, Department of Earth sciences, Ottawa, Ontario [2]Royal Tyrell Museum of Palaeontology, Drumheller, Alberta [3]University of Tsukuba, Ibaraki, Japan [4]McGill University, Earth and Planetary Sciences, Montréal, Québec

Introduction: The Cretaceous-Paleogene (KPg) boundary marks one of the most significant mass extinctions in Earth history. The leading hypothesis attributes the extinctions to a bolide impact with sulfate-rich rocks—the Chicxulub impact, but a major competing hypothesis suggests a major role for the emplacement of the Deccan continental flood basalts. Absolute age measurements for the largest Deccan eruptions and the KPg boundary suggest the two events were contemporaneous, but measurement uncertainties have so far thwarted attempts at resolving their relative timing. Using sulfur stable isotope measurements at two KPg sedimentary sections, we provide new insights into the relative timing of these two geologic events and their respective contribution to the KPg biotic turnover.

Sulfur isotopes: Both the Chicxulub impact and Deccan volcanism would have released massive amounts of sulfur (S) in the atmosphere. Impact-released S would have primarily been derived from late Maastrichtian seawater and the ≈3-km-thick sequence of Cretaceous evaporite- and carbonate-bearing target rocks at the impact site, whereas S released by Deccan volcanism would have an igneous origin. Maastrichtian seawater, Upper Cretaceous evaporites, and Chicxulub target evaporites have $\delta^{34}S$ values centered around ≈18‰[1], while sulfate aerosols collected at basaltic vents have much lower $\delta^{34}S$ values (≈8‰)[2].

KPg sedimentary sections: We measured whole-rock sulfur content and isotopic composition ($\delta^{34}S$) at high resolution across the KPg boundary at two sections (Knudsen's Coulee Section, KCS; Knudsen's Farm Section) in Alberta, Canada. We focus our discussion on the extremely well-preserved KCS, which features lithological, paleontological, and geochemical markers indicative of the terrestrial KPg boundary, including a three-part boundary claystone layer representing the initial ballistic melt ejecta, an early-formed 'fireball' layer of condensed vapor from the impactor and target rocks, and a later-formed layer of fine Ir-rich particles and sulfate aerosols.

Results: Sulfur contents and $\delta^{34}S$ values show similar behavior at both sections (Fig. 1A, 1B: KCS shown), with, below the boundary claystone, extremely low (<0.2 wt%) S contents and mildly varying $\delta^{34}S$ values (≈6.5‰±2‰). This provides a favorable backdrop for monitoring the addition of ^{34}S-rich sulfur to the system ($\delta^{34}S \times [S]$, Fig. 1C). Mixing curves (not shown) show the ^{34}S-enriched sulfur is derived from two distinct sources, with measurements associated with the brief and intense pulse falling on a high (≈18‰) $\delta^{34}S$ curve, comparable to Chicxulub target rocks, and those associated with the broader pulses falling on a lower (≈8‰) $\delta^{34}S$ curve, comparable to sulfate aerosols from oxidized volcanogenic SO_2.

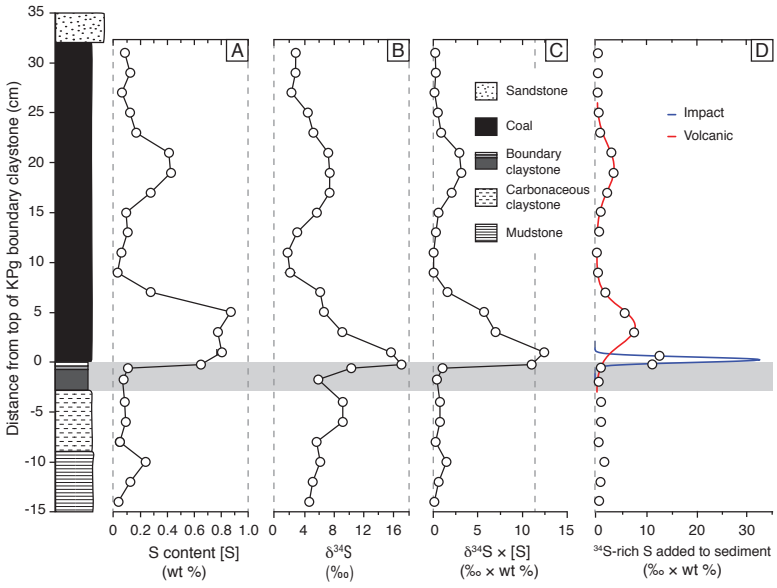

Fig. 1 Whole-rock S content [S] (A) and $\delta^{34}S$ values (B) at the Knudsen's Coulee KPg section. Data points represent 2 cm-thick sample intervals (smaller intervals in boundary claystone). (C) Plot of $\delta^{34}S \times [S]$ representing the amount of ^{34}S-rich S added to the sediment. (D) Modeled data. The shaded area indicates the boundary claystone, divided into a three-part micro-stratigraphy.

Discussion: The environmental scenario we propose places the onset of a major Deccan eruptive phase, lasting ≈90 kyrs, at the KPg boundary, contemporaneous with the Chicxulub bolide impact (Fig. 1D). A subsequent eruptive phase started ≈120 kyrs post-impact, lasting ≈90 kyrs. Deccan eruptions may have delayed the recovery of marine and terrestrial ecosystems after the impact, but our results highlight the Chicxulub impact as the primary extinction trigger.

References: [1] Paytan et al. (2004) *Science,* 304, 1663-1665; C. Koeberl, (1993) *Geology,* 21, 211-214 [2] Mather et al. (2006) *JGR*, 111.

THROUGH THE ICE, EXPOSING THE OCEAN: IMPACT BREAKTHROUGH PARAMETERS FOR EUROPA Rónadh Cox and Aaron W. Bauer, Geosciences Department, Williams College; rcox@williams.edu

Introduction: The idea that impacts could deposit organic and other compounds on Europa's surface is well established, but whether and how these materials might be transported to a subsurface ocean remains in question [*1*]. Previous studies have shown that Europa's ice shell is vulnerable to impact breaching [*2, 3*], and this analysis quantifies the conditions under which impacts might penetrate to water. Impact exposure of the ocean would provide a conduit for surface-subsurface exchange of biogenic materials.

Methods: We used the iSALE hydrocode [*4-6*] to model ice overlying water. We simulated ice thicknesses (T) from 1-40 km to cover the range of likely values for Europa [*7*]. Impactors were ice spheres of density 910 kg/m^3. Median impact velocity at Europa is about 26 km s^{-1} [*8*], but since high impact velocities require smaller time steps, we ran simulations at lower velocity (15 km s^{-1}) and scaled projectile size to produce the energies of interest [*9*]. Impactor diameters (26 km s^{-1} equivalent) ranged from 200-5000 m .

Impact outcomes and breakthrough criterion: Craters form when the ratio between impact energy and ice thickness is small (in thick ice or for small impactors). But as energy increases, transient crater depths (d_t) approach the ice-water contact [*3, 9*]. Surface-to-ocean communication occurs when the full ice thickness is melted or vapourised [*3, 9*]. The transition from non-penetrating craters to ocean-exposing melt-through events comes at $d_t \approx 0.8T$, where post-impact melting and rebound of the sub-crater ice combine to produce a surface-to-ocean water column; so we take $d_t = 0.8T$ AS the breakthrough criterion.

Largest possible non-penetrating craters: The upper limit on crater size at Europa depends on ice thickness. For ice 40 km thick, the largest possible non-penetrating crater has transient diameter (D_t) ≈80 km, which would produce a final diameter ≈160 km: there are no craters of this size on Europa. For 20 km ice, the upper limit for a crater-producing event is D_t ≈40 km, which is close to the estimated D_t for Europa's largest mapped craters [*10*]. This may be telling us that the likely ice thickness on Europa is in the 15-20 km range, which lines up with results from other lines of evidence [*7*].

Likelihood of breakthrough: All ice thicknesses tested are subject to full penetration by impactors with geologically short return times at Europa. The return time for a 5-km diameter cometary impact (100-km crater) is about 50 m.y. [*8*]. Such an object impacting 40 km-thick ice at 26.5 km s^{-1} produces d_t 38 km deep, with subsequent melt-through to ocean. For ice 10-20 km thick, the breakthrough criterion is met by impactors 0.8-2 km diameter (return times 3-15 million years [*8*]). Most estimates for Europa's ice thickness are in the 10-20 km range [*7*], so we expect that Europa's ice can be breached on timescales of 10^6- 10^7 m.y.

Evidence for breakthrough at Europa? Impact penetration to liquid has been proposed to explain features of Callanish and Tyre, Europa's largest craters [*10, 11*]; and also as a mechanism for forming chaos terrane [*2, 12-14*]. Our numerical models support these interpretations and suggest a need to consider impact breakthrough as a geomorphic process on Europa.

Implications of impact breakthrough: Exposure of the ocean via impact represents a protracted opportunity for transfer of materials into the subsurface realm because refreezing is estimated to take 10^5-10^6 years [*14*]. Although mass delivered by the hole-forming impactor is unlikely to end up in the ocean [*1*], ejecta from subsequent impacts might well land on its receptive, still molten surface. Cometary organic matter can survive and be retained by Europa's gravity field [*15*]; such material, released and impelled by subsequent impacts elsewhere on the moon, might fall onto older but incompletely frozen impact sites, and thence into the subsurface ocean.

References: [1] Pierazzo E. and Chyba C.F. (2002) *Icarus, 157*, 120-127. [2] Cox R. et al. (2008) *Meteoritics and Planet. Sci., 43*, 2027-2048. [3] Turtle E.P. and Pierazzo E. (2001) *Science, 294*, 1326-1328. [4] Ivanov B. A. et al. (1997) *Intl. J. Impact Eng. 20*, 411-430. [5] Melosh H.J. et al. (1992) *JGR, 97*, 14,735-714,759. [6] Wünnemann K. et al. (2006) *Icarus, 180*, 514-527. [7] Billings S.E. and Kattenhorn S.A. (2005) *Icarus, 177*, 397-412. [8] Zahnle K. et al. (2003) *Icarus, 163*, 263-289. [9] Turtle E.P. and Ivanov B.A. (2002) *PSe XXXIII,Abstract #1431,* [10] Moore J.M. et al. (2001) *Icarus, 151*, 93-111. [11] Greenberg R. and Geissler P. (2002) *Meteoritics and Planet. Sci., 37*, 1685-1710. [12] Billings S.E. (2004) *M.S. Thesis*, U. Idaho. [13] Billings S.E. and Kattenhorn S. A. (2003) *LPS XXXIV, Abstract #1955,* [14] Buck L. et al. (2002) G*RL, 29*, no. 2055. [15] Pierazzo E. and Chyba C.F. (2000) *LPS XXXIII, Abstract #1656.*

A Model of Localized Shear Heating with Implications for the Morphology and Paleomagnetism of Complex Craters. D. A. Crawford[1] and P. H. Schultz[2], [1]Sandia National Laboratories*, Albuquerque, NM, USA, [2]Brown University, Providence, RI, USA.

Introduction: The need for a dynamic weakening mechanism to facilitate the collapse of a transient cavity to produce the complex crater shape has been well documented. Several have been proposed: acoustic fluidization [1], thermal softening due to shock melting [2] and frictional melting along fault planes [3]. Several studies have stressed the potential importance of frictional melting during the impact process [4-8]. In the present work, we develop a numerical model of shear failure and frictional heating within faults and demonstrate how this model can play a role in explaining complex crater morphology and in the acquisition of remnant magnetization.

Model: Our starting point is the damage model of Collins et al. [9], where the yield strength of fully damaged material follows a Coulomb friction law and thermal softening of bulk material occurs approaching the melting point. We extended the model by estimating statistical crack spacing based on strain rate, a determination of shear heating within cracks and heat loss via conduction away from cracks. With this extension, thermal softening can occur as the temperature within a crack approaches the melt temperature. The model has been added to CTH [10] as the Brittle Damage with Localized Thermal Softening (BDL) model.

Discussion: The BDL model is dependent on estimates of crack spacing. In the examples shown in Figs. 1-2, we've chosen crack spacing (L) to follow a power law, $L=L_0 \dot{\varepsilon}^{-n}$, where $\dot{\varepsilon}$ is strain rate. We've chosen values of L_0 and n to produce crack spacing of 2-7 m for terrestrial crater diameters of 1–280 km. With EOS, strength and conductivity properties appropriate for granite, the BDL model predicts thermal crack widths of 0.3-3 cm and characteristic cooling times of 10-1000 s. over the size range studied. Frictional heating within each crack is proportional to $\mu L \dot{\varepsilon} P$, where μ is the friction coefficient (which decreases with temperature) and P is pressure. With the crack spacing and widths in these examples, 0.1-1% of rock volume is affected by this process.

Implication 1: As shown in Fig. 1, temperatures within cracks approach the melting point of granite (~2000 K) and persist for a period of time dependent on crater scale. For simple craters, the characteristic cooling time of cracks is significantly smaller than the crater formation time ($T_c << T_f$) so there is little time for thermal softening to influence crater development. For central peak craters T_c is comparable to T_f so thermal softening can influence the development of a central peak but decay rapidly enough to "freeze" the peak at the end of crater formation. For larger craters, thermal softening persists long enough for central peak overshoot to occur with implications for peak ring and multi-ring basin development.

Implication 2: The high temperatures acquired by some fault materials in this model would allow magnetic carriers to acquire thermal remanence of the magnetic field present at the time. If the cooling time is rapid enough, as it seems here for simple and central-peak craters, the acquired remanence may be of an impact-generated field [11] or the ambient field distorted by the presence of impact-generated plasma.

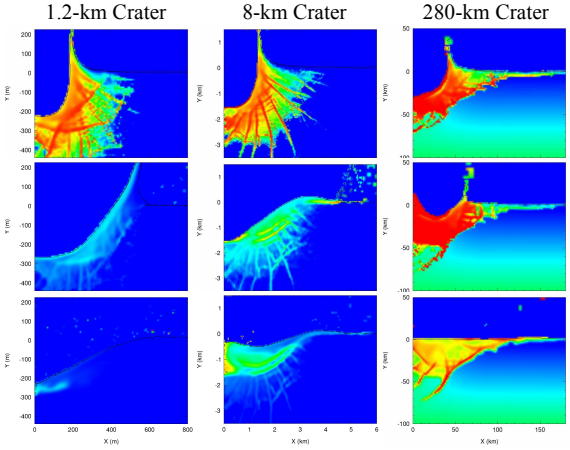

Fig. 1. Fault temperature using the BDL model for three simulated terrestrial craters at three representative times (top→bottom is beginning→end of crater formation). Blue ≤ 350 °K, Green = 1175 °K, Red ≥ 2000 °K.

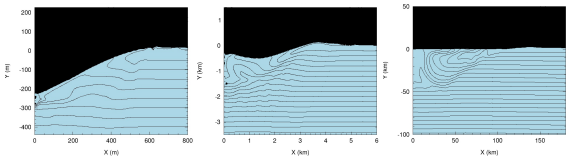

Fig. 2. Predicted final crater cross-sections after motion has ceased. The 1.2- and 8-km simulations straddle the simple-to-complex transition which occurs at 2-5 km.

References: [1] Melosh, H.J. (1979), *JGR*, 84, 7513-7520. [2] O'Keefe, J.D., Ahrens, T.J. (1999), *JGR* 104:E11, 27091-27104. [3] Dence, M.R. et al. (1977), *Impact and Explosion Cratering*, Roddy, D.J. et al. eds., Pergamon, NY, 247-275. [4] Schultz, P.H. (1996), *JGR*, 101, 21117-21136. [5] Spray, J.G. (1998), *Geol. Soc. London Sp. Pub.*, *140*, 171-180. [6] van der Bogert et al. (2004), *MAPS,* 38:10. [7] Senft, L.E., Stewart, S.T. (2009), *EPSL,* 287, 471-482. [8] Spray, J.G. (2010), *Ann. Rev. Earth Planet. Sci.*, *38*, 221-254. [9] Collins, G.S., et al. (2004), *MAPS*, 39:2, 217-231. [10] McGlaun, J.M. et al. (1990) *Int. J. Impact Eng.*, *10*, 351-360. [11] Crawford, D.A., Schultz, P.H. (1999) *Int. J. Impact Eng., 23*, 169-180.

*Sandia is a multi-program laboratory operated by Sandia Corporation, a Lockheed Martin Company, for the United States Department of Energy under Contract DE-AC04-94AL85000.

ZIRCONS AS A PROBE OF EARLY LUNAR IMPACT HISTORY. C. A. Crow[1], K. D. McKeegan[1], J. D. Gilmour[2], S. A. Crowther[2], D. J. Talor[1]. [1]ESS, University of California Los Angeles. (E-mail: ccrow@ucla.edu.) [2]SEAES, University of Manchester.

Introduction: Lunar zircons are among the oldest minerals on the Moon and their ages have been used to investigate its early magmatic and impact history. Zircons are ideal for investigating the early lunar bombardment because (1) low initial Pb results in high precision U-Pb age measurements, (2) these crystallization ages of lunar zircons all predate the proposed cataclysm at 3.9 Ga, (3) zircons incorporate both U and Pu, so we can measure both U-Pb crystallization ages and fissiongenic Xe degassing ages for the same crystal. We report preliminary U-Xe degassing ages in conjunction with Pb-Pb ages for two Apollo 14 zircons.

Samples: A total of seven zircons were separated from ~5g of Apollo 14259, a very mature lunar soil [1]. Three of the zircons were chosen for Xe analyses on the basis of their estimated U contents and large sizes (>300μm). The size requirement was determined during our previous Xe analyses of lunar zircons [2].

Method: U-Pb and Pb-Pb ages of all seven zircons were measured with the UCLA Cameca ims-1270 ion microprobe. The three large zircons were then irradiated in the UC Irvine Nuclear Reactor to induce ^{235}U fission in order to determine the U-Xe age [3]. Xe isotopes were measured with the University of Manchester Refrigerator Enhanced Laser Analyser for Xenon.

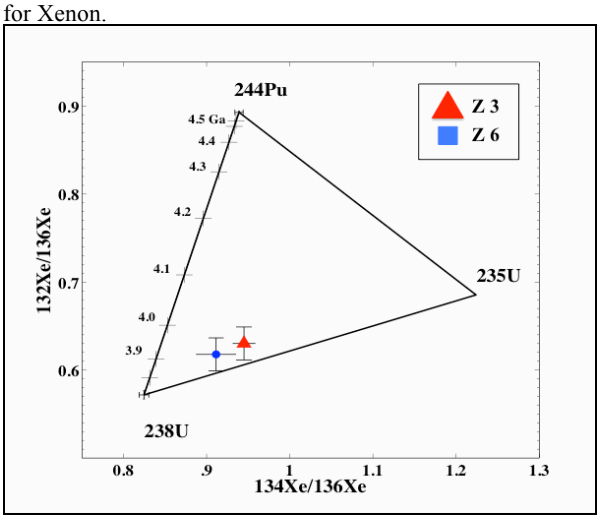

Figure 1: Results of Xe isotopic analysis for 2 large lunar zircons with blank, spallation, and air corrections. Both zircons had high temperature releases consistent with a mixture of spontaneous fission of 238U and induced fission of 235U.

Results: The Pb-Pb ages of the three large zircons are 4205±14 Ma (Z3), 4251±8 Ma (Z6), and 4190±22 Ma (Z7). Two of the grains (Z3 and Z7) are slightly discordant and both show evidence of a Pb mobility event within the last ~300 Myrs. Two of the three zircons (Z3 and Z6) produced sufficient xenon for precise xenon isotope ratios to be determined; the other did not due either to low U concentration or recent Xe degassing. Both zircons are consistent with a mixture of ^{235}U and ^{238}U fission, but neither shows evidence of ^{244}Pu (Table 1). All three zircons formed before the extinction of ^{244}Pu, so the absence of plutogenic Xe suggests that the zircons degassed more recent than 3.9 Ga, or they did not incorporate Pu during formation. We will present preliminary U-Xe degassing ages for both lunar zircons at the time of the meeting.

Table 1

Sample	132Xe/136Xe	134Xe/136Xe
Z3	0.618±0.019	0.911±0.024
Z6	0.630±0.019	0.944±0.013

References: [1] Meyer C. 2006. Lunar Sample Compendium,15455, (http://curator.jsc.nasa.gov/lunar/compendium.cfm). [2] Crow C. A., McKeegan K. D., Gilmour J. D., Crowther S. A., Taylor D. J. 2012. Abstract #1639. 43rd Lunar & Planetary Science Conference. [3] Turner G., Busfield A., Crowther S. A., Harrison M., Mojzsis S. J., Gilmour J. 2007. *Earth and Planetary Science Letters* 261: 491-499.

DISCOVERY OF MAFIC IMPACT MELT IN THE CENTRAL UPLIFT OF THE VREDEFORT BASIN.

C.L. Cupelli[1], D.E. Moser[1], I.R. Barker[1], J. R. Darling[2], J.R. Bowman[3], J. Wooden[4], and B. Dhuime[5].
[1]University of Western Ontario, 1151 Richmond Street, London, Ontario, Canada, N6A 5B7, (ccupelli@uwo.ca, Desmond.Moser@uwo.ca); [2] University of Portsmouth, Burnaby Building, Burnaby Road, Portsmouth, P01 3QL. [3]University of Utah, 115 S 1460E, Salt Lake City, Ut 84112, [4]Stanford University, 450 Serra Mall Stanford, CA 94305-2004; [5] University of Bristol, Wills Memorial Building, Queens Road, Bristol, UK, BS8 1RJ.

Introduction: The large (~250-300 km diameter [1]) Vredefort impact structure in the Archean crust of southern Africa provides us with an analogue for studying the crust-crater dynamics of impact modification of ancient lithosphere. No evidence of the impact melt layer expected for a Vredefort-scale event has been recognized, presumably due to 2.02 Ga of post-impact erosion [2]. Impact modeling, however, predicts that the Vredefort structure was overlain by a melt sheet several kilometers thick [3], similar to that of the Sudbury structure. A previous report of a 0.5 m-wide impact-age norite dyke [4] was subsequently re-interpreted as 'pseudotachyllite' that was locally derived [5].

Methods: We have tested the impact origin of the 'type' norite dyke at Vredefort and conducted additional detailed mapping in the region in search of similar mafic rocks. Tests included the examinination of contact relationships, shock microstructural state of accessory phases (e.g. EBSD of zircon) and host minerals, U-Pb and Hf isotopic analysis of unshocked and shocked zircons, and Ti-in-zircon thermometry.

Detailed mapping at 10 m grid spacing was initially carried out in the area of the 'type' gabbro-norite dyke [4]. Geochronology mineral separation was conducted at the Jack Satterly Geochronology lab at the University of Toronto and SIMS U-Pb isotopic analysis and Ti-thermometry were conducted at the Stanford/ U.S.G.S. SHRIMP-RG facility according to previously published procedures [6]. Electron nanobeam techniques including cathodoluminescence (CL) , electron diffraction (EBSD) and Energy Dispersive Spectroscopy (EDS) were performed with a Hitachi SU6600 VP-FEG-SEM at the University of Western Ontario Zircon and Accessory Phase Laboratory (ZAPLab) with internal protocols [7]. Hf Laser Ablation ICPMS isotopic analyses were conducted at the University of Bristol, UK. according to previously published procedures [8,9].

Results and Discussion: Outcrops of gabbronorite as much 10 m across were located within Archean Inlandsee Leucogranofels (ILG) gneiss at two locations. Unlike the polydeformed gneissosity of the ILG, the texture of the gabbronorite is massive to weakly foliated, exhibiting a strong foliation at one margin in a zone containing cm-scale inclusions of ILG. The form of the gabbronorite bodies, and their mineral textures, are consistent with an origin as dm-scale dykes and lenses that experienced minor recrystallization during solidification. Pyroxene and plagioclase are unshocked, the former exhibiting exsolution lamellae. Unshocked grains of igneous zircon and baddeleyite are intergrown with pyroxene, ilmenite and plagioclase. In contrast, shock microstructures in accessory phases of the ILG are abundant despite local impact melting and recrystallization. A subpopulation of similar shocked and recrystallized zircons, interpreted as xenocrysts, occurs in some samples of the gabbronorite. Zircon U-Pb SHRIMP ages for the unshocked gabbronorite zircon overlaps the ID-TIMS age for the impact of 2019±2 Ma. The εHf values of igneous grains are consistent with gabbronorite derivation by melting of a crustal reservoir with an Archean model age (e.g. the Witwatersrand basin). Ti-in-zircon temperatures are well-above average for endogenic crustal melts, ranging from 790˚C to 900˚C like those from the mafic base of the Sudbury impact melt sheet [10].

Our mapping, textural, microstructural, isotopic and thermometry data prove an impact origin for these mafic meta-igneous rocks, wheras historically an impact origin has not been accepted due to recrystallized textures and a local mineral fabric. We propose that these characteristics were acquired during post-impact crater modification and cooling, due to, for instance isostatic adjustment following central crater excavation and rebound. Other deeply eroded remnants of early cratering in Archean crust could appear similar, with the geochemical and textural signatures of the Vredefort bodies serving as a benchmark in the search for Early Earth impact melt residua.

References: [1] Therriault, A.M., Reid, A.M., and Reimold, W.U. (1993) [abs]: *LPS*. 24:1419-1420. [2] Gibson, R.L., Reimold, W.U., and Stevens, G. (1998) *Geol.* 26: 787-790. [3] Ivanov, B.A. (2005) *Solar Sys. Res*, 39(5), 381–409. [4] Moser, D.E. (1997) Geol. 25(1), 7-10. [5] Gibson, R.L., and Reimold, W.U. (2008) *Council for Geosci. Pretoria*, 97. [6] Mazdab, F.K. and Wooden, J.L. (2006) *GCA*,70(18), A405. [7] Moser, D. et al. (2011) *Can. J. Earth Sci*. 48. [8] Hawkesworth, C.J. and Kemp, A.I.S. (2006) *Chem. Geol.* 226, 144. [9] Fisher, C.M. et al. (2011) *Chem. Geol.* 286, 32. [10] Darling, J., Storey, C. and Hawkesworth, C. (2009) *Geol. 37, 10.*

SPHERULE SIZE DISTRIBUTION AND LITHOLOGY IN THE DALES GORGE SPHERULE BED.

A.E.K. Davatzes[1] and M. Enos[1]. [1]Department of Earth and Environmental Science, Temple University (1901 N. 13th St. Philadelphia, PA 19122) (alix@temple.edu)

Introduction: Models of impact plumes have calculated the size of spherules produced by the condensation and crystallization of molten and vaporized rock [1,2]. Within the Hamersley Group of Western Australia are several spherule layers representative of numerous impacts. The Dales Gorge spherule layer (DGSL) is preserved in a sequence of rocks representative of a low-energy, submarine environment; it is composed of below wave-base, fine-grained siliceous sediments and banded-iron formations [3]. The DGSL is a thin layer of sand-sized spherules formed from an impact event dated to about 2.49 Ga [3]. The spherule layer is distal fall-out of an impact-associated vapor plume and represents a relatively instantaneous depositional event on a global scale [3].

Methods: Four thin sections representative of the thickness of the bed have been petrographically analyzed and >600 spherules counted and measured for long and short axis diameters. Each spherule was classified according to the classification scheme in table 1.

% of Type	Description
15%	**Massive** stilpnomelane; may contain vesicles
43%	Stilpnomelane **rimmed** of K-spar &/or opaques
16%	**Random**ly-oriented K-spar
5%	**Radial**: inward-radiating K-spar
5%	Multiple compositionally distinct **layers**
16%	**Miscellaneous**

Table 1: Spherule types classified based on the classification scheme in [4].

Discussion: All of the spherules in this section had a short to long axis ratio of approximately o.8. Spherule diameters range from 0.05mm to 0.69mm (Fig. 1). This full range was only observed in the miscellaneous category of spherules. The histogram of all types peaks at 0.30-0.35mm (Fig 1B) and the layered spherules, in particular, are tightly clustered around this peak (Fig 1A). This is due to the fact that layered spherules are only identified when the thin section cut is through the center of the spherule. The other spherules types will often be measured as a non-central cut of the spherule, resulting in an underestimate of diameter. Still, it is important to note there are slight variations in spherule types, particularly the shift toward larger spherules in the spherules with a feldspar rim (Fig. 1A). The massive stilpnomelane and randomly-oriented feldspar spherules are shifted to the lower sizes (Fig. 1A), and some of these may be layered spherules cut along the edge.

Though there are some variations by type, they are not nearly as pronounced as what is seen in the Paleoarchean spherule layers in the Barberton greenstone belt [5]. They are also significantly smaller in size as compared to the older Barberton spherules [5]. Comparison of all of the Archean impacts show variations in composition and size distribution consistent with differences in original impactor size and composition as well as target rock composition. Ongoing spherule measurements of separates and microCT scanning is helping to further elucidate the size distribution of spherules.

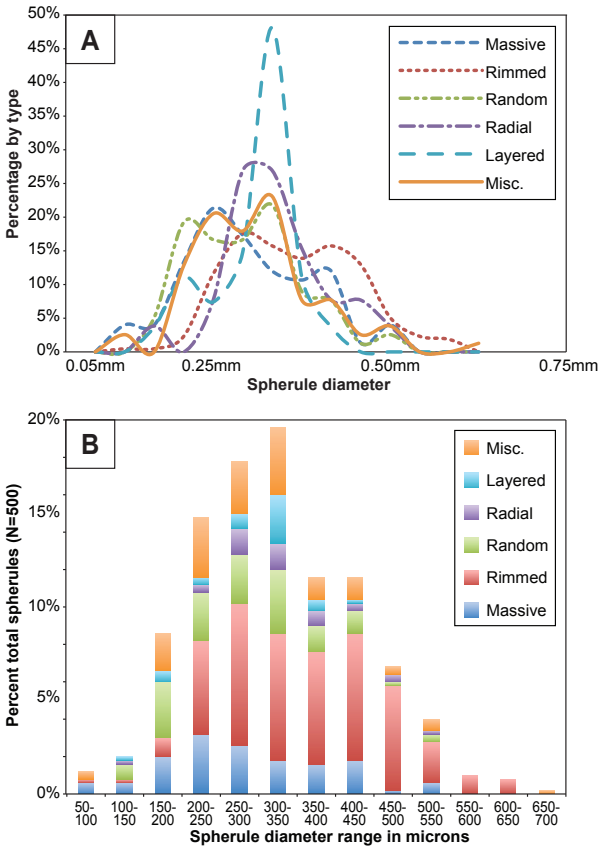

Figure 1: (A) spherule diameter normalized to percentage of type. (B) stacked histogram of spherule types.

References: [1] Melosh and Vickery (1991) *Nature* 350, 494 – 497. [2] Johnson, B.C., Melosh, H.J., (2012) *Icarus* 217, 416-430. [3] Simonson, B.M. et al. (2009) *Precambrian Research* 169, 100-111. [4] Sweeney, D. and Simonson, B.M. (2008) *Meteoritics & Planetary Science* 43, 2073-2087 [5] Davatzes, A. E. (2011) *42nd LPSC Conference*.

Acknowledgments: Funding for fieldwork was provided by the Temple University Provost Summer Research Award to AEKD. Funding for undergraduate research from the Temple UR program.

THE EARLY IMPACT HISTORIES OF METEORITE PARENT BODIES. T. M. Davison[1,2], D. P. O'Brien[3], G. S. Collins[1] and F. J. Ciesla[2], [1]Impacts and Astromaterials Research Centre, Department of Earth Science and Engineering, Imperial College London, London, SW7 2AZ, UK. (thomas.davison@imperial.ac.uk) [2]Department of the Geophysical Sciences, The University of Chicago, 5734 S. Ellis Ave., Chicago, IL 60637, USA. [3]Planetary Science Institute, 1700 E. Ft. Lowell, Ste 106, Tucson, AZ 85719, USA.

Introduction: The early Solar System was a violent place for young planetesimals. Collisions with other planetesimals were common, and would have affected the evolution of the bodies that would go on to become asteroids and meteorite parent bodies. As meteorites provide our strongest evidence of conditions in the early Solar System, a full understanding of the histories of their parent bodies is vital.

Methods: A large number of planetesimals would have been present in the early Solar System, each with their own collisional history determined by a series of chance encounters with other planetesimals, and depend on the number, sizes and timing of the collision events. Therefore the impact history of a parent body through time cannot be solved analytically.

In this Monte Carlo model, the impact histories of many thousands of meteorite parent bodies are simulated: Collisions are allowed to occur on the surface until either the body is disrupted, or 100 Myr of model time has elapsed. The frequency, impactor size and velocity of the impacts are chosen based on simulations of the dynamical and collisional evolution of a population of planetesimals and planetary embryos during planet formation [1, 2, 3]. Two dynamical models were used: one with Jupiter and Saturn on orbits with their current inclination and eccentricity ('EJS') and one with the giant planets on near-circular, coplanar orbits, similar to that in the Nice model ('CJS'). The collateral effects of each collision are determined based on the impact parameters: crater sizes can be determined from crater scaling laws (e.g. [4], and references therein); impact heating [5] and disruption [6] can be estimated using shock physics calculations.

Results: Parent bodies were separated into two categories: those that were catastrophically disrupted within the first 100 Myr, and those that survived 100 Myr without a disruptive impact. For a 100 km radius parent body in the CJS model, on average 7.6% of bodies were disrupted within the first 100 Myr. For those bodies that were not disrupted, ~ 850 collisions with impactors > 150 m in radius were predicted by the model. On average, there was one collision per parent body of impactors > 5 km in radius, and one in five parent bodies would have experienced a collision with an impactor > 10 km in radius.

Both the number of impacts and the specific internal energy increase due to impacts show that the first ~ 10–20 Myr is the most important time for impact heating: the same period that radiogenic heating from short-lived radionuclides (e.g. ^{26}Al) was important.

Discussion: A model for the formation of the CV chondrite parent body [7] to account for the unidirectional magnetic field requires that a parent body of ~ 100 – 300 km radius accreted a crust of ~ 6 – 20 km thickness during heating by ^{26}Al. The interior of the body differentiated, and the surviving, undifferentiated crust was the source of the pristine CV chondrites. The crust must have have remained undisturbed while the parent body was being heated and the magnetic field was in place (~ 10 Myr), to prevent foundering.

In the Monte Carlo model, for 100 km radius parent bodies ~ 5 collisions per parent body penetrated to 6 km. Around one in four parent bodies experienced an impact that penetrated to 20 km. While less than 1% of 100 km radius parent bodies survived the first 10 Myr without a collision penetrating to 6 km, around 80% survived without a collision that penetrated to 20 km. For 250 km parent bodies, more collisions can be expected: ~ 23 collisions per parent body penetrated to 6 km, and each parent body experienced ~ 1 collision that penetrated to 20 km. No 250 km radius parent bodies survived 10 Myr without a collision that penetrated to 6 km, and ~ 40% of bodies survived without a collision that penetrated to 20 km. Therefore, it seems unlikely that the CV parent body could have developed in the way proposed by [7] if the crust was ≤ 6 km thick; our Monte Carlo model predicts that for the CV chondrite model to work, a thicker crust was required. If a 20 km crust was present, around 30 parent bodies of 100 km radius and one body of 250 km radius that matched the CV chondrite criteria would have survived to 100 Myr and remained in the asteroid belt.

We will use the model to further constrain the thermal and impact histories of the H chondrite, CB chondrite and IAB/winonaite parent body.

Acknowledgements: This work was supported by STFC grants ST/J001260/1 & ST/G002452/1 and NASA PGG grants NNX09AG13G & NNX09AE36G.

References: [1] O'Brien D.P. and Greenberg R. (2005) *Icarus*, 178:179–212 [2] O'Brien D.P. (2009) *Icarus*, 203:112–118 [3] Bottke W.F. Jr. et al. (2005) *Icarus*, 179:63–94 [4] Melosh H.J. (1989) *Impact cratering: A geologic process*. Oxford University Press, New York [5] Davison T.M. et al (2010) *Icarus*, 208:468–481 [6] Jutzi M. et al. (2010) *Icarus* 207:54–65 [7] Elkins-Tanton L.T. et al. (2011) *EPSL* 305:1–10

LA-ICP-MS and textural analyses of impact spherules from the 2.54 Ga Bee Gorge spherule layer, Western Australia

A. Deutsch[1], K. Metzler[1], J. Berndt[2], F. Langenhorst[3], [1]Institut f. Planetologie, WWU Münster, Wilhelm-Klemm-Str. 10, D- 48149 Muenster, Germany, deutsca@uni-muenster.de; [2]Institut f. Mineralogie, WWU Münster, D-48149 Münster; [3]Institut f. Geowissenschaften, FSU Jena, D- 07745 Jena, Germany.

Introduction: Impact ejecta deposits are rather rare in the sedimentary record of the Earth but the well-preserved Archean to Paleo-Proterozoic marine deposit in Western Australia and R.S.A. contain up to m-thick impact ejecta layers [1]. While source craters are unconstrained, wide regional distribution and the spherules size argue for large-scale impact events [2].

Rationale, samples & techniques. Two major issues are discussed in the context of these large-scale ejecta layers: (i) where was/is the source crater and what was the composition of the target there, and (ii) how can we interpret the textures of the spherules in terms of temperature, time, and deposition regime. We have analyzed samples S64-1 and Y52-ID, from the the Bee Gorge spherule layer, Hamersley Basin, W.A., using light and electron microscopy, electron microprobe, and laser-ablation mass spectrometry.

Results & discussion. – *Texture and deformation features of the spherules*. As described [3] acicular to lath-shaped K-feldspar is the major phase in the spherules; typically forming an outer rim with radially grown xx or – less frequently – randomly oriented needles in a kind of meshwork. Of special interest are pairs of deformed spherules which appear to be fused together ("agglutinated" [3]) prior to incorporation in their host sediment, and the distinction from deformed spherules, coalescent by compaction and probably pressure solution. We found spherule clusters consisting of 10 or more sub-µm-sized spherules with deformed outlines. The main characteristics of these clusters, making up about 10 vol% of the layer, are: (i) Composed of ≥ 90 vol% of spherules; (ii) very few inter-spherule material; (iii) close-fit textures with mutual spherule deformation; (iv) coexistence of deformed and undeformed spherules; (v) size-sorted spherules, and (vi) few admixed spherule fragments.

If textures of the observed spherule clusters are not due to post-depositional compaction, they can probably be interpreted as result of collision and sticking of melt droplets during ejection, leading to mutual viscous deformation, followed by rapid cooling. If this is correct, a certain fraction of spherules must have passed the water column during deposition already in the shape of clusters. The entire ejecta layer consists of similarly sized spherules which is also true for the spherule clusters. Obviously size sorting have occurred already during flight prior to cluster formation and is not the result of reworking and sorting in the sediment. Interestingly, spherule (chondrule) clusters with the same textural properties have been recently described from unequilibrated ordinary chondrites [4].

Geochemistry. K-spars in and at the outer rim of the spherules, and the matrix show very different trace element budgets, indicating that the matrix represents background sedimentation (Fig.1). In the spherules very rarely low signals for Pt, and Ir were recorded. Except for PG elements, our data on very small volumes are in good agreement with previous results [1].

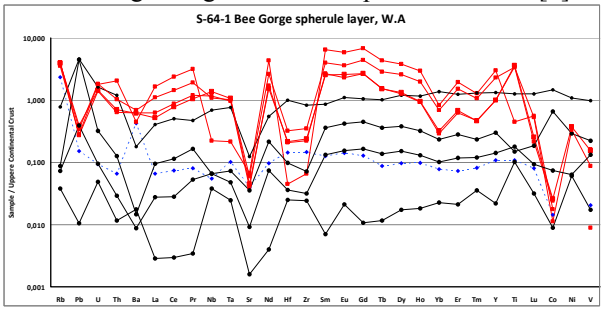

Fig. 1. Element distribution (LA-ICP-MS data) in the K-spar volumes of the spherules (**red**), the spherule center (**blue**), and the fine-grained matrix (**black**) normalized to UCC [5].

In line with [6], we interpret the K-spars xx as pseudomorphs after plag which probably crystallized during cooling of the impact melt droplets similar as proposed for microkrystites. The trace element budget of different spherules is quite similar, indicating a common source, and only minor changes during alteration. If trace element budget is primary, it can not be matched directly to a common crustal lithology but we concur with [1] that the a target basaltic in composition is likely the source for the Bee Gorge spherules.

References. [1] Simonson B.M. et al. (2009) *Precambrian Res* 175, 51-76. [2] Artemieva N. and Simonson B.M. (2012) *LPS* 43, abstr. #1372. [3] Sweeney D. and Simonson B.M. (2008). *MAPS* 43, 2073-2087. [4] Metzler K (2012) *MAPS* 47,2193-2217. [5] Rudnick R.L. and Gao S. (2003) *Treatise in Geochemistry* 3, 1-64 [6] Scally A. and Simonson B.M. (2005) *Aus J Earth Sci* 52, 773-783.

Acknowledgements. We are grateful to Bruce Simonson (Oberlin College) for providing the samples, for very helpful discussion and critique.

MINERALOGY OF IMPACT MELT AT COPERNICUS CRATER: INSIGHTS INTO MELT EVOLUTION AND DIVERSITY Deepak Dhingra and Carle M. Pieters, Geological Sciences, Brown University, 324, Brook Street, Providence, RI 02912 (deepak_dhingra@brown.edu)

Introduction: Impact melt deposits occurring on planetary surfaces could be considered as a tertiary crust formed due to recycling of pre-existing (primary or secondary origin) material. Melt produced at large impact craters could crystallize to form igneous-like rocks or may cool with significant glassy component. Either form can be intimately mixed with clasts of host material. Mineralogy of impact melt has been extensively studied both in terrestrial and extra-terrestrial samples [e.g. 1, 2]. However, remote mineralogical assessment of impact melt in the context of local geology has been less common. On Earth, erosion and vegetation often obscures exposures but geologically young craters on other planetary surfaces provide an excellent opportunity to analyze and evaluate melt mineralogy in great detail. We present a remote sensing perspective of impact melt mineralogy highlighting its spatial diversity as it exists at the geologically young complex crater Copernicus on the Moon, utilizing high spectral and spatial resolution data from recent missions.

Geologic Setting: Copernicus is a 96 Km diameter complex crater with terraced walls and a cluster of central peaks, located on the Earth facing side of the Moon. The crater has an extensive ray system and defines the youngest stratigraphic unit in the lunar time scale. The original target has been suggested [3] to be (from top to bottom): i) Mare Basalts ii) Imbrium Ejecta iii) Megaregolith iv) lower crust containing norites and probably some olivine [e.g. 4]. Copernicus overall composition highlights the originally heterogeneous target with a generally feldspathic northern part and more mafic southern part.

Impact Melt Distribution and Diversity: Subsequent to crater formation impact melt is emplaced in variety of morphological forms such as flows, ponds and spherules. Impact melt at Copernicus spans from the floor (where it occurs extensively) to the walls (occurring as ponds and flows) and beyond the crater rim. Several morphological forms are observed with a different melt to mega-clast ratio and thereby different cooling history. We are mapping this diversity at Copernicus with the objective of understanding impact melt composition, its variation and relationship with the morphological form as well as pre-impact target lithology. Our recent remote sensing analysis at Copernicus [5] has led to the discovery of a large scale mineralogical heterogeneity in the impact melt, likely related to the diverse lithology of the original target.

New Results: Melt mineralogy on the floor of Copernicus shows variability in the crystallinity with the NW quadrant (relatively free of large clasts) displaying relatively stronger spectral signatures as compared to the SW and NE quadrants (densely populated by mega-clasts) which usually display weaker bands. Isolated large boulders at times display detectable absorptions.

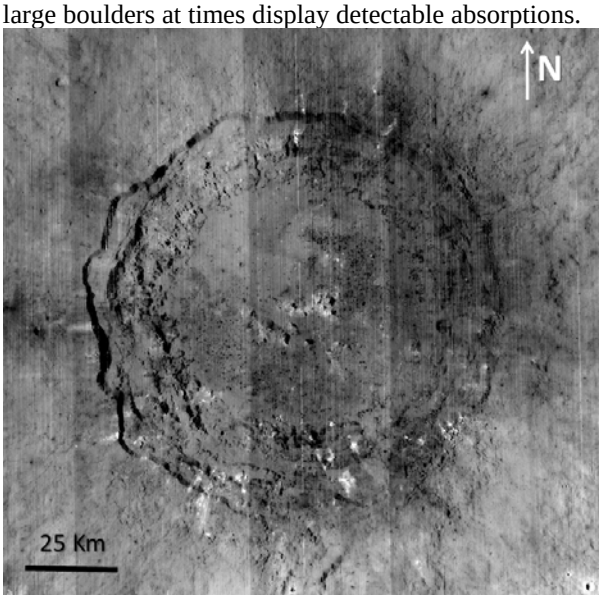

Fig. 1 Moon Mineralogy Mapper (M^3) Near IR ratio mosaic of Copernicus Crater designed to highlight quenched glass and olivine/pyroxene-rich deposits (brightest regions are more abundant)

Morphological mapping suggests that the mega-clasts may be coated by thin-veneer of impact melt which might have cooled faster as compared to the clast-free impact melt in the NW quadrant. As compared to the mega-clast rich NE and SW quadrants, collapse pits on the crater floor (which expose material below the surface) show detectable absorptions suggesting that there is a spectrally neutral coating at the top with more crystalline layers beneath. Impact melt glass displaying spectral bands (referred as quenched glass in spectroscopic studies) has been reported for the NW crater floor, walls and part of the rim from telescopic and spacecraft observations [6,7], and we are also characterizing this component.

References: [1] Ryder G. & P.D. Spudis (1987) *JGR*, **92**(B4), E432-446 [2] Tompkins S. & C.M. Pieters (2010) *MAPS*, **45**,1152-1169 [3] Schmitt H. H. et al. (1967) USGS Map I-515 [4] Pieters C. M. and D. E.Wilhelms (1985) Proc. 15th LPSC, Part 2, J. Geophys. Res., C415–C420 [5] Dhingra et al., (2013) *GRL*, **40**, 1043–1048, [6] Smrekar S. & Pieters C.M. (1985) *Icarus*, **63**, 442-452 [7] Pieters C.M. et al. (1994) *Science*, **266**, 1844-1848

MAPPING THE RITCHEY CRATER CENTRAL UPLIFT, MARS. N. Ding[1, 2], V. J. Bray[2], A. S. McEwen[2], S. S. Mattson[2], M. Chojnacki[2], L. L. Tornabene[3, 4], C. H. Okubo[5], [1]Faculty of Earth Sciences, China University of Geosciences (Wuhan), Wuhan, Hubei 430074, China. [2]Lunar and Planetary Laboratory, University of Arizona, Tucson, Arizona, USA, [3]Dept. of Earth Sciences & Centre for Planetary Science and Exploration, Western University, London, ON N6A 5B7, Canada. [4]SETI Institute, Mountain View, CA 94043, USA. [5]U.S. Geological Survey, Flagstaff, Arizona, USA. (ningding@lpl.arizona.edu)

Introduction: The central uplifts of large impact craters can expose bedrock and ancient crust that are otherwise buried [1, 2]. One example is the central peak of the 79 km diameter Ritchey crater (28.8°S, 309°E). Ritchey Crater is near the boundary between Hesperian ridged plains and Noachian highland terrain units on Mars [3]. In Coprates Chasm ~ 700 km to the north of Ritchey Crater, the deepest exposed bedrock is rich in low-calcium pyroxene (LCP) intruded by olivine-rich dikes, and interpreted as primitive crust produced in a magma ocean, overlain by altered Noachian bedrock rich in phyllosilicates, then topped by Noachian and Hesperian lava flows [4]. The stratigraphy of Argyre basin ~ 700 km south of Ritchey has been interpreted as an olivine and LCP basal unit overlain by bedrock rich in high-calcium pyroxene (HCP), then capped by phyllosilicate-rich Noachian units [5].

The central uplift of Ritchey crater is ~20 km wide. High Resolution Imaging Science Experiment (HiRISE) images of the peak reveal fractured massive bedrock and megabreccia [c.f. 2] with large clasts that appear to have been raised from depth. The stratigraphic uplift in a crater of this size is ~7.7 km [6], comparable to the depth of exposures in Coprates Chasm. Compact Reconnaissance imaging Spectrometer for Mars (CRISM) spectral parameter maps [7] reveal LCP, HCP, olivine, and hydroxylated silicates.

Our goal is to map the 3-dimensional geology of the central uplift of Ritchey and reconstruct the pre-impact stratigraphy, to better understand the Noachian stratigraphy of Mars. We are also mapping impactite deposits on the central uplift to help us constrain the relationship between breccia, pre-existing megabreccia, and other rock units. We update our progress [8] in this abstract.

Results: *Units*: We mapped nine units on Ritchey central uplift: (1) exposed bedrock (BR); (2) large-scale megabrecia (MB); (3) a clast-rich deposit (C) where fractures are either absent or obscured; three units often covered by polygons (interpreted as impactites produced by the Ritchey impact by [2]), namely, (4) polygonal-spot (PS), (5) polygonal-bright (PB), (6) polygonal-dark (PD) terrains, two of which (PS and PD) appear to be draped; (7) unconsolidated aeolian deposits (S); and two bedrock/clast-rich units that are thinly draped by aeolian deposits and are therefore transitional between units (1-3) and unit S, namely (8) a transitional bedrock/megabreccia (TB) unit and (9) a transitional clast-rich deposit (TC). The center of the central uplift contains a cavity ~2 km across. Most of the MB unit appears outside this central cavity, and most of the BR unit lies at even greater distances from it, in the outermost third of the uplift structure. These two units are predominantly exposed on the eastern and southern sides of the uplift. CRISM data for this region shows that most bedrock (BR) exposures are LCP-rich but also contain a small amount of HCP-rich material. The C and TC units are mainly distributed in the outermost parts of the central uplift and extend to the crater floor. Our analysis of CRISM data shows that these units are mainly LCP-rich materials. PS, PB and PD are usually found in lower elevations or on flat terrain within the central uplift and are mainly distributed in the west and north areas of the central uplift. The S unit has a low albedo and recognizable aeolian bedforms (e.g., ripples) found across Mars. The ripples display a regular NW-SE orientation indicating the direction of the prevailing wind.

Structural geology: We find several outcrops of conjugated joints in the northern and southern regions of the central uplift; their directions of greatest principal stress (σ_1) are nearly NNW-SSE. One outcrop, located northwest of the central uplift, exhibits a fault cross-cutting veins or dikes with a left-lateral offset of ~20-25 m. Another region, in the southern part of the central uplift, contains tensional joints. Throughout the entire uplift, joints are primarily confined to the BD and/or TB units, and are interrupted by surrounding units. This phenomenon suggests that these joints formed during the cratering process.

References: [1] Caudill C. M. et al. (2012) *Icarus,* 221, 710. [2] Tornabene L. L. et al., (2012) *3rd Early Mars abstract*. [3] Scott D. H. and Tanaka K. L. (1986) *USGS Map* I-1802-A. [4] Flahaut J. et al. (2012) *Icarus*, 221, 420-435. [5] Buczkowski D.L. et al. (2010) *JGR,* 115, E12011. [6] Grieve R. and Pilkington M. (1996) *AGSO Journal of Australian Geology and Geophysics* 16, 399. [7] Sun V. Z and Milliken R. E. (2013) LPSC 44, #2675. [8] Ding N. et al. (2013) LPSC 44, #2798

ELEMENT PARTITIONING PROCESSES BETWEEN IRON-RICH PROJECTILES AND SILICA-RICH TARGETS IN HYPERVELOCITY IMPACT EXPERIMENTS. M. Ebert[1], L. Hecht[1], A. Deutsch[2], T. Kenkmann[3] [1]Museum für Naturkunde Berlin, D-10115 Berlin, Germany (matthias.ebert@mfn-berlin.de); [2]Institut f. Planetologie, WWU Muenster, D-48149 Muenster, Germany; [3]Institut für Geo- und Umweltnaturwissenschaften, ALU Freiburg, D-79104 Freiburg.

Introduction: The investigation of projectile traces in impact materials is of great value for confirming a impact origin and for reconstructing the type of extra-terrestrial material that penetrated the Earth [1]. In this study we present experimental results about how impact energy, water-saturation of the target, and target porosity affect (i) projectile dissemination into the various impactites, and (ii) partitioning of projectile elements during mixing of projectile and target melts.

Experimental setup: In the context of the MEMIN program [2], we have performed impact experiments at the two-stage acceleration facilities of the Fraunhofer Ernst-Mach-Institute (Freiburg, Germany) using steel D290-1 projectiles, and targets of quartzite and quartz-rich sandstone blocks; some of the latter have been saturated with water. Projectile masses of 0.067 and 7.323 g and an impact velocity of about 5 km*s^{-1} result in impact energies of ~0.76 kJ and 81 kJ, respectively.

Results: During the high dynamic cratering process a large number of molten projectile droplets were incorporated into melts of target material. In general a metal melt coexist with a silicate melt, although the latter may exhibit further separation into immiscible melts at the sub-µm scale (see below).

Element partitioning processes: The target and projectile melts have experienced significant chemical modifications during the impact. Interelement ratios of the projectile tracers Cr, V, Co, Mo, and W within the contaminated target melts are strongly modified from the original ratios in the steel. This fractionation process is most likely the result of differences in the lithophile or siderophile character of the projectile tracer elements, or more precisely, of differences in their reactivity with oxygen [2] during interaction of metal melt with silicate melt. The element map in Fig. 1 clearly shows that Cr (and V) of the projectile droplets nearly totally partition into the quartzite melt, whereas the siderophile Co (Mo and W) almost entirely remain in the projectile droplets. The element ratios in the original steel are significantly changed within the projectile melt droplets.

Effects of experimental conditions: Several impact experiments were carried out with a quartzite target with almost no *porosity*. Electron microprobe investigations of highly shocked ejecta from these experiments suggest enhanced element fractionation processes during the impact compared to the experiments with the sandstone target (0% vs. ~23 % porosity). Partitioning of the projectile elements Cr, V, and especially Fe into the target melt is more enhanced in experiments with quartzite compared to those with sandstone. Some metal droplets are surrounded by a Fe-rich silicate melt (*Lfe*; Fig.1) and small Cr-V-rich minerals (probably spinels). These *Lfe* rims and the Cr-V-rich minerals, however, are completely absent in sandstone experiments at similar impact velocities. Furthermore, the highly shocked ejecta of the quartzite target has a higher amount of silica glasses, a lower content of projectile droplets, and shows often melt textures suggesting liquid immiscibility between Fe-rich and Si-rich silicate melts. Similar features were described for melt rocks of the Wabar crater [3].

The geochemical processes between projectile and target melts were obviously not affected by the degree of *water-saturation* and by the *impact energy*. This is true at least for the applied experimental conditions.

Conclusions: Our laboratory experiments yield results very similar to observations in nature, e.g., at Meteor Crater and the Wabar craters [3, 4]. From our perspective, small scale geochemical processes, like (i) partitioning of projectile elements into target melts, (ii) the associated phase separation into Fe-rich and Si-rich melts, and (iii) strong alteration of the ratios of meteoritic tracer elements in impact melts from the respective ratios in the projectile seem to be common feature during mixing of projectile and target melts.

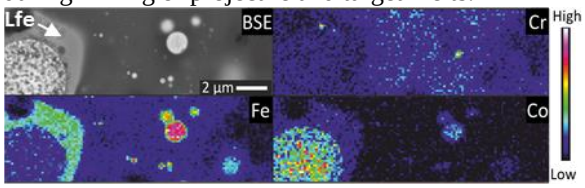

Fig. 1 WDX element maps of a highly shocked ejecta fragment with quartzite melt (dark grey), *Lfe* rim and steel projectile droplets (whitish spheres).

References: [1] Palme H. et al. (1981) *GCA* 45, 2417-2424 [2] Ebert M. et al. (2013) *MAPS* 48, *134-149* [3] Hamann C. et al. (2012) *EPSC* 2012, Abstract #2012-745-1. [4] Mittlefehldt D.W. et al. (2005) *GSA SP* 27, 367-390.

Acknowledgements: This work is supported by the German Science Foundation DFG (He-2893/8-1, Ke-732/18-1, DE-401/23-1).

CRATER FORMATION AFTER SHALLOW IMPACTS – HOW DO ELLIPTICAL CRATERS FORM?

D. Elbeshausen[1] , K. Wünnemann[1] and G. S. Collins[2], [1]Museum für Naturkunde, Invalidenstr. 43, 10115 Berlin, Germany. [2]Department of Earth Science and Engineering, Imperial College London, London SW7 2AZ, UK.
http://www.isale-code.de; dirk.elbeshausen@mfn-berlin.de

Introduction: Elliptical impact craters often exert a fascination, despite (or due to) their rare occurrence among the generally symmetric shape of impact structures on planetary surfaces. Nevertheless, our knowledge on the formation of these craters is limited. Why do some impacts result in a circular crater whereas others form elliptical shapes? How does the formation of elliptical craters differ from those of circular craters? Is the formation process comparable to those of elliptical craters formed at subsonic speeds? How does crater formation work at the transition between circular to elliptical craters? By conducting more than 800 three-dimensional (3D) hydrocodes simulations we investigated these questions in a quantitative manner.

Model stup: We used the 3D-hydrocode iSALE-3D [1,2] for our simulations. Assuming terrestrial gravity conditions (g=9.81 m/s^2) we varied the impact angle α from 90° (vertical impact) to 5°. We used impact velocities of U=8 km/s, 12 km/s, and 18 km/s and varied the projectile diameter L over more than one order of magnitude (L=0.25, 0.5, 1, 2.5, and 4 km). We used the Tillotson equation of state [3] with material properties of granite. We employed a Drucker-Prager rheology model, which assumes shear strength Y_s being a linear function of cohesion, internal friction, and pressure P (Y_s=Y_{coh} + $f \cdot P$). This allows for studying the effect of cohesion (Y_{coh}=0, 5, 20, 100, and 200 MPa) and the coefficient of internal friction (f=0, 0.2, 0.4, 0.5, 0.7, and 1.0) separately and independent from each other.

Results: We were able to reveal how these parameters affect the final shape (ellipticity) of craters. We found that elliptical craters are excavated as a result of shock compression (similar to circular craters, but in contrast to subsonic impacts producing elliptical craters by material displacement). The transition from circular to elliptical crater formation can be roughly described by three different regimes (see Fig. 1). The onset of elliptical impact crater formation happens quite abrupt; the corresponding threshold angle seems to depend on cratering efficiency (ratio of projectile size to crater diameter).

References: [1] Elbeshausen D. and Wünnemann K. (2011). In: Proc. of 11th Hypervelocity Impact Symposium (HVIS), Fraunhofer Verlag. [2] Elbeshausen D. et al. (2009) Icarus, 204 (2), pp. 716–731. [3] Tillotson J.H. (1962). Report GA-3216, General Atomic, San Diego, CA.

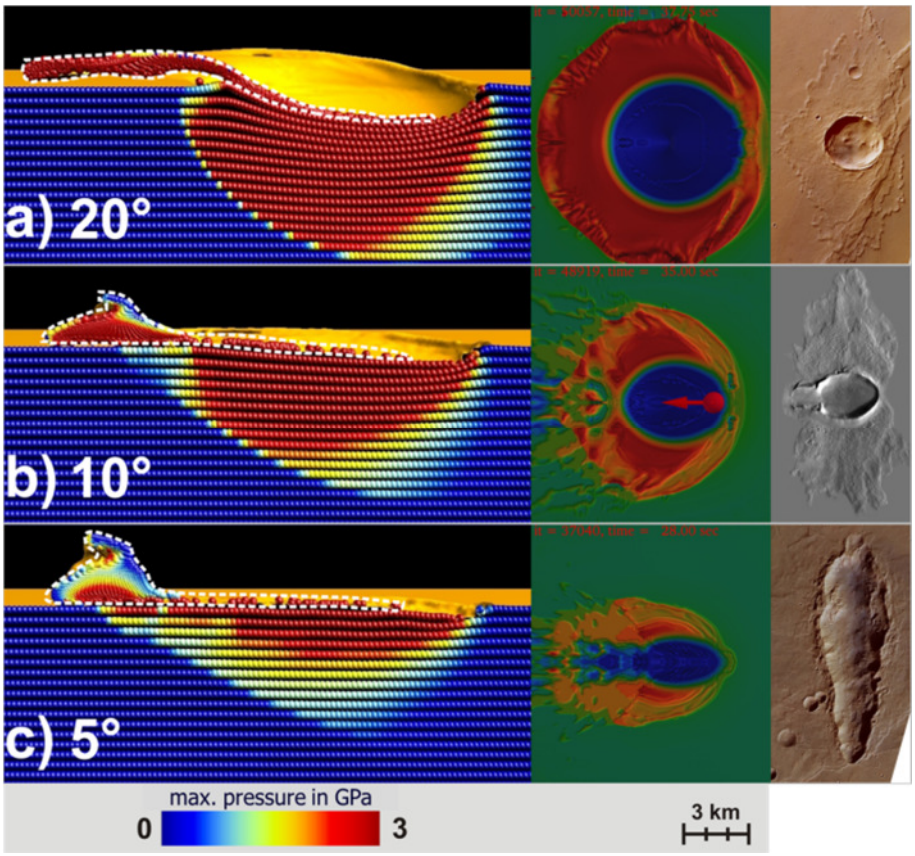

Figure 1: Snapshots of early (left) and late stage crater formation (middle) for three characteristic impact angles (L=4 km, U=8 km/s, Y_{coh}=5 MPa, f=0.3). **Left:** Tracers show peak pressures in a range from 0 GPa (blue) to 3 GPa (red). Tracers belonging to the projectile are framed with a white dashed line. **Middle:** Corresponding craters at a late stage. Projectile material has been removed in post-processing to obtain insights in the "real" crater structure. **Right:** Examples for Martian craters which might be associated with a similar formation process. Top: Crater in the Melas Dorsa region showing an ellipticity of 1.12 (*@ESA/DLR/FU-Berlin, Neukum*). Middle: This crater on Mars shows a butterfly-pattern as well as a secondary structure caused by projectile motion (*©NASA/JPL/ASU*). Bottom: This highly elliptic crater (south of Huygens-Crater) has been formed by an extremely shallow impact event (*©ESA/DLR/FU-Berlin, Neukum*).

Acknowledgment: This work was funded by the Helmholtz-Alliance HA-203 / "Planetary Evolution and Life" by the Helmholtz-Gemeinschaft Deutscher Forschungszentren (HGF).

Modelling Cu-Ni-PGE vein arrays within an Offset Dyke environment of the Sudbury Igneous Complex.

John S. Fedorowich, and Chris O'Connor, Itasca Consulting Canada Inc.

Arrays of Cu-Ni-PGE veins are found within Offset Dykes in the footwall to the Sudbury Igneous Complex, and present an important resource for mining over the last century. The chalcopyrite vein systems have three main elements: 1) a set of discrete failure surfaces which ultimately open as veins; 2) sets of shear fractures and small faults that extend from and are interconnected with the veins demonstrably controlling the vein openings, and 3) fluid over-pressuring as demonstrated by vein geometries.

From their arrangement, shapes, and spacing relationships it is thought that the chalcopyrite arrays are tectonic veins associated with small fault displacements, which were active in the late stages of dyke emplacement. In order to test this hypothesis and to provide an independent measure of vein patterns, a numerical modelling experiment was carried out using the Universal Discrete Element Code (UDEC). Vein simulations were performed in fully coupled mechanical-hydraulic analysis in two orientations; longitudinal and transverse to a vein array. Applied paleostress orientations for the models were obtained from the orientation distribution and shear sense of the small faults that control veins.

Results of the modeling and comparison with vein patterns from various Sudbury deposits are presented.

SHATTER CONES AND ASSOCIATED SHOCK-METAMORPHIC MICRODEFORMATIONS IN MINERALS – THE CASE OF THE SUDBURY IMPACT STRUCTURE, CANADA. L. Ferrière[1] and G. R. Osinski[2], [1]Natural History Museum, Burgring 7, A-1010 Vienna, Austria. (ludovic.ferriere@univie.ac.at), [2]Dept. Earth Sciences/Centre for Planetary Exploration, University of Western Ontario, London, ON, Canada.

Introduction: Shatter cones are the only diagnostic evidence of hypervelocity impact that develop on a macro- to megascopic scale [e.g., 1]. They have been reported in extremely different lithologies, with large variations of cone size (cm to m), and generally occurring in-situ only in the central part of the impact structure. Different models for their formation exist in the literature [2-7], but none of them account for all of the current field observations of shatter cones [7-9].

Here, we report on macroscopic and petrographic investigations of shatter cone samples from the Sudbuy impact structure. This work is part of an ongoing study of shatter cones from several impact structures, combining observations on the occurrence, distribution, and characteristics of shatter cones at the scale of the impact structure with macroscopic and microscopic observations of (shocked) minerals, to infer the course of events that result in the formation of shatter cones.

Results and Discussion: Shatter cones were observed, documented, and sampled at dozens of outcrops (Fig. 1), mainly from the South Range of the Sudbury structure (only a few from the North Range). They mainly occur within quartzites (or metamorphosed sandstones), more rarely in conglomerates, and in a few rare cases in gabbro (reported here for the first time in this lithology). At each outcrop, basic description and structural measurements were recorded. In the laboratory, petrographic and shock metamorphic investigations were conducted using an optical microscope. All together 14 thin sections of shatter cone samples were investigated. The entire area of each thin section was investigated under the optical microscope (with a magnification of 200x), and all mineral grains, especially quartz grains, were subjected to a systematic analysis of their properties.

In term of shatter cone distribution, our observations are very consistent with earlier studies of shatter cone distribution at Sudbury, such as by [10] – but see also [11]. However, with the help of B. Church (UWO, London, Canada), we were able to document an occurrence of shatter cones (up to ~1 m in size) in a quartzite outcrop located at ~35 km away from the outer limit of the Sudbury Igneous Complex, which is of interest in terms of reconstructing the original diameter of the Sudbury structure. In previous studies of shatter cones at Sudbury, they were not reported at such a great distance.

Our petrographic study confirms that microdeformation features occur in shatter cones from the Sudbury structure, including random penetrative fractures and kink bands in micas. It is notable, however, that no grains with either planar fractures (PFs), planar deformation features (PDFs), or feather features, were detected. This is interesting as recent work by [9] have clearly shown that shock-induced deformations in minerals, especially PFs and PDFs in quartz, are relatively abundant in shatter cones. Thus, either the investigated samples did not experienced peak shock pressures high enough to form PFs and/or PDFs, or these features were then annealed. In the present case it is possible that both processes are responsible for the observations.

References: [1] Dietz R. S. (1968) In *Shock metamorphism of natural materials*, French B. M. and Short N. M., Eds, Baltimore: Mono Book Corp. pp. 267–285. [2] Johnson G. P. and Talbot R. J. (1964) Air Force Institute of Technology, USA, 92 pp. [3] Gash P. J. S. (1971) *Nature Phys. Sci., 230*, 32–35. [4] Baratoux D. and Melosh H. J. (2003) *EPSL, 216*, 43–54. [5] Sagy A. et al. (2002) *Nature, 418*, 310–313. [6] Sagy A. et al. (2004) *JGR, 109*, B10209, 20 pp. [7] Wieland F. et al. (2006) *Meteoritics & Planet. Sci., 41*, 1737–1759. [8] Osinski G. R. and Spray J. G. (2006) Proc. 1st Int. Conf. on Impact Cratering in the Solar System, ESA SP-612. [9] Ferrière L. and Osinski G. R. (2010) *LPS XXXXI*, Abstract #1392. [10] Bray J. G. and geological staff (1966) *J. Geol., 74*, 243–245. [11] Osinski et al. (2013) this conference.

Fig. 1: Exposure view of shatter cones in quartzite from the Sudbury structure (Canada).

REVISED FRAGMENTATION MODEL OF PLANET-SIZED COLLISIONS. T. Fujita[1], H. Genda[2], H. Kobayashi[3], H. Tanaka[4], and Y. Abe[1], [1]Department of Earth and Planetary Science, The University of Tokyo (tfujita@eps.s.u-tokyo.ac.jp), [2]Earth-Life Science Institute, Tokyo Institute of Technology, [3]Department of Physics, Nagoya University, [4]Institute of Low Temperature Science, Hokkaido University

Introduction: Collisions between planetesimals or a planetesimal and a protoplanet are thought to occur frequently in the stage of planet formation and let them grow up. The critical impact energy for catastrophic disruption 'Q_D^*', where the largest remnant has half the target mass, has been well investigated under various conditions (e.g., [1]), and such a catastrophic impact was regarded as important process for planet formation (e.g., [2]).

However, recent studies (e.g., [3]) suggested that cratering impacts with specific impact energy much less Q_D^* were also important and the mass of growing planets was limited by such cratering impacts. Therefore, in order to develop the more accurate theory of planet formation, it is important to investigate how much fragments cratering impacts produce.

Here, we perform high-resolution impact simulations in gravity-dominant region. We reestimate Q_D^* and check the resolution convergence, because resolution of the impact calculations in the previous studies seems to be not enough. We also investigate the relation between the total mass of ejected fragments and impact energy.

Method: Using the smoothed particle hydrodynamics method (SPH) [4], we systematically perform the hydrodynamic simulations of collisions between planetesimals at various impact energies with about 5 million SPH particles. We reexamin Q_D^* and derive a scaling law representing a relation between total mass of ejected material and impact energy. Specifically, in our simulations bodies with different size collide head-on or obliquely against 100km- and 10km-diameter bodies at different speed, and the amount of the total mass of ejected material can be calculated.

Results: We find that the newly obtained Q_D^* is about one order of magnitude smaller than that of the previous work [2] due to higher-resolution simulations and the more accurate analytical method. This means collisions between planetesimals or a planetesimal and a protoplanet are more destructive than previously thought.

In the case of collisions with impact energy less than Q_D^*, as shown in Fig.1, the total mass of fragments (M_{frag}) is not linear with the specific impact energy (E_{imp}) due to the curvature of the target sphere. The relation can be described as $M_{frag} \propto E_{imp}^{1.4}$ for 100km-sized target as an example and is different from the expectation of [1]. On the other hand, in the case of collisions with very low impact energy, M_{frag} is linear with E_{imp} because the effect of the curvature is so slight that such collisions can be regarded as like a crater-forming impact; a sphere collides against a flat ground. Therefore, the scaling law representing the relation between M_{frag} and E_{imp} is described based on these two facts. Moreover, we find this scaling law depends upon E_{imp} uniquely. In addition, this scaling law is independent on target size and varied by impact angle.

We will present our analytical method and results of 10km-sized target or the oblique collision in detail on our poster.

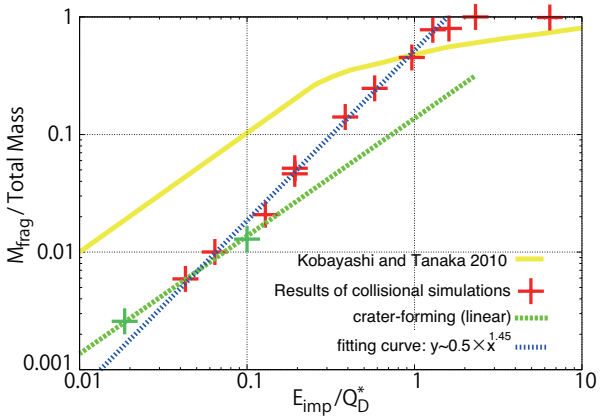

Fig 1. Total mass of fragments (M_{frag}) normalized by total mass as a function of the impact energy (E_{imp}) normalized by Q_D^* in the cases of head-on collision with 100-km sized target. The scaling law we derive is shifted down compared with [1] for $E_{imp}/Q_D^* < 1$.

References:

[1] Benz, W. and Asphaug, E. (1999) *Icarus, 142,* 5. [2] O'Brien, D. P. and Greenberg, R. (2003) *Icarus, 164,* 334. [3] Kobayashi, H. and Tanaka, H. (2010) *Icarus, 206,* 735. [4] Genda, H. et al., (2012) *ApJ, 744,* 137.

IRON REDOX VARIATIONS IN AUSTRALASIAN MUONG NONG-TYPE TEKTITES. G. Giuli[1], M.R. Cicconi[1], A. Trapananti[2], S.G. Eeckhout[3], G. Pratesi[4], E. Paris[1], and C. Koeberl[5]. [1]Scuola di Scienze e Tecnologie, sez. Geologia, Università di Camerino, Italy; E-mail: gabriele.giuli@unicam.it; [2] CNR-IOM OGG c/o ESRF, Grenoble, France; [3]European Synchrotron Radiation Facility (ESRF), Grenoble, France; [4]Dip. Scienze della Terra, Università di Firenze, Italy; [5]University of Vienna and Natural History Museum, Vienna, Austria.

Introduction: Muong Nong-type tektites differ from common splash form tektites by being larger, with irregular blocky shape, having a layered structure, being chemically heterogeneous, and (in some cases) containing undigested precursor minerals. Usually, dark layers are less abundant and, in thin section, they seem embedded in a light-colored matrix. Systematic chemical and physical variations are observable between dark and light colored layers. In particular, light-colored layers display a relatively higher Al and Fe content and a lower Si content with respect to dark layers. Moreover, the light layers have a higher refractive index (see [1] and references therein for a more complete description of Muong Nong-type tektites from the Australasian tektite strewn field).

Previous unpublished XANES data (collected on powder samples obtained by hand-picking separation of dark and light layers) showed small but detectable differences in the Fe oxidation between dark layers and light layers, the former being slightly but reproducibly more oxidized.

A new set of data has been acquired with an X-ray micro-beam on thin sections of 2 Muong Nong-type indochinite samples across the boundary between a dark layer and the light matrix in order to confirm whether or not there are systematic variations of the Fe oxidation state across the layers in the Muong Nong-type tektites. Moreover, 2D maps were collected to show qualitatively the spatial distribution of the Fe oxidation state..

Experimental: The XANES data and 2D XAS maps have been collected at the ID26 and BM08 beamlines respectively (ESRF, Grenoble, F) using a Si (311) monochromator (beam size at the sample of 55 x 120 µm for XANES and 200 x 200 µm for the 2D maps). Background subtracted pre-edge peaks have been fitted with sums of two to three pseudoVoigts components according to the procedure described in [2-3].

Results: Experimental XANES spectra are similar to those of other tektites [2,4,5]. However, reproducible changes occur in the pre-edge peak centroid energy of both samples: spectra collected within the dark layer display a pre-edge peak reproducibly ≈0.2 eV at higher energy than spectra collected within the light matrix. This difference in energy position is >4 times the estimated energy reproducibility and, therefore, is significant. We estimate the $Fe^{3+}/(Fe^{2+}+Fe^{3+})$ ratios in the light matrix and dark layer of the 2 studied samples to be 5 % and 15 % (±5), respectively. Moreover, XRF maps collected for one sample at selected X-ray energies (7400 and 7105 eV and the two pre-edge peak maxima at 7112 and 7114 eV ca.) were used to elaborate maps displaying spatial variations of the pre-edge peak shape related to the Fe redox state. Despite the very small differences in the Fe redox state between dark layers and light matrix, the features present in the maps roughly reproduce the shape and position of the dark streaks, confirming that in the dark streaks Fe is slightly more oxidized than in the light matrix.

References: [1] Koeberl, C. (1992) *Geochimica et Cosmochimica Acta*, 56, 1033-1064; [2] Giuli G. et al. (2002) *Geochimica et Cosmochimica Acta*, 66, 4347-4353; [3] Giuli G. et al. (2011) *American Mineralogist*, 96, 631-636; [4] Giuli G. et al. (2010) *Geological Society of America Special Paper* 465, 645-651; [5] Giuli G. et al.(2010) *Geological Society of America Special Paper* 465, 653-660.

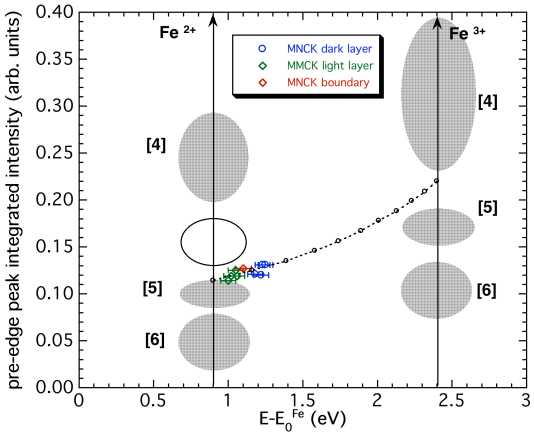

Fig. 1: pre-edge peak integrated intensity vs. centroid energy obtained from Fe K-edge microXANES spectra along a transect through the boundary between a dark streak and light matrix.

MAPPING TERRESTRIAL IMPACT CRATERS WITH THE TANDEM-X DIGITAL ELEVATION MODEL. M. Gottwald[1], T. Fritz[1], H. Breit[1], B. Schättler[1], A. Harris[2], [1] German Aerospace Center, Remote Sensing Technology Institute (DLR-MF), Oberpfaffenhofen, D-82234 Wessling, Germany, manfred.gottwald@dlr.de, [2] German Aerospace Center, Institute of Planetary Research (DLR-PF), Rutherfordstraße 2, 12489 Berlin, Germany

Introduction: We use the global digital elevation model (DEM) generated in the TanDEM-X mission for mapping confirmed terrestrial impact craters. The TanDEM-X mission generates a global DEM with unprecedented properties. It permits both for simple and complex craters detailed investigations of the morphology of the particular structure and of the surrounding terrain of outstanding quality.

Methodology: The DEM derived in the TanDEM-X mission [1] is generated from data of the German X-band TerraSAR-X and TanDEM-X satellites, launched in June 2007 and June 2010, respectively. This DEM achieves global coverage together with an accuracy in the sub-10 m range and a spatial resolution of 12 m at the equator. Thus it exceeds the quality of current elevation models generated from space-borne remote sensing data, e.g., SRTM X-band (15 m / 30 m with limited coverage) considerably.

We apply the TanDEM-X DEM to the impact crater record of the exposed entries in the well-appreciated *Earth Impact Database* of the Planetary and Space Science Center at the University of New Brunswick, Canada [2]. As of April 2013, this database lists 184 entries with 122 being of 'exposed' type. The selected approach provides very high confidence that only structures of confirmed impact origin are analyzed. Our initial purpose is to generate a TanDEM-X impact crater catalogue including, e.g., high precision maps together with cross sections yielding elevation profiles. The catalogue can be used for further detailed studies or the development of search algorithms for potential impact features in selected areas.

Early Assessment: We have already browsed the database of quality monitoring products generated in the DEM processing environment when individual X-band acquisitions are processed to yield the interim raw DEM data, including high resolution DEM images (2D and 3D), at the locations of the exposed *Earth Impact Database* entries. In total we identified 109 sites where the TanDEM-X DEM displays either a simple, complex (mostly eroded) or partially submerged structure. Two exemplary maps, the Haughton impact crater on Devon Island and the recently added Tunnunik structure on Victoria Island are illustrated in Fig. 1. Fig. 2 shows two TanDEM-X DEM elevation profiles for the Haughton impact.

First quantitative conclusions such as relations between detectability and crater properties can be drawn. It is obvious that even in the early assessment based on quicklook-type data the lower detection limit in suitable terrain corresponds to a diameter of only about 100 m.

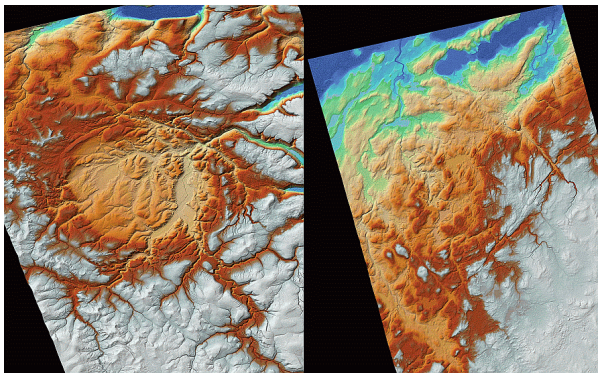

Fig. 1: Two TanDEM-X DEM maps of impact craters with Haughton (left) and Tunnunik (right). Color coding differs in both images.

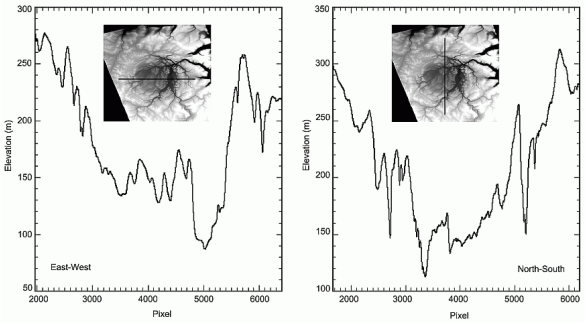

Fig. 2: East-west (left) and north-south (right) elevation profiles through the Haughton crater.

Conclusions: Our preliminary analysis has shown that the TanDEM-X DEM can be a powerful tool for the study of terrestrial impact craters. We will apply our analysis successively to the entire data set as the operational TanDEM-X DEM scenes will become available in 2013-2014 thus generating the intended impact crater catalogue of confirmed structures for reference purposes.

References: [1] Krieger G., et al. (2007) *IEEE Trans. Geosci. Remote Sens., 45, 11,* 3317-3341. [2] Earth Impact Database, Planetary and Space Science Center (PASSC), University of New Brunswick, Canada (http://www.passc.net/).

ONAPING FORMATION, RIES SUEVITE AND MELT-FUEL-COOLANT-INTERACTION (MFCI). R. A. F. Grieve[1], G. R. Osinski [1,2], and A. Chanou[1], [1]Department of Earth Sciences/Centre for Planetary Exploration, University of Western Ontario (rgrieve@nrcan.gc.ca), [2]Department of Physics and Astronomy, University of Western Ontario, 1151 Richmond Street, London, ON, N6A 5B7, Canada.

Introduction: Recently, it was concluded that the ~ 1.5 km thick Onaping Formation, which overlies the Sudbury Igneous Complex (SIC), at the Sudbury impact structure did not conform to the characteristics of "suevite" – an impact melt-bearing breccia first defined at the Ries impact structure, Germany. An alternative working hypothesis for the origin of the Onaping was developed. Namely, it formed through an extended and changing series of MFCI explosions, resulting from the violent interaction of seawater with the still molten impact melt sheet (what was to become the SIC) at Sudbury [1]. Most recently, MFCI has also been offered as the process forming suevite at the Ries impact structure and, by extension "suevite" breccias in a number of other terrestrial impact structures [2, 3]. Here, we review some of the basic characteristics of the Onaping Formation (OF) and the Ries suevite (RS) to assess whether both are likely to have been produced by the same post-impact process of MFCI.

Comparison of Basic Characteristics:

Stratigraphy. The OF lies above the SIC and is internally layered, with different lithologies. Currently, it is subdivided into: Basal Onaping Intrusion, Garson (see, however, [4]), Sandcherry and Dowling members [5], which form a lithological sequence, which, in general, can be traced around the entire Sudbury basin [1, 5]. Previous mapping of the OF also indicated distinct lithological units; although, the terminology differed somewhat. Contacts tend to be gradational between OF members and clasts of Sandcherry occur in the lower Dowling. Internal "breccia in breccia" textures also occur within the Sandcherry and Dowling.

The RS is not known to lie above an impact melt sheet. Although there are variants of the RS, they are determined less by distinct lithological and stratigraphic differences but more by geologic context, e.g., "crater suevite" in the central basin and "outer suevite" overlying Bunte breccia ejecta [2, 3].

Internal structures. While initially appearing chaotic, the OF is generally bedded and graded, becoming finer with stratigraphic height [5, 6]. Graded bedding becomes more pronounced towards the top of the OF. Within individual members of the, OF there are identifiable variants, such as the "Equant Shard" and Fluvial" variants within the Sandcherry member [5].

The RS is generally regarded as being non-sorted, with only isolated local internal structure. There is, however, a 17 m thick "graded suevite", within the crater suevite, which has been, most recently, attributed to reworking and water deposition [2, 3].

Shock metamorphism. Although it was the discovery of PDFs in quartz in grantoid clasts in the OF that was the original basis for designating the OF as a "suevite" [7], shock effects are relatively rare in the OF. Peredery [8] noted that 90% of the lithic clasts in the OF were unshocked. To date, shock effects in mineral clasts in the OF has never been documented [1, D. Ames, pers. comm., 2009]. In contrast, only 10% of the lithic clasts in the (outer) RS are unshocked [9]. Although the lithic clasts in the crater RS appear to record somewhat lower grades of shock [2], shock effects are also present in mineral clasts in the RS.

"Melt" clasts. Technically, there are no "melt" clasts in the OF, as they are completely devitrified. The "vitric" clasts in any particular sample, however, tend to have similar shapes (which vary between lithologies) and sizes [1, 5]. They also do not contain lithic or mineral clasts.

In contrast, the melt clasts in the RS have "a wide range of sizes, shapes, and textures" [2]. In some cases in the (outer) RS, they have preferred orientations, indicative of lateral flow [10]. In addition, the melt clasts in the RS contain relatively abundant mineral and lithic clasts, often displaying shock effects.

There is also a major difference in the geochemical variation between individual "melt" particles in the OF compared to the RS [5, 2], although hydrothermal alteration is a complicating factor in the OF [5].

Concluding remarks: Different petrography implies different petrogenesis. Given the major differences in the basic characteristics of the OF and RS, it is difficult to reconcile that they had the same origin through a MFCI process. Either the interpretation of the MFCI origin of the OF or the RS is incorrect or, perhaps, both are incorrect and other process(es) are responsible. Clearly, further work and discussion is needed.

References: [1] Grieve R. A. F. et al. (2010) *MAPS, 45*, 759-782. [2] Stöffler D. et al. (2013) *MAPS, 48, 1-75.* [3] Artemevia N.A. (2013) *MAPS, 48, doi:10.111/maps.12085.* [4] Coulter et al. (2013) this conference. [5] Ames D. E et al. (2008) *Econ. Geol. 103, 1057-1077.* [6] Muir T. L. (1984) *OGS Sp. Pap. 1, 449-489.* [7] French B. M. (1967) *Sci., 156, 1094-1098.* [8] Peredery W. V. (1972) *GAC Sp. Pap. 10, 49-59.* [9] Engelhardt W. (1997) *MAPS, 32, 545-554.* [10] Meyer C. (2011) *BGSA, 123, 2312-2319.*

NUMERICAL MODELING OF SEISMIC SIGNALS GENERATED BY HYPERVELOCITY IMPACTS IN COMPARISON TO EXPERIMENTAL OBSERVATIONS N. Güldemeister[1], D. Moser[2], K. Wünnemann[1], T. Hoerth[3] and F. Schäfer[3], [1]Museum für Naturkunde, Leibniz-Institut für Evolutions- und Biodiversitätsforschung, Berlin, Germany. (nicole.gueldemeister@mfn-berlin.de) [2]Technische Universität München, Non-destructive Testing Laboratory, München, Germany. [3]Fraunhofer-Institute for High-Speed Dynamics, Freiburg, Germany.

Introduction: Meteorite impacts can be considered as a source for seismic shaking similar to earthquakes. Shock waves that attenuate and turn into seismic waves result in seismic signals that have been recorded in explosion experiments [1] and in hydrocode models of large impact events [2]. To determine how much of the kinetic energy E_{kin} of the impactor is turned into seismic energy E_{seis} can be investigated experimentally or by numerical models. The ratio of E_{seis}/E_{kin} is the so-called seismic efficiency k which depends on material properties and is usually estimated to range between 10^{-2} and 10^{-6} [1,3].
In the framework of the "MEMIN" (multidisciplinary experimental and modeling impact crater research network) project the stress wave was recorded in a suite of hypervelocity impact experiments on a decimeter scale [4] by acoustic emission (AE) technique and newly developed pressure gauges. An important complementary method to analyze wave propagation is numerical modelling. The study aims at the validation and calibration of material models against static observations (US tomography) and dynamic measurements of the acoustic signal. Considering a nonporous quartzite and a porous sandstone target we focus on the detection of the propagation of the elastic wave. In a further step these data may be used to quantify the seismic efficiency of hypervelocity impacts.

Methods: We used special AE transducers attached to all sides of the target block at different distances from the impact point. Additionally, we employed pressure gauges, developed and manufactured at Fraunhofer EMI that allow for relating the measured voltage signal with mechanical stress amplitudes. The experimental setup enables to determine the attenuation of the signal with distance. For the numerical models we used the multi-material, multi-rheology hydrocode iSALE [e.g. 5] coupled with ANEOS [6] for quartzite [7] and the ε-α compaction model [5, 8]. The model accounts for the linear dependency of wave velocity on porosity [8]. Elastic wave velocities were determined to be 5000 m/s for nonporous quartzite and 2800 m/s for porous sandstone by ultrasound measurements before the experiment. Numerical gauges recorded thermodynamic and mechanical parameters as a function of time. Thus, the elastic waves and the arrival of the first wave signal can be analyzed.

Results: First-arrival-times of impact-induced waves picked from time-series recorded at impact experiments into quartzite and sandstone targets are plotted vs. distance in Fig. 1. We obtained a wave velocity of about 5090 m/s experimentally and 4900 m/s numerically for the quartzite target (Fig. 1). For the sandstone target the velocity is 2700 m/s in the experiment and 2900 m/s in the numerical model (Fig.1). The pressure gauges yielded a velocity of about 2900 m/s. The dynamic measurements are all in excess of the US velocity of 5000m/s (quartzite) and 2800 m/s (sandstone). Generally, we find a good agreement between numerical and experimental data in terms of the arrival time and signal phase. We estimated the seismic efficiency k of $2 \cdot 10^{-2}$ for quartzite and of $3 \cdot 10^{-4}$ for sandstone using the expressions in [1,3]. The seismic efficiency is significantly smaller for porous targets and thus less seismic energy is induced.

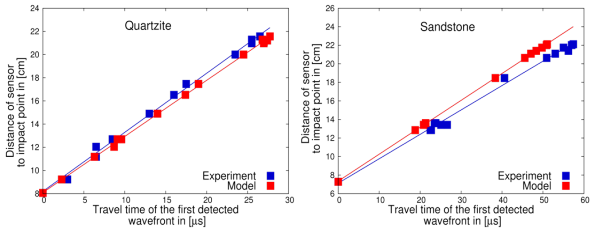

Fig. 1: Linear propagation of the elastic wave front. The plot shows the distances of different sensors versus first arrival time for quartzite (**left**) and sandstone (**right**).

Discussion: It is in general possible to use acoustic emission technique to record the seismic signal during laboratory impact experiments. The dynamically obtained results (AE, pressure gauges and numerical model) verify static ultrasound measurements. The experimentally determined propagation speed of the seismic signal during impact events agrees well with numerical models for quartzite and sandstone targets. The propagation velocity of the elastic wave is reduced in porous material. Thus experiments on the laboratory scale enable a good validation and calibration of numerical models against experimental observations. Additionally, we will use special sensors to determine pressure amplitudes to further calibrate our material models. Rigorously tested material models will enable to quantify the seismic efficiency of meteorite impacts by numerical models. The present results are generally consistent with estimates from the literature. However, further improvements will allow for a much more accurate determination of seismic shaking generated by meteorite impact.

Acknowledgements: This work was funded by DGF grant WU 355/6-1.

References: [1] Schultz P.H. and Gault D.E. (1975) *Earth, Moon Planets, 12*, 2, 159–177. [2] Ivanov B.A. (2004) *Sol. Sys. Res., 39*,381-409. [3] Richardson J.E. et al. (2005) *Icarus, 179*, 325-349. [4] Kenkmann T. et al. (2011) *MAPS, 46*, 890-902, 2011. [5] Wünnemann K. et al. (2006) *Icarus, 180*, 514–527. [6] Thompson S. L. and Lauson H. S. (1972) SC-RR-71 0714, 119pp. [7] Melosh H. J. (2007) *MAPS*, 42: 2035–2182. [8] Collins G.S. et al. (2011) *Int. J. Imp. Eng., 38*, 434-439.

LIQUID IMMISCIBILITY AND DISEQUILIBRIUM TEXTURES IN QUENCHED IMPACT MELT OF THE WABAR AND TENOUMER CRATERS. L. Hecht[1,2], C. Hamann[1,2], D. Schultze[3], M. Ebert[1,2], and W.U. Reimold[1], and R. Wirth [4] [1]Museum für Naturkunde Berlin (MfN), D-10115 Berlin (lutz.hecht@mfn-berlin.de), Germany, [2]Freie Universität Berlin, Institut für Geologische Wissenschaften, D-12249 Berlin, Germany, [3]Technische Universität Berlin, Angewandte Geowissenschaften, D-13355 Berlin, Germany, [4]Deutsches GeoForschungs-Zentrum (GFZ), D-14473 Potsdam, Germany.

Introduction: Preserved heterogeneities in quenched impact melt may serve as a tool to better understand its genesis. Heterogeneity of impact melt may have several reasons including incomplete homogenization of target lithologies, variation in the amount of admixed meteoritic material, as well as subsequent fractionation or alteration process during cooling and crystallization [1]. Liquid immiscibility has rarely been described for impact melts but is likely more common than previously thought. Impact melt of two craters or crater fields have been studied to better understand the causes of impact melt heterogeneity and the processes of chemical target-projectile mixing.

Wabar impact melt: The impact glass sample from the Wabar craters (Saudi Arabia) is composed of a highly siliceous, vesicular, and texturally heterogeneous glass with flow bands and schlieren of more or less Fe-rich glass that resembles the black melt variety of [2]. In detail, Wabar black melt is composed of an emulsion of three compositionally different melts that quenched to a phase-separated glass (Fig. 1): It is dominated by a highly siliceous glassy matrix (Lsi) that contains ubiquitously and homogenously dispersed droplets and spheres of a Fe- and Ca-rich ultrabasic glass (Lfe), and numerous, but lesser frequent, metallic FeNi-spheres. Around large FeNi-spheres (>10 μm), corona-like structures occur (Fig. 1) composed of Lfe with ~20 vol% of small (1–4 μm) Lsi droplets. These textures suggest that significant amounts of Fe were supplied from the meteoritic FeNi-spheres when they mechanically mixed with target melt. The strong increase in Fe induced liquid immiscibility with various ratios of Lfe/Lsi.

Tenoumer impact melt: Impact melt bombs from the Tenoumer crater (Mauritania) range from andesite to basaltic andesite in composition and were mainly formed from a mixture granitoid and mafic target rocks [3,4]. Depending on the whole rock composition the impact melt is composed of various amount of mainly plagioclase (pl), clinopyroxene (cpx), orthopyroxene (opx), olivine (ol), fe-oxides, and interstitial glass. The textures (e.g. atoll-shaped olivine, acicular px and pl) and mineral assemblages indicate strong disequilibriaum conditions during crystallization. Rapid crystallization was also likely the cause of phase separation into a Ca- and Fe-rich melt (Lfe) and a Si- and K-rich melt (Lsi) observed within the interstitial glass matrix (Fig. 2). Furthermore, the Lfe may itself show crystallization of Ca-Fe-rich minerals.

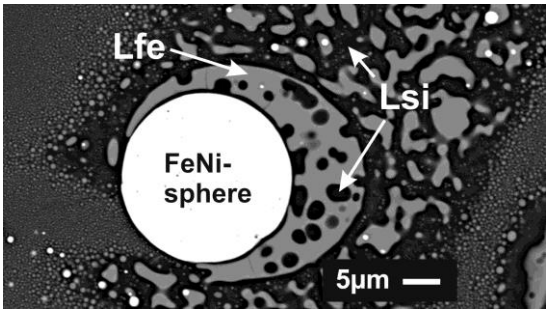

Fig.1 BSE image of Wabar impact glass. Abbreviations see text.

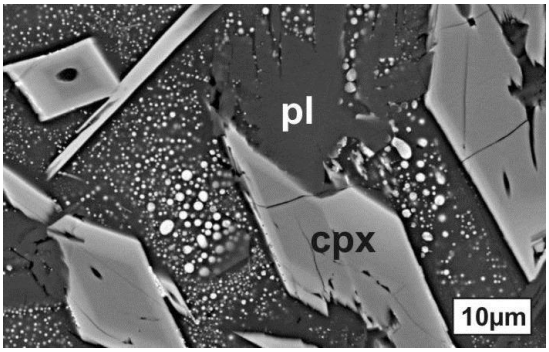

Fig.2 BSE image of Tenoumer impact melt rock. White droplets are Lfe in Lsi. Abbreviations see text.

Conclusions: Phase separation into coexisting liquids may occur if the melt composition is shifted (towards a two-liquid field) due to mixing of different target rocks or rapid crystallization as in the case of the Tenoumer impact melt. In case of the Wabar impact melt liquid immiscibility is a consequence of chemical interaction between projectile (Fe meteorite) and target melt that were mechanically mixed during or before cooling. The emulsion textures and relative proportions of Lfe and Lsi document the successive supply of the meteoritic material and associated chemical fractionation processes.

References: [1] Koeberl C. et al. (2013) *Elements, 8,* 37-42. [2] Hörz F. et al. (1989) *Proc. Lunar Sci. Conf. 19th,* 697–709. #1522. [3] Pratesit G. et al. (2005) *Meteoritics & Planet. Sci., 40,* 1653-1672., [4] Fudali R.F. (1974*) J. Geophys. Res., 79,* 2115-2121.

New data on the Belize tektites. V.H. Hoffmann[1,2], M. Kaliwoda[3], R. Hochleitner[3], J.H. Cornec[4],. M. Funaki[5]. [1]Faculty of Geosciences, Dept. Geo.-Env. Sciences, Univ. Munich, Germany, [2]Dept. Geosciences, Univ. Tuebingen; [3]Mineralogical State Collection, Munich, Germany ; [4]1867 S. Marion St., Denver CO 80210; [5]NIPR, Tokyo, Japan; Email: viktor.hoffmann@alice.de

Introduction:

New findings of apparent tektites have been made in Belize during the last years, probably in situ, and the existence of a Central American tektite strewn field was reported [1,2]. Two investigated Belize tektites gave an Ar-Ar age of 820 ± 40 ka [3,4], recently a slightly younger age of about 780 ka could be obtained by [5]. Both radiometric age constraints are indistinguishable from the ages of the Australite-Indochinite tektite strewn field (~770 ka). However, additional geochemical studies on Belize tektites reported different signatures in comparison to the Australite-Indochinite tektites. Pantasma structure in Nicaragua was proposed as a possible impact crater [6].

Methodology

A Belize tektite sample was investigated by magnetic means and LASER Micro Raman Spectroscopy within our pilot study.

A set of magnetic parameters has been studied: NRM (natural magnetic remanence), IRM (isothermal magnetic remanences), magnetic susceptibility (at various fields and frequencies). The magnetic signature of the Belize tektite will be compared with published and new original data obtained on tektites and other natural glasses [7].

A Horiba Xplora Integrated confocal LASER micro-Raman system was used; most of our investigations were performed with the 532 nm LASER. Magnifications were between 100 and 1000x, a long-distance 100x lens was used in general. Acquisition times were 3-5 sec with accumulation numbers of 2-5.

Results and interpretation

The NRM and IRM values (mass specific in 10^{-3} Am^2/kg) obtained on the Belize tektite (NRM: 7.96, IRM 19.9-26.4) were found to be much higher than those of the other tektites investigated or published so far (NRM in the range of 10^{-6} to 10^{-9}; IRM in the range of 10^{-4} to 10^{-7}). Our Belize tektite sample was artificially magnetized (hand magnet?). Magnetic remanences can be carried only by ferro(i) magnetic phases being present in a sample. The Belize tektite should contain significant amounts on ferro(i) magnetic material (eg native iron or iron oxides; native iron blebs are known from other tektites). Optical microscopy showed numerous (sub-) micron-sized opaque particles, some of them could be native iron (under investigation). The NRM/IRM properties clearly discriminate our Belize tektite sample from all other known tektites to our best knowledge [own data and 8-10].

Magnetic susceptibility value (137 10^{-9} m^3/kg, mass specific) of the Belize sample is also higher than that of most of the other investigated tektites and compares well with the values of the Tikal glasses/tektites [own data and 8-11]: Tikal glass mean value 120, range 109-134 [8], range of other tektites 40-117), reflecting the higher content of Fe-bearing phases in our sample (see above).

LASER micro Raman spectroscopy gave the typical spectra of natural silica-rich glasses which are characterized by the following typical features [7], fig. 1: (i) Quite noisy signal showing more or less high background, (ii) high fluorescence background at higher wave numbers (from 1000 1/cm), (iii) two broad bands centred around 450-600 1/cm and 850-1100 1/cm

The high fluorescence background is an indicator of the high degree of amorphization. Additionally, sharp Raman bands are observed in the Belize tektite at higher wave numbers in some cases, similar to the features reported for example in impactites or fulgurites[7 and refs. herein].

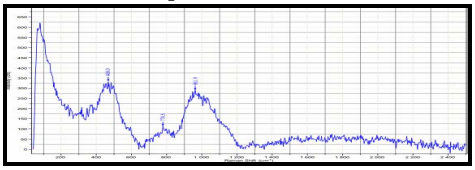

Fig. 1: Typical Raman spectrum found on a Belize tektite.

Currently a number of additional Belize tektites are under investigation within our project. We hope that this will provide a sufficient database to allow further interpretations and conclusions in terms of the potential existence of a new strewn field or a link to the Australasian tektite strewn field.

References

[1] Povenmire H. et al., 2011. 42nd LPSC, #1224.[2] Cornec J., Cornec L., 2010. The Sequel. [3] Povenmire H. et al., 2012. 43rd LPSC, #1260. [4] Schwarz W.H. et al., 2012. Paneth Coll., #0210. [5] Gantert N. et al., 2012. Paneth Coll., #0190. [6] http://www.pantasma.com [7] Hoffmann V. et al., 2013. Corals 2013, Vienna. [8] Senftle F.E. et al., 2000. JGR 105/B8, 18921-18925. [9] De Gasparis A.A., et al., 1975. Geology 3, 605-607 [10] Senftle F.E., Thorpe A., 1959. GCA 17, 234-247. [11] Werner T., Borradaile G.J., 1998. PEPI 108, 235-243.

OLDEST IMPACT STRUCTURES ON EARTH – THE CASE STUDY OF THE SUAVJÄRVI STRUCTURE (RUSSIA). M. S. Huber[1], J. Plado[2], and L. Ferrière[3], [1]University of Vienna, Vienna, Austria, (matthew.huber@univie.ac.at), [2]University of Tartu, Tartu, Estonia, [3]Natural History Museum, Vienna, Austria.

Introduction: The so-called Suavjärvi structure is considered to be the oldest confirmed impact structure on Earth [e.g., 1]. It is located in Karelia, Russia (63°07' N, 33°23' E) in a somewhat remote area. It was first described in 1986 [2], and more recently a publication written in English [3], somewhat expanded the previous arguments that were proposed earlier in [2]. A field expedition was organized to the Suavjärvi structure to revisit the previously described localities NE of the lake (and a few additional exposures), but we were unable to reproduce any of the field observations. No evidence of impact metamorphism was detected.

Background: The Suavjärvi structure has been described as an impact structure, with a target consisting of Archean crystalline basement rocks of the Svecofennian Shield and an infill of "megabreccia" overlain by Jatuli Formation conglomerates. These conglomerates were used to constrain the age of the structure to 2200-2700 Ma [3] (An age of 2400 Ma is given by [2]; age also listed in [1]; however, no justification for this age is provided). The structure is located around the ~3-km wide Lake Suavjärvi, with an "apparent diameter" of 16 km based on a poorly illustrated Landsat image [3]. However, no circular features appear on recent satellite imagery. Microphotographs of quartz grains described as "shocked quartz grains" are used by [2, 3] as an evidence of shock metamorphism.

Field Campaign: In July, 2012, we spent one week at the Suavjärvi structure. Prior to the field investigation, a map from an earlier expedition was obtained from M. Naumov (VSEGEI) that included the locations of outcrops. A large number of these outcrops were visited, in addition to traverses around the Lake Suavjärvi to any apparent outcrops that could be found. The area is wet, heavily vegetated, low-lying land, with relatively few outcrops.

The outcrops labeled on the map as "polymict impact breccia", and referred as being a "megabreccia" [2, 3], were found to consist primarily of granite and schist. Although the outcropping rocks had clearly undergone metamorphic deformation (folds and faults were clearly visible), they could not be described as a breccia, but rather entire outcrops consisting of massive granite or schist. The so-called "polymict impact breccia" and the "Archean basement" outcrops were indistinguishable in the field, and very few outcrops of Jatulian sediments were found.

Samples: Oriented rock samples were drilled from outcrops. So far, ten thin sections were prepared and carefully investigated for shock metamorphism. No shocked quartz grains were detected in these samples.

Interpretation: Neither evidence from our field campaign, nor evidence from our thin section investigations suggest an impact origin for the Suavjärvi structure. No "key point" of evidence reported by [2, 3] could be reproduced; There is no "megabreccia" or "polymict impact breccia" at the structure, and shocked quartz grains could not be found. We find no evidence to support the conclusion that the Suavjärvi structure was generated by a hypervelocity impact.

The structure, therefore, appears to be representative of the general geology of the region. Lake Suavjärvi is likely a post-glacial lake. The few "shocked quartz grain(s)" that were described in [2 & 3] are unconvincing as being shocked, and perhaps represent quartz grains with metamorphic deformation lamellae, which can sometimes be mistaken for shock lamellae [e.g., 4]. Thus, we recommend that the samples identified to contain "shocked quartz" be studied further. Based on our observations, we recommend the Suavjärvi structure not be considered an impact structure unless convincing evidence is provided.

Discussion: Accepted forms of evidence of impact structures are well established [e.g., 4]. Amongst the evidences that are accepted for demonstrating hypervelocity impact, shocked quartz are often taken as the most convincing. However, a number of studies, including [2, 3] and [5], provide photomicrographs of microstructures that are unlikely to be shocked quartz. We recommend that all impact structures be confirmed only if full details of the evidence of shock metamorphism are made available, including measurements of "shock lamellae" in quartz, complete with images of the grains, and preferably with techniques in addition to optical microscopy to confirm the interpretation.

Acknowledgments: We would like to thank the Barringers for the Barringer Family Fund for Meteorite Impact Research and M. Naumov for providing the outcrop map that helped make this study possible.

References: [1] Earth Impact Database. [2] Maschak M. S., Orlova J. V. (1986) *Meteoritika, 45*, 137–141. [3] Maschak M. S., Naumov M. V. (2012) *MAPS, 47*, 1644–1658. [4] French B. M., Koeberl C. (2010) *Earth-Sci. Rev., 98*, 123–170. [5] Garde et al. (2012) *EPSL, 337–338*, 197–210.

A NESTED OR COMPOSITE SHATTER CONE STRUCTURE IN THE SOUTH RANGE OF SUDBURY. D. M. Hurwitz[1], M. Zanetti[2], M. P. Lucas[3], D. Anders[4], G. Kramer[1], O. Thomson[5], D. A. Kring[1], G. R. Osinski[4]. [1]LPI, Center for Lunar Science and Exploration, Houston, TX; [2]Dept. Earth and Planetary Sciences, Washington Univ., MO; [3]Dept. of Earth and Planetary Sciences, Univ. of Tennessee, TN; [4]Centre for Planetary Science and Exploration, Univ. Western Ontario; [5]Univ. Puerto Rico Mayagüez

Introduction: The 1.85 Ga Sudbury impact structure, Ontario, Canada, ranks among the largest impact structures on Earth with an apparent diameter of ~200 km [1]. Sudbury is known for its well-developed shatter cones [2], features that indicate deformation by impact-induced shock waves [e.g., 3]. Early mapping efforts indicate that shatter cones developed in a belt up to ~18 km wide around the basin [4-6], generally confined to brecciated target rocks that bound the central Sudbury Igneous Complex. During a recent effort to update these distribution maps [7], we identified a possible composite cone containing smaller nested shatter cones in an outcrop located in the southeast quadrant of Sudbury (coordinates 46.5309°N, 80.8421°W). Similar composite cones have also been identified in association with the Vredefort structure [e.g., 8,9].

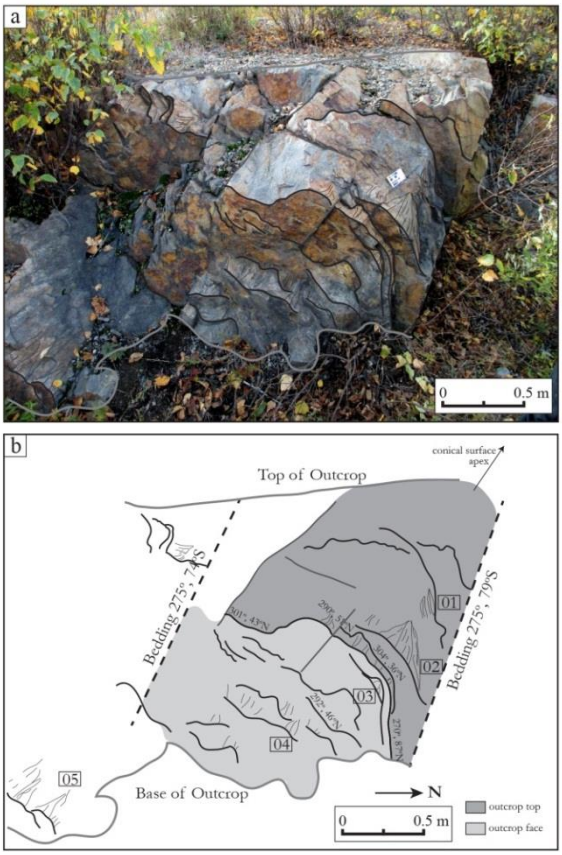

Figure 1: (a) Nested shatter cones in this outcrop are interpreted to represent a composite cone. (b) Sketch of the outcrop shown in (a), showing locations of secondary (parasitic) shatter cones (thin black lines).

Figure 2: Parasitic shatter cones on the side of the outcrop (feature 01, Fig. 1b). Lineations converge at an apex, a characteristic trait of shatter cones.

Observations: The survey area is within the South Range of the Sudbury impact structure, northeast of the city of Sudbury. Outcrops in this area contain target metasediments and quartzites. In one location (Fig. 1), there are a series of stacked, curvilinear foliations, some of which contain clusters of lineations (Fig. 1b). In five of these identified clusters, the lineations approach convergence, a texture that is consistent with well-developed shatter cones (e.g., Fig. 2). We measured trends and plunges for clustered lineations to identify trends in shatter cone orientation.

Interpretations: Observations suggest that this outcrop is a swarm of shatter cones oriented around a central cone-shaped core. We therefore interpret this layered sequence of embedded shatter cones as a single large, ≥1.5 m wide composite cone. Trends of parasitic shatter cone axes appear to be correlated with that of the larger composite cone, with small cone axes pointing up and towards the apex of the composite cone. The composite cone is consistent with formation from a shock wave radiating from a point source that was locally modified to produce a diffraction-like pattern of nested cones.

References: [1] Grieve et al. (2010), *MaPS*, *45*, 759; [2] Dietz and Butler (1964), *Nature*, *204*, 280; [3] Gash, (1971), *Nature Phys. Sci.*, *230*, 32; [4] Bray, et al. (1966), *J. Geology*, *74*, 243; [5] Dietz, (1972), *Geol. Assoc. Canada, Spec. Paper 10*, 29; [6] French (1972), *Geol. Assoc. Canada, Spec. Paper 10*, 19; [7] Osinski et al. (2013) *Large Meteorit. Impact*, *5*, this meeting; [8] Albat and Mayer (1989), *Tectonophys.*, *162*, 265; [9] Wieland et al. (2006) *MaPS*, *41*, 1737.

JETTING DURING THE VERTICAL IMPACT OF A SPHERICAL PROJECTILE. B. C. Johnson[1] and H. J. Melosh[1,2], [1]Department of Physics, Purdue University, 525 Northwestern Avenue West Lafayette, IN 47907, USA (johns477@purdue.edu), [2]Department of Earth, Atmospheric, and Planetary Sciences, Purdue University, 550 Stadium Mall Drive, West Lafayette, IN 47907, USA.

Introduction: Early in the contact stage of an impact, highly shocked luminous material is ejected at low angles forming an impact flash [1]. The impact flash forms when a jet of material squirts from the contact point of the target and the projectile. This jetted material reaches velocities greater than the impact velocity. Although jetting during the oblique convergence of two thin plates (often driven by shaped charges) [2] is well studied, the process of jetting in bolide and planetesimal impacts has received little attention [3,4]. Here we present the first numerical models that resolve jetting during impacts of spherical projectiles on flat targets.

Methods: We use the axisymmetric iSALE hydrocode to simulate a 10 km diameter impactor striking a half space target. We study impact velocities ranging from 2-20 km/s, stepping by 2km/s. For this preliminary study, we use the Tillotson equation of state for Aluminum to represent both the target and the projectile [5]. As we are only interested in the most highly shocked high velocity material, we do not consider any material strength.

To best resolve the jetting process, our models require the unprecedented resolution of 6.35 m or 800 cells per projectile radius. Although we include the gravitational acceleration of Earth and use a fixed impactor size, the high velocities of jetted material allow us to scale our results using hydrodynamic similarity.

Results: In the oblique convergence of thin plates, jetting occurs when the shock velocity is greater than the velocity at which the collision point moves along the plates [2]. Using the Hugoniot for the material of interest, this jetting criterion yields a critical impact angle, below which jetting does not occur, where the impact angle is the angle between the free surfaces of the impacting plates. During the impact of a spherical body on a flat target, the impact angle ranges from 0 to $\pi/2$ from the time that the sphere contacts the surface to the time that the sphere is buried halfway into the target. Thus, as the impact progresses the impact angle will inevitably reach and surpass the critical angle and jetting should initiate [4].

The critical angle increases monotonically with impact velocity. For this reason the most impressive example of jetting occurs in our 2 km/s impact. As **Figure 1** shows, material is ejected at velocities up to ~7 km/s, almost 3.5 times the impact velocity. The highest velocity material comes from 1828 m from the symmetry axis implying a critical angle of 21.4 degrees. This is somewhat larger than the critical angle of 16.5 degrees, calculated using the simple geometric relation of Ang (1990) and the Hugoniot for Aluminum. This discrepancy likely implies that we do not have high enough resolution to resolve the exact moment of jet initiation. Although the initiation of jetting is abrupt, the transition between the jet and the normal ejecta curtain is smooth. Rarefactions propagating from the free surface of both the projectile and the target are probably responsible for this smooth transition.

We define jetted material as any material ejected at a velocity greater than the impact velocity. With this definition, the 2 km/s impact velocity yields the highest mass of jetted material at 3.4×10^{-2} projectile masses. Although jetting is an extreme process where melting and vaporization can occur at very low impact velocities, in terms of mass involved, jetting does not play a major role in the process of impact cratering.

References: [1] Eichorn G. (1975) *Planet. Space. Sci., 23*, 1519-1525. [2] Walsh J. M. et al. (1953) *J. Appl. Phys., 24*, 349-359. [3] Ang J. A. (1990) *Int. J. Impact. Engng., 10*, 23-33. [4] Melosh H. J. and Sonnet C. P. (1986) *Origin of the moon, conference proceedings* 621-642. [5] Tillotson J. H. (1962) General Atomic Report GA-3216.

Acknowledgements: We gratefully acknowledge the developers of iSALE, including Gareth Collins, Kai Wünnemann, Boris Ivanov, Jay Melosh, and Dirk Elbeshausen. This research is supported by NASA NNX10AU88G.

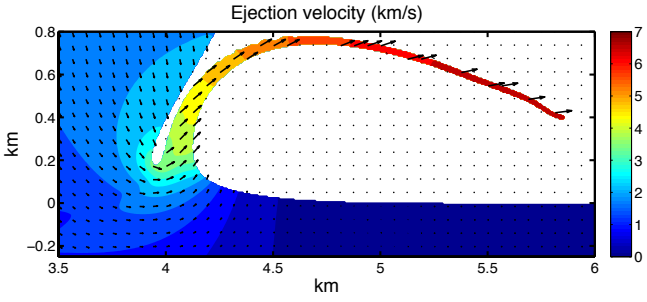

Figure 1: Material colored according to velocity 0.75 s after a 10 km diameter aluminum impactor strikes an aluminum half space at 2 km/s. The vectors show the direction of the material velocity. Note that the x-axis starts 3.5 km from the symmetry axis.

THE LINKS BETWEEN TARGET PROPERTIES AND LAYERED EJECTA CRATERS IN ACIDALIA AND UTOPIA PLANITIAE, MARS. E. Jones and G. R. Osinski, Centre for Planetary Science and Exploration/Dept. Earth Sciences, University of Western Ontario, 1151 Richmond Street, London ON, N6A 5B7, ejones68@uwo.ca.

Introduction: Martian craters with fluidized ejecta – including single-layered, double-layered and multiple-layered craters – have been studied extensively, with their formation generally suggested to be linked to varying concentrations of subsurface volatiles [1,2]. A new and extensive catalogue on martian impact craters [3,4] classifies crater ejecta along with their location, diameters and ejecta extents, potentially providing new information on the links between these morphologies and the subsurface. We examine this catalogue with an aim to identifying how these morphologies are interrelated within Acidalia and Utopia and how target properties may control the occurrence of layered ejecta. These regions have been previously identified as showing large numbers of Late Hesperian/Amazonian aged layered ejecta craters potentially related to past volatile rich sedimentary deposits [5,6].

Results: Single layer ejecta (SLE) craters smaller than 10 km diameter are the dominant impact morphology in Utopia, but large numbers of double-layer (DLE) craters are also present. Few craters within both Utopia and Acidalia do not show the layered ejecta morphology. From our study region, a crater in Utopia 3–12km diameter has a ≥70% chance of displaying layered ejecta. If layered ejecta is indicative of subsurface volatiles, then volatiles in Utopia were most strongly concentrated at the depths excavated by 7–9 km diameter craters (actual excavation depths not modeled here), and increase with diameter/depth up to this limit. The potentially high fraction of small (<5 km diameter) DLEs indicates that shallow volatiles may have been recently abundant at shallow depths (100s of metres) in Utopia, if the ejecta classification of these craters is accurate. This is consistent with radar evidence of possible substantial ice deposits at ~50–90m depth in Utopia [7,8].

Acidalia shows the highest preference for DLE craters. From Figure 1, for craters 6–11 km in diameter, there is a ≥50% probability that it will be a DLE. This indicates a significant association of DLEs to subsurface layers within this region and target conditions that are more favorable to the DLE morphology than SLE. Onset diameters of DLE craters in Acidalia are significantly deeper than typical for DLEs at that latitude, potentially related to the depletion of volatiles at shallow depths. This region is likely depleted in significant amounts of water ice within the top 1 km; although possible ice-rich material has been detected further to the south [9] and the water-equivalent-hydrogen content is 8% [10].

The catalogue ejecta extent data was also examined to calculate ejecta mobility ratios. High ejecta mobility ratios are taken to indicate lower effective viscosity of the ejecta flow, potentially related to higher entrained volatiles content [11]. Most SLE craters have a low ejecta mobility ratio <2. The highest values >3 are clustered within Utopia and Arcadia in the northern hemisphere and are associated with craters <10km diameter. These trends are, therefore, not determined only by latitude as clear regional correlations are observed [13].

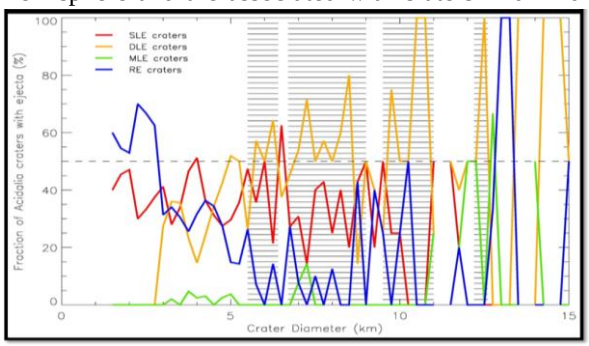

Figure 1: The proportion of each crater morphology within diameter bins in Acidalia. Craters in blue were identified in the catalogue as showing only radial ejecta. Excavation depth is proportional to crater diameter.

Conclusions: Our results indicate that craters with more than one layer of ejecta may be associated with subsurface volatiles, whereas single layered ejecta craters may be influenced more strongly by particle size and cohesion and be less sensitive to volatiles than DLE and MLE craters. Some sources of error and potential regions of mis-classification in the catalogue are identified.

References: [1] Kuzmin, R. (1980) *LPSC XI*, 585-586; [2] Mouginis-Mark, P. (1981) *Icarus, 45*, 60-76; [3] Robbins, S. and Hynek, B. (2012) *JGR, 117*, E05004; [4] Robbins, S. and Hynek, B. (2012) *JGR, 117*, E06001; [5] Costard, F. and Kargel, J. (1995) *Icarus, 114*, 93-112; [6] Barlow, N. and Perez, C. (2003) *JGR, 108*, 1-10; [7] Plaut, J. et al. (2009) *LPSC XC, abstract* #2312; [8] Nunes, D. et al. (2010) *JGR, 115*, 1-20; [9] Picardi, G. et al. (2005) *Science, 310*, 1925-1928; [10] Maurice et al. (2011) *JGR, 116*, 1-41; [11] Mouginis-Mark, P. (1979) *JGR, 84, 8011-8022*; [12] Barlow, N. (2005) *Large Meteorite Impacts III*, Geological Society of America, 433-442; [13] Costard, F. (1989) *Earth, Moon, and Planets, 45*, 265-290

THE CENTRAL UPLIFT OF SPIDER CRATER, WESTERN AUSTRALIA. T. Kenkmann[1] and M. H. Poelchau[1], [1]Institute of Earth and Environmental Sciences, Albert-Ludwigs Universität Freiburg, Albertstraße 23-B, 79104 Freiburg, Germany, Thomas.kenkmann@geologie.uni-freiburg.de.

Introduction: The Spider impact crater, Australia (13 x 11 km Ø, N16°44'27'', E126°05'21'') named after the peculiar appearance of its central uplift, is situated on the Kimberley-Plateau in Western Australia. J. E. Harms was the first who recognized the structure around 1960, but twenty years later a cryptovolcanic origin was still favored [1]. Shoemaker and Shoemaker [2, 3] mapped the site in 1984-85. McHone [4, 5] and Abels [6, 7] investigated the structure by means of remote sensing analyses. While most authors favored an oblique impact from N to NW to explain the northerly dipping thrust stacks [2, 3], Abels [6, 7] argued that pre-impact topography and the (very) gently dipping limbs of the broad Mt. Barnett syncline might account for the asymmetric structure.

We undertook a field survey of the central uplift at Spider in 2007. The nearest infrastructure is the Gibb River Road and the Mount Barnett Roadhouse. Access to the structure is restricted as it is part of the Mount Barnett pastoral lease under declared Aboriginal homeland. We present micro- and macrostructural field data along with a simple kinematic model that explains the structure of the central uplift.

Microstructures: Twelve samples were analyzed for petrography and shock metamorphism using optical microscopy, four from the central dome, six from the thrust systems and two from outside the crater (Pentecost sandstone). The samples of the core region are strongly deformed to monomictly brecciated Warton Sandstone (1.7 Ga), the oldest unit at Spider. This pure quartzitic sandstone shows some planar deformation features (PDFs) and very abundant planar fractures (PFs), many of them contain feather features (FFs) [8]. Shock effects propagate from quartz grains into the surrounding quartz cements suggesting that the rocks were completely lithified and of low porosity when the impact occurred. Shatter cones are ubiquitously present in the central dome. Pentecost sandstone samples from the surrounding thrusts show a quartz arenite with clayey and Fe-rich seams surrounding the quartz grains. The deformation varies from weakly deformed to shocked. The shocked samples show abundant transgranular fractures, PFs, FFs, and a few PDFs. Shatter cones occur only in the vicinity of the central dome. Between the thrusts occur narrow zones of monomict and polymict lithic breccias. They contain a fine-grained lithic matrix (5-10 µm) in which angular fragments of quartz, chert, siltstone (50-100 µm) are embedded.

Macrostructures and kinematic model: The central uplift consists of two imbricate thrust stacks that surround the core of the structure, indicating N-S shortening with a preferred material transport top to southerly direction (Fig. 1). Dipping of beds within the imbricate stacks ranges between 20-80° (40° mean dip) and shows no systematic change from N to S. The traces of each thrust are bent and their strike gradually shifts from N to S. To explain the change in orientation of the thrust slices from up range to downrange a very simple approach of vector summation in a horizontal plane might be helpful: An idealized flow field during crater collapse at a vertical incidence is represented by purely radial convergent flow lines. This flow field is combined with a flow field consisting of parallel flow lines of outward decreasing magnitude that are pointing from up range to downrange. The latter trajectory field is expected when a tangentially impacting projectile transfers momentum to a target. Simple vector addition of the two flow fields results in curved trajectories whose orientations are perpendicular to the strike of the thrusts. The imbricate stacks initiated up-range and migrated down-range simultaneously with the uplift of the central core. Three-dimensional numerical modeling is necessary to fully resolve the trajectory field in time and space. This is currently planned.

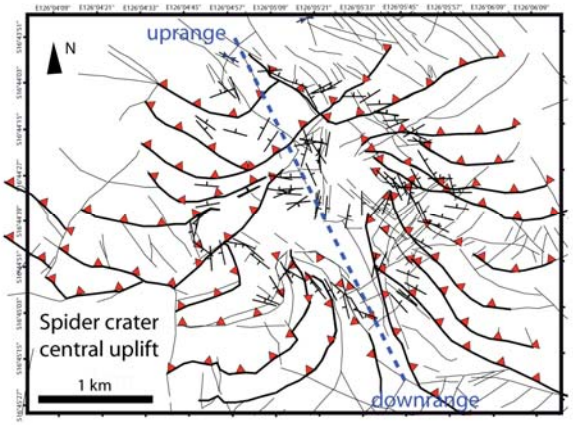

References: [1] Harms J. E. et al. (1980). *Nature 286*, 704-706. [2] Shoemaker E. M. & Shoemaker C. S. (1988). *GSA, Abstracts 20*, A147. [3] Shoemaker E. M. & Shoemaker C. S. (1996). *AGSO Journal of Australian Geology & Geophysics, 16*, 379-398. [4] McHone J. F. et al. (2002a) *Met. Planet. Sci., 37*, 407-420. [5] McHone J. F. (2002b) *LPSC XXXIII, abstract 1990*. [6] Abels, A. (2001) *LPSC XXXII*, abstract 1408. [7] Abels, A. (2005) *Aust. J. Earth Sci. 52*, 653–664. [8] Poelchau, M.H. & Kenkmann, T. (2011) *JGR 116*.

REVISITING THE DIAMETER OF THE WEST CLEARWATER LAKE IMPACT STRUCTURE, QUEBEC, CANADA. M. C. Kerrigan[1], G. R. Osinski[1], and L. L. Tornabene[1]. [1]Centre for Planetary Science and Exploration, Dept. of Earth Sciences, University of Western Ontario, 1151 Richmond St., London, ON, Canada, N6A 5B7 (mkerrig@uwo.ca)

Introduction: The Clearwater Lake complex (56°10N, 74°20W) in Quebec, Canada, is a double impact structure, expressed as two adjacent circular lakes (Fig. 1). East Clearwater Lake is approximately 21 km in diameter while West Clearwater Lake measures 32 km across. West Clearwater also has a prominent ring of islands 18 km across and some small, low-lying islands in the centre of the lake. In early studies of West Clearwater the 32 km diameter of the lake is used as the diameter of the crater whether the study described the crater as being of volcanic [1] or impact origin [2]. In this study we focus on West Clearwater Lake using remote sensing data to examine the surrounding terrain for structural features associated with an impact crater rim morphology outside of the lake area.

Crater Geology. The target lithology for this impact structure is Precambrian granitic gneiss of the Canadian Shield with small outcrops of Ordovician limestone [3]. The impact event is dated at ~290 Mya [4] and the geology of the lake islands display a sequence of lithic and impact melt-bearing breccias, and a fine-grained to clast-rich impact melt sheet [3].

Methodology: Several remote sensing datasets are utilised in this study including: a 1:50,000 Digital Elevation Model from Natural Resources of Canada, Landsat Enhanced Thematic Mapper+ (ETM+) and Advanced Spaceborne Thermal Emission and Reflection Radiometer (ASTER) visual-near infrared (VNIR) and short wavelength infrared (SWIR) data. The topographic, morphologic, and structural expression of the terrain surrounding the crater was assessed by eye mapped over a colourized shaded-relief map of the area within ArcGIS v.10 (Fig. 2).

Results and Discussion: An overall east-west direction of the topography and the many smaller lakes is apparent in the shaded-relief map. This is associated with westward flow during the Laurentide glaciation [5]. In some areas, however, particularly towards the south and west of the lake, ridges and valleys appear curvilinear and concentric with the shoreline, as well as others which trend more north-south. These may represent radial faults and fractures emanating from the centre of the crater. While some of these possible faults and fractures have been overprinted by the subsequent glaciations, they nevertheless form a faint "halo" feature surrounding the lake at a diameter of ~65 km from the centre of the lake (Fig. 2); this halo has also been observed in Radarsat 1 data [5]. Whether this represents the actual crater rim remains to be determined but this work highlights the difficulty in identifying the rim in eroded complex impact structures.

Fig. 1: True colour Landsat ETM+ image of Clearwater Lake complex. Note the general east-west lineation highlighted by small lakes throughout the region.

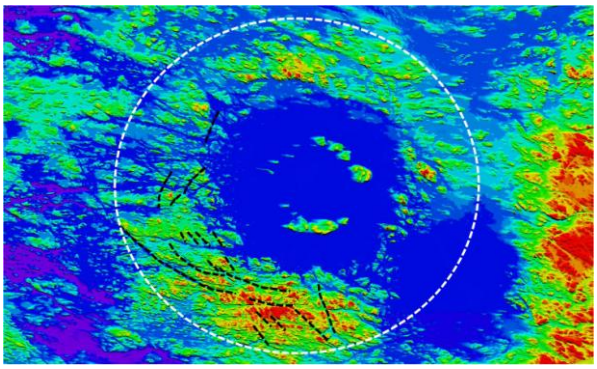

Fig. 2: Shaded-relief map of West Clearwater Lake generated using standard processing and mosaic techniques for Digital Elevation Models (DEMs) with the Environment for Visualizing Images (ENVI) software package. Possible faults are marked in black and potential crater rim limit highlighted with the white circle.

Future Work: Multiple radial topographic profiles across the impact structure, as well as multiple sun-angled shade-relief maps will be used to create ai improved structural map of the site. Spectral information and additional observations made from these remote sensing datasets will assist in the preparation for future fieldwork, geologic mapping, and planning traverses and locations where interpretations can be ground-truthed.

References: [1] Kranck S. H. and Sinclair G. W. (1963) *Geol. Survey Can. Bull. 100*. [2] Dence M. R. et al. (1965) *J. Roy. Astron. Soc. Can. 59*, 13–22. [3] Phinney W. C. et al. (1978) *Lunar and Planetary Sci. Conference Proceedings. 9*, 2659-2694. [4] McDonald I. (2002) *Meteoritics and Planetary Sci. 37*, 459-464. [5] Smith S. K. et al. (1999) *Canadian Journal of Remote Sensing. 25*, 218–228.

MINERALOGY AND GEOCHEMISTRY OF POST-IMPACT SEDIMENTARY INFILL OF THE CRATER MOAT AND CARBONATES OF THE CRATER FLOOR, WAQF AS SUWWAN IMPACT STRUCTURE. H. N. Khoury[1], E. M. Salameh[1], and W.U. Reimold[2], [1]Department of Geology, The University of Jordan, Amman 11942; e-mail: khouryhn@ju.edu.jo; salameli@ju.edu.jo, [2]Museum für Naturkunde – Leibniz Institute of Evolution and Biodiversity Research, Invalidenstrasse 43, 10115 Berlin, Germany; e-mail: uwe.reimold@mfn-berlin.de; also Humboldt-Universität zu Berlin, Unter den Linden 6, 10099 Berlin, Germany.

Introduction: The Waqf as Suwwan complex impact structure in eastern Jordan of about 6.5 km diameter was formed as a result of the impact of an extraterrestrial projectile, presumably in late Cretaceous to Eocene times [1, 2, 3, 4]. The structure offered a plethora of structural geological information, especially regarding the deformation of a central uplift. Three boreholes were drilled into the moat around the central uplift structure. The deepest borehole was drilled to the north and outside of the central uplift to a depth of 140 m. The first 11 m core reveals the presence of fluvial sediments (wadi deposits) that are dominated by chert breccias. The rest of the core is made up of upper Cretaceous limestone and dolomite. Brecciation and fracturing with vertical, as well as inclined (45^0 and 30^0) fractures occur throughout the cores. Forty samples were subjected to mineralogical, petrological, chemical and stable isotope analyses.

Results: The top 11m fluvial sediments of the core are parapolymictic breccias made up of crypto- to micro-crystalline and fibrous, angular, brecciated and cracked lithics. Chert is the major component, together with micritic and biomicritic limestone lithics. Quartz grains are angular to sub-angular, bimodal with a predominance of silt over sand size. Few quartz crystals exhibit wavy extinction, some with intense microfracturing. Secondary dolomite and sparry calcite are embedded in the micritic matrix. The only possible shock deformation is suggested by sporadic, intense fracturing in zircon and quartz. Neither PF, PDF, nor FF has been observed. The rest of the core is made up of fractured and brecciated limestone and dolomite. Calcite and dolomite crystals in the carbonates are locally characterized by intense twinning and other deformation. Stable isotope data ($\delta^{13}C$ and $\delta\ ^{18}O$) show no deviation from their upper Cretaceous and Eocene carbonate equivalents in Jordan (Fig. 1).

Conclusion: The results are combined to indicate that the drilled strata below the wadi deposits represent a level of unshocked or at best very weakly (< 5 GPa) shocked crater floor. This fact further suggests that the entire impact structure is very deeply eroded. The stratigraphic information from drilling indicates that the age of the impact is constrained to post-late Eocene age. Unfortunately, still no directly datable lithologies have been incurred to confirm this with absolute age data[4].

Acknowledgments: The University of Jordan, the Ministry of Higher Education of Jordan (Scientific Research Support Fund), Alexander von Humboldt Foundation (AvHF), University of Ottawa are thanked for their support of the study. Part of the analytical work of HK was done at the Museum for Natural History Berlin, Germany, with support from the DAAD and AvHF. The isotope analyses were carried out at the University of Ottawa.

References: [1] Kenkmann, T., Reimold, W. U., Khirfan, M., Salameh, E., Konsul, K. and Khoury, H. (2010) The complex impact crater Jebel Waqf as Suwwan in Jordan: effects of target heterogeneity and impact obliquity on central uplift formation. *The Geological Society of America, Special Paper* 465. [2] Salameh, E., Khoury, H., Reimold, W.U., and Schneider, W. (2008) First Large Meteorite Impact Structure Discovered in the Middle East: Jebel Waqf As Suwwan, Jordan: *Meteoritics and Planetary Science*, v. 43, p. 1681-1690. [3] Salameh E., Khoury H. and Schneider W.: Jebel Waqf as Suwwan, Jordan: a possible impact crater – a first approach. *Zeitschrift der deutschen Gesellschaft für Geowissenschaften* 157: 319-325. [4] Salameh1, E., Khoury, H. and. Reimold, W.U. (2013) Drilling the Waqf as Suwwan impact structure. *International Journal of Earth Sciences.* Under Review.

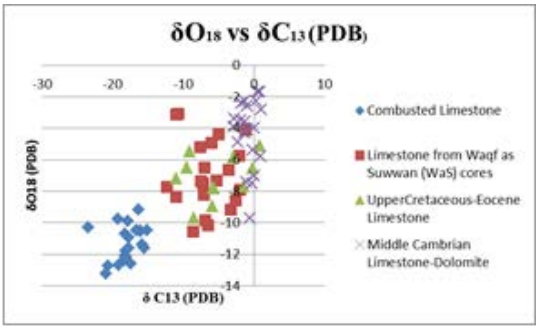

Fig. 1. Stable isotope data (δO18 and δC13) of lim - stone from Waqf as Suwwan (WaS) cores compared with equivalent upper Cretaceous-Eocene, combusted and Paleozoic carbonates.

Thermal Evolution of Lunar Impact Basins and Implications for Mascon Formation

Walter S. Kiefer[1], Ross W. K. Potter[1], Patrick J. McGovern[1], Gareth S. Collins[2], and David A. Kring[1], [1]Lunar and Planetary Institute, 3600 Bay Area Blvd., Houston TX 77058, kiefer@lpi.usra.edu , [2]Impacts and Astromaterials Research Centre, Dept. Earth Science and Engineering, Imperial College London, London SW7 2AZ, UK.

The gravity field of the Moon has long been known to have large positive free-air gravity anomalies over impact basins such as Imbrium and Orientale [1-3]. Large gravity highs over topographically low basins are not generally expected, and these observations require the presence of high density material somewhere in the crustal column beneath the impact basin. Although extrusive basalt flows are present at many but not all mascon basins, the available constraints on basalt flow thicknesses [4,5] are such that surface basalts by themselves can not account for the observed gravity anomalies. Thus, the consensus has been that some degree of super-isostatic mantle uplift beneath large impact basins is necessary [6-9]. Several recent studies have explored ways in which visco-elastic relaxation of the initial impact basin structure may create the required super-isostatic uplift of the mantle, either due to solidification of the impact melt pool beneath the basin center or by flow driven by an outer annulus of sub-isostatic material [10-13].

Post-impact Thermal Evolution

The impact energy associated with the formation of a large lunar impact basin significantly heats the lunar mantle beneath the impact zone. For an impact appropriate for the Orientale basin, hydrocode simulations using iSALE show that the resulting volume of partially molten mantle is roughly 150 km in radius and extends to a depth of about 200 km, with a total melt volume of $\sim 1\text{-}2 \cdot 10^6$ km^3 [14]. This material has a density deficit of -30 to -60 kg m^{-3} relative to the ambient mantle and thus is a major contributor to the density structure that drives visco-elastic flow.

Existing visco-elastic flow models consider only conductive cooling of the melt pool. Due to the size of the melt pool, the conductive cooling time exceeds 10^8 years and is longer than the visco-elastic evolution timescale. However, due to the melt pool buoyancy, convective flow of the mantle plus melt system will also be important, resulting both in a much smaller cooling timescale and in advective redistribution of molten material. The buoyant melt will tend to rise up and flow laterally outward from the basin center, and the resulting thinner melt layer will cool more rapidly. Approximating this flow as a gravity current [15, 16], the melt pool may thin to one third of its original thickness in just a few million years. Porous flow in the partially molten melt pool may also be important. These changes in the buoyancy field are likely to significantly modify the post-impact visco-elastic flow beneath the basin and thus may degrade the fit to the gravity data. Finite element mantle convection models with strongly temperature-dependent rheology are being performed to further quantify this evolution.

Volcanic Intrusion Mascon Model

The crust below the impact zone is pervasively fractured (porosity 15-20% [17]), forming a reservoir for magma ponding within the crust. As an alternative model of mascon gravity anomalies, we proposed a layer of intrusive sills and dikes that thermally anneal the pore space and increase the density of the crust [18, 19]. At Orientale, the peak rate of volcanic extrusion was about 200 million years after the impact [5], allowing time for the lithosphere to cool and thicken after the impact and support a super-isostatic volcanic load. For likely densities and porosities of the feldspathic crust and intrusive basalt [20], the observed gravity anomaly [2] can be explained with an intrusive basalt layer with an effective thickness of 1.8 km. Extrusive volcanism is typically only about 0.2 km thick on the Orientale floor [5], so in this model the intrusive magmatism is about 90% of the total magmatism. This is consistent with typical intrusive/extrusive magmatism ratios observed on Earth. If applied to all lunar mascons, this model would be a significant enhancement to the inferred volume of lunar volcanism. An intermediate model, with mascon contributions from both visco-elastic evolution and intrusive volcanism, is also possible.

References [1] Muller and Sjogren, Science 161, 680-684, 1968. [2] Konopliv et al., Icarus 150, 1-18, 2001. [3] Zuber et al., Science 339, 668-671, 2013. [4] Williams and Zuber, Icarus 131, 107-122, 1998. [5] Whitten et al., JGR 116, 2010JE003736, 2010. [6] Wise and Yates, JGR 75, 261-268, 1970. [7] Neumann et al., JGR 101, 16,841-16,863, 1996. [8] Hikida and Wieczorek, Icarus 192, 150-166, 2007. [9] Namiki et al., Science 323, 900-905, 2009. [10] Melosh et al., LPSC 43, abstract 2596, 2012. [11] Andrews-Hanna, Icarus 222, 159-168, 2013. [12] Dombard et al., GRL 40, 2012GL054310, 2013. [13] Freed et al., LPSC 44, abstract 2037, 2013. [14] Potter et al., JGR, in press, 2013. [15] Griffiths and Campbell, JGR 96, 18,295-18,310, 1991. [16] Bercovici and Lin, JGR 101, 3291-3309, 1996. [17] Wieczorek et al., Science 339, 671-675, 2013. [18] Kiefer et al., Early Solar System Bombardment Workshop, abstract 4026, 2012. [19] Kiefer, JGR 118, 2012JE004111, 2013. [20] Kiefer et al., GRL 39, 2012GL051319, 2012.

ACCRETIONARY LAPILLI (CARBONATE SPHERULES) AT THE CRETACEOUS-PALEOGENE ('KT') BOUNDARY IN BELIZE (CENTRAL AMERICA). D. T. King, Jr.[1] and L. W. Petruny[1], [1]Geology Office, Auburn University, Auburn, Alabama 36849 USA.

Introduction: The Cretaceous-Paleogene (KT) boundary stratigraphy in Belize consists of four main units: (1) a terminal Cretaceous paleosol (< 1 m; exposed at the village of Armenia on the Hummingbird Highway [1, 2]); (2) a fine-grained bed containing accretionary lapilli (~ 1-3 m; exposed at Albion Quarry on Albion Island near the town of San Antonio [3] and on the highway at Armenia [1, 2]); (3) an impactoclastic breccia bed (~ 8-15 m; exposed at Albion Island [1, 3, 4]); and an impactoclastic bed of rounded pebbles (exposed at Progresso Lagoon [2], on the highway at Armenia [1], and in various sites in the Cayo District [5]). Not all these units are found together in the same places. This paper focuses on the accretionary lapilli (i.e., impact-produced carbonate spherules) that occur at Albion Island and Armenia.

Albion Island 'KT' stratigraphy: In a large road materials quarry on Albion Island (a small area surrounded by diverging braches of the Rio Hondo), a basal impactoclastic clay layer, ~ 1-2 m thick, crops out that contains abundant accretionary carbonate spherules. These spherules range in size from a few mm to about 1 cm [3, 4]. Above this layer lies an ejecta diamictite [3] or impactoclastic breccia (the Albion impactoclastic breccia [4]), which is ~8-15 m thick. This impact glass-bearing breccia is characterized by thick sedimentological units or bedding that has been enhanced by horizontal shearing. The unit contains normal and reverse size grading, clast imbrication, flow lamination, and isolated and linked aggregates of clasts (i.e., clast clustering) [4]. In addition, most carbonate clasts within the Albion impactoclastic breccia are compact bladed to compact elongated and have surficial markings consistent with high-velocity particle interactions [4]. The Albion impactoclastic breccia is truncated by a local unconformity, which is overlain by modern soils at Albion Island and micritic Lower Paleogene limestones in an adjacent area of México [1, 4].

Albion Island's spherules: These accretionary lapilli or carbonate spherules range in size from a few mm to ~ 1 cm. These spherules are typically strongly compressed and generally lack distinctive internal structure such as layering. However, a small percent of these spherules have discernable internal layering and a small percent have distinct nuclei as well. These nuclei are small carbonate grains, not glass. All Albion Island carbonate spherules have been subjected to intensive diagenesis and attendant recrystallization. Their present carbonate phase is dolomite [6] and the crystal size is typically micritic (a few microns). Even though impact-produced glass fragments are apparently missing from the Albion Island spherule bed, there are clay spherules that may have been originally glassy impact spherules [6].

Armenia 'KT' stratigraphy: On the north side of the Hummingbird Highway at the village of Armenia, Belize, an outcrop includes the upper beds of the Maastrichtian Barton Creek dolostone, which is overlain by a lateritic clay bed (paleosol) containing dolostone boulders [1]. This is in turn overlain by an accretionary spherule-bearing carbonate-rich clay layer (~ 2-3 m), which contains broken impact glass fragments [1, 7]. Above the spherule-bearing layer lies a limestone conglomerate bed, which contains abundant rounded and polished limestone clasts averaging several cm in diameter [1, 7]. The matrix of this bed has yielded some quartz grains with multiple sets of PDFs [6]. The limestone conglomerate bed is overlain by a local unconformity, which is blanketed by modern soil.

Armenia's spherules: Accretionary lapilli or carbonate spherules from Armenia range in size from less than one mm to ~ 1.5 cm. A typical spherule consists of a core (usually a carbonate grain, but in some instances an angular, impact-produced glass fragment), which is surrounded by concentric layers of clayey calcium carbonate. The surface (or "shell") of each concentric layer is typically harder than the lower part of the layer. Concentric layers range in thickness from < 0.001 mm to > 1 mm and are structureless to vaguely laminated [7]. Some layers are silty. It is likely that the carbonate in each concentric layer was deposited as microcrystalline lime, but has now converted to calcite. Aggradational recystallization among calcite crystals is evident in thin section, and this may have accompanied the lime-to-calcite conversion [7].

References: [1] Pope K.O. et al. (2005) *GSA Spec. Paper 384,* 171-190. [2] King Jr. D.T. et al. (2004) *GCAGS Transactions,* 54, 289-304. [3] Ocampo A.C. et al. (1996) *GSA Spec. Paper 307,* 75-88. [4] King Jr. D.T. and L.W. Petruny (2003) *Impact Markers in the Stratigraphic Record,* Springer Verlag, 203-229. [5] Pope K.O. and A.C. Ocampo (2000) LPS XXXI Abstract #1419. [6] Pope K.O. et al. (1999) *Earth & Planet. Sci. Lett.,* 170, 351-364. [7] King Jr. D.T. and L.W. Petruny (2013) LPS XLIV Abstract #2747.

POROSITY: THE REASON FOR SiO_2 MELT FORMATION AT EVEN 5 GPa SHOCK PRESSURE. EXPERIMENTS WITH TARGETS OF 3 DIFFERENT POROSITIES VS MESOSCALE MODELING.

A. Kowitz[1], N. Güldemeister[1], W.U. Reimold[1,2], R.T. Schmitt[1], and K. Wünnemann[1]; [1]Museum für Naturkunde, Leibniz-Institut für Evolutions- und Biodiversitätsforschung, Invalidenstrasse 43, 10115 Berlin, Germany. [2]Humboldt-Universität zu Berlin, Unter den Linden 6, 10099 Berlin, Germany. E-mail: astrid.kowitz@mfn-berlin.de; nicole.gueldemeister@mfn-berlin.de

Introduction: The identification of impact craters formed in porous sandstone targets, on the basis of recognition of shock deformation features, is a complex task, especially concerning the interaction of the shock wave with open pores. There is a serious lack of diagnostic shock features, particularly for the low shock-pressure range, which is addressed in this project focusing on shock deformation experimentally generated in porous sandstone and for comparison in dense quartzite at pressures of <20 GPa. We aim to establish a shock classification scheme for porous, quartz-bearing rocks. The laboratory impact experiments were accompanied by meso-scale numerical modeling and enable a detailed description and quantification of thermo-dynamic parameters during single pore collapse.

Methods: Three series of shock recovery experiments (impedance method) [1] were conducted from 2.5 to 17.5 GPa with cylinders of two different layers of dry Seeberger sandstone (L3, porosity Φ ~25-30 vol.% (Fig. 1a); L5, Φ ~12-19 vol.%) and a quartzite (< 0.2 vol.% Φ). Numerical models were computed with the hydrocode iSALE [2] coupled with the ANEOS for quartzite [3] using a virtual experimental set-up similar to the experimental one.

Results: The determined fracture density shows that until 12.5 GPa the dense quartzite is significantly less fractured (143 f/mm) than the porous sandstone (~209 f/mm) followed by an increase in fracture density up to 17.5 GPa (277 f/mm). In contrast, the samples of L3 achieve their peak fracturing at 12.5 GPa (209 f/mm) followed by a decrease to 17.5 GPa (113 f/mm). The number of fractures in the L5 samples is intermediate between quartzite and L3. Backscattered electron (BSE) SEM images demonstrate that in the sandstones pores are entirely closed even at an initial shock pressure of only 2.5 GPa. Here, we have observed diaplectic quartz glass and/or SiO_2 melt, both of which are distributed heterogeneously (Fig. 1b); these phases rarely occur at 5 GPa (L3) but increase in frequency up to ~85 vol.% (L3) at 17.5 GPa. In the sandstone samples with lower porosity (L5) the onset of glass formation starts at higher pressures (7.5 GPa) and does not reach such high amounts. In contrast, within the quartzite there is no glass/melt formation up to 17.5 GPa. The meso-scale numerical models also show a complete closure of pores already at low initial pressures (<6 GPa). Detailed analysis of the closure of single pores indicates localized amplifications of shock pressure up to 3-4 times the average shock pressure in the porous material (Fig. 1c).

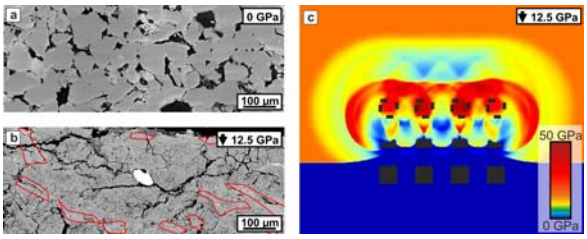

Fig. 1. SEM-BSE images of **(a)** unshocked and **(b)** shocked (12.5 GPa) Seeberger sandstone (L3). Note the total closure of pore space, the intense fracturing, and the heterogeneous distribution of diaplectic quartz glass and/or SiO_2 melt (red-framed areas). **(c)** Shock pressure distribution during pore collapse (snapshot). Note the total closure of pores (black) and the pressure amplification up to 4 times (dark red) at locations of primary pores.

Discussion: Shock compression of porous sandstone results in distinctly different effects than observed in non-porous rocks, especially at low shock pressures. Despite our low shock pressures, the formation of diaplectic quartz glass and SiO_2 melt was observed in L3 already at 5 GPa, whereas these phases usually occur only at 30-35 GPa and >45 GPa, respectively, in shocked quartz single crystals [1]. Furthermore, their amount decreases distinctly with decreasing porosity because the crushing mechanism is strongly dependent on porosity and leads to a distinctly heterogeneous distribution of localized shock pressure and temperature amplification in the target and therefore to a heterogeneous distribution of shock effects (e.g., fractures, local occurrence of diaplectic quartz glass and SiO_2 melt) (Fig. 1b, 1c). Our attempts at quantification of shock amplification (up to 3-4 times) due to pore space collapse using meso-scale modeling are in good agreement with observations on our shock experiments. According to Kieffer et al. [4] our samples of L5 can be classified by their amount of glass/melt to shock stage 1b, which then does not agree with their proposed pressure estimations. The samples of L3 can be classified to stage 1b to 3, which partly agrees with their shock pressure estimations. Nevertheless, a first step in improving a classification scheme for porous sandstone has been achieved.

Acknowledgements

This work was funded through DFG research unit FOR-887 (MEMIN) projects WU 355/6-1 and RE 528/8-2.

References

[1] Stöffler D. and Langenhorst F. (1994) *Meteoritics & Planet. Sci.*, 29, 155-181. [2] Wünnemann K. et al. (2006) *Icarus*, 180, 514–527. [3] Melosh H. J. (2007) *Meteoritics & Planet. Sci.*, 42, 2035–2182. [4] Kieffer S. W. et al. (1976) *Contrib. Mineral. Petrol.*, 76, 41-93.

EXPLORATION OF THE SCHRÖDINGER PEAK-RING BASIN ON THE LUNAR FARSIDE. David A. Kring[1], Jack O. Burns[2], Joshua B. Hopkins[3], Scott Norris[3], and T. Joseph W. Lazio[4], [1]Center for Lunar Science and Exploration, USRA-Lunar and Planetary Institute, Houston TX 77058 (kring@lpi.usra.edu), [2]Center for Astrophysics and Space Astronomy, University of Colorado, Boulder CO 80309, [3]Lockheed Martin Space Systems, Denver CO 80127, [4]Jet Propulsion Laboratory, Pasadena CA 91109.

Introduction: A multi-year assessment of the NRC's report outlining *The Scientific Context for Exploration of the Moon* [1] produced a global landing site report with locations where those scientific objectives could be addressed [2]. The landing site report concluded that the Schrödinger peak-ring basin is one of the scientifically-richest landing sites on the Moon.

That study prompted a closer look at the geology of the Schrödinger basin for mission opportunities. Within the context of the Constellation Program, in which astronauts would land and be able to explore with a Lunar Electric Rover (LER), three landing sites with traverses and sample stations were designed [3]. Subsequently, with the addition of M^3 and LROC data, outcrops of distinct lithologies were identified [4, 5].

The mission paradigm has changed, however. At the moment, the capability to land astronauts on the surface is not being developed. The Orion Multi-Purpose Crew Vehicle, however, is being prepared for an Exploration Flight Test (EFT)-1 on a Delta IV in September 2014. Exploration Mission One (EM-1) with Orion on the Space Launch System (SLS) is scheduled for 2017; this is an un-crewed flight around the Moon with a free return trajectory. EM-2 follows in 2021 with a crewed lunar orbit-capable system.

Lunar L2-Farside Mission: The Orion has the capability for a mission that operates within view of the Schrödinger basin on the lunar farside [6]. In this type of mission, astronauts would be sent to an orbit around the Earth-Moon L2 point ~60,000 km above the surface. In parallel, a robotic asset could land within Schrödinger basin and collect samples for return to Earth. The lander and rover would maintain contact with Earth through Orion (Fig. 1). Moreover, astronauts on Orion could teleoperate the vehicle to reduce mission risk, enhance scientific return, and test operational concepts for future missions.

Objectives: The Schrödinger basin is located in what is likely to be the modification zone of the South Pole-Aitken basin. Schrödinger is the second youngest basin, within the oldest basin, so a sample return mission to that location has the potential of determining the duration of the basin forming epoch and addressing the two highest science priorities in the NRC [1] report. The basin-forming impact uplifted material from great depth, producing a peak ring of crystalline rock massifs suitable for testing the lunar magma ocean hypothesis.

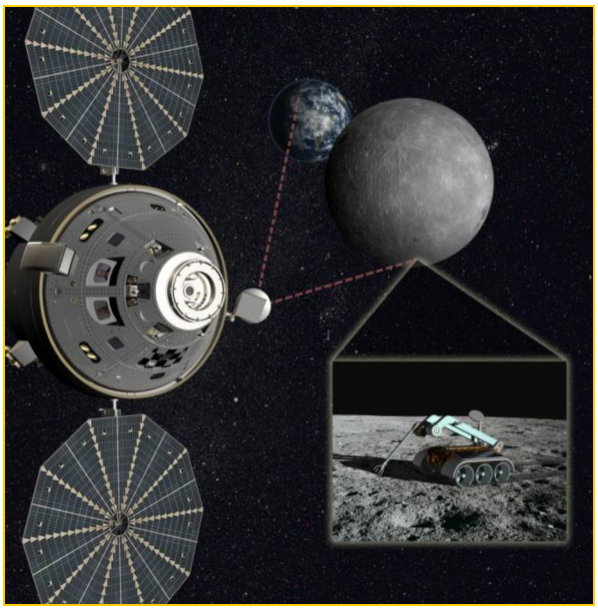

Fig. 1. Schematic picture of the Orion MPCV L2 mission in which astronauts teleoperate a rover on the lunar farside.

That material, when combined with material within impact breccias and exposed in the basin walls, will provide a cross-section through a substantial portion of the lunar crust. Magmas eventually erupted onto the basin floor, producing mare basalt flows and a spectacular pyroclastic vent, providing an opportunity to probe the thermal and magmatic evolution of the Moon's mantle. The pyroclastic vent may have important in situ resource utilization (ISRU) potential too.

Schrödinger is so large and such a scientifically rich site that multiple mission opportunities exist there. In addition to the geologic objectives described here, it is an excellent site for the deployment of a low radio frequency telescope to detect the effects of the Universe's first stars and galaxies on the intergalactic medium [6].

References: [1] National Research Council (2007) *The Scientific Context for Exploration of the Moon*, 67p. [2] Kring D. A. and Durda D. D., editors (2012) *A Global Lunar Landing Site Study to Provide the Scientific Context for Exploration of the Moon*, LPI Contrib. No. 1694, 688p. [3] O'Sullivan K. M. et al. (2011) *GSA Spec. Pap.*, *477,* 117–127. [4] Kramer G. Y. et al. (2013) *Icarus*, *223*, 131–148. [5] Kumar P. S. et al. (2013) *JGR*, *118*, 18p., doi:10.1002/jgre.20043. [6] Burns J. O. et al. (2013) *J. Adv. Space Res.*, in press.

INTERPRETING THE DEPTH OF ORIGIN OF THE SCHRÖDINGER PEAK RING AND IMPLICATIONS FOR OTHER IMPACT BASINS. David A. Kring, Georgiana Y. Kramer, and Ross W. K. Potter, Center for Lunar Science and Exploration, USRA-Lunar and Planetary Institute, 3600 Bay Area Blvd., Houston, TX 77058 USA (kring@lpi.usra.edu).

Introduction: Uplifted impact basin peak rings can be used to probe planetary interiors. On the Moon, the ~320 km diameter Schrödinger basin is the best preserved basin of its size and has an extraordinary peak ring with which to evaluate the differentiation of the lunar magma ocean. The peak ring has a diameter of ~150 km and rises 1-2.5 km above the basin floor, providing an immense cross-section of the deep crust and possibly upper mantle. Dramatic exposures of anorthositic, noritic, and olivine-bearing (troctolite?) lithologies have been detected with Kaguya, Chandrayaan-1, and Lunar Reconnaissance Orbiter data [1-3]. Key to interpreting them, however, has been estimates of the lithologies' depths of origin.

Competing models: For lunar central peak craters, Cintala and Grieve [4] pointed out that uplifted melt cannot form the bedrock peaks, implying the minimum depth of origin for central peaks is the maximum depth of melting. They derived an analytical equation relating structural uplift with final crater diameter [5]. If one applies that equation to Schrödinger, one obtains an estimate for structural uplift of 94 km, which should have exposed material from the lunar mantle.

Schrödinger, however, is a peak ring basin, not a central peak crater. Cintala and Grieve [5] suggested an alternative uplift model for structures of this size. Rather than having the topographically exposed structure rising from the crater center, they suggested it rises from a ring of rock bounding the region of impact melted material. In this model, peak ring lithologies come from shallower depths than the maximum depth of melting. This model is appealing, because it is consistent with the observation of crustal anorthosite, rather than mantle lithologies, in some lunar peak rings [5]. This model has also been recently amplified by Head [6].

We prefer to interpret the Schrödinger peak ring with an alternative model wherein central peaks and peak rings are produced by a similar central uplift process, but in which the central uplift collapses to form the peak ring. This is a model highlighted by hydrocode modeling (e.g., [7,8]) and consistent with observations of the Chicxulub impact structure.

While this model treats the process of uplift in peak ring craters and central peak craters in the same way, one cannot use the equation of Cintala and Grieve [5] to calculate the depth of origin for material in the peak ring. The collapse of the central uplift in the formation of peak ring basins alters the amount of final uplift and distribution of lithologies. During the collapse, for example, the material in the central uplift flows outward, producing nappe-like structures that collide with the inward collapsing walls of the transient crater. The material exposed in that collapsed central structure are not the deepest uplifted units, but rather lithologies that are derived from only a fraction of the transient crater depth. That implies a crustal origin (e.g., 20-30 km depth) for the lithologies within the Schrödinger peak ring, although faulting through the collapsed peak ring [9] could juxtapose and expose units from a range of depths.

Conclusions: This model provides continuity in the processes that produce central peaks (e.g., in Copernicus) and peak rings like that in the Schrödinger basin. Because it generates surface exposures that are derived from depths significantly less than that of the transient crater, it is also consistent with the observations of anorthosite in many lunar peak rings. For the specific case of the Schrödinger basin, the model implies the lithologies in the peak ring will be dominated by crustal lithologies.

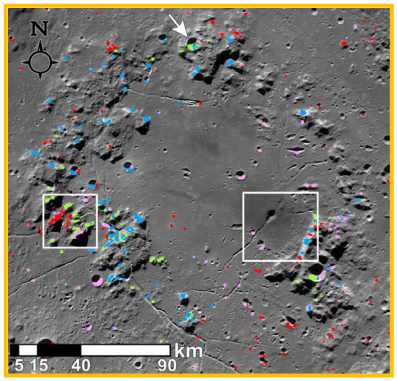

Fig. 1. Peak ring within the Schrödinger basin; anorthositic (blue), noritic (red), and olivine-bearing (green) areas where lithologies are identified; and 3 possible sample sites.

References: [1] Ohtake M. et al. (2009) *Nature*, *461*, 236–240. [2] Yamamoto S. et al. (2012) *Icarus*, *218*, 331–344. [3] Kramer G. Y. et al. (2013) *Icarus, 223,* 131–148. [4] Cintala M. J. and Grieve R. A. F. (1994) *GSA Spec. Paper 293*, 51–59. [5] Cintala M. J. and Grieve R. A. F. (1998) *Meteoritics & Planet. Sci., 33,* 889–912. [6] Head J. W. (2010) *Geophys. Res. Lett., 37,* L02203, doi: 10.1029/93JE01278. [7] Collins G. S. et al. (2002) *Icarus, 157,* 24–33. [8] Ivanov B. A. (2005) *Sol. Syst. Res., 39,* 381–409. [9] Chandnani M. et al. (2013) *LPS XLIV,* Abstract #1908.

Formation of Sudbury Breccia by Shock Compression and Cataclasis

B. Lafrance, B. S. Kamber, and D. E. Ames

Pseudotachylitic Sudbury breccia formed in basement rocks below an impact melt sheet represented by the present-day Sudbury Igneous Complex (SIC). Its origin has been attributed either to shock compression and cataclasis during propagation of an impact shock wave, to frictional melting and cataclasis during large slip displacements along crater collapse superfaults, or to injection of superheated melts from the overlying impact melt sheet into dilational fractures that opened during collapse of the crater. In an effort to test these models, the compositions of Sudbury breccia in the North Range and South Range of the Sudbury impact structure are compared to the compositions of the rocks hosting the breccia and to the average composition of the SIC. Major and trace element systematics suggest that the breccia formed *in situ* by mixing of its comminuted host rocks. The distinct chemical composition of the SIC argues against the involvement of the impact melt sheet in the makeup of the breccia. The similarity in the compositions of the breccia and its host rocks further argues against the generation of the breccia along superfaults followed by its injection into the fault wall rocks. The strong local host control on chemical and clast compositions of the breccia indicates that it formed *in situ* by shock-induced compression and cataclasis of its host rocks during propagation of the shock wave. Further comminution and cataclasis of the host rocks occurred along pre-existing anisotropies and fractures that formed and were reactivated during the growth and collapse of the transient crater, as indicated by the presence of breccia clasts within breccia.

IMPORTANCE OF TRISHEAR DEFORMATION FOR MINERAL EXPLORATION IN THE SOUTHERN SUDBURY BASIN, ONTARIO, CANADA. I. Lenauer[1] and U. Riller[2], [1]SRK Consulting Inc. (Canada), Suite 1300 151 Yonge St, M5C 2W7 Toronto Canada, iris.lenauer@gmail.com, [2]Institut für Geologie, Universität Hamburg, Bundesstrasse 55, 20146 Hamburg, Germany.

Objective: Understanding post-impact shape change of the 1.85 Ga Sudbury Igneous Complex (SIC), the relic of a deformed impact melt sheet, and its host rocks, is paramount for Ni-, Cu- and PGE-mineral exploration in the periphery of the Sudbury Basin. Non-cylindrical folding and northwest-directed reverse faulting are commonly accepted as the main deformation processes that caused the synformal and asymmetric geometry of the SIC. In the southern Sudbury Basin, greenschist-facies metamorphic tectonites make up the South Range Shear Zone, which accommodated northwest-directed reverse shearing and structural uplift of the southern SIC. The southern SIC is characterized by large variations in the dip of inclined SIC-host rock contacts and foliation surface as well as layer thicknesses and observed strain gradients. By contrast, impact-induced quartz-dioritic dikes in host rocks, so-called Offset Dikes, appear to have experienced little rotation, evident by vertical ore-rich fingers within the Dikes, believed to have formed under the influence of gravity [1]. These observations call for a deformation mechanism that can account for considerable variation in the rotational components of the southern SIC and its host rocks.

Background information: The ca. 2.5 km thick Main Mass of the SIC is composed from base to top of norite, quartz-gabbro and granophyre layers and is underlain by shocked Archean basement and Paleoproterozoic cover rocks. The basal layers of the SIC, notably the so-called Sublayer, the Offset Dikes and the immediate host rocks of the SIC are the prime target of current mining activity. Lithological contacts of the SIC generally dip toward the centre of the Basin and indicate substantial departure, i.e., rotation, of SIC segments from the original subhorizontal impact melt sheet geometry. Removal of the rotational component of the southern SIC requires tilting of these rocks to the SE by approximately 50 degrees. However, such magnitude of wall rock tilting appears to conflict with the subvertical orientation of ore-rich fingers in the Offset Dikes and excludes solid-body rotation of the southern SIC and its host rocks as a single coherent unit.

Trishear deformation of the southern SIC:

We present evidence that the orientation of layers and foliation surfaces in the southern SIC can be explained by trishear fault propagation folding. A key characteristic of trishear deformation is the transfer of localized displacement on a basal thrust fault to distributed deformation within a triangular zone, the trishear zone. Outside the trishear zone the hanging wall is translated without internal distortion. Trishear deformation of the southern SIC accounts for: angular discordances between the upper and basal contact of the SIC, local overturning of the southern SIC, steepening of planar mineral fabrics from northwest to southeast, thickness variations in the SIC layers, and the presence of the South Range Shear Zone as a zone of enhanced strain fabric intensity.

Significance of trishear deformation for mineral exploration: Although the SIC and its Paleoproterozoic host rocks deformed simultaneously after the impact event, a considerable strain gradient is observed between the granophyre and norite layers of the southern SIC and adjacent host rocks. Evidently, layer thickness was affected by post-impact strain and thus, tectonic thinning. Rotation of lithological contacts is largely controlled by simple-shearing and bulk thinning. Layer rotation in the SIC is greatest within the zone of trishear deformation, causing overturned SIC-host rock contacts. Proterozoic rocks south of the SIC show lower intensity of post-impact deformation and smaller quantities of deformation than is apparent in the SIC. This can be explained by trishear deformation in which the Paleoproterozoic rocks chiefly form the hanging wall which was translated without being affected by large strains. Depending on the location of mineral deposits relative to the South Range Shear Zone, rotation and strain vary significantly in mineral deposits. Accordingly, Offset Dike segments located at large distances to the SIC are expected to show little amounts of internal deformation and rotation. This has important consequences for assessing the geometry of sulfide-rich fingers in Offset Dikes.

References:

[1] Lightfoot, P.C., and Farrow, C.E.G., (2002). *Econ. Geol., 97*, 1419-1446.

A SYSTEMATIC MULTI-YEAR FIELD CAMPAIGN AT THE MISTASTIN LAKE IMPACT STRUCTURE, LABRADOR, CANADA. M. M. Mader[1], C. L. Marion[1], G. R. Osinski[1,2], A. E. Pickersgill[1], A. C. Singleton[1], and L. L. Tornabene[1], [1]Centre for Planetary Exploration/Dept. Earth Sciences, 1151 Richmond St., University of Western Ontario, London, ON, N6A5B7, Canada (gosinski@uwo.ca).

Introduction: The systematic study of mid-size impact structures was one of the three main recommendations for focused research programs resulting from the first Bridging the Gap conference in 2003 [1]. For this reason, the research group at the University of Western Ontario, Canada, led by G. R. O., has been focusing on the comparative study of complex impact structures in the 20 to 40 km diameter size range in a variety of different target rocks. Structures being studied include Clearwater East and West (Canada), Haughton (Canada), Ries (Germany), Rochechouart (France), Slate Islands (Canada), Tunnunik (Canada), and Mistastin Lake – the focus of this contribution.

Mistastin Lake impact structure: The Mistastin Lake impact structure is located in northern Labrador, Canada (55°53'N; 63°18'W) has an apparent crater rim diameter of ~28 km and was formed ~36 Ma [2]. The original crater has been differentially eroded; however, a subdued rim and distinct central uplift are still observed [3]. The inner portion of the structure is covered by the Mistastin Lake and the surrounding area is locally covered by soil/glacial deposits and vegetation. The target rocks at Mistastin are dominated by granodiorite, mangerite, and anorthosite – the latter making Mistastin an ideal scientific analogue for the Moon. It is notable that this structure has only previously been mapped in reconnaissance fashion [4].

Methodology: Fieldwork was conducted over the course of 3 summers (2009 – 2011) and subsequent laboratory work is ongoing with a variety of undergraduate and graduate thesis work focusing on this structure. Below, we outline the highlights from these studies over the past 4 years.

Central uplift: The central uplift of the Mistastin Lake structure is in the form of the 3 by 4 km Horseshoe Island in the middle of Mistastin Lake. Field mapping has resulted in a new geological map for the island. A major finding has been the discovery of impact melt rock at one site located in the central area of the island and 4 sites along the eastern coast where impact melt-bearing breccia dykes are exposed. The latter have been interpreted as being intruded during the excavation stage of crater formation and injected into fractures in the host rock [5]. A systematic study of shock effects in the central uplift rocks is ongoing. Early efforts have focused on shock effects in plagioclase with some interesting results, including the scarcity of planar deformation features in distinct contrast to the co-located quartz [6].

Crater rim: Structural field geology combined with remote sensing images of the crater rim region have confirmed the presence of a topographic ring of hills at 28 km diameter, consistent with this being the apparent crater rim. The presence of several terraces formed by collapse during the modification stage of crater formation have been recognized both in the field and on satellite images [7].

Impactites: Despite the potentially multiple episodes of glaciation, one of the unique properties of Mistastin is the presence of several semi-continuous sequences of impactites exposed in streams and rivers draining in to Mistastin Lake. These exposures afford excellent opportunities to study the nature of impactites and their emplacement. A general sequence for exposed impactite units, from the base upwards, is: autochthonous to parachthonous lithic (monomict) breccias, allochthonous lithic (polymict) breccias, allochthonous impact melt-bearing breccias, and allochthonous impact melt (e.g., Fig. 1).

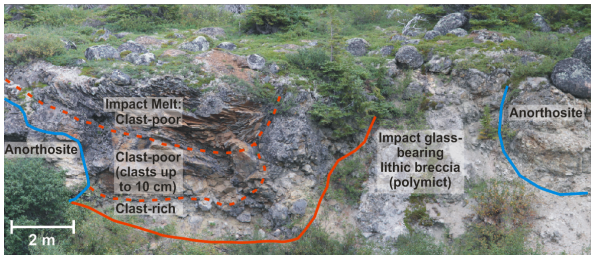

Figure 1. Impactites exposed at Coté Creek, Mistastin Lake impact structure. From [8].

Impact melt rocks at Mistastin have been studied in detail and demonstrate that the melt was derived from ~73% anorthosite, ~7% mangerite, and ~20% granodiorite [9]. The underlying breccia units are heterogeneous and studies are still ongoing; however, they are interpreted as proximal ejecta deposits [8].

References: [1] Herrick, R.R. and Pierazzo, E. (2003) *LPI Contribution No. 1162*. [2] Mak, E.K. et al. (1976) *EPSL, 31*, 345–357. [3] Grieve, R.A.F. (1975) *GSA Bull*, *86*, 1617–1629. [4] Currie, K.L. (1971) *Bull. Geological Survey of Canada 207*. [5] Singleton, A.C. et al. (2011) *42nd LPSC, Abstract #2250* [6] Pickersgill, A.E. et al. (2013) *44th LPSC*, Abstract #2471. [7] Mader, M.M. et al. (2013) *44th LPSC*, Abstract #2517. [8] Mader, M. et al. (2011) *41st LPSC*, Abstract #2505 [9] Marion, C.L. and Sylvester, P.J. (2010) *Planet. Space Sci.*, *58*, 4, 552–573.

MAPPING SUDBURY BRECCIA IN THE NORTH RANGE OF THE SUDBURY IMPACT STRUCTURE, CANADA. C. L. Marion[1], G. R. Osinski[1], R. A. F. Grieve[2], J. Bailey[3], A. Péntek[3], D. Smith[3] and J. Clayton[1], [1] University of Western Ontario, Dept. of Earth Sciences, 1151 Richmond St. London, Ontario, N6A 5B7, cmarion3@uwo.ca, [2]Earth Sciences Sector, Natural Resources Canada, Ottawa, ON, K1A 0E4. [3]Wallbridge Mining Company Limited, 129 Fielding Road, Lively, Ontario, Canada P3Y 1L7.

Introduction: Sudbury Breccia is a term applied to various breccia units at the 1.85 Ga, ~200 km diameter Sudbury impact structure, Ontario, Canada. One sub-type of Sudbury Breccia is interpreted as pseudotachylyte, which has a clast-poor to clast-rich dark aphanitic matrix and occurs in the form of veins or in large anastomosing bodies within the crater floor (Fig. 1). The leading formational hypotheses include in-situ frictional melting during crater modification such as along large displacement superfaults [1-2]; shock-induced cataclasis and comminution of the target rocks during propagation of the shock wave [3]; or impact melt injection from the overlying melt sheet into dilational fractures in the crater floor [4]. The large bodies of pseudotachylyte at Sudbury occur in a variety of shapes and sizes as well as matrix and clast content and textures [5].

Sudbury Breccia has been reported to occur up to 80 km away from the footwall contact with the Sudbury Igneous complex. The research community generally encounter outcrops in limited areas in public spaces, along road cuts such as along HWY 144 and in the mining districts where permitted. However these occurences may not be representative of the many tens of km^2 in the forested areas in between. Recently, ore mineralization within the Sudbury Breccias in the North Range footwall [e.g. 6] has drawn attention to industry to enable efficient localization of the mineralized occurences.

Objective: In collaboration with Wallbridge Mining Company Limited, we are systematically mapping the extent of Sudbury Breccia in the North Range footwall in addition to many small-scale maps of individual outcrops to identify any major changes in texture with distribution, and presence of mineralization. Here we present a preliminary map and results of an outcrop visited in Summer 2012.

Methodology: Grid mapping was completed to include cm-scale clasts hosted by the breccia and identify any and all host and clast lithologies. Sampling was completed with a Pomeroy Core Drill and 1" diamond drill bit. Petrography and analysis of these samples is ongoing and will include X-ray Fluorescence to determine if the composition of the melt matrix at this site is of local origin.

Results: The Ministic Lake Road turnoff outcrop is part of a km-scale series of Sudbury Breccia outcrops mapped along the regional contact between the Levack gneiss complex and the Cartier batholith. It is truncated by a pre-impact diabase dyke. Both vein and large bodies of Sudbury Breccia are present in this outcrop, although no ore mineralization has been observed. In each of the large breccia bodies, all of the above mentioned target rocks are represented in the clast population. Of particular interest are diabase clasts hosted by a breccia body apparently 28 m from the dyke, indicating moderate displacement. There is no exposed link between these bodies. In outcrop, both actinolite and epidote alteration were observed along with microfaults that may be pre-impact. The outcrop is approximately 37 m long by 5 m high and is dipping between 45° and 80° away from the road. A grid map was completed to include clasts > 5 cm and converted to digital format. Six 1-inch cores were collected from the various lithologies, and made into thin sections for petrographic analyses.

Future Work: Further petrographic analysis are required to identify all mineral phases within the matrix and target rocks as well as bulk geochemical analyses to compare wall rock and breccia composition. We plan to map many more of these outcrops, well off the beaten trail.

References: [1] Spray J. G. and Thompson L. M. (1995) *Nature*, 373, 130-132. [2] Spray J. G. (1998) Geological Society, London, Special Publications, 140, 195-204. [3] Lafrance B. and Kamber B. S. (2008) *Precambrian Res.*, 180, 237-250. [4] Riller U. et al. (2010) *Geology*, 38, 619-622. [5] Rousell D. H. et al. (2003) *Earth Sci. Reviews* 60, *147*–174. [6] Péntek A. et al. (2013) *Econ. Geol*. 108, 59-78.

Figure 1. Sudbury Breccia at the Ministic Lake Road turnoff outcrop. A glassy to aphinitic dark coloured matrix with clasts of multiple lithologies. Pen for scale.

LASER GUN SHOCK EXPERIMENTS ON IMPACT VAPOR PLUMES AND ITS IMPLICATION FOR ORIGIN AND EVOLUTION OF PLANETARY ATMOSPHERE. T. Matsui[1], K. Kurosawa[1], S. Ohno[1], T. Kadono[2], and S. Sugita[3], [1]Planetary Exploration Research Center, Chiba Institute of Technology (2-17-1, Tsudanuma, Narashino, Chiba 275-0016, JAPAN), [2]School of Medicine, [2]Univ. of Occupational and Environmental Health, [3]Dept. Complexity Sci. and Eng., Univ. of Tokyo.

Introduction: Atmospheric compositions and pressure are among the most important boundary conditions to investigate the evolution of the surface environment of planets [e.g., 1, 2]. Hypervelocity impacts are thought to play a key role in the origin and evolution of planetary atmospheres. Shock compression/heating and subsequent rapid decompression induce a variety of physical and chemical processes [e.g., 3]. The understanding of physical/chemical behavior of impact vapor plumes is important to investigate the number of geological events [e.g., 4-8]. Such events, however, have not been understood well because of the lack of reliable experimental data on impact-induced vaporization due to experimental difficulties.

In this paper, we describe our experimental approaches for understanding impact-induced vaporization. Recently, high-power lasers used in the studies on nuclear fusion allow us to address extreme conditions on a phase space produced by >10 km/s impacts in a laboratory. We conducted a series of laser gun shock experiments using geologic samples. Then, we applied the results to the geological problems, including atmospheric blow-off on the early Earth and a killing mechanism at the K/Pg impact event.

Experiments: Laser gun shock experiments were carried out using GEKKO-XII HIPER facility at Osaka University. The experimental setup and procedure are described in detail in our previous studies [9-13].

***P-T* Hugoniot measurement for Mg_2SiO_4:** We obtained the Hugoniot curve for forsterite on a pressure – temperature (*P-T*) plane up to 1.2 TPa using the direct drive technique. We captured time-resolved optical signal from a shocked sample using a streaked spectrometer and a VISAR. Figure 1a shows the obtained *P-T* Hugoniot curve for forstereite. The peak shock temperature at >400 GPa is much lower than the M-ANEOS prediction, suggesting that shock-heated forsterite has a higher heat capacity [13, 14]. Such high heat capacity leads to a higher entropy gain, resulting in a higher degree of vaporization after decompression than was previously thought.

Atmospheric blow-off on Earth: The eroded atmospheric mass due to an impact from planets can be calculated based on the *P-T* Hugoniot curve and the sector blow-off model [5]. We investigate the change in the atmospheric pressure on the early Earth during the late veneer phase with a stochastic model [15]. We found that the pre-existing atmosphere on the early Earth is likely to be in a complete loss during the late veneer phase [14].

Chemical composition of impact vapor plumes: We conducted the direct measurements of the chemical composition in impact vapor plumes using the flyer acceleration technique. A natural anhydrite ($CaSO_4$) sample was used as a target to investigate sulfur chemistry in vapor plumes. A quadrapole mass spectrometer (QMS) was used to measure the SO_3/SO_2 molar ratio. Figure 1b shows the SO_3/SO_2 molar ratio as a function of peak shock pressure. We found that SO_3 is the dominant species in impact-induced $CaSO_4$ vapor plumes at a wide range of peak shock pressure [12].

The K/Pg mass extinction due to acid rain: Our results indicate that a huge amount of SO_3 should be released into the atmosphere after the K/Pg impact. The high SO_3/SO_2 ratio leads to an intense global acid rain rather than global cooling proposed as the killing mechanism in the previous studies [e.g., 12, 15].

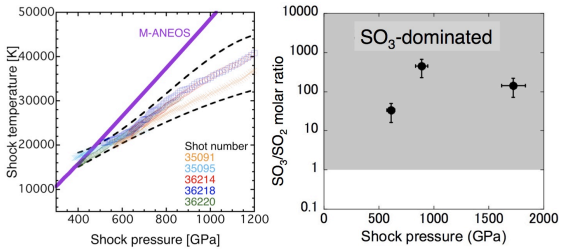

Figure 1. (a) The *P-T* Hugoniot curve for forsterite. (b) The SO_3/SO_2 ratio as a function of shock pressure.

References:

[1] Matsui and Abe (1986) *Nature, 319,* 303. [2] Matsui and Abe (1986) *Nature, 322,* 526. [3] Melosh (2007) *MAPS, 42,* 2079. [4] Ćuk and Stewart (2012), *Science*, *338*, 1047. [5] Vickery and Melosh (1990), *GSA special paper, 247*, 289. [6] Mukhin et al. (1989), *Nature*, *340*, 46. [7] Ohno et al. (2004), *EPSL, 218,* 347. [8] Johnson and Melosh (2012), *Icarus, 217*, 416. [9] Kadono et al. (2010), *JGR, 115*, E04003. [10] Kurosawa et al. (2010), *GRL, 37,* L23203. [11] Kurosawa et al. (2012), *JGR, 117,* E04007. [12] Ohno S. et al. (2012), *17th SCCM, 1426*, 851. [13] Kurosawa et al. (2012), *17th SCCM, 1426*, 855. [14] Hicks et al. (2006), *PRL*, *97,* 025502. [15] Kurosawa et al. (2013) *44th LPSC,* Abstract #2537.

SECONDARY CRATERS OF LARGE CRATERS AND BASINS ON EUROPA AND GANYMEDE: EJECTA SIZE-VELOCITY DISTRIBUTIONS ON ICY BODIES. William B. McKinnon and Kelsi N. Singer, Department of Earth and Planetary Sciences and McDonnell Center for the Space Sciences, Washington University in St. Louis, MO 63130 (mckinnon@wustl.edu).

Introduction: We have mapped fields of secondary craters around three large primary craters on Europa and Ganymede and estimated the size and velocity of the fragments that formed the secondaries using updated scaling equations for ice impacts [1]. We characterize the upper envelope of the fragment size-velocity distribution to obtain a power-law function for the largest fragments at a given ejection velocity. We compare our power-law velocity exponents to the exponents found by Vickery for similar studies of mercurian, lunar, and martian craters [2,3]; for all but basin-scale impacts, fragment size apparently decreases more slowly with increasing ejection velocity than on rocky bodies. Spallation theory provides estimates of the size of ejected spall plates at a given velocity [4], but this theory predicts fragments considerably smaller than are necessary to form most of our observed secondaries. In general, ejecta fragment sizes scale with primary crater diameter and decrease with increasing ejection velocity by $1/v_{ej}$ or greater.

Secondary Craters on Icy Satellites: The relationship between the size and velocity of fragments ejected during large cratering events on icy satellites is poorly known. Yet knowledge of the size-velocity distribution (SVD) of ejected fragments is critical to understanding the contribution of ejecta to the overall population of small craters and thus to the paramount issue of age dating by means of crater counts [e.g., 5]. Only one (preliminary) study has previously mapped and determined the SVD for such secondaries, from the crater Pwyll on Europa [6]. Here we consider three large primaries on Europa and Ganymede, including the largest preserved multiring impacts on Europa (Tyre, below) and Ganymede (Gilgamesh).

The size, depth and range from the primary of a given secondary crater allows us to calculate the size and velocity of a secondary-forming fragment via crater scaling [7]. Quantile regression fitting characterizes the decline in maximum fragment size with increasing ejection velocity v_{ej} according to $d_{frag,max} = Av_{ej}^{-\beta}$. Based on ejection physics we expect to see trends when comparing the SVDs of different secondary fields with the size of the primary, surface gravity, tensile strength of the target, etc. For the two large icy satellites considered here, β values (99th percentile) are near 1 for the three midsized craters (crater diameters in km are given in the figure below), while Gilgamesh has a much steeper $\beta \sim 3$; however, no trend for a steeper velocity dependence with increasing primary size is apparent for the Moon or Mercury (see figure and also [8,9]). While the velocity exponents for the icy midsized craters are consistently lower than those found for terrestrial craters of similar size, $\beta = 1$ is actually predicted by spallation theory [4]. Moreover, $\beta \approx 1+$ can be shown to be consistent with maximum lunar ejecta block scaling [10] (K.R. Housen, pers. comm.).

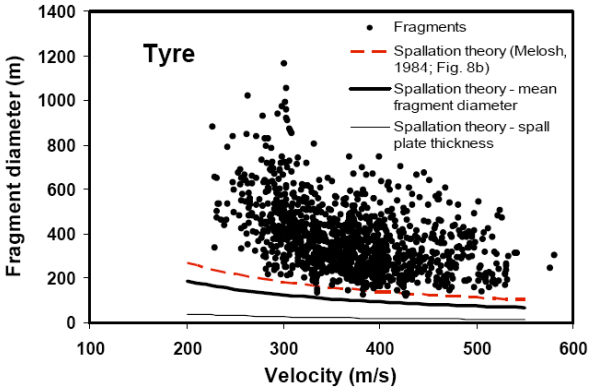

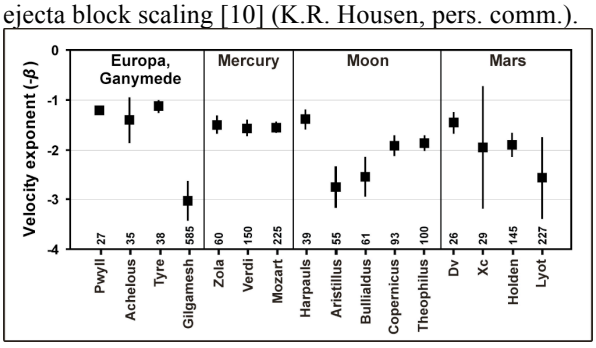

Larger craters on the same body eject larger fragments (as described by the pre-exponential factor A). Spallation theory [4], however, underpredicts the largest ejecta fragment size at a given velocity by a factor of several, as illustrated by the figure at left. Curves illustrate predicted spall plate thickness, a larger average spall fragment size (by $\sqrt[3]{100}$), and a stress-wave estimate (dashed curve). We suspect fragments cluster.

Acknowledgment: This work supported by NASA PGG.

References: [1] Singer K.N. et al. (2013) *Icarus,* submitted. [2] Vickery A.M. (1986) *Icarus, 67,* 224–236. [3] Vickery A.M. (1987) *GRL, 14,* 726–729. [4] Melosh H.J. (1984) *Icarus, 59,* 234–260. [5] McEwen A.S. and Bierhaus E.B. (2006) *AREPS, 34,* 535–567. [6] Alpert A.J. and Melosh H.J. (1999) *LPS XXX,* Abstract #1881. [7] keith.aa.washington.edu/craterdata/scaling/theory.pdf. [8] Hirase Y. et al. (2004) *PSS, 52,* 1103–1108. [9] Hirata N. and Nakamura A.M. (2006) *JGR-Planets, 111,* 3005. [10] Bart G.D. and Melosh H.J. (2010) *Icarus, 209,* 337–357.

A HOLEY CONUNDRUM: DISTINGUISHING BETWEEN ANCIENT CALDERAS AND DEGRADED IMPACT CRATERS ON MARS. J. R. Michalski[1,2], J. E. Bleacher[3] and S. P. Wright[4], [1]Planetary Science Institute, Tucson, Arizona, 85719, USA; michalski@psi.edu, [2]Dept. of Earth Sciences, Natural History Museum, London, UK, [3]NASA Goddard Spaceflight Center, Greenbelt, Maryland, USA. [4]Dept. of Geology and Geography, Auburn University, Auburn, Alabama.

Introduction: The surface of Mars contains thousands of impact craters exhibiting a range of stages of preservation from youthful craters with well-preserved morphological evidence for impact to ancient craters in which most diagnostic features attributable to impact origin have been removed by erosion [1]. We suggest that some of the most ancient basins Mars, commonly assumed to have formed by impact, are in fact large calderas that formed through explosive volcanism early in Martian history [2].

Approximately 70% of the Martian surface has been resurfaced by volcanism though a significant fraction is from yet unrecognized sources [3]. In fact, while Hesperian and Amazonian volcanic constructs are easily recognized from their classic shield morphologies, relatively little is known about Noachian volcanism – either because those constructs have been strongly modified by erosion [4] or because ancient volcanoes were of a fundamentally different character than more youthful volcanoes [2]. Distinguishing between an impact versus volcanic origin for many ancient Martian basins is complicated, but hugely important for understanding the geologic evolution of the Martian crust.

Observations in Arabia Terra: The Arabia Terra region is one of the most ancient parts of the Martian crust. In northern Arabia Terra, we have identified at least 8 large (20-100 km-diameter) basins that are unlikely to have formed from meteor impact. Many of these features have been dismissed previously as degraded impact craters. Yet, these features generally do not preserve any clear evidence for impact processes; no morphologic evidence for central uplifts, uplifted rims, ejecta, or inverted stratigraphy is observed in remote sensing data. While all of these features could have been removed by erosion, significant resurfacing of ancient impact craters generally results in lower crater depth/diameter ratios than what is observed in these basins [1-2].

The type-example of an ancient caldera, termed here a plains-style caldera complex, is Eden Patera (Figure 1), which is a large, irregularly shaped topographic depression (~55 km by 85 km in diameter, NW-SE and SW-NE respectively) located at 348.9 E, 33.6 N within Noachian-Hesperian ridged plains of likely volcanic origin (Figure 1). Other features in northern Arabia Terra contain evidence for collapse associated with volcanic activity. Siloe Patera (6.6 E, 35.2 N) is a set of nested, deep depressions that reach ~1750 m below the surrounding plains. Euphrates Patera is an irregularly shaped depression that reaches 700 meters depth below the surrounding lava plains and contains several benches in the interior that might be explained by sequential episodes of collapse or lava lake high stands. Semeykin Crater is a large, scalloped depression surrounded by lava plains and friable deposits, which also contains mounds of friable materials in its interior and ridged plains along the exterior. A suite of features, Ismenia Patera, Oxus Patera, and Oxus cavus are located together near 0E, 38.5 N. The two patera exhibit scalloped, breached rims composed of layered materials.

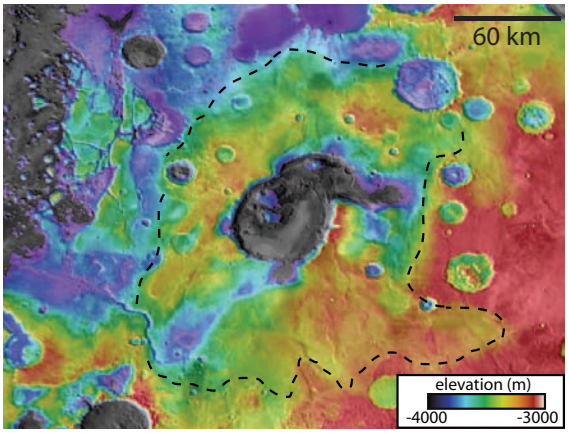

Figure 1: MOLA colorized elevation data are draped over THEMIS daytime infrared data showing Eden Patera, a plains-style caldera complex in Arabia Terra, Mars.

Implications: We suggest that some ancient basins on Mars represent a fundamentally new type of volcanic construct on Mars: plains-style caldera complexes. Ancient, degraded impact craters certainly exist in the Noachian Martian crust, but further work must be done to distinguish between degraded impact craters and ancient calderas. Plains-style caldera complexes might have formed in an early phase of explosive volcanic activity on Mars.

References: [1] Robbins, S. J. and B. M. Hynek, JGR 117, E05004, 2012. [2] Michalski, J.R., J.E. Bleacher, and S.P. Wright, 43rd LPSC, abstract 1263, 2013. [3] Greeley, R. and P. Spudis, Rev. Geophys. 19, 13-41, 1981. Golombek, M. P. et al., JGR 111, 1-14, 2006.

HYDROCODE SIMULATION OF THE TRANSITION FROM CENTRAL PEAK TO PEAK-RING CRATER MORPHOLOGY FOR THE MOON. C. Milbury[1] , B. C. Johnson[1] and H. J. Melosh[1], [1]Department of Earth, Atmospheric, and Planetary Science, Purdue University, 550 Stadium Mall Drive, Hampton Hall, Room 3233, West Lafayette, IN 47907 (cmilbury@purdue.edu).

Introduction: The observed transition from simple to complex crater morphology is driven by gravitational collapse of the transient crater. The mechanism that causes the transition from complex to peak-ring crater morphology is still debated. There are two dominant models that have been proposed to explain this transition in crater morphology. Both the central peak collapse model [1, 2] and the nested melt cavity model [3, 4] predict the observed morphological features and depth to diameter ratios. By calculating peak and peak ring volumes, Bray et al. [5] showed that the data tend to support peak-ring formation by collapse of the central peak.

In this study, we systematically investigate this change in crater morphology using the iSALE hydrocode and varying the Acoustic Fluidization (AF) parameters over a broad range of values. We will identify where melt is produced and calculate the melt volume so these can be compared with the nested melt cavity model predictions.

Background: Melosh [6] was the first to put forward the idea of AF, which is the temporary behavior of fractured rock as a viscous fluid. It is triggered by intense, short-wavelength vibrations within the target and it occurs mostly within the crater collapse phase of the impact process. Wünnemann & Ivanov [7] carried out simulations using the AF model to match the observed depth to diameter ratios over a range of crater sizes for the Moon, Earth, and Venus.

Methodology: We use the following model parameters in our simulations: an equation of state granite crust and a dunite mantle, an impact velocity of 17 km/s, a lunar gravity of 1.62 m/s^2, a target heat flow of 18 mW/m^2, and a melt temperature of 1373 K. We systematically vary the AF parameters, Υ_T and Υ_η, to understand how they affect crater morphology. Υ_T is a scaling factor related to the decay time and controls the amount of time the target is subject to AF, and Υ_η is the viscosity-scaling parameter [7].

For each model run, the crater depth, diameter, and central peak height and width are compared to those determined by Kalynn et al. [8] for lunar complex craters using topographic data. The impactor size will be increased such that the characteristics for larger impact structures can be examined. Figure 1 shows the temperature profile 700 s after impact with a 7 km diameter dunite impactor. These will be compared with specific craters on the Moon, and the gravity signature associated with these craters will also be modeled using data from NASA's Gravity Recovery And Interior Laboratory (GRAIL) mission.

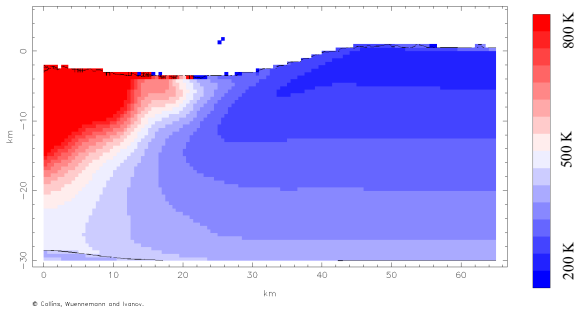

Figure 1. The temperature profile 700 s after impact.

Discussion: Understanding this observed change in crater morphology has implications beyond the Moon. The transition from central peak to peak-ring craters and these types of craters is observed throughout the solar system. Alexopoulos & McKinnon [9] documented this transition for Venusian craters using Arecibo and Venera radar images and Magellan radar data. Since the MESSENGER mission arrived at Mercury, an increasing number of complex and peak-ring craters have been identified [10]. Nycz & Hildebrand [11] used Viking and Mars Orbiter Camera images to identify and classify 680 impact structures on Mars. They showed a size and morphological progression similar to that of [9]. Multiringed basins are not unique to terrestrial bodies; they have been observed on Jupiter's icy moons [12].

Investigating this transition is clearly important and it may help to shed new light into the cratering process and the mechanism that causes this tobserved transition in crater morphologies.

References: [1] Morgan, J. V. et al (2000) *EPSL, 183*, 347-354. [2] Collins, G. S. et al. (2002) *Icarus, 157*, 24-33. [3] Head J. W. et al (2010) *GRL, 37*, L02203. [4] Baker D. M. et al (2011a) *Icarus, 214*, 377–393. [5] Bray V. J. et al. (2012) *GRL, 39*, L21201. [6] Melosh (1979) *JGR, 84*, 7513-7520. [7] Wünnemann K. and Ivanov B. A. (2003) *PSS, 51*, 831-845. [8] Kalynn J. et al. (2013) *GRL, 40*, 38-42. [9] Alexopoulos J. S. and McKinnon W. B. (1994) *SPGSA, 293*, 29-50. [10] Baker D. M. et al., (2011b) *PSS, 59*, 1932-1948. [11] Nycz J. C. and Hildebrand A. R. (2003) *MPSA*, #5255. [12] Schenk P. M. and McKinnon W. B. (1987) *Icarus, 72*, 209-234.

TRACING LOWER CRUST AND UPPER MANTLE ON THE SURFACE OF THE MOON. Katarina Miljkovic[1] and Mark A. Wieczorek[1], [1]Univ Paris Diderot, Sorbonne Paris Cité, Institut de Physique du Globe de Paris, 75013 Paris, France (miljkovic@ipgp.fr).

Introduction: The global crustal thickness map of the Moon derived from GRAIL gravity measurements shows that the lunar crust is thinner than previously thought. The nearside crust is on average 30 km thick. The crustal thickness on the farside varies from about 30 km in the South Pole-Aitken (SPA) basin up to 60 km in the highlands [1]. Previous studies suggest that during basin formation, the amount of excavated mantle depends on the target material rheology [2,3]. This work investigates whether these crustal thicknesses, together with different target properties could have caused the excavation of the underlying mantle material during impact basin formation, how much and where would that material be located within the impact site.

Method: Numerical modeling of lunar impact basins was made using iSALE-2D, a multi-material, multi-rheology shock physics hydrocode [4,5]. An infinite-half space target mesh in 2-D was divided into crust and mantle layers, represented by basaltic and dunite rock, respectively. The material parameters: ANEOS, strength and failure model were used from [6,7]. Thickness of the pre-impact crustal layer was fixed at 30 or 60 km. Impactor size ranged from 15 to 90 km and impact speed was 17 km/s, which covered a range of impact basins from small peak-ring to large multi-ring basins. Lunar nearside and farside were represented by vertical temperature profiles derived from lunar 3-D thermal evolution models [8] with variations that correspond to the location on the surface (i.e. PKT, highlands) and the time basins formed (~4.0 Ga ago).

Results: Impact basins form via the growth of a deep, bowl-shaped transient cavity that is gravitationally unstable and is followed by a complex collapse into final morphology. The collapse of the transient crater is combined of inward motion of the cavity walls and prominent uplift of the cavity floor [2,6], both of which depend sensitively on the shear strength and temperature of the crust and upper mantle [9]. The uplift of the transient crater floor brings up the underlying layers of lower crust and upper mantle closer to the surface, where surface exposure is possible, depending on target properties and impact size.

Numerical modeling shows that in a 30-km-thick crust, the formation of peak ring and multi-ring basins is accompanied by exposures of upper mantle on the surface, with highest concentrations of mantle material in regions between the peak (or inner) ring and topographic rim. Depending on the size of the melt pool formed within the basin center, these exposures mostly concentrate at the melt pool edge, where the melt pool is also the shallowest. Similarly in a 60-km-thick crust, the lower crust becomes mostly exposed, with little or no upper mantle involved. Materal uplifted and deposited on the surface is heavily mixed in with the upper crust layers. In addition, depending on the crustal properties, during final stages of crater modification a fine layer of fractured crust could cover up the exposed underlying material.

Comparison with observations: The hyperspectral mapping obtained by the Spectral Profiler (SP) onboard SELENE/Kaguya shows global distribution of olivine-rich [10] and pure anorthosite (PAN)-rich [11] sites on the Moon. Olivine is associated with the upper mantle, and PAN with lower crust [10,11]. The olivine-rich exposures are found mainly on the nearside, where crust is globally thinner than on the farside. Some olivine was found in the SPA and Moscoviense basins, which are the regions of the thinnest crust on the farside. Furthermore, those olivine exposures are distributed along the concentric regions within the basins, mainly along the mare or crater rims [10]. Similar patterns are found in the highland region with the PAN exposures being concentrated along the crater rims [11].

Conclusions: Numerical modeling of lunar impact basin formation, for basins ranging from peak-ring to multi-ring showed that uncovering and excavation of the lower crust and upped mantle material are likely products of basin formation in the thin crust, and for larger basins in the thick crust. If the observed exposures of olivine and PAN are indeed the highest concentrations of the underlying material exposed to the surface, then our numerical modeling is in agreement with the observations.

References: [1] Wieczorek et al. (2013) *Science, 339,* 671-675. [2] Potter, R. W. K. et al. (2012) *GRL*, 39, L18203. [3] Stewart, S. T. (2011) *42nd LPSC*, Abstract #1633. [4] Amsden, A. A. et al. (1980) *LANL report* LA-8095, 105. [5] Collins, G. S. et al. (2004) *Meteorit. Planet. Sci.* 39, 217–231. [6] Ivanov B.A. et al. (2010) *GSA special paper* 465, 29–49. [7] Pierazzo, E. et al. (2005) *Large Meteorite Impacts III,* vol. 384. [8] Laneuville, M. et al. (2013) *JGR*, submitted. [9] Miljkovic, K. et al. (2013*) 44th LPSC*, Abstract #1926. [10] Yamamoto, S. et al. (2010) *Nature Geoscience*, 3, 533-536. [11] Nakamura, R. et al (2013) *44th LPSC*, Abstract #1988.

Acknowledgements. This work was funded by the UnivEarthS LabEx project of the University of Sorbonne Paris Cité.

CARBONATE-RICH IMPACT-MELT FROM MOROKWENG IMPACT STRUCTURE, SOUTH AFRICA.

S. Misra[1], D. Ray[2], and M. A. G. Andreoli[3, 4], [1]SAEES, University of KwaZulu-Natal, Durban-4000, South Africa (misras@ukzn.ac.za).; [2]PLANEX, Physical Research Laboratory, Ahmedabad-380009, India; [3]Necsa - NLM, P. O. Box 582, Pretoria 0001, South Africa; [4]School of Geoscience, University of the Witwatersrand, Wits 2050, South Africa.

Introduction: The Morokweng impact crater (centered 26°20′S, 23°32′E) in the North West Province of South Africa was formed at 145±2 Ma ago by an impact of a LL-6 chondrite [1]. The target rocks of this impact crater mostly include Archaean granitoids, mafic gneisses, greenstones, mafic to acid lavas, and ultramafic cumulate rocks along with the overlying Proterozoic and Phanerozoic (Karoo) cover rocks. More specifically, the Proterozoic supracrustals include extensive dolomitic carbonates and BIF of the Griqualand West Supergroup [2]. The preserved thickness of the impact-melt probably exceeds ~870 m [1] and was interpreted to have formed dominantly from the granitic target along with significant mafic igneous rocks and minor quartzite [3]. In the present abstract, we report our preliminary observation on cores provided by the De Beers company from boreholes drilled ~15 Km SW of the Morokweng town (26°15′30″S, 23°41′30″E), an area blanketed by sand and calcrete of the Cenozoic Kalahari Group [2]. The study of these cores suggests the presence, at least locally, of a carbonates-rich impact-melt component in the Morokweng crater.

Sample descriptions and analytical procedure: In the present study, we have investigated a set of a dozen core samples 70 mm in diameter and up to 8 cm in length. The cores are representative of extensive breccia intersected in boreholes drilled in the early 1990s by the De Beers Company at the site of a magnetic anomaly within the Archaean basement rocks (Dr. C. Smith, personal communication). The clasts in the breccia predominantly consist of granite (generally intensely fractured and discoloured) and sulphide-bearing amphibolite. Occasionally, very fine grained clasts, dark grey or red colour, were also noted. The chemical analyses for the present study were done at PLANEX, Physical Research Laboratory, Ahmedabad, India, with a Cameca Sx 100 electron microprobe equipped with wavelength dispersive spectrometer (WDS) with large crystals (LPET and LLiF) under the following analytical conditions: 15 keV accelerating voltage, 20 nA sample current, ≤1 μm bean with PAP correction.

Petrography: A core sample marked 834/2 (depth unspecified) from the De Beers bore hole has been investigated for the present study. Under the microscope, the rock consists of angular fragments of granitoid of two main sizes (fewer large clasts scattered among smaller ones) within a very fine grained, red-coloured matrix, not clearly resolvable under an optical microscope.

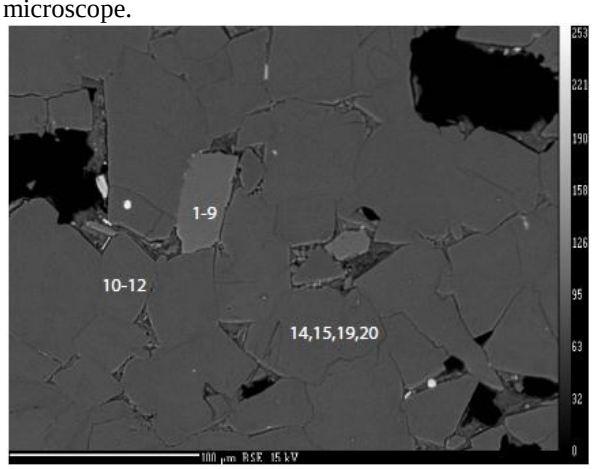

Fig. 1. BSE image of finer grained, red-coloured matrix from De Beers borehole core marked 834/2 (see text; numbers define analytical spots).

BSE image of the finer fraction of the rock sample is shown in figure 1. It mostly consists of subhedral prismatic grains of rectangular shapes, which are in contact with each other showing cumulate-type texture.

Analytical data: Analyses 1-9 were carried out on a prismatic grain with corroded boundary, which was found to be a potash feldspar xenocryst. The rest of the analyses (10-12, 14, 15, 19, 20) established that the matrix material was mainly a dolomitic melt with significant proportions of MgO (~17-23 wt %) and CaO (~36-38 wt %). Our further analyses on other spots of the thin section further confirmed that most of the red matrix consists of euhedral to subhedral dolomite crystals < 100μm in maximum size.

Discussion: Our preliminary investigation on the De Bears borehole suggests that the matrix of the impact breccia consists of dolomitic melt. This suggests the involvement of significant volumes of Griqualand West carbonates as a target rock, at least locally, during the excavation of the Morokweng crater. Given the presence of a melt in the breccia and of common PDFs in the granite clasts (M Andreoli, unpublished data) we conclude that the De Beers boreholes cores intersected a volume of suevite, a rock type previously misinterpreted as Dwyka Group diamictite [3].

References: [1] Maier W. D. et al. (2006) *Nature, 441*, 203-206. [2] Andreoli M. A. G. et al. (1999) *GSA Spec. Paper, 339*, 91–108. [3] Koeberl C. and Reimold W. U. (2003) *GCA, 67*, 1837-1862.

Crater Profile Analysis using High Resolution Laser Altimetry Data Sets. J. Montgomery[1] and J. McDonald[2], [1]Georgetown University, Washington, DC 20057, jmontgomery@cs.georgetown.edu, [2]DePaul University, Chicago, IL 60604, jmcdonal@cs.depaul.edu.

Introduction: Impact craters play an important role in planetary chronology and geomorphology. Analyzing impact crater morphological features, such as crater diameter and frequency is a critical step in determining the age of celestial bodies[1]. However, the accuracy of impact crater measurements can vary depending on the type of remote sensed data used and on the method used to measure impact crater features. Such efforts have been greatly aided by the new topographical data sets from planetary orbiting satellites such as the mars and lunar orbiters [2], which have provided maps as detailed as 1024 px/degree. Unfortunately current tools are either unable to use this new dataset at all due to the sheer volume of data or are unable to allow feature identification and analysis at interactive speeds. We present a novel approach which integrates feature exploration with precise crater profile measurements using high-resolution laser altimetry (128, 512 or 1024 px/degree) data sets rendered at interactive frame rates on consumer graphics hardware.

Impact crater morphometry is essential in studying landform processes of planetary bodies. For example, crater formation and size/frequency distribution rely on measurements of feature sizes and slopes on the body's surface. These measurements can be derived either from stereographic images obtained from visual spectrum cameras or from altimetry data products which have traditionally been of much lower resolution. The present work focuses on altimetry products because the accuracy and resolution of the current data sets provided by NASA are competitive with the higher resolution stereographic data previously available. Morphometric analysis based on height measurements derived from low resolution data can differ by as much as ± 250 meters when compared with high resolution data products[3] and slope calculations can suffer dramatically from such inaccuracies.

The primary tool for measuring crater morphology is the crater profile, which is a cross section plot of a crater's elevation and diameter. Crater profiles can be generated manually from altimetry data. Unfortunately, one of the most common methods for using altimetry data uses an add-on tool for ARCGIS [4]. This system requires importing a low-resolution shade-relief terrain model which is rendered offline. Therefore the computations are often based on data from a secondary image rather than from the original altimetry data set.

mVTK is a visualization and data exploration software package that dynamically renders visualizations of high resolution digital terrain models in gridded record datasets (GRD) at interactive speeds. It does this by exploiting the power of consumer graphics hardware [5]. To facilitate the use of mVTK for impact crater morphometry, we have extended mVTK with the addition of tools for crater profile measurements. These measurements are computed directly from the high-resolution LOLA/MOLA GRD datasets based on user input with a mouse.

The system provides equidistant cartographic projections using the full-resolution gridded data files provided by NASA and provides both false-color and shade-relief visualizations. These projections are interactively rendered allowing the user to explore the planetary surface in real-time [6]. Once the user has chosen the desired planetary feature, the user can select a linear path along the surface to generate a crater profile. The profile generated by mVTK uses the same high-resolution altimetry data that was used for cartographic projection and is also computed and rendered using graphics hardware.

To compute distances and slopes, the user simply selects two points on the profile graph. These points are mapped back to the original unmodified high-resolution gridded data and both the longitudinal and vertical distances are computed. These distances allow the following crater measurements which are essential to the analysis of crater formation:

- Rim-to-rim and rim-to-peak distances
- Rim height
- Crater floor and peak widths
- Crater wall and peak wall slopes

These measurements are essential to impact crater categorization and to the analysis of crater formation, such as, simple crater to complex crater transitioning characteristics [7]. Measuring crater features are in important part of chronology and crater morphology analysis. This presentation will demonstrate how mVTK provides a method that directly uses high-resolution altimetry data to improve the accuracy of such measurements.

References:

[1] G. Neukum et al. (2001), *Space Science Review*, 96, 55-86. [2] D.E. Smith et al. (2010) *Geo. Research Letters*, 37, L18204. [3] P.V. Radhadevi et al. (2012) *LPS 43rd*, Abstract #2303. [4] T. Kneissl et al.. (2010) LPS 41st, Abstract #1638. [5] R. Rost, et.al. *The OpenGL Shading Language* (*3rd Edition*), Addison Wesley Professional, July 2009. [6] J. Montgomery and J. McDonald (2012) *,Proc. SPIE*, 85390E. [7] V.J. Bray et al. (2012) *LPS 43rd*, Abstract #1694.

MOON MINERALOGY MAPPER OBSERVATIONS OF SOUTH POLE – AITKEN: CONSTRAINTS ON BASIN FORMATION. D. P. Moriarty[1] and C. M. Pieters[1], [1]Dept. of Geol. Sci., Brown Univ., Providence, RI, Daniel_Moriarty@Brown.edu

Introduction: With a diameter of ~2500 km and a maximum depth of ~12-14 km, The South Pole – Aitken basin (SPA) on the lunar farside is one of the largest (and oldest) impact basins in the solar system [1-6]. As such, SPA is key to understanding large impact processes as well as the structure of the lunar interior. Here, we compare impact basin formation models to Moon Mineralogy Mapper (M^3) observations.

Vertical Impact Model: The simplest basin formation models invoke vertical impacts. For a SPA-scale vertical impact, scaling relationships predict total excavation of crustal materials from the transient cavity [e.g. 7]. Large quantities of melt are formed, primarily from mantle materials [7-9]. Uplift and collapse of melted mantle materials at the center of the forming basin result in sloshing of these materials over the rim of the transient cavity and emplacement overlying exterior crustal materials [7,10]. Extensive collapse of the transient cavity deforms and translates materials inward and results in a final topographic depression larger than the transient cavity by a factor of ~2 [7]. This results in a two-zone basin structure: an inner zone comprised of mostly mantle melt and an outer zone comprised of mantle melt overlying crustal materials [7].

Model Variations: *Melt sheet differentiation*. Melt bodies can differentiate under certain conditions (low viscosity, slow cooling, and convection) [11]. If a melt sheet fully differentiates, individual exposures of the melt sheet would not represent the bulk composition [9,12]. However, the stratigraphy formed via differentiation is sensitive to the bulk composition [9]. *Oblique impact*. Vertical impacts are statistically unlikely, the most likely impact angle on any planetary body being 45° [13]. For a given transient crater volume, highly oblique impacts reduce the total volume of impact melt produced and shift the melt region shallower and downrange [14]. Oblique impacts also result in a muted central uplift as well as less melt retention in the basin interior [7,10]. *Low-speed / large projectile*. For a given transient crater volume, low-speed / large projectile impacts produce less melt [8,15]. Additionally, excavation and melting occur in shallower zones. A larger impactor cross section could trap more crustal materials in the melt region, effecting the bulk melt composition [16]. An oblique impact by a very large impactor would cause impactor decapitation and energy decoupling, preserving a large transient cavity with pre-impact stratigraphy [15]. *Clast-rich melt*. Many models treat melted materials as a strengthless fluid. This in unrealistic, as crater modification and partial melting would result in clast-rich melts [16]. The inclusion of clasts results in two-phase flow and limits the overshoot of melt beyond the transient cavity rim during mantle uplift and collapse [16].

M^3 Observations: For this study, a survey of compositional units was performed for NW SPA using M^3 data. Although the lunar mantle is expected to contain significant olivine, observations of SPA have revealed a paucity of the mineral [17-21]. This is consistent with three SPA impact scenarios: (1) shallow excavation and melting resulting from a highly oblique and/or low-velocity impact (sampling mostly lower crustal materials), (2) an upper mantle lacking significant olivine (implying mantle overturn did not occur [17]), or (3) sequestration of olivine at unsampled depths via melt sheet differentiation [9]. (3) would also require a mechanism to constrain mantle melt to central SPA (such as clast-rich melt flow), since thinner melt deposits in outer SPA are less likely to differentiate and sequester olivine at unsampled depths.

Central SPA is dominated by low-Ca pyroxene (LCP), which is exposed in craters of various sizes (suggesting that it is pervasive over a range of depths) [18-20]. Outer SPA exhibits juxtapositions of LCP- and plagioclase-rich materials, also at a wide range of depths. The scale of heterogeneity in this region ranges from 100s of meters to ~100 km. If SPA impact ejecta (mafic melt and breccia) was emplaced over the crust surrounding the transient cavity, large-scale mixing and deformation of these layers may occur during the modification stage, producing the observed heterogeneity [7]. The inward motion of external materials during collapse may also explain the occurrence of plagioclase-rich crustal materials near the basin center (such as in the central peaks and ejecta of Alder). Characterizing the petrogenesis of individual LCP-rich exposures through quantitative spectral analysis will further constrain the basin formation process.

References: [1]Stuart-Alexander, D. (1978) *USGS Map, 1-1047*. [2]Wilhelms, D. E. et al. (1979) *Geol. Atlas Moon, I-1162*. [3]Spudis, P. D. et al. (1994) *Science, 266*, 1848-1851. [4]Zuber, M. T. et al. (1994) *Science, 266*, 1839-1843. [5]Wieczorek, M. A. and R. J. Phillips (1999) *Icarus, 139*, 246-259. [6]Garrick-Bethell, I. and M. T. Zuber (2009) *Icarus, 204*, 399-408. [7]Potter, R. W. K. et al. (2012) *Icarus, 220*, 730-743. [8]Pierazzo, E. et al. (1997) *Icarus, 127*, 408-423. [9]Vaughan, W. M. and J. W. Head (2013), *LPSC, XLIV*, #2012. [10]Osinski, G. R. et al. (2011) *EPSL, 310*, 167-181. [11]Warren, P. H. (1993) LPSC, XXIV, 1481. [12]Morrison, D. A. et al. (1998) *LPSC, XXIX*, #1657. [13]Shoemaker, E. M. (1963) *The Moon, Meteorites and Comets*, 301-336. [14]Pierazzo, E. and H. J. Melosh (2000) *Icarus, 145*, 252-261. [15]Schultz, P. H. and D. A. Crawford (2011), *Geo. Soc. Am. Special Papers, 477*, 141-159. [16]Stewart, S. T. (2011), *LPSC, XLII*, #1633. [17]Hess, P. C. and E. M. Parmentier (1995) EPSL, 134, 501-514. [18]Pieters, C. M. et al. (1997) GRL, 24, 1903-1906. [19]Pieters, C. M. et al. (2001) JGR, 106, E11, 28.001-28.022. [20]Moriarty, D. P. et al (2013) LPSC, XLIV, #3039. [21]Yamamoto, S. et al. (2010) Nat. Geosci., 3, 533-536.

Atomic Records of Inner Solar System Impact Processes from U-Pb Dating Phases

D.E. Moser[1], I.R. Barker[1], K.T. Tait[2], J.R. Darling[3], K.R. Chamberlain[4], A.K. Schmitt[5], C.L. Cupelli[1], D. A. Reinhard[6], D. Olson[6], P. H. Clifton[6], D. J. Larson[6], B.Gault[7], M. Bugnet[7], M B. Shaulis[8], T.J. Lapen[8], A.J. Irving[9]
[1]University of Western Ontario, London, CAN (desmond.moser@uwo.ca), [2]Royal Ontario Museum, Toronto, CAN; [3]University of Portsmouth, Portsmouth, UK; [4]University of Wyoming, Laramie, Wyoming, USA; [5]UCLA, Los Angeles, USA; [6]CAMECA, Madison, WI 53711, USA; [7]CCEM, McMaster University, Hamilton, CAN; [8]Univ. of Houston, Houston, USA; [9]University of Washington, Seattle, USA.

Introduction: Time is of the essence in the reconstruction of planetary processes, and the extremely sluggish volume diffusion rates of elements such as U, Pb, O, Hf and trace elements in the geochronology minerals such as zircon and baddeleyite, together with their resistance to breakdown during shock metamorphism [1], make them ideal recorders of inner Solar System evolution. These micro-minerals, relatively common in planetary crusts and achondrites, can also preserve microstructures diagnostic of impact environments, with zircon sometimes capturing the entire shock loading and unloading sequence [2]. Here we present case studies from the Earth, Moon, Asteroid Belt and Mars illustrating the new records of shock metamorphic processes, ages and environments obtainable from U-Pb geochronology phases.

Methods: The advances we present are made possible by integration of electron nanobeam measurements of orientation and chemical microstructure with isotopic analyses, ideally using *in situ* techniques such as SIMS (UCLA), laser ablation ICPMS (Univ. of Houston), or the relatively new technique of Local Electrode Atom Probe (LEAP) Tomography (CAMECA). Electron nanobeam analyses were performed at the Zircon and Accessory Phase Laboratory (UWO ZAPLab) using a Hitachi SU6600 VP-FEG-SEM with cathodoluminescence (CL) , electron diffraction (EBSD), Energy Dispersive Spectroscopy (EDS) [2], and by atomic resolution STEM (CCEM).

EARTH: A natural laboratory for response of U-Pb and other isotopic systems to shock pressure and heating is the central uplift of the ~250 km diameter Vredefort impact basin of South Africa, where we can examine mineral response across a large shock-metamorphic pressure and thermal gradient from collar to center. Shock microtwins, first discovered in the collar, persist through extreme post-schock heating in the pyroxene hornfels post-impact thermal aureole, sometimes nucleating coarse granules of impact age. Crystallographically controlled planar and curviplanar features, impact melt glass, and pervasive crystal-plastic deformation track the sequence of shock loading, unloading and crater modification [2]. These records survive modern fluvial transport over hundreds of kilometers [3]. Monazite shock microstructures also vary radially from planar features to polycrystalline granular at center [4]. Impact-related Pb loss, age disturbance and plasticity are minor to absent in the outer zone of post-shock heating, and begins approximately at the 800°C isograd [2]. This is a useful template for reconstructing shock histories on other planets.

MOON: Micrograins of zircon and baddeleyite in lunar breccia NWA 2200 [5] exhibit a diversity of microstructures analogous to those in samples from the Vredefort and Ries craters. An example of polystage igneous and impact processes is evident in an anhedral zircon grain, in an apparently undeformed gabbro clast, exhibiting shock microtwin lamellae and crystal-plastic deformation. Our spatially correlated SIMS U-Pb dating are revealing a 400 million year window of early lunar processes.

ASTEROID BELT: Recent SIMS dating of eucrite zircon yield a 50 million year age range interpreted as protracted crystallization from 4.56 Ga [6]. We observe complex CL zoning in a 4.54±0.1 Ga eucrite zircon, as well as crystal-plastic deformation and low-angle grain boundaries, allowing that deformation-assisted Pb-loss could account for variations in U-Pb ratos in asteroidal material.

MARS:. Our microstructural analyses and SIMS dating of shocked, igneous micro-baddeleyites in the highly shocked basaltic shergottite NWA 5298 resolve a longstanding debate in martian geochronology. Our results demonstrate 'young' igneous activity on Mars at 187±33 Ma through melting of an ancient ~4 Ga reservoir, and subsequent shock-resetting of some baddeleyite grains during Earthward launch and growth of 'ejectic' zircon near quenched melt pockets [7]. Analysis of a recently discovered population of martian regolith zircon, baddeleyite and monazite is underway [8], and it is likely that documentation of their age and microstructure will reveal additional insight into impact phenomena and environments in the inner solar system.

References: [1] Krogh, T.E., Kamo, S.L., & Bohor, B.F. (1996) *Geophys. Monog.*, 95, 343-353. [2] Moser, D. E. et al. (2011) *Can. J. Earth Sci.* 48, 117–139. [3] Erickson, T.M. et al. (2013) *GCA* 107, 170-188. [4] Moser, D.E. (1997) *Geology* 25, 7-10. [5] Darling, J.R. (abs) ESBD 2012 CMU, Pittsburgh. [6] Zhou, Q. et al.. (2013) *GCA* 110, 152-175. [7] Moser D.E. et al. (2013). *Nature*, in press. [8] Moser, D.E. et al. (2013) *Meteoritical Society*, Edmonton, CAN (Abs).

Deciphering lithological contact of granophyre dikes with bedrock granites at Vredefort dome, South Africa

N. Nakamura[1], and Meyer[2] [1]Department of Earth Science, Tohoku University, 980-8578, Japan, [2]Kopjeskraal Country Lodge, P O Box 1922, Parys, 9585, South Africa

Introduction: The Vredefort impact structure contains a suite of granophyric dykes, referred to as the Vredefort Granophyre, occurring within and at the edge of the Archaean basement core. This unique melt rock occurs as vertical ring dikes along the contact between sedimentary collar and core of Archaean granites, and as vertical dikes extending northwest-southeast and northeast-southwest in the granitic core. It has known that the granophyre rocks have an unusual composition and high content of recrystallized sedimentary inclusions compared to common intrusive igneous rocks with similar SiO2 content (61 to 70 percent by weight) [1]. Although there have been a lot of mineralogical and isotopic studies, the lithological contact has not been studied due to the lack of the outcrop. During the field survey, we found the lithological contact of the Vredefort granophyre with bedrock granites near the Kopjeskraal Country Lodge, Vredefort, South Africa. Here we report the petrological and magnetic studies of the contact.

Geological background: The Vredefort Granophyre is an impact melt that was injected downward into fractures in the heavily shocked and metamorphosed granite. This unit contains inclusions that are predominantly composed of quartzite, feldspathic quartzite, arkose, and granitic material with minor proportions of shale and epidiorite. Despite the granitic materials, the granophyre represents a stable paleomagnetic remanence [2].

Result and Discussion: Figure 1 represents surface stray magnetic field over the contact in the thin section by using scanning magneto-impedance magnetic microscope [3]. White color is an upward stray field and black is a downward field from the thin section surface. Granite shows a heterogeneous distribution of coarse-grained magnetite, instead granophyre shows a highly magnetic stray field. This highly magnetic portion agrees well with a ballen texture of mafic minerals. Also the contact is not discontinuous boundary such as faulting, but is the solid-state. Therefore, we can explore the thermal history of the contact from the petrological observations. In this presentation, we will give a cooperative studies of petrology and paleomagnetism.

References: [1] Therriault, A. M., Reimold, W. U. and Reid, A. M. (2004) *South African Journal of Geology, 100,* 115-122. [2] Salminen et al. (2009) *Precambrian Research, 168,* 167-184. [3] Uehara, M. and Nakamura, N. (2007) *Rev. Sci. Instrument, 78,* 043708, doi:10.1063/1.2722402

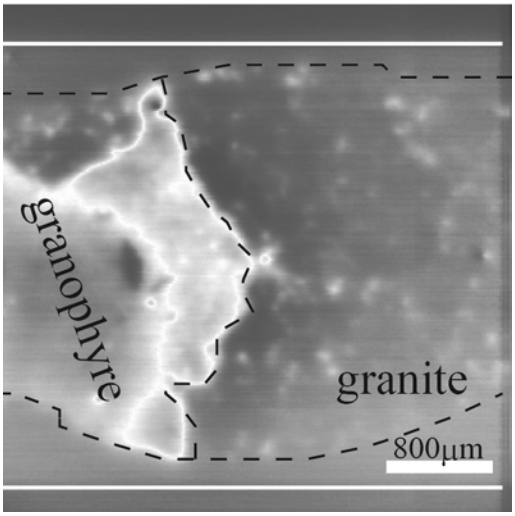

Figure 1: Stray magnetic field image of the Vredefort Granophyre and bedrock granite. The contact is a solid state and shows a distinct lithological difference. Highly magnetic portion near contact represents ballen-like texture within a cryptocrystalline texture.

SULFIDES IN IMPACT CRATERS. M. V. Naumov, Karpinsky All-Russia Geological Research Institute (VSEGEI), 199106 Sredny pr., 74, St.Petersburg, Russia, m_naumov@mail.ru).

The Sudbury structure presents a case of the world class Ni-Cu-PGE sulfide ores generated by a meteorite impact [1]. There is no evidence for similar sulfide deposits being associated with any other known impact structure elsewhere in the world; some small-scale impact-related base metals deposits had been reported before [*see* 2, 3 for references], though. This fact begs the question: is Sudbury unique or some factors favorable for sulfide accumulation in impact craters could be revealed? To solve the problem, it is necessary to study the sulfide mineralization in different impact craters. Apart from economic aspects, this mineralization could be of interest as an example of sulfide formation during the melting of upper crustal rocks without the input of abyssal matter; it could be considered as an indicator of crystallization conditions of impact melts as well.

In this report, data on sulfide mineralization in Russian impact craters including three large ones – Popigai (100 km), Kara (65 km), and Puchezh-Katunki (80 km) are summarized to show principal features of distribution and composition of sulfides within impact structures. These craters are distinct in their inner structure, target rock compositions, amount and mode of distribution of impact melt; thus, sulfide occurrences in various impact-related environments are considered. When compared with other impact structures including Sudbury, the data represented give a good basic knowledge to simulate probable impact-derived processes leading to the sulfide concentration.

To date, any sulfides were reported from about 35 impact structures. In many of them, only pyrite is mentioned; however, a detailed study reveals commonly a wide range of sulfides. The list of sulfides (and tellurides) known in astroblemes includes altaite, arsenopyrite, bornite, bravoite, chalcocite, chalcopyrite, galena, marcasite, molybdenite, millerite, pentlandite, pyrrothite, pyrite, sphalerite, and talnachyte. They occur in all impact lithologies including crater lake sediments. However, their appearance is amounted commonly to scattered dissemination or thin veins alone. Three genetic groups of sulfide associations are distinguished: (1) pre-impact, (2) syngenetic, (3) epigenetic.

Pre-impact sulfides are those, which are already in existence prior the impact, they undergo modification and redistribution during impact, though. A millerite-pentlandite-chalcopyrite assemblage (replaced partly by pyrite/marcasite) in Popigai crater is a case. Two other groups resulted mostly from modification, transfer, and redeposition of pre-impact sulfide matter. This is argued, e.g., by the correlation of sulfur isotope composition between pre-impact and impact-generated sulfides [4]. If composition and abundance of the latter are determined to a large extent by original sulfide oiccurences in target, their distribution and possible concentration depends on conditions of impact melt solidification and post-impact hydrothermal fluids.

Syngenetic sulfides are formed by impact melt crystallization. They are represented mostly by pyrrhotite; pentlandite, millerite, and chalcopyrite are common. Characteristic elements are Fe, Ni, Cu, and Co. Syngenetic mineralization was found out in Popigai, Boltysh, Kara, Moroqweng, East Clearwater etc, but Sudbury gives an only economic case.

Epigenetic sulfides are derived from the impact-generated hydrothermal circulation. A chalcopyrite-galena-sphalerite-marcasite-pyrite association is typical (Lockne, Siljan Ring, Kara, Puchezh-Katunki, Zapadnaya and other impact structures including Sudbury). Characteristic elements are Fe, Cu, Zn, and Pb.

Thus, an impact event can produce two genetic types of sulfide mineralization: (1) syngenetic low-sulfur Co-Ni-Cu mineralization (millerite pentlandite chalcopyrite pyrrhotite) in impact melts and (2) hydrothermal high-sulfur Cu-Pb-Zn-Ag mineralization (galenite sphalerite chalcopyrite pyrite) in diverse impact lithologies. These types are observed in all astroblemes studied in detail including Sudbury. Both types can form economic occurrences. When impact structures comprising sulfide deposits, and sulfide-lacking astroblemes being compared, some factors favorable for sulfide concentration in impact structures can be distinguished: (a) geochemical and metallogenic enrichment (specialization) of target by metals; (b) heterogeneous target comprising lithologies contrasting in composition; (c) formation of a voluminous impact melt sheet screened by a thick suevite/breccia cover; (d) predominance of massive impact melt rock among impact-derived lithologies; (e) formation of heterogeneous (due both original and crystallization differentiation) impact melts; (f) wide spread occurrence of post-impact hydrothermal processes.

References. [1] Naldrett A. J. (1984) Magmatic sulfide deposits – Geology, geochemistry, and exploration. *Berlin, Springer*, 727 p. [2] Grieve R.A.F. and Masaitis V. L. (1994) *Int. Geol. Rev., 36*, 105-151. [3] Reimold W.-U. et al. (2004) In Koeberl C. and Henkel H. (eds.) *Impact Tectonics*, Springer, 479-552. [4] Naumov M. V. (2004) *Trans. Rus. Acad. Sci., 399A, No. 9*, 1283-1289.

MAPPING OF LAYERED BEDROCK IN MARTIAN CRATERS: INSIGHTS IN TO CENTRAL UPLIFT FORMATION. A. M. Nuhn[1], L. L. Tornabene[1], G. R. Osinski[1], and A. S. McEwen[2]. [1]Centre for Planetary Science and Exploration/Dept. Earth Sciences, University of Western Ontario, London, ON, N6A 5B7 Canada (anuhn4@uwo.ca), [2]Lunar and Planetary Laboratory, University of Arizona, Tucson Arizona, USA.

Introduction: Central uplifts within complex impact craters expose faulted, rotated, and deformed deeply-seated bedrock from the subsurface and thus provide important insights with respect to the subsurface geology of planetary bodies [1,2] Details of the mechanics of central uplift formation, including weakening mechanisms, remain poorly constrained. In this study, three Martian complex craters with central uplifts exposing layered bedrock were selected for detailed mapping. The craters are all ~30 km in diameter, contain well-exposed bedrock, and are located in Hesperian ridged plains volcanic geological unit [3]. Here, we present the results of preliminary morphologic and structural mapping of these three unnamed Martian craters.

Data and Methods: The Mars Reconnaissance Orbiter (MRO) carrying the High Resolution Imaging Science Experiment (HiRISE) provides images and Digital Elevation Models (DEMs) with resolutions as high as ~0.25 and ~1.0 m/pixel, respectively [4]. HiRISE data can resolve small-scale features on central uplifts that allow detailed structural and morphological mapping.

HiRISE images as the base layer and ESRI ArcGIS and JMARS software were used to map the three craters in our study. Geological units were mapped by correlating similar unit morphologic characteristics. Mapping of structural features include dykes, faults, folds, and layer orientations. Morphologic and structural mapping is complete for the crater that exhibits the best exposure out of the three craters.

Results and Discussion:

Layered Bedrock. This morphological unit consists of darker-toned, lava layers alternating with lower-standing, weaker, lighter-toned, lower albedo, sedimentary or volcanogenic (possibly ash) layers [1-2, 5-6]. These layers are assumed to have been relatively flat-lying prior to impact. The layers are reported to have a mixture of strong spectral signatures of olivine and high calcium pyroxene; typical of basalts and consistent with a volcanigenic origin [6]. There are multiple exposures of bedrock that appears to have been fractured, folded, faulted, and uplifted into large megablocks that occurred during crater formation [2].

Folding and Faulting. The uplifted layered megablocks range from 100's to 1000's of metres in diameter and expose almost vertical overturned beds, consistent with the observations of Wulf et al. [7] at Martin crater. These blocks can sometimes be partially covered by impact melt and aeolian deposits. Radial folding of a few 100 metres in width and minor displacements of a 20 - 30 meters can be clearly seen within these large megablocks. The folding may be a series of faults referred to as a radial transpression ridge [8] consistent with high strain rates and the non-ductile behavior of rocks during an impact event.

The megablocks are clearly bounded by radial faults with larger displacements that contain a great deal of breccia.

Uplift of the blocks. All three of the crater's central features display varying elevations and diameters of uplift. This may be due to the influence of the target lithology and/or varying degrees of erosion to the surface. It is possible that the pre-existing layered volcanic and wrinkle ridges known to occur in this area cause pre-existing weakening within the target rock that allows these blocks to form. Also, one of the craters rests near a contact of older Noachian target lithology and the Hesperian volcanics, which also may contribute to the different size and exposure of the megablocks.

Breccia Dykes. Dykes within the three layered central uplifts exhibit displaced, tabular bodies, and are typically oriented approximately radially with respect to the centre of the crater. They crosscut the layered bedrock in all three of the selected layered central uplifts but are themselves offset by faults that are necessarily later. The dykes range from ~1 to 50 m in width and up to 1 km in length. Some well exposed dykes contain clasts in a smooth low albedo matrix, supporting the hypothesis that some may be breccia dykes.

Future Work: Future work in this study will measure strike and dip of the central uplifts using HiRISE DEM's, to further understand structural deformation. Mapping other craters with central uplift bedrock morphologies that include megabreccia and massive-fractured bedrock types will also be completed to see similarities and differences in regards to there formation and these target types [5, 9].

References: [1] Tornabene et al. (2012) 3rd Early Mars abstract. [2] Caudill et al. (2012) Icarus, 221, 710-720. [3] Scott D. H. and Tanaka K. L. (1986) USGS Map I-1802-A. [4] McEwen et al., (2007) JGR, 32: L21316. [5] Tornabene L.L. et al. (2010) LPSC XVI, Abstract #1737. [6] Quantin C. et al., (2012) Icarus 221, 436-452. [7] Wulf et al.,2012, Icarus 220, 194-204, terrestrial crater studies. [8] Kenkmann and Dalwigk. (2000) *Meteor. & Plan. Sci.*, 35, 1189-1201.. [9] Tornabene et al., (2013) this conference.

EVIDENCE FOR IMPACT INTO ICE RICH TERRAIN AND MELTING TO PRODUCE GLACIATION AND VALLEY NETWORKS IN THE AEOLIS/ZEPHYRIA REGION, MARS. J. W. Nußbaumer[1], [1]Johannes Gutenberg University, Mainz, Germany.

Introduction: Paleochannels have been identified, which are interpreted to be the result of melting of ice. A 30 km diameter impact basin (Fig. 1) in the Aeolis/Zephyria region near the dichotomy boundary is characterized by small valley networks (Fig. 2) that are partly located radial to the crater rim. Large glacial deposits, interpreted to be the remains of debris covered glaciers, have been identified in the area surrounding the crater. The spatial association between the crater and the paleochannels suggest that the impact was responsible for their formation.

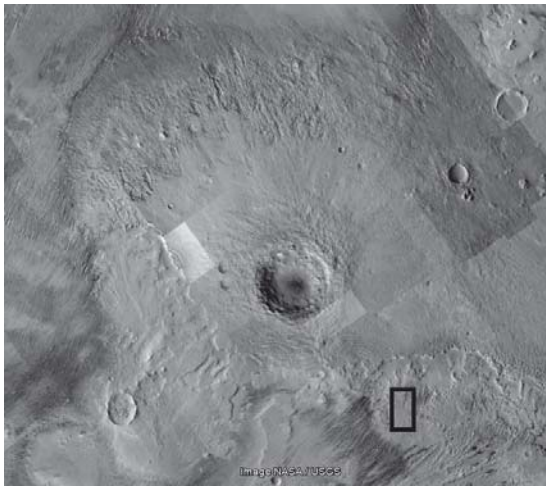

Fig. 1: CTX Image mosaic of an impact crater in the Aeolis/Zephyria region. Black box marks position of Fig. 2.

Ejecta deposit: The release of water is initiated by the melting of ice from the deposition of hot ejecta deposits over its surface. Such a mechanism would generate fluvial features in the absence of a climatic regime favorable for fluvial activity.

Conclusions: I propose that the valley networks originated from the release of water due to the deposition of hot ejecta over ice deposits present in the area during the impact event. Glacial deposits have been identified elsewhere on Mars [1-6]. Water sources originate from the melting of snow/ice deposits, extensive fluvial features in close proximity to the large crater in a region interpreted to have experienced significant glacial activity.

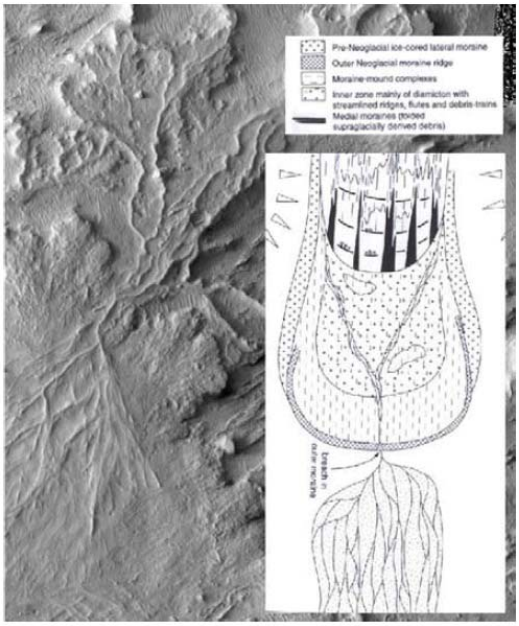

Fig. 2: Themis Image V05875001(left) and terrestrial analog (right, glacier and drainage system, Svalbard, adapted from [7]), suggesting the action of glacial meltwater as a water source for fluvial channels.

The spatial relationship between the valleys and the main crater suggest, that they are related. The hot ejecta deposit associated with the impact provides an explanation for the melting of ice deposits that were present on the plateau at the time of impact.

References: [1] Christensen, P. R. (2003) *Nature* 422, 45–48. [2] Dickson, J. L. et al. (2008) *Geology* 36 (5), 411–415 [3] Head, J. W. et al. (2006) *Geophys. Res. Lett.* 33, doi:10.1029/2005GL024360. L08S03. [4] Levy, J. S. et al. (2007) *J. Geophys. Res.* 112, doi:10.1029/2006JE002852. E08004. [5] Newsom, H. E. (1980) *Icarus* 44, 207–216. [6] Shean, D. E. et al. (2007) *J. Geophys. Res.* 112, doi:10.1029/2006JE002761. E03004. [7] Evans, D. (2005), *Hodder Arnold*, 544pp.

REVISITING THE DISTRIBUTION AND PROPERTIES OF SHATTER CONES AT THE SUDBURY IMPACT STRUCTURE, CANADA. G. R. Osinski[1], L. Ferrière[2], D. A. Kring[3], D. Anders[1], K. Armstrong[4], D. Baker[5], M. Bamberg[6], C. Beddingfield[7], T. Gaither[8], T. Harrison[1], M. S. Huber[2], D. Hurwitz[3], S. Jaret[9], G. Kramer[3], Y. Kuriyama[10], M. Lucas[7], C. L. Marion[1], C. Mercer[11], C. Mount[12], C. Neish[13], A. Nuhn[1], L. Ostrach[11], A. Pickersgill[1], E. Pilles[1], R. W. K. Potter[3], A. Ryan[11], M. Sharp[14], N. Swartz[15], O. Thomson[16], M. Veto[11], M. M. Wielicki[17] S. Wright[18], M. Zanetti[19], [1]Canadian Lunar Research Network/Centre for Planetary Exploration, University of Western Ontario, [2]Natural History Museum & University of Vienna, [3]Lunar and Planetary Institute, [4]Portland State University, [5]Brown University, [6]DLR, [7]University of Tennessee, [8]United States Geological Survey, Flagstaff, [9]Stoney Brook University, [10]Japan Aerospace Exploration Agency, [11]Arizona State University, [12]Northern Arizona University, [13]NASA Goddard Space Flight Center, [14]University of Maryland, [15]Temple University, [16]University of Puerto Rico Mayaguez, [17]UCLA, [18]Auburn University, [19]Washington University in St. Louis (gosinski@uwo.ca).

Introduction: Shatter cones are one of the most characteristic features of hypervelocity impact events and remain the only diagnostic shock metamorphic criterion recognizable in the field [1]. At Sudbury, shatter cones were first recognized in 1964 and provided the first definitive evidence for the impact origin of this structure [2, 3]. Since then, shatter cones have been used to confirm the existence of dozens of impact craters on Earth. However, several contrasting models for their origin exist [4–7] and the exact formation mechanism(s) remains unclear.

Despite being recognized at Sudbury almost 50 years ago, shatter cones have received relatively little attention. The original map of Guy-Bray published in 1966 [8] was updated slightly by Dressler in 1984 [9]. A recent compilation by Ames et al. [10] differs from these previous maps and includes new observations based on unpublished work by J.P. Golightly. Understanding shatter cones at Sudbury is important for several reasons, not least because they can help to infer the original size and geometry of this deformed structure based on knowledge of how shock attenuates away from the point of impact. At the same time, observations at Sudbury may shed light on the formation mechanism(s) of shatter cones.

Here, we present the first results of a new multi-year research program that aims to systematically map the distribution of shatter cones and their physical properties around the Sudbury structure. This effort was initiated by G.R.O. and L.F. in 2010 and took a major step forward in Fall 2012 as part of the "Impact Cratering Short Course and Field Training Program", organized by the Canadian Lunar Research Network, the Centre for Planetary Science and Exploration, and the Lunar and Planetary Institute, through the auspices of the NASA Lunar Science Institute. The objectives are to: 1) determine the spatial distribution and radial extent of shatter cones around the Sudbury structure; 2) determine their orientation and identify if there are any systematic variations around the structure; and 3) investigate the morphology, morphometry, and microscopic shock effects of shatter cones around the Sudbury structure.

Methodology: The location of each outcrop was documented using Global Positioning System (GPS) units (provided). The following was recorded at each outcrop: basic description of the lithology in which shatter cones occur; size and how well developed (i.e. 3D full cones or only flat ones) of the cones; whether the apex of the shatter cones points downwards or upwards; trend and plunge of the shatter cone striations: strike and dip of the bedding. Cone measurements were plotted on a lower hemisphere equal area projection (Schmidt net) to determine cone orientation.

Results: Our initial results are broadly consistent with earlier studies of shatter cone distribution in the South Range of the Sudbury structure. In the North Range, however, the cluster of well developed shatter cones in the Milnet region identified by (8) could not be reproduced. In general, shatter cones appear more abundant in the South Range than the North Range. Many of the outcrops studied possessed shatter cones with apices pointing in multiple directions, often in completely opposite directions. This is in keeping with observations from other terrestrial craters (11, 12) and is not explained by current models for shatter cone formation (4–7). Other observations include a possible master cone (13) and intriguing relationships with Sudbury Breccia.

References: [1] French B. M., Koeberl C. (2010) *Earth Sci. Rev.,* 98, 123–170. [2] Dietz R. S. (1964) *J. of Geol.* **72**, 412–434. [3] Dietz R. S., L. W. Butler (1964), *Nature* **204**, 280–281. [4] Johnson G. P., Talbot R. J. (1964), Air Force Institute of Technology, Dayton, Ohio. [5] Sagy A. et al. (2002) *Nature* **418**, 310–313. [6] Baratoux D., Melosh H. J. (2003) *EPSL* **216**, 43–54. [7] Gash P. J. S. (1971) *Nature Phys. Sci.* **230**, 32–35. [8] Bray J. G. (1966) *J. Geol.* **74**, 243–245. [9] Dressler B. O. (1984) in *The Geology and Ore Deposits of the Sudbury Structure* pp. 99–136. [10] Ames D. E. et al. (2008) *Econ. Geol* **103**, 1057–1077. [11] Osinski G. R., Spray J. G. (2006) *ESA Sp. Pub. SP-612 (CD-ROM).* [12] Wieland F. et al. (2006) *MAPS* **41**, 1737–1759. [13] Hurwitz D. et al. (2013) this conference.

STRUCTURAL MAPPING OF THE TUNNUNIK IMPACT STRUCTURE, NWT, CANADA: INSIGHTS IN TO CENTRAL UPLIFT FORMATION. G. R. Osinski[1,2], R. Francis[1], J. Hansen[3], C. L. Marion[1], A. E. Pickersgill[1], and L. L. Tornabene[1], [1]Dept. of Earth Sciences & Centre for Planetary Science and Exploration, University of Western Ontario, London, ON, N6A 5B7, Canada, [2]Dept. Physics and Astronomy, University of Western Ontario, London, ON, N6A 5B7, Canada, [3]Canadian Space Agency, St. Hubert, QC, J3Y 8Y9, Canada (gosinski@uwo.ca).

Introduction: Complex impact craters are characterized by a structurally complicated rim or so-called terraced zone, a down-faulted annular trough containing a lens of impact melt rocks and/or breccias, and an uplifted central area. Based initially on observations of the Moon, there is an apparent progression with increasing crater size from central peak, central-peak basin, to peak-ring basins [1]. Despite the fundamental nature of central uplifts, there remains considerable debate as to the exact formation mechanisms, timing, weakening mechanisms, and the effect of target lithology. In this contribution, we report on structural mapping of central uplift of the newly confirmed Tunnunik complex impact structure in the Canadian High Arctic based on fieldwork carried out in summer 2012.

Tunnunik: The Tunnunik impact structure is situated adjacent to the Collinson Inlet on the Prince Albert peninsula on northwestern Victoria Island, NWT, Canada. It's impact origin has recently been documented through the presence of shatter cones [2, 3] and planar deformation features in quartz [4]. The age of Tunnunik is poorly constrained at >130 <450 Ma [2]. Based on mapping carried out in 2010 by our group, Tunnunik has an apparent crater diameter of 28 km [3]. The target rocks consist of flat lying sedimentary rocks. The youngest rocks currently exposed at the surface today are the Ordovician to Silurian Thumb Mountain and Allen Bay Formations. Younger Devonian-age rocks may have been present at the time of impact but no preserved evidence was found. Older target rocks include, from youngest to oldest, the Cambro-Ordovican Victoria Island Formation, the Cambrian-age Stripey Unit, Tan Dolostone Unit, and the Clastic Unit. The oldest rocks exposed in the centre of the present-day structure are of the Neoproterozoic Wynniatt Formation of the Shaler Supergroup. Neoproterozoic diabase dykes intrude the latter.

Structural geology: Mapping of the rim region of Tunnunik documented the presence of listric faults out to a radius of 14 km, providing the apparent crater diameter estimate of 28 km noted above. While exposure regionally is poor to moderate, one of the unique aspects of the Tunnunik impact structure is an ~2 km long canyon cut through the edge of the central uplift (Fig. 2), thus providing an unprecedented view in to the internal structure of mid-size complex impact structure.

Fig. 1. Originally flat-lying rocks deformed by inwards-directed thrust faulting in the centre of the structure. The cliff face is ~100 m high.

Detailed structural mapping of the canyon revealed the generally outward-dipping nature of the target rocks; however, orientations range from ~20° to nearly vertical. In some regions, large several 100 m-size blocks are upturned and maintain their internal bedding structures (Fig. 1). In other regions, target rocks are oriented less steeply and bedding parallel thrust faults are exposed. Overall, the central uplift of this structure comprises a series of imbricated blocks of variable thickness bounded by thrust faults. Kinematic indicators show that movement is in towards the centre of the structure, consistent with the inwards and upwards motion during central uplift formation. Internally, the blocks display no obvious signs of deformation, except shatter cones, and large zones of breccia that seem to be required by the acoustic fluidization model for weakening [5], are notably absent.

Acknowledgements: We thank the Polar Continental Shelf Project (PCSP) for logistical support, and NSERC, Canadian Space Agency (CSA), MDA, and INAC for funding. Edward Tabarah and Jean-Marc Comtois from the CSA are thanked for supporting J. Hansen's participation in this project as part of an ongoing field geology program for Canadian astronauts.

References: [1] Stöffler, D. et al. (2006) *Rev. Min. Geochem*, 519–596. [2] Dewing, K. et al. (2013) *MAPS*, *48*, 2, 211–223. [3] Osinski, G.R. et al. (2013) *44th LPSC*, Abstract #2099. [4] Pickersgill, A.E. and Osinski, G.R. (2013) *44th LPSC*, Abstract #2602. [5] Melosh, H.J. and Ivanov, B.A. (1999) *Ann. Rev. Earth Planet. Sci.*, *27*, 385–415.

SPIRAL FEATURES AND THE CORIOLIS EFFECT ON VESTA'S BASIN RHEASILVIA. K. Otto[1], R. Jaumann[1,2], K. Krohn[1], K.-D. Matz [1], F. Preusker[1], T. Roatsch[1], F. Scholten[1], I. Simon[1], K.Stephan[1], C. A. Raymond[3] and C. T. Russell[4], [1]Deutsches Zentrum für Luft- und Raumfahrt (DLR), Institute of Planetary Research, Germany (Rutherfordstraße 2, 12489 Berlin, (katharina.otto@dlr.de), [2]Institute of Geosciences, Freie Universität Berlin, Germany, [3]California Institute of Technology, Jet Propulsion Laboratory, Pasadena, USA, [4]Institute of Geophysics and Planetary Physics, University of California, Los Angeles, USA.

Introduction: The Dawn space craft orbited asteroid Vesta for one year arriving in August 2011 [1]. The on-board Framing Camera (FC) collected image data with a resolution up to 20 m/pixel [2]. Stereo images from the High Altitude Mapping Orbit (HAMO, 60 m/pixel) were used to construct a Digital Terrain Model (DTM) of Vesta's surface [3].

The FC images and the DTM revealed a large impact basin in the southern hemisphere, named Rheasilvia. Rheasilvia's central peak located at 75°S and 301°E nearly coincides with Vesta's south pole. Its diameter of about 500 km has the dimension of Vesta's diameter (525 km) [2, 4]. This and Vesta's relatively short rotation period of 5.3 hours indicate that the Coriolis force is likely to have an effect on mass motions within the Rheasilvia basin [5]. Indeed, a pervasive spiral deformation pattern has been observed [6].

Figure 1: Spiral pattern in Vesta's southern hemisphere. Shown is a stereographic projection (equal angle) on a sphere of 255 km.

The Coriolis Effect: The Coriolis force is a fictional force associated with rotating systems. The rotation deflects the motion perpendicular to the rotation axis to cause curved trajectories. The Coriolis force F_C is given by

$$\vec{F_C} = -2m\vec{\Omega} \times \vec{v} \quad (1)$$

where *m* is the mass of the moving body, Ω the angular velocity of the rotating body and *v* the velocity of the moving object. The trajectory of a mass moving in the horizontal plane on a rotating sphere is described by a circle with inertial radius *R*. The inertial radius is dependent on the magnitude of the velocity *v*, the latitude ϕ and the magnitude of the angular velocity Ω. It is given by

$$R = \frac{|\vec{v}|}{2|\vec{\Omega}| \sin \phi}. \quad (2)$$

Note that the radius is only dependent on the speed of the moving body but not on its mass. Solving Eq. 2 for the velocity *v* yields

$$|\vec{v}| = 2R|\vec{\Omega}| \sin \phi. \quad (3)$$

Method: We mapped the most prominent curved features of the spiral deformation pattern in the Rheasilvia basin and used the data to calculate their three dimensional location. A reference spheroid of 285 km by 229 km was used to approximate Vesta's shape and to determine the three dimensional location. At each point along a curved feature we approximated a circle and determined the inertial radius *R*. Knowing the angular velocity Ω, the latitude ϕ and the inertial radius *R*, we calculated the velocity of the motion using Eq. 3.

Results: The velocities were plotted against the DTM profile of each feature. We analysed the correlation of elevation and velocity to find implications for the mass wasting type.

References: [1] Russell, C. T. et al. (2013) Dawn completes its mission at 4 Vesta, *Meteorit. Planet. Sci.*, 1-14. [2] Jaumann, R. et al. (2012) Vesta's shape and morphology, *Science, 336*, 687-690. [3] Preusker, F. et al. (2012) Topography of Vesta from Dawn FC stereo images, *EPSC 2012*, Abstract epsc2012-428-1. [4] Russell, C. T. et al. (2012) Dawn at Vesta: Testing the protoplanetary paradigm, *Science, 336*, 684-686. [5] Jutzi, M. et al. (2013) The structure of the asteroid 4 Vesta as revealed by models of planet-scale collisions, *Nature, 494*, 207-210. [6] Schenk, P. et al. (2012) The geologically recent giant impact basins at Vesta's south pole, *Science, 336*, 694-697.

PSEUDOTACHYLITE BRECCIA VEINS FROM DHALA IMPACT STRUCTURE, NORTH CENTRAL INDIA: TEXTURE, MINERALOGY AND GEOCHEMICAL CHARACTERIZATION. J.K. Pati[1], W.U. Reimold[2,3], A. Greshake[2], C.K. Koeberl[4], and P. Pati[1], [1]Department of Earth and Planetary Sciences, Nehru Science Centre, University of Allahabad, Allahabad-211 002, India(jkpati@yahoo.co.in); [2]Museum für Naturkunde Berlin, Invalidenstrasse 43, 10115 Berlin, Germany (uwe.reimold@museum.hu-berlin.de), [3]Humboldt-Universität zu Berlin, Unter den Linden 6, 10099 Berlin; [4]Department of Lithospheric Research, University of Vienna, Althanstrasse 14, A-1090 Vienna, Austria (christian.koeberl@univie.ac.at).

Introduction: Pseudotachylitic breccia veins and larger occurrences are known from large impact structures (Vredefort, Sudbury, Manicouagan, Araguainha) as well as from relatively smaller structures (Rochechouart, Slate Islands). This is the first report of pseudotachylitic breccia veins in basement granitoids from the Dhala structure, north central India [1]. They occur in vertical borehole MCB-10 at N25°17'59.7" and E78°8'31".

Results: The Dhala structure was drilled by the Atomic Minerals Directorate for Research and Exploration (AMDRE), Department of Atomic Energy, of the Government of India in about 60 locations up to depths of nearly 600 m, in a regional search for uranium. The mesoscopic pseudotachylitic breccia occurs in MCB-10 at 348.15, 384.90, 389.90, 401.85, 452.75, 484 and 502.55m depths as veins, pods, networks of or single anastomozing veinlets with thickness ranging from less than a mm to about 5 cm. In the core samples, multiple crosscutting PTB veins with sharp boundaries with the host granite are noted, and in places clastic debris off the wall (rip-off clasts) are observed within the vein. In thin section, these bluish grey to dark grey veins have sharp but irregular contacts with the host granitoids and are generally highly altered. The extensively iron-stained granitic host rock shows sericitization and the mafic phases are mostly chloritized. Locally cataclastic granite is cut by post-cataclasis carbonate veinlets. Two types of PTB veins are observed: 1. Distinct vein type cataclastic breccias at the microscopic scale with minor amounts of actual groundmass showing locally heavily altered domains, possibly representing comminuted clastic debris. 2. Extremely altered dark grey PTB veins (chloritized groundmass, saussuritized feldspar, heavily iron-stained matrix, and chloritization of biotite ± hornblende). There are distinct and euhedral phenocrysts obviously grown from a melt phase in larger (> several mm in width) occurrences. The groundmass is fine-grained similar to the texture of a crystallized melt phase, but is always extensively altered.

Eighteen samples comprising host rock and PTB vein material were sliced from drill core from various depths and analyzed for their major, minor (incl. REE) elemental compositions by XRF and INAA. The average LOI value in PTB samples is 5.8 wt.%) and is distinctly higher than that of the host rocks (1.9 wt.%). The SiO_2 content of the host rocks ranges between 60.4 to 77.7 wt.%, and the Na_2O+K_2O values vary from 7.02 to 10.75 wt.% indicating the general granitic composition. Their modal mineralogy (quartz + alkali feldspar ± plagioclase ± biotite ± hornblende) and texture also classify the host rocks as granitoids. The PTB veins have relatively low average SiO_2 content (40.0 wt.%) with high MgO values (average: 12.3 wt.%), and they are similar to silica-undersaturated mafic rocks in their Ni/Cr ratio <1. Possibly the preferential dissolution of hydrous phases into the melt, breakdown of biotite±hornblende, and alteration by Fe-rich solutions may have lead to the formation of magnetite and could be responsible for the change in major element chemistry from the granitoid to PTB vein compositions. Interestingly the granitoids and the PTB samples, in general, show identical REE patterns with average total REE < 260 ppm, LREE enrichment, HREE depletion and negative Eu anomaly (Eu/Eu*=0.38-0.73).

Conclusions: These highly altered PTB veins and the granitoid hosts with contrasting major element chemistry but identical REE pattern possibly formed as fracture fillings during the modification stage. They could have also been locally generated due to frictional melting, or some of the thin veinlets might be shock veins.

References: [1] Pati J.K. et al. (2009) *Meteoritics & Planet. Sci., 44*, A121.

Acknowledgements: JKP thanks the AMDRE, Govt. of India for the permission to study and sample borehole cores used in the present study.

.

CONTRIBUTIONS TO THE SUDBURY IGNEOUS COMPLEX AND THE DEPTH OF EXCAVATION: EVIDENCE FROM ONAPING FORMATION ZIRCON. J. A. Petrus[1], J. A. Ayer[1], D. G. F. Long[1], P. C. Lightfoot[2], and B. S. Kamber[3], [1]Laurentian University, Sudbury, Canada (jpetrus@laurentian.ca), [2]Vale, Sudbury, Canada, [3]Trinity College Dublin, Dublin 2, Ireland.

Introduction: It is now generally accepted that the Sudbury Igneous Complex (SIC) is a differentiated melt sheet [1] created by a large meteorite impact 1.85 Ga ago [2]. However, there remains considerable debate over the depth of excavation and the target lithologies that contributed to the SIC [3,4]. Recent work by Darling et al. showed that the Pb isotope composition of offset dykes in the South Range of the impact structure could be explained as a mixture of 80% Huronian metasediment (HMS) and 20% Superior Province gneisses [3]. From this, they concluded that the depth of excavation was shallow, implying that the impact must have been oblique. Earlier work by Mungall et al. argued on the basis of geochemical data that the depth of excavation was much deeper, requiring a significant contribution from lower continental crust [4].

In this study, zircon from the Onaping Formation (OF) (Sudbury impact crater-fill sequence, rich in target rock lithic fragments [5]) are compared to those found in HMS, Superior Province granitoids, South Range gneisses (SRGs), and other target lithologies in terms of their U-Pb geochronology in an effort to identify which rocks contributed to the SIC.

Samples and Methods: The OF was sampled in four localities, covering a wide geographic area and different members of the formation. The HMSs are represented by samples from the Mississagi and Gowganda Formations, and a quartzite block in the OF. Hitherto unreported lithologies are the SRGs, which were sampled in the vicinity of Lively (2 from outcrop, one from drill core). On the northern side of the impact structure, a variety of Superior Province granitoids were also analyzed. The OF, HMS and SRG zircon were analyzed by LA-ICP-MS, while the Superior Province granitoids were analyzed by SHRIMP.

Results: In total, more than 2700 zircon were analyzed. The U-Pb geochronology of each group is summarized below.

Huronian Metasediments. Detrital zircon in these samples form a tight distribution around 2720 Ma with several Mesoarchean grains.

Superior Province Granitoids. The granitoids have discrete and tight age clusters, ranging from 2729 Ma to 2621 Ma. There is a general N to S younging trend.

Onaping Formation. The majority of zircon yielded Neoarchean ages. Populations outside of this main group tend to be small and correspond to the age of the impact itself or known Paleoproterozoic target rocks. Although a proportion of the Neoarchean grains can be explained as contributions from HMS and Superior Province gneisses, there are many 2550-2650 Ma zircon that are not so easily attributed to previously known target rocks.

South Range Gneisses. Two of the samples analyzed yielded ages similar to the Creighton granite (2390 Ma and 2430 Ma) and therefore probably represent more strongly deformed varieties of this intrusion type. One sample (SRG-A), however, appears to be approximately 2600 Ma old with evidence for thermal overprinting (possibly from the emplacement of the Murray and Creighton granites), as well as partial resetting at ca. 1 Ga due to the Grenville orogeny. This particular specimen is the only known 2600 Ma rock in the immediate impact area and could be a piece of basement to the HMSs.

Discussion: The abundance of 2550-2650 Ma zircon found in the OF cannot be accounted for by contributions from any previously known lithology. However, the distribution of zircon in one of the newly reported SRGs matches this otherwise unexplained but prominent group of zircon. In an earlier study, Ames et al. also noted 2600 Ma zircon in the OF and suggested that they were derived from the lower crust, but due to their limited dataset, these authors did not recognize how widespread they were [6]. Thus, it appears that a previously unrecognized lithology has contributed significantly to both the OF and presumably the SIC.

In light of this discovery, Pb isotope data were acquired for SRG-A and were found to be very similar to HMS, lending further support to the idea that SRG-A could represent the otherwise unexposed Southern Province basement. Furthermore, the similarity of Pb isotope composition between SRG-A and HMS complicates the assessment of contributions to the SIC via Pb isotope data. Finally, if SRG-A is truly basement material for the HMSs, the depth of excavation likely exceeded the estimates of Darling et al. [3], alleviating the requirement for an oblique impact. A more detailed petrological and geochemical study of gneissic basement in the South Range is required.

References: [1] Therriault A. M. et al. (2002) *Econ. Geol.*, 97, 1521-1540. [2] Davis D. W. (2008) *Geology*, 36, 383-386. [3] Darling J. R. et al. (2010) *Geochim. Cosmochim. Acta*, 74, 5680-5696. [4] Mungall J. E. et al. (2004) *Nature*, 429, 546-548. [5] Grieve R. A. F et al. (2010) *Meteoritics & Planet. Sci.*, 45, 759-782. [6] Ames D. E. et al. (1998) *Geology*, 26, 447-450.

TIMING RELATIONSHIP BETWEEN RADIAL AND CONCENTRIC OFFSET DYKES AT SUDBURY, ONTARIO: A CASE STUDY OF THE FOY AND HESS OFFSET DYKES. E. A. Pilles[1], G. R. Osinski[1], R. A. F. Grieve, D. Smith[2], and J. Bailey[2] [1]Dept. Earth Sciences/Centre for Planetary Science and Exploration, University of Western Ontario, London, ON, N6A 5B7, epilles@uwo.ca [2]Wallbridge Mining Company Limited, Lively, ON, P3Y 1L7

Introduction: The Sudbury impact structure is host to the largest Ni-Cu-PGE deposits in North America [1]. Among these are the so-called Offset Dyke (OD) deposits, such as Copper Cliff Mine which hosts ~15% of the known Sudbury ore [2]. Despite their economic value, there is still much controversy regarding their origin. Using the Foy and Hess ODs as a case study, we employ a combination of field mapping, microscopy, and geochemical analysis to attempt to answer some of these pressing questions. The results of this research will lead to new exploration strategies for locating new ore deposits in the Sudbury footwall.

Background: Offset Dykes are igneous intrusions genetically linked to the Sudbury impact event. The primary rock type is granodiorite; although, historically the lithology of ODs is referred to as quartz diorite. They range from ~1 m to ~400 m thick, and ~100 m to ~50 km in length. They commonly exhibit two phases: an inclusion-rich phase commonly associated with ore deposits, and an inclusion-free phase [3].

Foy Offset Dyke. Foy is the longest of the radial dykes, hosted by the north range Archean granitoids, greenstones, and gneisses. The southern segment extends northwest for 16 km, it is then offset to the east, where it extends north for ~20 km. The dyke ranges from 50 m to 400 m thick. Where it connects to the embayment the primary composition is inclusion-rich pyroxene-granodiorite, containing granite, diabase, and gneiss clasts. Further north there are both inclusion-free and inclusion-rich phases [4]. The primary mineralogy of the ODs is epidote + biotite + chlorite + amphibole + albite + quartz + calcite [5]. The age of the dyke has been determined as $1.852\ ^{+4}/_{-3}$ Ga [6].

Hess offset dyke. The Hess is the longest concentric dyke, extending ~50 km in the north range, varying from 10 m to 100 m thick. The lithology varies between two phases of grano-diorite: sulphide-poor inclusion-free phase enclosing a sulphide-rich and inclusion-rich phase[7]. The inclusion-rich phase includes clasts of granite, gneiss, norite, anorthosite, and heterolithic breccia resembling footwall breccia [7].

Results: *Field work.* Field mapping and sampling was completed at the intersection of the Foy and Hess ODs. An area of approximitely 1 km^2 was mapped at a 1:50 scale to determine the distribution of clasts >30 cm in diameter. No contact between the Hess and Foy was apparent in the field despite excellent exposure. Inclusions were found in two distinct locations: granitoid inclusions from the batholith host rock were found up to 5 m away from the OD - host rock contact, and within the inclusion-rich phase, which is found in the core of the Hess and Foy dykes. Inclusions of granitoid, diabase, gneiss, and the inclusion-poor phase were found. The contact between the two phases was sharp, but gradational. A 'transition zone' marked the gradual change from inclusion-free to inclusion-rich phases, ranging from ~1cm to 100 cm thick.

Petrography. Petrographic analysis of this transition zone shows that the minerals have a strong preferred orientation – even if the phases themselves lack foliation – and a high concentration of biotite and chlorite. The inclusion-free phase is typically coarser grained, with higher quartz-albite content. The inclusion-rich phase typically finer grained and contains more biotite. Sulfides in the latter phase are more common, coarser and euhedral.

Geochemistry. Major oxides were determined from the matrix of the OD samples from both phases of the Hess and the Foy. Results were typical of ODs [8], and showed little variation between Foy and Hess or between the inclusion-free and inclusion-rich phases.

Discussion: The lack of a distinct contact between the Hess and Foy dykes suggests that the concentric and radial dykes were emplaced at the same time. The presence of the inclusion-free phase inside the inclusion-rich phase suggests that the inclusion-free phase was emplaced first. The presence of large granitoid inclusions near the OD-country rock suggests rapid, violent emplacement. Further work on the Hess and Foy ODs is necessary to ascertain the timing relationship between the different phases and the radial and concentric dykes.

References: [1] Farrow, C. E. G. & Lightfoor, P. C. (2002) *CIM, 54,* 273-297. [2] Scott, R. G. & Benn, K. (2002) *Economic Geology, 97,* 1447-1458. [3] Murphy, A. J., & Spray, J. G. (2002) *Economic Geology,* 97, 1399. [4] Tuchscherer, M. G. & Spray, G. (2002) *Economic Geology, 97,* 1377-1397. [5] Fleet, M. E., Barnett, R. L., and Morris, W. A. (1987) *Canadian Mineralogist, 25,* 499-514. [6] Ostermann, M., Scharer, U., & Deutsch, A. (1996) *Lunar and Planetary Institute Contribution, 922,* 38-39. [7] Wood, C. R. (1998) *M Sc. Thesis UBC.* [8] Lightfoot, P. C. et al. (1997) *Economic Geology, 92,* 647-673.

EXPERIMENTAL CRATERING IN QUARTZITE, TUFF AND SANDSTONE: FINAL AND TRANSIENT CRATER VOLUMES. M. H. Poelchau[1], T. Kenkmann[1], T. Hoerth[2], A. Deutsch[3], K. Thoma[2], F. Schäfer[2]. [1]Institut für Geo- und Umweltnaturwissenschaften, Universität Freiburg, D79104 Freiburg, Germany, [2]Fraunhofer Ernst-Mach-Institut (EMI), Freiburg, [3]Institut f. Planetologie, WWU Münster, (michael.poelchau@geologie.uni-freiburg.de).

Introduction: The MEMIN research unit is investigating the role of sedimentary target materials on the cratering process. Following experimental campaigns that focused on dry and water-saturated sandstone targets [1,2] we have expanded the range of target materials to quartzite and tuff.

Cratering Experiments: Seven impact experiments were performed at the two-stage light-gas gun facilities of the Ernst-Mach Institute [3] on quartzite and tuff targets. Spherical D290-1 steel projectiles with diameters of 2.5 and 12 mm were accelerated to ~5 km/s. Targets were 20 cm edge length cubes and 80x80x50 cm blocks.

Quartzite and tuff as target materials were chosen to cover a wider range of porosities in comparison to the previously used sandstone (23% porosity). The quartzite has <1% porosity; its uniaxial compressive strength (UCS) is 292 MPa. The tuff has 40% porosity and a UCS of 23.1 MPa.

Results: Crater volumes in dry tuff, quartzite and dry sandstone targets are all similar for the same impact conditions, despite the large range of target strengths. While both the target's strength and porosity are parameters that can reduce crater size, these two parameters are usually inversely correlated for geological materials. Saturating pore space with water leads to an increase in crater volume in both tuff and sandstone by reducing the dampening effects of porosity on the shock wave, while keeping the target's UCS constant.

Strength Scaling: As both porosity and strength are important factors for crater size, π-group scaling can be used to factor out the effects of target strength. Experiments in low-strength sandstone and tuff targets with higher porosities have much lower cratering efficiencies than expected for (non-porous) π_3 values of the quartzites (π_3 factors in target strength, density, and impact velocity). Increasing pore-space saturation effectively reduces porosity effects on crater volume and cratering efficiency, and these values lie closer to the non-porous quartzite trend.

Transient Craters: Due to the interaction of the shock wave with free surfaces of the target, large pieces of spalled material are ejected. This alters the crater morphology and increases crater volume. To discern spall effects from the excavation process and to determine the volume of the transient crater, parabola are fitted to the scanned crater profiles following a method described in [2,4].

Transient crater volumes are only ~15-50% of the volumes of the "final" craters. On average, quartzites have smaller transient craters (13-26%) than sandstones (21-50%) or tuffs (27-33%), relative to final crater volumes. Somewhat surprisingly, transient crater volumes are also smaller in large-scale experiments performed at the EMI's "XL" light gas gun [3]. E.g., sandstones impacted by 10-12 mm projectiles have transient craters with 31±7% of the final crater volume, while sandstones impacted with 2.5 mm projectiles have 47±2%. These values imply that spallation is increased in quartzites and in large-scale experiments.

There are several possible explanations for the observed spall behavior. The increase in spallation in quartzites may be related to higher crack propagation speeds than in sandstone [5], or to the correlation between spall thickness and the target's tensile strength, which are proposed to be directly proportional [6].

The increase in spallation in large-scale experiments may be correlated to projectile size. Larger projectiles generate a longer pressure pulse upon impact. These longer pressure pulses increase the number of tensile fractures formed and also reduce the pressure threshold at which tensile fractures form [7,8]. On the other hand, the target block geometry (cubes vs. flatter cuboids) may influence how the shock wave is reflected from the back of the target, potentially causing a second wave of spallation.

Outlook: Constraining target effects on cratering and differentiating between excavation and spall processes help to produce detailed data sets that serve to validate numerical models [9]. In turn, these models help to understand planetary scale cratering processes.

Acknowledgements: The MEMIN program is supported by the DFG (Research Unit FOR-887).

References: [1] Kenkmann T. et al. (2011) *M&PS, 46,* 890–902. [2] Poelchau et al. (2013) *M&PS, 48*, 8-22. [3] Lexow et al. (2013) *M&PS, 48,* 3-7. [4] Dufresne et al. (2013) *M&PS, 48,* 50-70. [5] Kimberley et al. (2013) *Acta Materialia, 61*, 3509–3521 [6] Melosh H. J. (1984) *Icarus 59*, 234–260. [7] Meyers M. A. (1994) Dynamic behavior of materials. New York: Wiley, 668 p. [8] Ahrens T. J. and Rubin A. M. (1993) *JGR 98,* 1185–1203. [9] Güldemeister et al. (2013) *M&PS*, *48*, 115-133.

ORIENTALE BASIN: FORMATION PROCESSES AND STRUCTURE INFERRED FROM HYDROCODE MODELING R. W. K. Potter[1,2], D. A. Kring[1,2], G. S. Collins[3], W. S. Kiefer[1,2], and P. J. McGovern[1,2], [1]Center for Lunar Science and Exploration, Lunar and Planetary Institute, 3600 Bay Area Blvd, Houston, TX, 77058, USA, [2]NASA Lunar Science Institute, potter@lpi.usra.edu; [3]Dept. Earth Science and Engineering, Imperial College London, London, SW7 2AZ, UK

Introduction: As the youngest and best-preserved lunar multi-ring basin, Orientale has been used as the archetype for investigating basin formation processes and structure (e.g., [1,2]). Numerous aspects of Orientale, however, remain uncertain, e.g., transient crater dimensions and melt volume. Here, we summarize the results of [3], where we numerically modeled the Orientale basin-forming event to resolve some of the uncertainties associated with its formation and structure.

Methods: Orientale-sized impacts were numerically modeled using the iSALE hydrocode (e.g., [4]). The target was divided into crust (60 km thick) and mantle layers, each with properties appropriate for their lunar counterparts. Two thermal profiles [5], estimating lunar thermal conditions at the time of Orientale's formation ~3.8 Ga, were used. Impactor diameter varied between 40 and 120 km; impact velocity varied between 10 and 20 km/s. All impacts were vertical.

Results: The location and thickness of Orientale's crustal annulus, inferred from gravity data [6], was used to constrain the models to find best-fit impact scenarios for each thermal profile.

Thermal Profile 1 (hot mantle). The best-fit scenario had a 50 km diameter impactor hitting at 15 km/s. A transient crater ~320 km in diameter was produced, similar in size to Orientale's Inner Ring (IR). Material was excavated from a maximum depth of 42 km (within the lower crust). The volume of mantle melt produced was 1.1×10^6 km^3. Analysis of material deformation suggests thrust and normal fault-like features at locations equivalent to Orientale's IR and Outer Rook Ring (ORR), respectively (Figure 1).

Thermal Profile 2 (cool mantle). The best-fit scenario had an 80 km diameter impactor hitting at 15 km/s. A transient crater 466 km in diameter was formed, slightly smaller than Orientale's Inner Rook Ring (IRR: 480 km). The maximum excavation depth was 55 km (within the lower crust). The volume of mantle melt produced was 2.4×10^6 km^3. Analysis of structural deformation showed thrust and normal fault-like features at locations equivalent to Orientale's IRR and Cordillera Ring (CR), respectively.

Melt volumes agree with previous work (~10^6 km^3; e.g., [7]), as does the absence of excavated mantle [8] and the inferred faulting within the basin [9]. The ORR has previously been suggested as marking the extent of the transient crater [10]; our models suggest a smaller diameter.

Discussion: Though thermal conditions similar to TP2 cannot be ruled out, the best-fit impact scenario using TP1 appears more appropriate for the Orientale-forming event as: (1) normal fault-like features and material distribution around the ORR agree with previous work [9]; (2) only upper crustal material is found beyond the CR, agreeing with the highly feldspathic composition [11]; and (3) the elevation and radial location of the topographic high in the TP1 scenario matches observations [12].

Acknowledgments: We thank iSALE developers: Boris Ivanov, Jay Melosh, Kai Wünnemann and Dirk Elbeshausen.

References: [1] Head, J.W. (1974) *The Moon*, 11, 327-356. [2] Head, J.W. (2010) *GRL*, 37, L02203. [3] Potter, R.W.K. et al. (2013) *JGR*, in press, doi:10.1001/jgre.20080. [4] Collins, G.S. et al. (2004) *MAPS*, 39, 217-231. [5] Potter, R.W.K. et al (2012) *GRL*, 39, L18203. [6] Wieczorek, M.A. and Phillips, R.J. (1999) *Icarus*, 139, 246-259. [7] Vaughan, W.M. et al. (2013) *Icarus*, 223, 749-765. [8] Yamamoto, S. et al. (2010) *Nat. Geosci*., 3, 533-536. [9] Nahm, A.L. et al. (2013) *JGR*, 118, 190-205. [10] Fassett, C.I. (2011) *GRL*, 38, L17201. [11] Spudis, P.D. et al. (1984) *JGR*, 89, C197-C210. [12] Smith, D.E. et al. (2010) *GRL*, 37, L18204.

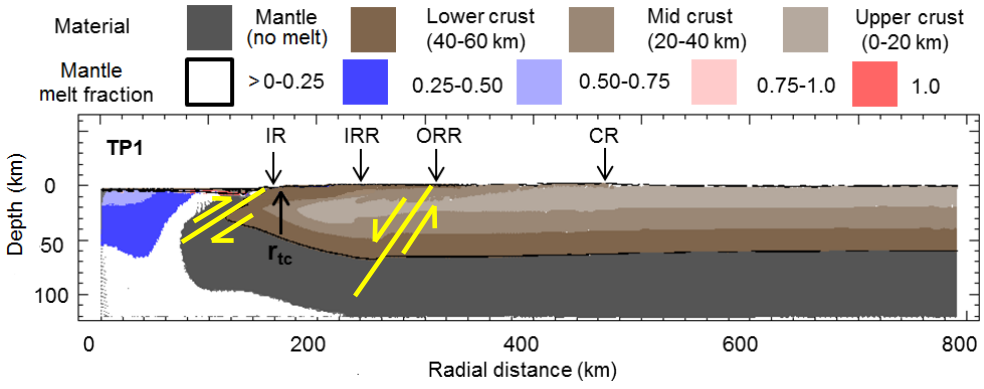

Figure 1: Material and mantle melt distribution, as well as inferred faulting, for the best-fit Orientale model using Thermal profile 1. Also shown: transient crater radius (r_{tc}) and Orientale ring structures.

Search for Impact Craters in Iran: Citizen Science as a Useful Method H. Pourkhorsandi, Department of Geology, Faculty of Science, University of Tehran, Tehran 14155-64155, Iran (hkhorsandi@khayam.ut.ac.ir)

Introduction: Developments in remote sensing and satellite imagery since 60's have had a major role in the recognition of about 170 terrestrial impact structures. Free access to satellite images has led to the investigation of earth's surface by specialists and non-specialists, at the result these attempts have led to the discovery of new impact craters around the globe (e.g. [1-4]). Middle East as a vast region consists only three confirmed impact structures (Wabar craters [5], Kamil [1] and Jabal Waqf es Suwwan [2] craters). Compared to the other regions of the world very few researches on this topic have been done in the Middle East.

Methods: In an attempt to identify new impact craters in Iran, we formed a group consisted of volunteers from Iranian amateur astronomers society to investigate: 1- Satellite images via Google Earth© to identify "circular" structures that maybe be related to meteoritic impacts. 2- Reports in ancient books about the probable meteorite impact related phenomena. 3- Old reports and stories among rural people. Members got familiar with the topic with prepared web materials and lectures.

Central and Eastern Iran images were divided to 30*30 km quadrilaterals. Each member investigates a segment with a standard method and reports the circular structures. Then we investigate it with more images, topographic and geological maps and data of the region and we do a field study if it' necessary.

Results: Two examples of the investigated structures are reported here.

a) A circular structure with a diameter of ~ 200m situated ~100km NW of Birjand city identified (33°21'57"N, 58°14'24"E) (Fig. 1). This feature is not mentioned in 1:100000 geologic map of the area [6]. A field study took place in summer 2012. The area is composed of dark color sedimentary rocks. Bottom of the structure is composed of black limestone and black shale and the rim lithology is terrigenous sedimentary rocks with sharp and regular layering and some folded layers (N,S rims). There is no sign of brecciation and/or meteoritic fragments in the region that are primary diagnostic indicators for small size impact craters (e.g. [7]). So it is unlikely to consider it as an impact crater. It is probable that the structure has formed by activity of the small stream that passes inside crater and three faults that intersect each other in the place.

b) In his book "the Raiders of the Sarhad" General Dyer explains about a crater formed by a meteorite fall, based on local people said: "The old man had told him that, one night when he was a youth, something had exploded in the sky and fallen to the earth, punching a hole one hundred feet deep in the plain" [8]. There is a picture of this hole in [9](Fig. 2); based on crater shape it is unlikely to be an impact craters and is very similar to a sink hole.

This feature is not mentioned in maps. It is situated ~130km SW Zahedan (28°24'52" N, 60°34'44" E). In a field study in 2011, we find out that the crater is completely been filled with fine grained sediments and there is no evidence of a meteorite related phenomenon. Based on local's descriptions and the picture of the Gwarkuh crater it does not in the least suggest a meteorite crater ([10] also concluded the idea) and almost certainly it was a sink hole.

Beside these structures, field studies on another craters in Iran are in progress, the outcomes of which will be announced in the near future.

References: [1] Folco L. et al. (2011) *Geology*, 39, 2, 179-182. [2] Salameh E. et al. (2008) *MAPS*, 43, 10, 1681-1690. [3] Glikson Y. et al. (2008) *AJES*, 55, 1107-1117. [4] Kofman R. S. et al. (2010) *MAPS*, 45, 9, 1429-1445. [5] Wynn J.C. and Shoemaker E.M. (1998) *SciAm*, 279, 5, 36-43. [6] *Geological Map of Sarghanj (1:100000).* (1995) GSI. [7] French B. M. and Koeberl C. (2010) *Earth-Sci. Rev.* ,98, 1-2, 123-170. [8] Dyer R. E. H. (1921) *the Raiders of the Sarhad*, H.F. & G. Whitherby, London, 268pp. [9] Skrine C.P. (1931) *GEOGR J*, 78, N, 321-340. [10] Spencer L. (1933) *GEOGR J*, 81, 3, 227-243.

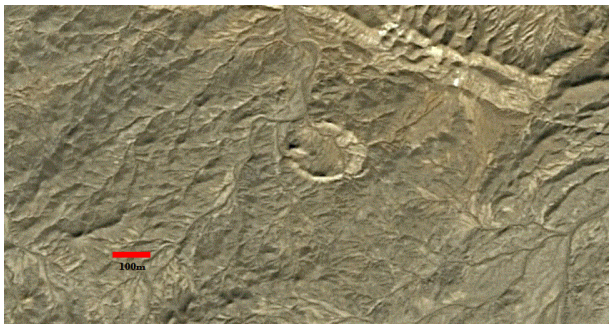

Fig 1. Satellite image of a circular structure in Eastern Iran. (maps.google.com)

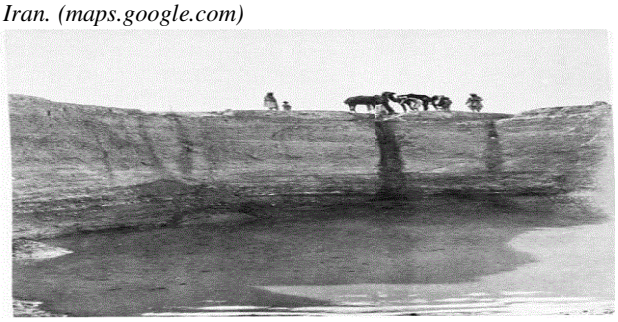

Fig 2. Gwarkuh Crater. From Skirin C.P. [9].

VREDEFORT PSEUDOTACHYLITIC BRECCIAS AND VREDEFORT GRANOPHYRE: CHEMISTRY AND ISOTOPE CHEMISTRY FAVOR FORMATION OF PTB SANS VG-LIKE COMPONENT. W.U. Reimold[1,2], T. Mohr-Westheide[1], M. Thirlwall[3], and L. Fischer[1] , [1]Museum für Naturkunde, Invalidenstrasse 43, 10115 Berlin, Germany (uwe.reimold@mfn-berlin.de), [2]Humboldt-Universität zu Berlin, Unter den Linden 6, 10099 Berlin, Germany, [3] Department of Earth Sciences, Royal Holloway University of London, Egham, Surrey TW20 0EX, UK (m.thirlwall@gl.rhul.ac.uk).

Introduction: For years the generation of pseudotachylitic breccias (PTB) in impact structures has been controversial [1]. Variably, shock compression melting, decompression melting, friction melting, and combination of these processes were proposed for in situ melt generation. In contrast, a few have favored that PTB represent impact melt generated elsewhere and was intruded into the crater floor upon mixing with local material. Regarding Vredefort, they promoted ([e.g., 2] that impact melt (Vredefort Granophyre, VG) had intruded from the coherent melt sheet into the crater floor and mixed with local material.

Method: We have reevaluated the chemical data base for Vredefort PTB and amended it with additional major and trace element data (e.g., a further full suite of PTB and country rocks from Otavi Hill). We also discuss Rb-Sr, Sm-Nd, and U-Pb isotopic data for PTB from three major occurrences in Vredefort quarries, plus their host rocks, and for comparison VG and epidiorite samples. Also, a μ-X-ray fluorescence spectrometer (M6 Jetstream, Bruker) was used for comparison of chemical compositions of PTB and host granite in a 71 x 52 cm slab from Leeukop Hill. The instrument allows non-invasive element distribution analysis of large samples with relatively high spatial resolution of several 100 μm [4]. Finally, a previously used [3] site (188, Kopjeskraal Farm) with a wide VG dike was resampled for a complete cross-section (host granite-Granophyre dike-epidiorite). Samples were analysed by XRF for major and trace elements and these data are used to evaluate the claim that two generations (a felsic and a mafic one) of impact melt were present [3].

Results: (1) Major and trace element data for host rock-PTB pairs emphasize the significant comparability of the respective analyses. This pertains to bulk rock analysis as well as PTB groundmass microanalysis and clast population studies. Mixing calculations for the varied components of host rock at Otavi and Kudu confirm the conclusion that PTB compositions do NOT require an exotic, allochthonous component. (2) Major and trace element results [5] of < 0.5 cm PTB in mafic host rocks revealed, overall, good agreement between PTB composition (EMPA defocused beam analysis and host rock composition from XRF). Notable deviations can be explained by preferential melting of either plagioclase or hydrous ferromagnesian minerals at different proportions. (3) The isotopic results demonstrate that PTB and their host rocks have significantly different isotopic systematics from that of VG [6]. PTB and respective host rocks from different locations yielded different isotopic results for each locale. This further supports the chemical results that PTB melt was formed from local reservoirs (the respective host rocks), which are different from the reservoir of impact melt (mixture of the full crustal sequence affected by the impact). With respect to the ε_{Nd} values calculated for an age of 3.15 Ga, the approximate age for the Archean granitoids that represent the host rock to PTB and the major precursor component of VG, a significant variation between granitoid-hosted PTB and Granophyre is observed. (4) The μ-XRF derived element distribution maps of the complete slab of PTB and granitic host rock show very similar chemical compositions for the granitic host rock and the melt breccia. The two lithologies can be readily distinguished by their spectrographic "textures": Element distribution maps show medium-grained granite composed of individual mineral grains, whereas melt rock is characterized by a fine-grained matrix around host rock relics. Integration of count rates for several decimeter-sized areas in the host rock and the melt breccia, respectively, results in almost identical spectra for major and trace element abundances. (5) Finally, chemical, petrographic and microchemical analysis of the Kopjeskraal profile samples demonstrate that there is no so-called mafic VG phase. Epidiorite clasts are mixed into impact melt rock of normal composition, and clasts are partially assimilated into VG melt.

Discussion: Results support that PTB formed without admixture of an exotic component from local host lithology(ies) only, and that melt is derived from preferred melting of hydrous ferromagnesian minerals. A single Granophyre variety occurs at Kopjeskraal and presumably elsewhere on the Vredefort Dome.

References: [1] Mohr-Westheide T. & Reimold W.U. (2011) MAPS 46, 543-555. [2] Lieger D. et al. (2011) GCA 75, 4490-4514. [3] Lieger D. & Riller U. (2012) Icarus 219, 168-180. [4] Alfeld M. et al. (2013) J. Anal. At. Spec. 28, 760-767. [5] Mohr-Westheide T. (2011) PhD Thesis, Humboldt-Universität Berlin, 210 pp.. [6] Reimold W. U. et al. (2011) Abstr., MAPS, 46, Suppl., p. A196.

RECENT ADVANCES IN UNDERSTANDING TECTONICALLY INDUCED CRATER FLOOR MODIFICATION AT SUDBURY: IMPORTANCE FOR THE IDENTIFICATION OF Cu-Ni SULPHIDE EXPLORATION TARGETS. U. Riller[1], M. Clark[2], I. Lenauer[3], T. Santimano[4]. [1]Institut für Geologie, Universität Hamburg, Bundesstrasse 55, 20146 Hamburg, Germany, [2]McMaster University, Hamilton, Canada. [3]SRK Consulting Inc. (Canada), Suite 1300, 151 Yonge St, M5C 2W7 Toronto Canada. [4]Deutsches Geoforschungszentrum, Telegrafenberg, C 122, 14473 Potsdam, Germany.

Introduction: Understanding post-impact shape change of the 1.85 Ga Sudbury Igneous Complex (SIC), the relic of a deformed impact melt sheet, and its host rocks, is paramount for Ni-, Cu- and PGE-mineral exploration. Respective mineral deposits related to the layered Main Mass of the SIC are found: at its base, notably in the Sublayer; in its immediate periphery; and in the physically connected so-called Offset Dikes. Together with the Main Mass, overlying melt-breccias of the Onaping Formation and post-impact sedimentary rocks form the Sudbury Basin. Non-cylindrical folding and northwest-directed reverse faulting of the Main Mass are commonly accepted as the main deformation processes that generated this fold basin. In detail, however, individual segments of the SIC, notably the North Range, the South Range and the East Range, and their respective host rocks deformed by different mechanisms. These mechanisms are delineated as follows, along with their implications for occurrence of specific mineral deposits.

The North Range: The North Range is considerably less deformed than the East Range and the South Range. The North Range was affected mostly by discontinuous deformation and solid-body tilting of less than 30° toward the SE [1]. Consequently, geometric relationships of lithological contacts in the North Range remained largely pristine and, thus, offer insight into the original crater floor geometry. Analysis of high-resolution topographic data [1] suggests that the North Range SIC is ponded due to the possible presence of a peak ring [2]. The topography of the final crater floor, i.e., after thermal erosion of target rock, is characterized by amplitudes of up to 400 m over wave lengths of hundreds of metres to a few kilometres, and amplitudes of up to 1500 m over a wave length of about 25 km. The crater floor depressions are spatially associated with a thickened Quartz Gabbro–Norite layer and Sublayer hosting economically important sulphide mineral deposits. This relationship points to a viable exploration strategy [3].

The East Range: In terms of first-order structure, the East Range is made up by two synclines, the NE-lobe and the SE-lobe, and an anticline in between. Spatial analysis of the strike of Paleoproterozoic dyke segments in host rocks indicates the location of the anticline, referred to as the West-Bay Anticline [4]. The anticline is characterized by abrupt plan-view thickness variations in the lower SIC and curved faults displaying significant strike separations and repetition of SIC contacts. Sublayer embayments and associated Offset Dikes likely served as zones of mechanical weakness, at which the higher-order folds localized under NW-SE shortening. Ore bodies in the East Range are, thus, expected to be displaced on discontinuities adhering to NW-SE shortening.

The South Range: Deformation in the South Range is highly heterogeneous, evident by the orientation of metamorphic mineral shape fabrics and folds as well as shortening directions inferred from brittle shear faults [5, 6, 7]. Overall, deformation involved simultaneous shearing on the South Range Shear Zone and variable tilting of the SIC and adjacent target rocks [5], which can be explained by trishear deformation [7]. This deformation mechanism can account for large rotation magnitudes of, and strain intensities in, the SIC as well as rather low rotation magnitudes and strains in adjacent host rocks. Thus, trishear deformation has important consequences for the downward projection of sulfide-rich zones in Offset Dikes.

During trishear deformation the plan-view geometry of the SIC likely changed from convex outward to concave inward [7]. This shape change imparted local contact-parallel shortening that caused corrugation of SIC contacts and thickness variations of individual SIC layers. Such variations have important ramifications for estimating the sulphide content at the base of the SIC. In particular the thickness of the felsic Norite, which is depleted in sulphides, relates to the sulphide concentration at the base of the SIC [3]. Thus, caution is required not to overestimate potential sulphide concentrations at the base of tectonically thickened SIC segments.

References: [1] Dreuse, R. et al. (2010). *Terra Nova,* 22, 463–469. [2] Grieve, R.A.F., (2008) *MAPS,* 43, 855-882. [3] Keays, R.R, and Lightfoot, P.C. (2004). *Mineral. and Petrol.* 82, 217–258. [4] Clark, M.D. et al. (2012). *Can. J. of Earth Sci.,* 49, 1005-1017. [5] Santimano, T. and Riller, U. (2012) *Prec. Res.,* 200-203, 74-81. [6] Lenauer, I. and Riller, U. (2012a). *J. of Struct. Geol.*, 35, 40-50. [7] Lenauer, I. and Riller, U. (2012b). *Tectonophysics*, 558-559, 45-57.

IMPACT HEATING AND COUPLED CORE COOLING AND MANTLE DYNAMICS ON MARS. James H. Roberts[1] and Jafar Arkani-Hamed[2], [1]Johns Hopkins University Applied Physics Laboratory, 11100 Johns Hopkins Rd., Laurel, MD 20723 (James.Roberts@jhuapl.edu), [2]Dept. of Physics University of Toronto, 60 St. George St., Toronto, ON, Canada M5S 1A7 (jafar@physics.utoronto.ca)

Introduction: Several giant impact basins of mid-Noachian age have been identified on Mars [1], the youngest of which are demagnetized [2]. Passage of the shock waves generated by the hypervelocity impacts [3] that formed these basins would have increased the temperature of the interior [4], modified the pattern of mantle convection [5,6], and suppressed core cooling [7], potentially contributing to the cessation of dynamo activity [8]. Here, we investigate the thermal and dynamo evolution of Mars in response to heating by a basin-forming impact, which instantaneously change the temperature structure in the core and mantle. We study the thermal coupling of the core and mantle while both are simultaneously cooling, using coupled models of mantle convection and parameterized core cooling.

Modeling: At the time of an impact we introduce a temperature perturbation resulting from shock heating into the core and mantle [4,6]. The core temperature becomes stratified, largely erasing lateral variations [7]. Exploiting this symmetry, we couple a 1-D parameterization of core cooling to 2-D axisymmetric mantle convection models using the finite element code Citcom [9], appropriate for a single vertical impact scenario. This allows us to more accurately model the thermal evolution of both core and mantle, when the core is not necessarily adiabatic and convecting [10].

Results: Figure 1 shows the evolution of the temperature in the core and lower thermal boundary layer of the mantle. after the vertical impact of a 1000-km diameter rocky projectile at 10 km/s. Just after impact, the stratified core is stable to convection and the temperature may exceed 3000K just below the CMB. The top of the core cools into the mantle, and the lower mantle material is swept into a large hemispheric upwelling. The hot layer at the top of the core disappears after a few tens of My. Further core cooling results in formation of a convecting zone at the top of the core that propagates downwards as the thermal gradient becomes adiabatic at greater depths. As the convecting region of the core thickens, the magnetic Reynolds number increases (see Figure 2), and a strong dynamo is possible after ~120 My to 150 My.

Conclusions: A large basin-forming impact results in stable stratification of the core, and halts core convection and pre-existing dynamo activity for more than 100 My. Our results are consistent with electron reflectometry observations [2] that show a lack of remanent magnetism in the younger Noachian giant impact basins [1], and supports a causal link between basin formation and cessation of dynamo activity [5,8].

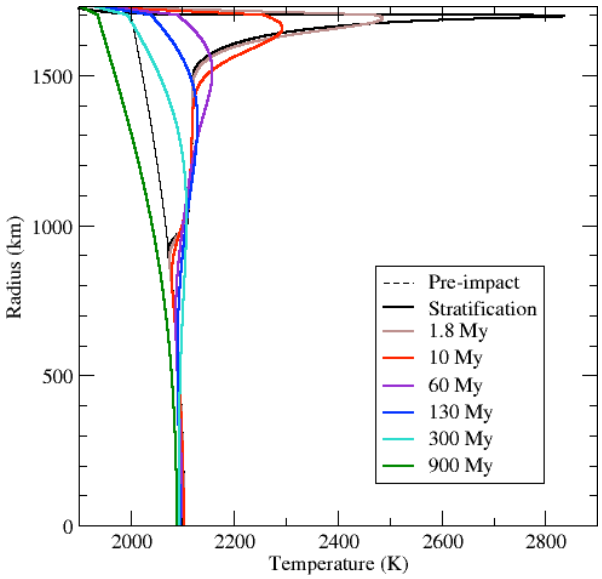

Figure 1: Radial temperature profile in the core and lower thermal boundary layer of the mantle following the impact heating.

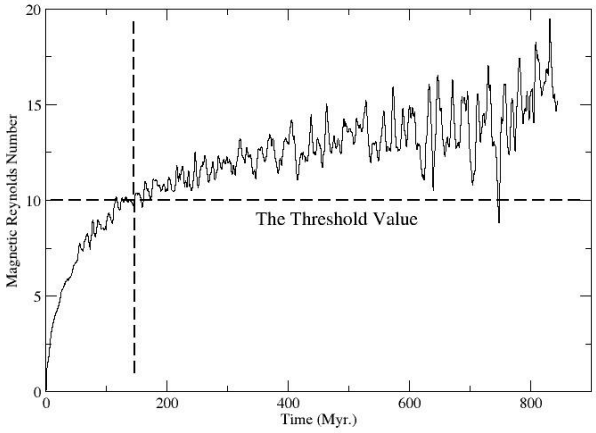

Figure 2: Post-impact evolution of the magnetic Reynolds number of the core for the case shown in Figure 1.

References: [1] Frey H. V. et al. (2008) *GRL, 35*, L13203. [2] Lillis R. J. et al. (2008) *GRL, 35*, L14203. [3] Pierazzo E. et al. (1997) *Icarus, 127*, 208-223. [4] Watters W. et al. (2009) *JGR, 114*, E02001. [5] Roberts J. H. et al. (2009), *JGR, 114*, E04009. [6] Roberts J. H. and Arkani-Hamed J. (2012), *Icarus, 218*, 278-289. [7] Arkani-Hamed J. and Olson P. (2010) *JGR, 115*, E07012. [8] Arkani-Hamed J. (2012) *PEPI, 196-197*, 83-96. [9] Roberts J. H. and Zhong S. (2004), *JGR, 109*, E06013. [10] Ke Y. and Solomatov V. S. (2009), *JGR, 114*, E07004.

The distinct behavior of sedimentary target rocks during the Chicxulub impact event: Observations at proximal and distal ejecta deposits at K-Pg sites El Guayal, La Lajilla, and drill cores UNAM-7 and ODP 207.

T. Salge[1,2], D. Goran[1], P. Schulte[3], and A. Deutsch[4], [1]Bruker Nano GmbH, Am Studio 2D, 12489 Berlin, Germany <tobias.salge@bruker-nano.de>, [2]Museum für Naturkunde, 10115 Berlin, Germany, [3]AF-Consult Switzerland Ltd, 5405 Baden, Switzerland, [4]Institut f. Planetologie, WWU Münster, 48149 Muenster, Germany.

Introduction: Ejecta deposits at the K-Pg boundary reveal that shocked carbonates are a common product of the Chicxulub impact into the carbonate-sulfate target of the Yucatán platform [1-4]. In order to better understand these impact processes, microscopic, EDS and EBSD studies of impactites were carried out.

Results, interpretations: (1) Drilled at the outer rim, 126 km of the Chicxulub crater center, core UNAM-7 contains a sequence of 126.2 m suevite topping a silicate melt-poor breccia with anhydrite megablocks [5]. The microcrystalline breccia matrix is dominated by calcium sulfate (51.8 %), calcium magnesium carbonate (30.6%), calcium carbonate (14.9 %), minor strontium sulfate (0.7 %) and feldspars (1.5 %). Dolomite spheroids with a polygonal to interlobate microstructure document deposition in molten state and slow cooling. A vesicle-bearing crystallization sequence in anhydrite, coated with silicate melt, indicates coherent melting and decomposition.

(2) EBSD studies of spherulitic calcite particles at the K-Pg deposit at El Guayal, Mexico (520 km SW the crater center [5]) reveal a fiber texture of elongated crystals with a preferred orientation distribution. The results indicate the presence of calcium carbonate melt which was ejected from upper target lithologies at T>1240 °C and P>40 bar [6] and crystallized at a high cooling rate of ΔT>100 °C/s [7]. A different microstructure is characterized by equiaxed crystals with a random orientation distribution at calcite particles of El Guayal and the K-Pg deposit at La Lajilla (1000 km W the crater center). This documents recrystallization by thermal stress at T>550 °C at a moderate cooling rate of ΔT~100 °C/s during atmospheric transport. At the polymict breccia of El Guayal, spherulitic calcite particles display a progression of microstructures from recrystallized to larger elongated grains towards the rim indicative for a formation at a low cooling rate of ΔT~10<100 °C/s [7]. Aggregates of recrystallized calcite with altered silicate melt indicate aggregation of viscous silicate melt with carbonate. Hence, the presence of pseudomorph pore space in altered silicate melt suggests CO_2 degassing at temperatures of ~660≥900 °C. The lack of anhydrite and rare presence of dolomite only in the lower subunits of El Guayal indicate that these minerals were strongly affected by decomposition.

(3) At the 2-cm-thin K-Pg ejecta deposit of ODP 207 in the Western Atlantic (4000 km SE from Chicxulub), the uppermost 1 mm contains shocked quartz and shocked carbonates [1,3]. Shocked carbonates consist predominantly of fine-grained, recrystallized calcite with minor, larger dolomite grains. They are associated with sodium halide and submicron-sized prismatic copper oxy halides. These observations point to a decarbonation of dolomite and calcite at T>778 °C with interaction of seawater.

Conclusions: UNAM-7 provides the first evidence for melting and dissociation of sulfates at the Chicxulub crater, and melting of dolomite. The abundant presence of shocked sulfates in core UNAM-7, and their absence at distal deposits may indicate that high-T processes for sulfates are restricted to a region close to the crater. It can be explained that the melting point for anhydrite at 1465 °C is very close to the temperature of the decomposition reaction [8]. Shocked carbonates from distal ejecta deposits are a clear proof for melting and dissociation. The rareness of dolomite and lack of anhydrite at distal ejecta deposits can be explained by a distinct response of these minerals:

(1) $CaSO_4 \Rightarrow CaO + SO_3$

(2) $CaMg[CO_3]_2 \Rightarrow CaCO_3 + MgO + CO_2$

(3) $CaCO_3 \Leftrightarrow CaO + CO_2$ $\Delta H° = 178$ kJ / mol

Compared to MgO, CaO is highly reactive in the interval of 300-700 °C if CO_2 is present [9]. Reformation of calcite during the fast back-reaction of CaO with CO_2 (and water) would cause a prolonged release of thermal energy that may have initiated a delayed vapor release in the ejecta plume evolution. In turn, this process could force the gas driven ejecta transport.

References: [1] Schulte P. et al. (2010) *Science* 327, 1214-1218. [2] Deutsch A. and Langenhorst F. (2007) *GFF* 129, 155-160. [3] Schulte P. et al. (2009) *GCA.* 73, 1180-1204. [4] Guillemette R.N. and Yancey T.E. (2008) *GSA Bull.*. 120, 1105-1118. [5] Salge T. (2007) *PhD thesis*, HU Berlin, 130 p. [6] Irving, A.J. and Wyllie, P.J. (1973) *EPSL,* 220-225. [7] Jones, A.P. et al. (2000) *Lect. Note Earth Sci.* 91, 343-361. [8] Ivanov B.A. et al. (2004). *LPSC XXXV*, #1489. [9] Aginier P. et al. (2001) *GCA,* 65, 2615-2632.

Acknowledgements: This research used samples provided by the Ocean Drilling Program (ODP); P. Claeys and J. Urrutia-Fucugauchi provided additional samples.

CLASSIFICATION OF SULFIDES, ARSENIDES AND TELLURIDES FROM THE SUDBURY IGNEOUS COMPLEX (SIC) USING FEATURE ANALYSIS AND SPECTRUM IMAGING WITH ADVANCED EDS.

T. Salge[1], L. Hecht[2], B. Hansen[1] and M. Patzschke[3]. [1]Bruker Nano GmbH, Berlin, Germany, tobias.salge@bruker-nano.de, [2]Museum of Natural History, Berlin, Germany, [3]Vale S/A, Santa Luzia-MG, Brazil.

Developments in energy dispersive X-ray spectrometry (EDS) offer advanced element analysis at high spatial resolution [1] for quantitative mineralogy and ore characterization [2]. This will be demonstrated for sulfides, arsenides and tellurides from the offset dike of the SIC that have been studied recently [3].

A BRUKER QUANTAX EDS system with an XFlash® Silicon Drift Detector (SDD) was used on a computer controlled field emmision SEM with stage control. Particles were detected by grey scale thresholds in the BSE micrograph. Spectra were acquired by point measurements in the center of each particle. Minerals were classified in seconds based on their composition using a truly standardless quantification routine without internal references.

Areas of interest were studied with high spatial resolution at the sub-µm scale. In order to decrease the excitation volume for generated X-rays, an accelerating voltage of 7 kV was used. Consequently, only low energy X-ray lines (Figs. 1 and 2) can be evaluated which is possible by using extended atomic database [4] integrated into the EDS software. EDS databases from spectrum images which provide complete spectra for each pixel of the SEM image permit data mining. For instance, the element identification can be improved by using the Maximum Pixel Spectrum function [5]. This function synthesizes a spectrum consisting of the highest count level found in each spectrum energy channel. Even elements which occur in only a few or just one pixel of an element map can be easily identified. Spectrum statistics can be improved using chemical phase mapping (Fig. 3), which detects similarly composed spectra with the help of mathematical methods (principal component or cluster analysis) or user defined areas.

It can be concluded that improvements in detector and pulse processor technology as well as software developments have expanded the EDS applications to applied mineralogy. The existence of high demand elements increases the value of existing ores. The analysis of features at the sub-µm scale using SEM-EDS can provide new insights for sulfide deposit models.

References: [1] Salge T. (2012) *Imaging & Microscopy, 14*, 19-21. [2] Salge T. et al. (2013) *Proc. 23rd IMCET, Turkey*, 357-367. [3] Hecht L. et al. (2010), *Proc. 11th IPS*, Sudbury, Canada. [4] Aßmann A. and Wendt M. (2003) *Spectrochim. Acta* 58,711–716. [5] Bright D.S. and Newbury D.E. (2004) *J. Microscopy* 216:186-193.

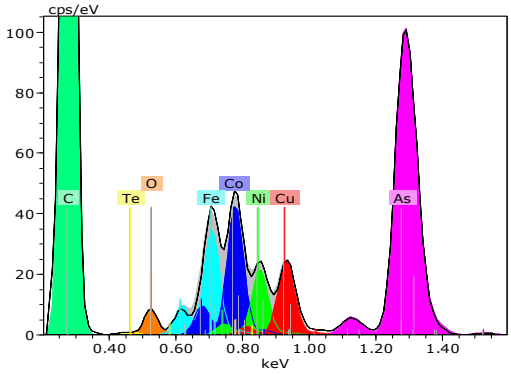

Fig. 1 Deconvolution result of the of the low energy range. The colored peaks represent the contribution of different elements.

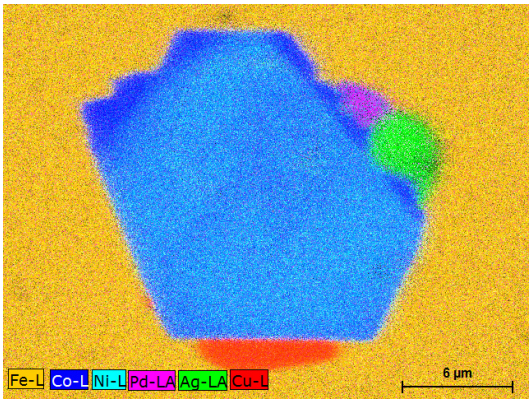

Fig. 2 Composite element map of sulfide mineralization of the Worthington dyke. The overlapping element lines were automatically deconvolved (XFlash 6|10, ≤124 eV Mn Kα, ≤41 eV C, 7 kV, 22 nA, ~97 kcps, 20 min, 45 nm pixel size.

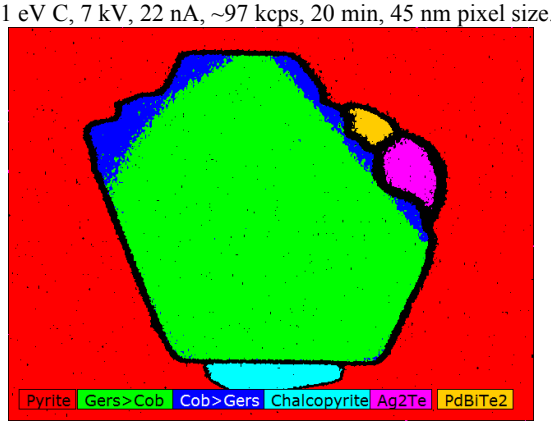

Fig. 3 Phase map considering the net intensity of Fe-L, Co-L, Ni-L, As-L, Pd-L, Ag-L, Cu-L, Bi-M, Te-L and S-K.

MICROBIAL TRACE FOSSILS PRESERVED IN IMPACT MATERIALS. H. M. Sapers[1,2], G. R. Osinski[1,2,3], N. R. Banerjee[1,2]. [1]Centre for Planetary Science and Exploration, University of Western Ontario, London, ON, Canada, 1151 Richmond St, N6A 5B7. [2]Department of Earth Sciences, ibid. [3]Department of Physics and Astronomy, ibid.

Introduction: Impact materials represent understudied microbial substrates with the potential to preserve evidence of life from early Earth as well as the potential for life on other planets. Meteorite impact events create unique microbial niches that may have been significant habitats on early Earth and are important astrobiological targets on other rocky bodies such as Mars [e.g. 1, 2]. Given the probable ubiquity of impact glasses in post-impact environments throughout the Solar System, it is important to understand the biological components and potential of such systems on Earth. Recently, microbial ichnofossils were described in meteorite impact glass from the Ries impact structure, Germany [3]. To the best of our knowledge there are only four other studies reporting *potential* fossil evidence of biological activity in impact systems. Here we compare and contrast the evidence from all these studies in an attempt to ascertain the astrobiological potential of meteorite impact structures.

Biosignatures: A biosignature is an observable feature produced through biological processes that cannot be attributed to abiotic phenomena [4]. Characterization of a putative biosignature, such as a morphological microfossil, must involve a suite of complimentary multi-scale, multi-analytical techniques to unambiguously demonstrate that the feature is both indicative of biological activity and that it cannot be formed through abiotic processes [e.g., 4-6]. Both morphological and geochemical evidence of biological process and/or behavior combined with a geological study of the host material illustrating syngenicity and antiquity with the substrate must be demonstrated [4, 6] Despite decades of research establishing biogenicity criteria [e.g., 6-8], demonstrating the unambiguous biogenic origin of putative microfossils remains challenging [e.g., 9].

Trace fossils in impact materials: To date, to our knowledge, there have been five reports of putative trace fossils in impact materials: microbial etching of hydrothermal minerals at the Ries impact structure [10], the presence of rod-shaped biomorphs in post-impact hydrothermally altered sediments from the Chesapeake Bay impact structure [11], evidence of extracellular polymeric substances in a hydrothermally precipitated calcite vein from the Siljan impact structure [1], a report of filamentous 'fossils' hosted in hydrothermally precipitated mineral assemblages within fractured impact breccia from the Dellen impact structure [12], and most recently, microbial tunneling in impact glasses from the Ries impact structure [3].

Three of these five studies; microbial etching at the Ries [10], rod-shaped biomorphs at Chesapeake Bay [11], and filamentous 'fossils' at Dellen [12], fail to recognize both multiple biogenicity criteria as well as a systematic study of the host material underscoring the difficulty in ascertaining the biogenicity of a putative trace fossil and the importance of following a multi-analytical approach to characterizing enigmatic features.

In the Hode et al (2009) study of mineralized EPS at the Siljan impact structure [1], rigorous microscopy and detailed geological context meet biogenicity criteria. It is worth noting, however, that the host material is not unique to an impact structure. The hydrothermal minerals, while precipitated in a impact-generated hydrothermal system, are common in non-impact associated hydrothermal systems. This study does add to a growing body of evidence highlighting the astrobiological significance of impact-generated hydrothermal systems on Earth and Mars [14].

The study of the microbially mediated alteration of impact glass at the Ries impact structure [3] not only presents both morphological and geochemical evidence of biogenicity, but also a systemic and thorough geological study of the host material. This study represents the first report of microbial activity preserved in material unique to the impact cratering process.

Conclusions: The goal of characterizing morphological microfossils is not only to identify attributes as uniquely produced by biological processes, but also to be able to recognize these attributes as unambiguous indicators of life. An understanding of the preservation of past biogeological processes directs our search for life beyond Earth on planets such as Mars.

References: [1] Hode, T. et al. (2009) *in J. Seckbach and M. Walsh, (Eds)*. Springer Science + Business Media B. V. 249-273. [2] Banerjee, N.R. et al. (2004) *LPSC XXXV* Abstract #1248. [3] Sapers, H.M. et al. (submitted) *Geobiology* [4] Cady, S.L. et al. (2003) *Astrobiology, 3,* 351-368. [5] Cady, S. and N. Noffke. (2009) *GSA Today 19*, 4-10. [6] McLoughlin, N., et al. (2007) *Astrobiology, 7,* 10-26. [7] Schopf, J.W. and M.R. Walter, (1983) *in J.W. Schopf, (Ed)*. Princeton University Press. 214-239. [8] Buick, R. (1990) *Palaios, 5*, 441-459. [9] Brasier, M.D. et al. (2002) *Nature, 416*, 76-81. [10] Glamoclija, M., J. Schieber, and W.U. Reimold, (2007) *LPSC XXXVIIII.* Abstract # 1989. [11] Glamoclija, M. (2007*) GSA Denver Annual Meeting*. Abstract #116-21. [12] Lindgren, P. et al. (2010) *Int. J. Astrobiol. 9*, 137-146. [14] Osinski, G. R. et al. (2013) *Icarus*, *224,* 347–363

MEGASCALE IMPACTS INTO VESTA'S SOUTH POLE. P. Schenk,[1] D. O'Brien[2], H. McSween[3], D. Buczkowski[4], R. Gaskell[5], F. Preusker[6], S. Marchi[7], A. Yingst[2], S. Mest[2], C. Raymond[8], C. Russell[9], and the Dawn Science Team. [1]Lunar and Planetary Institute, Houston (schenk@lpi.usra.edu), [2]Planetary Science Institute, Tucson, [3]University of Tennessee, Knoxville, [4]JHU/Applied Physics Laboratory, Laurel, [5]Planetary Science Institute, Pasadena, [6]DLR, Institute of Planetary Research, Berlin, [7]NASA Lunar Science Inst., Boulder, [8]Jet Propulsion Laboratory, Pasadena, [9]Univ. of California, Los Angeles.

Introduction: The large 505-km-wide South Polar impact basin, Rheasilvia, on Vesta is the largest impact feature with respect to planet diameter observed to date. As such, it provides a unique window into large impacts into planetary scale bodies under near disruption conditions. Here we present an overview of Dawn mission findings for this large impact feature from 1 year in orbit around Vesta.

Description: A 450-km class impact feature on Vesta was first observed in HST data [1]. The first discovery by Dawn on approach in 2011 was that the impact feature actually consisted of two large overlapping basins [2], part of the complex impact history of Vesta [3]. The older Veneneia basin is 395-km across and is half obliterated by the younger 505-km Rheasilvia basin. The floor of Veneneia is highly disrupted and partially covered by Rheasilvia ejecta so we will focus mostly on Rheasilvia, except to note that Veneneia is associated with outcrops of dark material.

Rheasilvia: This large basin, centered at 72°S, 279°W (Claudia system), has a "complex" morphology, with a narrow rim scarp, broad floor material, quasi-conical central peak or complex. We will describe each briefly. The rim is relatively simple but variable along its circumference. In some regions it is a low ridge reflecting a break in slope. In other areas it is a narrow inward-facing scarp of a few hundred meters to ~25 km relative heights. A few large slump features have been identified, but they are not contiguous around the rim and absent in some quadrants.

The basin floor is not flat anywhere but slopes gently inward. It is highlighted by an unexpected series of linear to arcuate low (1-2 km) scarps. These form an integrated (non-crosscutting) pattern across the entire floor. A large number of scarps arc away from the central complex in a clockwise fashion, forming a spiral pattern nearly unique in the Solar System.

The central complex is ~200 km wide and 22 km high on average and has a rugged morphology. Hollows could be indications of impact melt but regolith formation precludes confirmation. Arcuate scarps suggest partial collapse of the complex on one side.

Varying thicknesses of heavily striated material mantles areas north of Rheasilvia, extending to the equator and beyond. This material is interpreted as ejecta 1-10 km thick (provisionally), consistent with increasing degrees of crater erasure [3].

A set of spectacular large troughs extend along the equator. The geographic centers of these arcs are located within the basins, suggesting a causal relationship. We note that the troughs are not perfectly centered on the basins, however, suggesting a complex relationship. The only apparent radial features are a few sets of north-south crater chains.

Compositionally, the floor of Rheasilvia is heterogeneous [5]. Part of the floor is dominated by a diogenitic signature, which extends to the north beyond the rim suggesting partial excavation and ejection of deep crustal material. No unambiguous olivine signature has as yet been identified. The age of the basin is currently estimated at 1-2 Gyr [3].

Discussion: Volume calculations confirm that Rheasilvia was more than capable of ejecting enough material to form the Vestoid asteroid family and the HED meteoritie suite with it [2]. The lack of an olivine signature is not well understood, though gravity data are being interpreted with this question in mind. Impact modelers are working on refining their models using the new constraints, including trough formation. The high crater density on the troughs can be explained by ejecta landing after the stress waves pass.

One of the most surprising aspects of Rheasilvia has been the arcuate/spiral scarp pattern on the floor. These are interpreted as a record of the deformation pattern and stress field as the basin floor rebounded (and not to post-impact mass-wasting). The spiral pattern has been interpreted as due to failure during inward movement of floor material during post-excavation rebound. Two possible causes of the pattern have been suggested: coriolis deflection of floor material (the sense of rotation is correct) and failure patterns found in nature and experimentally in converging material. Both may be possible but discovery of similar patterns in natural crates suggests that coriolis may not be necessary. In the case of Rheasilvia, the absence of large volumes of impact melt leave these patterns exposed to view.

References: [1] P. Thomas, and others (1997), *Science* 277, 1492-1495. [2] P. Schenk, and others. (2012) *Science, 336,* 694-696. [3] S. Marchi and others. (2012) *Science, 336,* 690-693. [4] D. Buczkowski, and others (2012) *Geophys. Res. Lett., 39,* L18205. [5] H. McSween and others, *J. Geophys. Res.*, in press.

LARGE METEOR AND COMET IMPACTS AND ORIGIN OF LIFE. Harrison H. Schmitt, Department of Engineering, University of Wisconsin-Madison. P.O. Box 90730, Albuquerque, NM, (hhschmitt@earthlink.net).

Introduction: Sample, photo-geological, and mineralogical analyses related to the Moon and Mars provide the foundation for understanding the environment in which early life evolved in our Solar System. Data and conclusions from these analyses show that thermal and mechanical energy produced by a large size and frequency spectrum of meteor and cometary impacts dominated the pre-biotic surfaces of the Earth and Mars. This constituted a major potential factor in the environment in which the molecular precursors to life evolved here and probably on other terrestrial planets in other solar systems.

Early Earth Environment: Many types and compositional varieties of phyllosilicate minerals likely dominated the early Earth's surface environment. The remote identification of extensive phyllosilicate deposits in ancient Martian terrain supports this conclusion. Phyllosilicates would have been produced by rapid weathering of impact generated glass and rock and mineral debris in wet, salty, chemically complex, reducing (oxygen-poor) oceanic and early continental chemical niches. Phyllosilicate-rich locales would have been highly varied in their temperature and pressure regimes, favoring rapid evolution of different compositions and structures.

The Moon and, in a currently supportive role, Mars provide a record of the impact history of the inner solar system and therefore that of the Earth.[1] The Moon probably began its existence about 4.57 billion years ago [2] as a small planet of chondritic composition orbiting the Sun near or around the Earth that was subsequently captured intact by the Earth.[3] An alternative of lunar origin by giant impact assisted capture remains a favorite of computer modelers.[4] Whatever its origin as a satellite of Earth, at least the outer 500km of the Moon initially consisted of an impact-generated, volatile poor magma ocean[5] overlying a volatile-rich chondritic proto-core.[6] The sequential crystallization of silicate minerals from that magma produced a 34-43km thick crust[7] dominated by the calcium-aluminum silicate plagioclase including some iron-rich accessory minerals. As this crust became coherent enough to record continuing impacts, impact craters about 60km in diameter gradually saturated its surface.[8] In this same period of saturation-cratering, very large impacts occurred, forming basins of continental scale from about 1000 to 3200km in diameter, with the largest hypothesized as being the ~4.3? Gyr old Procellarum Basin followed by the ~4.2? Gyr old South Pole-Aitken at 2500km.[9]

After saturation cratering subsided, another period of large (300-1000km diameter) impact basin formation began, producing at least 45 such basins.[10] Apollo samples directly date two of the youngest of these large basins, Serenitatis and Imbrium, as having formed in that sequence 3.8-3.9 billion years ago.[11] The creation of the youngest large basin, Orientale, has not been dated directly; however, photo-geological analysis indicates that it formed about 3.8 billion years ago.[12]

From about 4.4 to 3.8 billion years ago, therefore, the upper ~35km of the Moon's crust consisted of a continuously re-formed calcium-aluminum silicate debris layer comprised of rock fragments within a matrix of much smaller mineral and glassy particles. Exposed to the same inner Solar System environment as the Moon, but with the addition of significant indigenous water in its crust and at its surface, the geological consequences of this violent impact history on Earth would be profound in terms of hydrous alteration of primary minerals. The same also can be said of early Mars.

Rock Alteration to Clays: On Earth and Mars, the fine crustal impact debris would alter rapidly to hydroxyl-rich phyllosilicates as that debris formed. Alteration of silicate minerals to phyllosilicates is a well-documented geological phenomenon at the Earth's surface and in its subsurface as well as in hot water (hydrothermal) environments near and beneath volcanic eruptions.[13] Silicates like feldspars that are rich in alkali elements and olivines that are rich in magnesium are particularly susceptible to such alteration. Of particular interest in this regard are minerals of the smectite group and, to a lesser extent, serpentine. Smectites[14] are composed of continuous two-dimensional sheets of SiO_4 tetrahedrons, with the composition Si_2O_5. Each tetrahedron shares three corners with other tetrahedra, resulting in an overall hexagonal mesh. Aluminum and ferric iron can substitute for silicon at the center of each tetrahedron with the ensuing charge imbalance satisfied by various cations placed between sheets. The resulting complex surface structures and geochemistry[15] of these minerals may offer significant potential for pre-biotic selective organization of organic molecules.

The remote identification of various phyllosilicates in the oldest surface regions on Mars provides strong clues as to those that may have been present at the surface of the early Earth. To date, most Martian phyllosilicates[16] are associated with the oldest visible terrains. They appear to be Fe/Mg- and Al-rich, specifically including members of the smectite group (saponite, nontronite vermiculite, and montmorillonite) as the most common. Spectral signatures of illite (or muscovite) and chlorite (or clinochlore) also have been detected. Varieties of the serpentines could explain some other, more local signatures. Hydrated silica and sorosilicate pumpellyites, with a broad range of compositions, also have been identified. At one specific location, an iron-magnesium smectite appears to be dominant and is overlain by hydrated silica, montmorillonite, and kaolinite.[17] Mars Exploration Rovers also discovered opaline silica at Gusev Crater and possibly at Meridiani Planum[18].

Clay's Potential Role in Origin of Life: The availability of a broad spectrum of phyllosilicate catalysts and structural templates for the organization of pre-biotic molecules, and their potential for enhancing the stability of their hosts in various pre-biotic environments, may have provided critical steps along the path to self-replicating macromolecules.[19] Phyllosilicate mineral surfaces also may have been the initial structural frameworks that organized amino acid formation as well as providing fixed availability of necessary inorganic components, such as phosphate-oxygen groups. Further,

some surface structures may have constituted the scaffolding for the first cells, later to be replaced by more evolutionarily advantageous organic systems.[20] For example, phyllosilicate scaffolds may have anticipated a RNA function in providing spatial organization for cellular metabolism, specifically offering protein attachment sites for hydrogen production.[21] Further, crystallographic mobility of sodium ions in phyllosilicates similarly may have anticipated the sodium channels in cell membranes that trigger bioelectrical events within cells.

References: [1] Wilhelms, D. E. (1987) *The Geologic History of the Moon*, USGS Prof. Paper 1348, 156; Hiesinger, H., and J. W. Head III (2006), in B. Jolliff, et al., eds., *New Views of the Moon,* Rev, Min. & Geochem., 60, Mineralogical Society of America, 1-2. [2] Taylor, S. R. (1982) *Planetary Science: A Lunar Perspective*, LPI, 409-431; Taylor, S. R., and T. M. East (1996) in A. Basu and S. Hart, eds., *Earth Processes: Reading the Isotopic Code,* AGU Geophys. Mono. 95, 41; Patterson, C., (1956) *Geochim et Cosmochim Acta*, 10, 230-237; Carlson, R. W., and G. W. Lugmair, in R. M., Canup and K. Righter, eds. (2000) *Origin of the Earth and Moon,* Univ. Arizona Press and LPI, 25-44. [3] Alfven, H., and G. Arrhenius (1972) *The Moon*, 5, 210-225; Taylor, S. R. (1982) *Planetary Science: A Lunar Perspective*, LPI, 424; Sputis, P. D. (1996) *The Once and Future Moon*, Smithsonian, 161-163; Taylor, S. R., and T. M. Esat (1996) in A. Basu and S. Hart, ed., *Earth Processes: Reading the Isotopic Code*, AGU Geophy. Monograph 95, 33-46; Jones, J. and H. Palme (2000) in R. M., Canup and K. Righter, ed., *Origin of the Earth and Moon,* Univ. Arizona Press and LPI, 197-216. [4] Canup, R. M., and K. Righter, ed., 2000, *Origin of the Earth and the Moon*, University of Arizona Press, 555p. [5] Wood, J. A., et al., 1970, *Proceedings LSC I*, 1, 965-988; Smith, J. V., et al., 1970, *LSC 1*, 1, p. 897-925; Taylor S. R., and P. Jakes, 1977, 1, p. 433-446; Warren, P. H., 1985, *Ann. Rev, Earth and Planet. Sci.*, 13, 201-240; C. B. Agee and J. Longhi, Eds., (1991) *Workshop on the Physics and Chemistry of Magma Oceans from 1 Bar to 4 Mbar*, Technical Report Number 92-03; Jones, J. and H. Palme (2000) in R. M., Canup and K. Righter, eds., *Origin of the Earth and Moon,* Univ. Arizona Press and LPI, 205-209; Shearer, C. K., et al. (2006) in B. Jolliff, et al., eds., *New Views of the Moon,* Rev. Min. & Geochem., 60, Min. Soc. Am., 240-253. [6] Schmitt, H. H. (2003) *Encyclopedia of Space and Space Technology*, H. Mark, ed., Wiley, New York, Chapter 1, 15-18. [7] Wieczorek, M. A., et al (2013) *Science*, 339, 671-675. [8] Wilhelms, D. E. (1987) *The Geologic History of the Moon*, USGS Prof. Paper 1348, 156. [9] Schmitt, H. H. (2003) *Encyclopedia of Space and Space Technology*, H. Mark, ed., Wiley, New York, Chapter 1, 32. [10] Sputis, P. D. (1993) *The Geology Of Multi-Ring Impact Basins: The Moon And Other Planets*, Cambridge University Press, Cambridge, 263 p.; Wilhelms, D. E. (1987) *The Geologic History of the Moon*, USGS Prof. Paper 1348, 64-65. [11] Stöffler, D., et al (2006) in B. Jolliff, et al., eds., *New Views of the Moon,* Rev. Min. & Geochem., 60, Min. Soc. Am., 569-573. [12] Wilhelms, D. E. (1987) *The Geologic History of the Moon*, USGS Prof. Paper 1348, 156; Stöffler, D., et al (2006) in B. Jolliff, et al., eds., *New Views of the Moon,* Rev. Min, & Geochem., 60, Min. Soc. Am., 573. [13] Velde, B. B., and A. Meunier (2010) *Origin of Clay Minerals in Soils and Weathered Rocks*, Springer-Verlag, Berlin, 406p. [14] Brindley, G. W., and G. C. Brown, eds. (1982) *Crystal Structures of Clay Minerals and Their X Ray Identification* (Mono, Min. Soc. Am.) 495p; Meunier, A. (1965) *Clays*, Springer-Verlag, Berlin, 472p; Bergaya, F., et al., eds., (2006) *Handbook of Clay Science, Volume 1 (Developments in Clay Science)*, Elsevier, 1224p. [15] Sposito, G., et al. (1999) *Proceed. of the Nat. Acad. Sci.,* 96, 3358-3364. [16] Fairén, A. G., et al. (2010) *Proceed. of the Nat. Acad. Sci.,* 107, 12095-12100; Carter, J., et al. (2009) *LPSC XL*, Abstract #2028; Mustard, J. F. (2008), *Nature*, 454, 305-309; Bibring et al. (2006) *Science*, 312, 400-404; Gendrin et al. (2005) *Science*, 307, 1587-1591; Poulet et al. (2005) *Nature*, 438, 623-627. [17] Bishop, J. L., et al. (2008) *Science,* 321, 830-833. [18] Squyres, S. W., et al. (2008) *Science*, 320, 1063-1067. [19] Ferris, J. P. (2006) *Phil. Trans. Royal Soc. London-Bio. Sci.*, 361, 1777-1786; Schmitt, H. H. (1999) Abstract, *GSA Ann. Meet*., A-44; Schmitt, H. H. (2006) in P. Blondel and J. W. Mason, eds., *Solar System Update*, Springer-Praxis, 126; Mojzsis, S. J., and T. M. Harrison (2000) *GSA Today*, 10, 4,1-6; Kring, D. A. (2000) *GSA Today,* 10, 8, 1-7. [20] Ertem, G., and J.P. Ferris (1996) *Nature*, 379, 238-240; Ertem, G., and Ferris, J. P. (1997) Jour. Am. Chem. Soc., 119, 7197-7201. [21] Delebecque, C. J., et al. (2011) *Science*, 333, 470-474. [22] Payandeh, et al. (2011) *Nature*, 475, 353-358.

NEW CONSTRAINTS ON MULTI-RING BASIN FORMATION. P. H. Schultz[1], D. A. Crawford[2], and K. L. Donaldson[1], [1]Brown University, Providence, RI, USA. [2]Sandia National Laboratories, Albuquerque, NM, USA.

Introduction: A new survey of the composition of central uplifts within craters and basins on the Moon reveals that most did not expose mantle material [1, 2]. This result places a new constraint on the formation and interior ring formation of large impact basins.

Background: Near-infrared studies using the Moon Mineralogy Mapper (M^3) on Chandrayaan-1 [1,2,3] reveal that relatively un-shocked, pure (≥ 99% plagioclase) anorthosite characterizes many central peaks and uplifted massif rings within basins. Even the inner rings of large basins such as Orientale, Crisium, Humorum, Hertzsprung, and Nectaris exhibit pure anorthosite, not exposed deep mantle materials, particularly where the crustal thickness ranges from 30 to 63km (from the GRAIL crustal thickness model [4]). Exposures of pure anorthosite mixed with mafic lithologies, however, generally occur where the crust is estimated to be between 22 and 32km, thereby leading to the conclusion that the pure anorthositic portion of the primary crustal thickness (likely derived from the early magma ocean) must have been at least 30km thick. Consequently, the inner rings of large basins are not derived from great depths. In models depicting a collapsed, deep transient crater, the uplifted interior rings of the large basins (>300km) on the Moon should come from below the anorthositic crust (into the mantle). This observation places new constraints on basin-formation models.

Discussion: Traditional views of crater and basin excavation depict a deep transient crater resembling a simple crater before undergoing collapse (and oscillations), thereby leading to a central peak or interior rings [e.g., 5]. This view has several implications. First, there should be a progression in compositions of the uplifted interior. Central peaks from smaller craters should sample the anorthositic crust, whereas the inner rings of large basins should expose deep mantle materials. Moreover, the final crater should not retain any expression of the initial conditions of coupling between the projectile and target. For convenience, the former model is termed here the "*oscillation model*" (*OM*).

A second view argues that the central structures within craters and basins retain signatures of the initial stage of cratering, best expressed by oblique impacts [6,7,8]. In this model, the interior ring of a large multi-ring basin marks the transition between the initial downward displacement and an annulus of lateral excavation. Consequently, the interior ring correlates with early-stage initial conditions (momentum controlled), whereas the transient excavation diameter relates to excavation of surrounding shocked and comminuted crust (energy controlled) limited in growth by gravity [7]. As a result, the interior ring should not sample the deep mantle; rather it should expose shallower depths, i.e., the anorthositic crust. This second model is termed here the "*lateral excavation model*" (*LEM*).

These two views have very different predictions for exposure depths and retention of initial conditions. For a collapsing transient crater (*OM*), the central peak or peak ring should contain materials derived from about 1/2 the transient crater depth. As a result, larger basins should expose greater depths and traces of initial conditions should be erased. For example, the central uplift of a 200km rim-rim diameter basin (~130 km transient diameter) could have exposed depths of greater than 60km. But the inner rings of large multi-ring basins (such as Orientale, Crisium, Nectaris) should have exposed mantle materials from greater depths (>100km). For the lateral excavation model, the central uplift delineates the edge of downward displacement from much shallower depths (~1/4 the transient crater diameter, i.e., the anorthositic crust).

In the *LEM*, the central uplift preserves evidence for first-contact conditions, including the impactor trajectory and size. As scale increases (or impact angle decreases), initial conditions comprise a greater fraction of crater growth, thereby becoming more obvious in expression, e.g., the elliptical or downrange-breached interior ring along with an uprange offset of the interior mascon within basins (e.g., Moscoviense, Orientale, Crisium, and Imbrium). The breached downrange ring results from retained momentum in the early-stage flow field [8], including shallow downrange scouring by the failed projectile.

Implications: Observations of pure anorthosite in the M^3 near-infrared data suggest a new approach for modeling of multi-ring basin formation [e.g., 9] is warranted. Multiple mechanisms with differing regimes of efficacy such as deep vs. shallow, or radially inward vs. outward may need to be combined to fully explain the observations. We will be using numerical simulation compared to experimental and remote sensing data to investigate combined mechanisms [e.g. 4, 9] to see if they can better explain the observations than a single mechanism alone.

References: [1] Donaldson, K. L. et al. (2012), *Second Conf. on Lunar Highlands*, LPI, #9024; [2] Donaldson, K. L. (2013), PhD thesis, Brown; [3] Cheek, L. C. et al. (2013), *J. Geophys. Res., Submitted*; [4] Wieczorek, M. A. *et al*. (2012), *Science,* doi:10.1126/science. 1231530; [5] Melosh, H.J. (1979), *JGR*, 84, 7513-7420; [6] Schultz, P.H. et al. (1981), *Proc. Lunar and Planetary Sci. 12A*, pp. 181-195; [7] Schultz, P.H. (1992), *J. Geophys. Res.*, *97*, No. E10, 16,183-16,248; [8] Schultz, P. H., and A. M. Stickle, A. M. (2011), LPSC 42, # 2611; [9] Schultz, P. H. (2012), *Geol. Soc. Amer. Fall Meeting,* #202-1; [10] Crawford, D. A. and Schultz, P. H. (2013), this volume.

MULTISPECTRAL ASSESSMENT OF IMPACT MELT DEPOSITS WITHIN COMPLEX LUNAR CRATERS. B. Shankar[1], G. R. Osinski[1], and I. Antonenko[1], [1]Centre for Planetary Science and Exploration/Dept. of Earth Sciences, University of Western Ontario, London, ON, Canada (bshanka2@uwo.ca)

Introduction: The release of high resolution multispectral data (with improved spatial and spectral detail) from the Lunar Reconnaissance Orbiter (LRO) and Chandrayaan-1 missions provides new opportunities to assess the morphologies and spectral characteristics of impact melt deposits from lunar complex craters in greater detail. Impact melt deposits represent shock-melted target rocks that range in morphologies from crater fill deposits to melt veneers, melt sheets, and ponded deposits [1]. Models indicate that the amount of melt generated increases with the size of the impact event [2]. The modification phase of crater formation determines where much of the impact melts are concentrated [3, 4], as collapsing crater walls and central uplifts in the transient cavity can transport impact melt materials beyond the crater rim.

This study focuses on the characterization and distribution of impact melt deposits using multispectral satellite datasets around two well preserved complex craters with varying central uplift morphologies, located on the lunar farside.

Study Sites: 1) Olcott (22°N, 117°E) is an 81 km diameter complex crater situated on the edge of the degraded Lomonosov-Fleming basin [5, 6]. The crater morphology includes a sharp rim, crater walls with terraces, and a cluster of central peaks on the crater floor. 2) Kovalevskaya (30°N, 129°W) is a 113 km complex crater located north-west of Orientale basin [7]. The crater morphology includes a well preserved crater rim, terraced walls, a flat crater floor, and a central uplift with two peaks of variable heights.

Methods: Impact melt deposits were identified primarily based on their visible characteristics, smooth, low albedo deposits that show obvious contrast when compared to their immediate surroundings, and deposits that do not have a volcanic source of origin [1]. Monochrome 643 nm LRO Wide Angle Camera (WAC) global mosaics at 100m/pixel resolution [8, 9], and high resolution panchromatic images from the Narrow Angle Camera (0.5 m/pixel) instruments on the Lunar Reconnaissance Orbiter [8] were used to identify the extent of the deposits.

Characterization of impact melt deposits was conducted by the fusion of multiple lunar datasets – combining spatial, spectral, and topographic data. Multispectral reflectance data in the UV-VIS-NIR range were derived from the Chandrayaan-1 Moon Mineralogy Mapper (M^3) [10] to provide compositional detail. Topographic information was acquired from the LRO Lunar Orbiter Laser Altimeter instrument [11].

Results: From image data, impact melt deposits are identified both within and beyond the crater floor at each of the study sites (cf., [5, 7]). The deposits are typically smooth and have low albedo. They fill the crater floor, occur as thin veneers over central uplifts, or pooled on crater terraces and beyond the crater rim. The aerial extent of mapped melt deposits is greater in Kovalevskaya than at Olcott crater [12]. M^3 reflectance data reveals a great detail about the rock compositions present at each crater site. Sampled spectral profiles of the morphological units within each crater indicate the presence of both low and high-Ca pyroxenes and plagioclase feldspar [5, 7, 12]. The distribution of mafic material is not ubiquitous, which alludes to the complexity of the target subsurface.

Discussion and conclusions: The identification of impact melt deposits around these complex impact craters is challenging, and limited only to visible datasets. Multispectral datasets are, however, useful in broadly determining the compositional and surface textural details of impact melts and provide a complimentary tool in understanding the impact cratering process [e.g. 5, 7, 12]. Our work shows that the spectral characteristics of the exterior melt deposits are typically undistinguishable from spectral characteristics of the crater floor. This is an indication that the melts emplaced beyond the crater floor are the same materials as the crater floor melts, consistent with a multi-stage ejecta emplacement process [4]. Future work will integrate data from the LRO Diviner mission [13] to provide additional opportunities to constrain the compositional details of identified melt deposits, and will be further investigated.

References: [1] Hawke, B. R., and Head, J. W. (1977). *SPCM*, pp. 815–841. [2] Cintala, M. J., and Grieve, R. A. F. (1998). *Meteoritics and Planet. Sci*, *33*, 889–912. [3] Melosh, H.J. (1989). 245p. [4] Osinski, G. R. et al. (2011). *EPSL*, *310*, 167–181. [5] Shankar, B. et al. (2012). *LPSC XLIII*, Abstract #1357. [6] Giguere, T. A. et al. (2003). *JGR*, *108*, 5118. [7] Shankar, B. et al. (2013). *LPSC XLIV*, Abstract #2094. [8] Robinson, M. S. et al. (2010). *Space Sci. Rev*. *150*, 81–124. [9] Speyerer, E. J. et al. (2011). *LPSC XLII*, Abstract #2387. [10] Pieters, C. M. et al. (2009). *Current Sci.*, *96*, 500–505 [11] Smith, D. E. et al. (2010). *Space Sci. Rev*., *150*, 209–241. [12] Shankar, B. (2013). *Ph.D. Thesis*, http://ir.lib.uwo.ca/etd/1137 [13] Greenhagen, B. T. et al. (2010) *Science*, *329*, 1507–1509.

MICROSCOPIC EFFECTS OF SHOCK METAMORPHISM IN ZIRCON FROM THE HAUGHTON IMPACT STRUCTURE, ARCTIC CANADA. A. C. Singleton[1], G. R. Osinski[1,2], [1] Centre for Planetary Science and Exploration/Dept. of Earth Sciences, University of Western Ontario, 1151 Richmond St., London, ON, N6A 5B7, Canada (asingle2@uwo.ca), [2]Dept. of Physics and Astronomy, University of Western Ontario, 1151 Richmond St., London, ON, N6A 5B7, Canada

Introduction: The features that result from the extreme conditions involved in an impact event are diagnostic of these events and can sometimes be related to specific pressure and temperature conditions [1, 2]. Zircon is recognized to be a highly refractory and resilient mineral, which has advantages over quartz, feldspar and other rock-forming minerals. Indeed, zircon is increasingly being seen as a useful indicator of shock metamorphism in the study of impact structures and impactites in general [2, 3]. The aim of this study is to investigate shock metamorphic effects in zircon from the Haughton impact structure, Canada, for the first time.

Geological Setting and Methodology: The Haughton impact structure is a 23 km, ~39 Ma, well-preserved complex crater situated near the western end of Devon Island, Nunavut, in the Canadian High Arctic (75°22'N, 89°41′W) [4, 5]. Over 300 samples of precambrian gneiss samples were collected from 36 sites within the clast-rich impact melt rock unit of this structure and from one site outside the structure. Fifty-two representative samples were selected and polished thin sections were made and investigated in transmitted and reflected light with a petrographic microscope. Select grains were then imaged using an SEM (scanning electron microscope) to provide more detailed information on the microstructures and zoning within the grains.

Results and Discussion: Shock effects identified in the sample set range from level 0 to level 7 indicating shock pressures ranging from 2 to 80 GPa. These shock levels were assigned using the methodology outlined by Singleton et al. [6].

A total of 255 zircon grains from seven representative samples were located, photographed and described using an optical microscope. In the description of each zircon, key descriptors were recorded, including the presence of fractures (linear, sub-linear, or non-linear), zoning, displacements, and granular texture. The percent of grains per sample containing each feature was then determined and the resulting data was represented using a bar graph. From examining this data some general trends may be noted. First, oscillatory zoning steadily decreases as the shock level increases. There does not appear to be a trend in the presence of non-linear and sub-linear fractures but it should be noted that the most highly shocked samples do not display linear fractures. Conversely, granular textures are only observed in samples that are shocked to level 5 or higher. The lack of linear fractures seems to correlate well with samples that show the so-called granular texture. This texture has been described by Wittmann et al. [3] as recrystallized amorphous $ZrSiO_2$ and redite that reverted to zircon.

This is likely do to the fact that the recrystallization that causes this granular texture disrupts the zircon's original crystallinity thus changing its cleavage surfaces. Displacement is present in all samples with the exception of the unshocked sample, suggesting that this is a shock-related feature.

A small number of zircons at shock level of 6 exhibited an unusual "microporous" texture. These grains are rare in this sample set and are found in sections along with fully recrystallized zircon grains. They appear to consist of smooth regions of recrystallized zircon and regions of the aforementioned texture (Fig 1). To the knowledge of the authors, this is the first recorded instance of it. In an attempt to explain the internal variations in texture of these grains, trace element maps were collected.

It is clear from this study that zircons have the potential to play an important role in the identification and understanding of impact structures. This study is the most extensive investigation of its type at Haughton and the focus on zircons adds to previous investigations on main phase shock metamorphism.

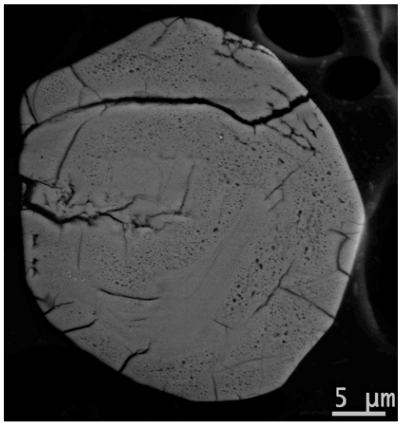

Figure 1. SEM image of recrystallized zircon showing microporosity texture.

References: [1] Stöffler, D. (1971) *JGR, 79,* No. 23. [2] French B. M. and Koeberl C. (2010) *Earth Sci. Rev. 98,* 123–170. [3] Wittmann, A. et al. (2006) *Meteoritics & Planet. Sci., 41*, 433–454. [4] Osinski, G.R. et al. (2005a) *Meteoritics & Planet. Sci., 40* ,1759–1776. [5] Sherlock, S. et al. (2005) *Meteoritics & Planet. Sci., 40,* 1759–1776. [6] Singleton, A. C. et al. (2011) *Meteoritics & Planet. Sci., 46,* 1774–1786.

LARGE METEORITE IMPACTS AND GENESIS OF PRECAMBRIAN GRANITES. M.S. Sisodia
Department of Geology, J.N. Vyas University, Jodhpur, 342005, India. sisodia.ms@gmail.com

Earth's continental crust is largely granitic (86%) thus granitoids have been a subject of comprehensive study for the Earth Science community. Extensive variation in composition, texture and emplacement of granites generated many conflicting views regarding its genesis, which as a consequence still remains an enigma. Chappell and White [1] classified granites into I-type and S-type based on their chemical and mineralogical composition. Granites resulting from melting of infra-crustal protolith and constituted of biotite, hornblende, sphene, magnetite with high Na_2O/K_2O ratio are called as I-type while the product of anatexis of sediments and constituted of muscovite, biotite, garnet etc but devoid of hornblende are called as S-type granites. Other authors later added, some more alphabets such as M-type (mantle granites), A-type (alkaline), C-type (crustal), and H-type (hybrid) to this classification. Granites are also classified as WPG (within plate granites), COLG (collision), VAG (volcanic arc), ORG (ocean ridge), IAG (island arc), CAG (continental arc), CCG (continental collision), POG (post orogenic), RRG (rift related), CEUG (continental epeirogenic) and OP (oceanic plagiogranites) on the basis of their tectonic environment [2]. Granites are invariably intimately associated with chemically erratic xenoliths and microgranular enclaves. How such xenoliths evolve within granites has been a matter of concern. To resolve this disorder 'restite- unmixing' hypothesis was proposed [3] but that was not accepted and was left to "rest-in-peace". Granites are also classified as Late-orogenic, Post-orogenic and Anorogenic on the basis of chemical composition associated with mountain building activity [4,5]. A geochemical classification on a three-tier strategy based respectively on iron ratio, modified alkali-lime index (MALI) and aluminium saturation index has also been proposed [6]. Experimental petrology has helped in resolving many rock genesis controversies [7] thus on the basis of experimental results scientists supported classification of granites based on mixing/hybridization of anatectic melts with mantle-derived magma [8]. The term 'Suite' is therefore used to define a group of igneous rocks derived from a common source [9] but the genetic significance of suite has always remained questionable because of chemically distinct variables found in all types of granites [10]. Although there are many controversies and confusion regarding genesis of granites but there exists a consensus that crustal anatexis and recycling of pre-existing crustal material has played a significant role in the petrogenesis of granitoids. Notwithstanding this consensus the earth science community has still no answer to explain crustal melting process, regions of magma generation and granitic intrusion mechanism. In the present paper two cases of impact derived granites are discussed to understand and elucidate the origin of granites due to impact.

Impact cratering is a fundamental process responsible for planetary accretion to shaping the planets. Small and big extra terrestrial bodies have continuously hit the Earth since its formation, similar to Moon and other planetary bodies. The effects of theses impacts on the Earth undergo erosion, weathering or get buried under sediments; nevertheless there are characteristic shock metamorphic features that help in the recognition of impact craters [11].

The molten rocks of Neoproterozic age, dominantly granites and rhyolites, covering an area of about 51 thousand sq km in western India, named as Malani Beds have been inferred to have evolved due to anorogenic felsic magmatism [12]. No consensus however exists regarding their nomenclature, origin and duration of magmatism [13, 14]. Recent survey of Malani Beds revealed the whole area as a highly eroded complex crater with diagnostic impact related features that divulge Malani rhyolite and granite as solidified impact melts [14]. In another case the Palaeoproterozoic felsic rocks, dominantly sheared and brecciated granites, occupying an area of about 750 sq km, structurally placed in a 'caldera' at Mohar area of Shivpuri district in M.P., India are debatably interpreted to have originated due to Plinian type volcanic explosion [15]. The observation of shock-metamorphosed features at Dhala confirmed the origin of these granites due to impact [16]. A 4.53 Ga old granite clast in the Adzhi-Bogdo meteorite [17] and 3.88 to 4.32 Ga old lunar granites [18] also corroborate probable impact origin. It is important to note that impacts generate a large volume of crustal melt that behave and look similar to effusive and intrusive volcanic products. The impact melts in larger cases form deposits of considerable thickness with polygonal joints similar to that observed in large igneous provinces. The centrally uplifted structures in complex crater cases that result due to rebound of the rocks compressed due to energy of the impact appear similar to the plutonic igneous rocks. Incomplete melting of crustal material after impact produces breccia or megabreccia that explains occurrence of erratic xenoliths and chemically heterogeneous enclaves found in granites. It can therefore be concluded that silicic large provinces especially of Precambrian age needs a re-examination to unearth their relation with the impacts, if any, in order to resolve the granite genesis enigma.

References: [1] Chappell B.W. and White A.J.R. 1974, Pacific geo., 8, 173-174. [2] Pearce J.A. et al 1984, J. Petrology, 17, 15-43. [3] White A.J.R. and Chappell B.W. 1977, Tectonophysics, 13, 7-22. [4] Rogers J.J.W. and Greenberg J.K. 1990, J.Geology, 98, 291-309. [5] Agrawal S. 1995, J.Geology, 103, 529-537. [6] Frost B.R. et al 2001, J. Petrology, 42, 2033-2048. [7] Tuttle O.F. and Bowen N.L. 1958, Mem.Geol.Soc.Am. 17, 153p. [8] Castro A. et al 1991, ESR, 31, 237-253. [9] Bayly M.B. 1968, Petrology, Prentice-Hall, 371p. [10] Whitten E.H.T. 1987, Am.J. Science, 287, 332-352. [11] French B.M. and Koeberl C. 2010, ESR, 98, 123-170. [12] Blanford W.T. 1877, Rec.Geol.Surv.India, 10, 10-21. [13] Bhushan S.K. and Chandrasekaran V. 2002, Mem. Geo. Surv. India, 126, 181p. [14] Sisodia M.S. 2011, Current Science, 101, 946-951. [15] Jain S.C. et al 2001, Geol. Surv. India sp.pub. 64, 289-297. [16] Pati J.K. et al 2008, MPSc, 43, 1383-1398. [17] Terada K. and Bischoff A. 2009, Astr.J., 699, 68-71.[18] Shih C.Y.et al 1993,G.C.Acta57, 4827-4841.

DISCOVERY OF NEW OFFSET DYKES AND INSIGHTS INTO THE SUDBURY IMPACT STRUCTURE.

D. A. Smith[1], J. M. Bailey[1], E. F. Pattison[2], [1]Wallbridge Mining Company Limited, dsmith@wallbridgemining.com, [2]Consulting Geologist, Retired (Inco).

Introduction: Offset dykes are part of the Sudbury Igneous Complex (SIC) which is interpreted as impact melt within the Sudbury impact structure [1].

In recent years, while exploring for Ni-Cu-PGE deposits, Wallbridge Mining Company Limited (Wallbridge) has mapped significant extensions to the Hess, Ministic, and Manchester Offset dykes; has identified the new Trill and Cascaden Offset dykes; and has identified several new types of dykes of possible SIC affinity including the Pele granophyre dykes, several quartz gabbro dykes and several pyroxenite dykes (Figure 1).

The geometry of these new dykes around the SIC and their observed field relationships provide new insights into the formation of the Sudbury impact structure and raise significant new questions.

Background: The SIC melt sheet forms a large differentiated body consisting of an upper granophyre layer underlain in sequence by quartz gabbro, norite, the lower ore bearing sublayer, and the underlying ore bearing Offset dykes. The Offset dykes fill radial and concentric fractures around the SIC and are traditionally separated into quartz diorite and inclusion quartz diorite phases that vary compositionally between quartz monzodiorite, granodiorite, and tonalite [1].

Discussion: The original pre-erosional extent of the crater and SIC is not known. The Foy and Hess Offsets show continuity in the field indicating that the radial and concentric Offset dykes were emplaced during one event [2]. If the dykes originate from the SIC, both likely intruded downwards into the footwall rocks from an overlying and now eroded portion of the crater and SIC, rather than through outward injection.

Small apophyses of the Offset dykes gradually terminate into pre-existing conjugate joint fractures suggesting passive intrusion and stoping of wall rocks, rather than forceful injection.

Inclusion free and at least two variants of inclusion bearing quartz diorite are observed in the Offset dykes. There appear to be gradational contacts between pyroxene, amphibole-biotite, and biotite bearing phases, which occur both with or without magnetite. Inclusion bearing phases contain inclusions of quartz diorite and are mostly associated with disseminated to massive Ni-Cu-PGE sulfide; however, mineralized examples of inclusion free quartz diorite do occur. The Offset dykes range from medium grained in thicker sections, to glassy and aphanitic within chilled margins and narrow aphosyses which are often spherulitic.

Several new types of dykes of possible SIC affinity have been identified. The Pele dykes are texturally and compositionally similar to the upper granophyre of the SIC, the quartz gabbro dykes resemble the middle quartz gabbro layer of the SIC, and a series of pyroxenite dykes resemble exotic pyroxenite inclusions described within the sublayer of the SIC [3].

The timing relationship of the new types of dykes is unclear. In particular, any mechanism for tapping of the upper granophyre and quartz gabbro layers for intrusion into the footwall rocks may provide constraint on the cooling history and/or the nature of the overlying now-eroded portions of the SIC.

Mafic to ultramafic inclusions within the sublayer have been much discussed and the identification of similar dykes in the footwall with mapped strike lengths of >5 km is noteworthy. These dykes may represent an ultramafic component to the SIC not previously documented.

Finally, the curvature of the concentric Hess Offset dyke may constrain the centre of the original crater to somewhere near the Copper Cliff Offset dyke to the south of the SIC, providing a possible constraint on the original size of the impact structure.

References: [1] Ames, D.E., and Farrow, C.E.G. (2007) GAC, SP5, 329-350. [2] Pilles, E. A., Osinski G. R., Grieve R. A. F., Smith, D. A., and Bailey, J. M. (2013) *this volume* [3] Lightfoot, P.C., Doherty, W., Farrell, K., Keays, R.R., Moore, M., and Pekeski, D. (1997) *OGS OFR*, 5959.

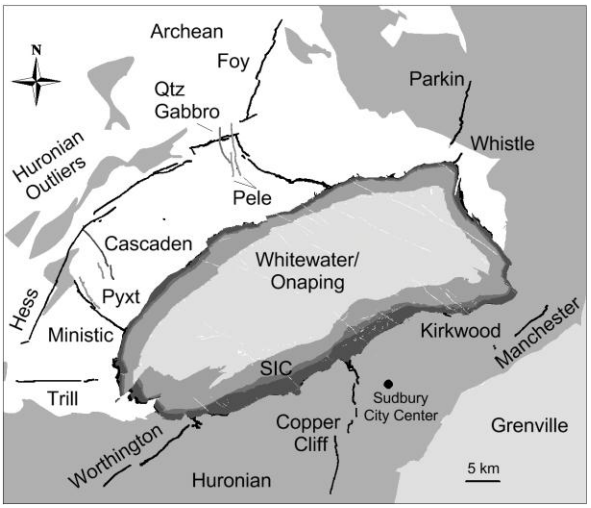

Figure 1. Impact related dykes at the Subury structure.

GEOPHYSICAL MAPPING AND MODELLING OF THE CHARITY SHOAL STRUCTURE, LAKE ONTARIO, CANADA. P. A. Suttak[1], J. I. Boyce[1] and D. Hrvoic[1], [1]School of Geography and Earth Sciences, McMaster University, Hamilton, ON L8S 4L8, suttakp@mcmaster.ca

Introduction: The Charity Shoal structure (CSS) is an enigmatic, crater-like depression located in eastern Lake Ontario, about 25 km south of Kingston. The CSS is defined by a raised bedrock rim, 1200-1400 m in diameter, enclosing a 19.5 m deep circular depression (Fig. 1A). The origin of the CSS is uncertain but it has been interpreted as a (Ordovician age?) meteorite impact [1]. A detailed geophysical survey was performed over the structure and 2-D magnetic forward modeling was conducted to evaluate its origin.

Methods: Magnetic, seismic and bathymetric surveys were conducted across a 9-km^2 grid over Charity Shoal in July, 2012. Sub-bottom seismic profiles were acquired with a 12-24 kHz chirp profiling system (Fig. 1C). 2-D forward modeling was conducted using GM-SYS^{TM} to evaluate three geological scenarios: 1) a meteorite impact in Precambrian basement, 2) a diatreme (Jurassic-age) and 3) a synclinal structure (depression) within the Precambrian basement.

Results: The CSS is defined by a ring-like magnetic high and central magnetic low (Fig. 1B). The total field magnetic anomaly is large (> 1500 nT) and cannot be accounted for by the 19.5 m deep basin within the Paleozoic bedrock.The anomalies large magnitude indicates a deep basin and/or demagnetization effects in the Precambrian basement rocks below the structure. Demagnetization effects are associated with meteorite impacts due to shock melting of target rocks but can also be produced by intrusive bodies with remanence directions that oppose the modern main field.

Forward modelling results verify that the observed total field anomaly requires a deep depression in Precambrian or a remanence opposing the main field. A volcanic intrusive origin is also unlikely, as the modelled diatreme produces complex, short wavelength anomalies not present in the observed signal. A simple structural depression (syncline) in the Precambrian basement can be fitted to the observed data but requires a magnetic susceptibility ($4x10^{-1}$ SI) larger than the mean value for Precambrian basement rocks in the region. The impact crater model best reproduces the observed anomaly when the basin is modeled as a 450 m deep parabolic impact crater in the Precambrian basement. The modeling results exclude the origin of the CSS as a shallow erosional feature and are most consistent with a meteorite impact or structural depression (syncline) within the Precambrian basement.

References [1] Holcombe T. L. et al., (2013) *Geo. Mar. Lett.*, DOI 10.1007.

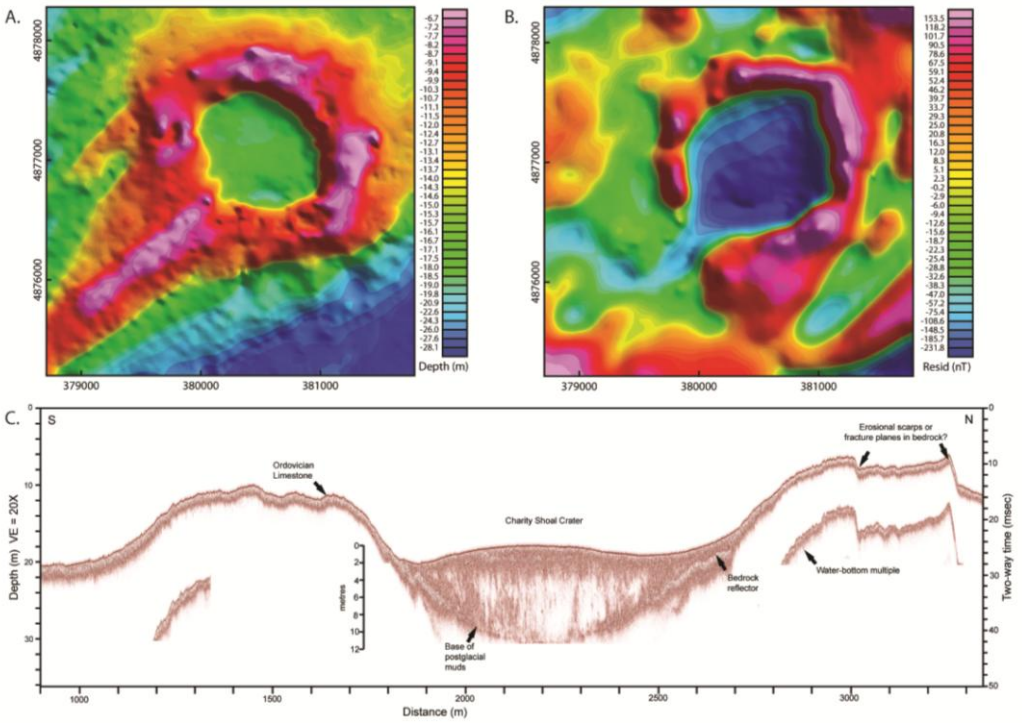

Figure 1. A. 200 kHz single-beam bathymetry. B. Residual magnetic field. C. N-S chirp seismic profile

SIZE DISTRIBUTION OF SPHERULES IN THE PARABURDOO SPHERULE LAYER. N. G. Swartz[1] , A. E. K. Davatzes[1], S. W. Hassler[2], [1]Department of Earth and Environmental Science, Temple University (1901 N. 13th St. Philadelphia, PA, 19122; nicholas.swartz@temple.edu), [2]The Wilderness Society (250 Montgomery St. San Francisco, CA 94104)

Introduction: The Paraburdoo Spherule Layer (PSL), a recently discovered spherule layer close to the Archean-Proterozoic boundary in the Paraburdoo Member of the Wittenoom Formation (Hamersley Basin, Western Australia,) presents an excellent opportunity to study and understand the temporal and spatial evolution of impact plumes [1]. The PSL is ideal for study because it is composed almost entirely of spherules, includes well preserved primary spinel and primary crystal textures, and lacks indications of post depositional reworking [1]. Analysis of the physical and chemical properties of PSL spherules may yield insights into the formation and evolution of the impact plume in which they formed and provide constraints for models of plume formation [2,3].

The focus of this study is on the distribution of spherule diameters in the PSL. Spherule size is controlled by temperature, viscosity, and velocity of materials in the vapor plume. Variation in spherule size will likely represent temporal and thermal heterogeneity within the plume [3]. A total of 762 spherules were identified, classified based on texture, and measured to establish size distributions, volumetric abundance, and the overall textural composition of the spherule bed.

Spherule Types: The PSL contains six types of spherules based on textures and current composition (Table 1). Although diagenetically altered, primary textures and spinel minerals are preserved in some spherules.

% Abundance	Spherule Types Descriptions
1.4	**Barred** texture, likely a relict texture of olivine; now a sheet-like phlogopite texture
44.9	**Fibrous** textures with no distinct orientation of K-feldspar crystallites
32.0	**Clay-rich** spherules with small inclusions of opaque materials
8.7	Massive **carbonate** replacement
2.2	Inward-directed **radial** fibrous fans of K-spar
10.8	**Miscellaneous**

Table 1: PSL spherule textures and abundances.

Methods: We made thin section samples along the vertical thickness of PSL sampls from two locations and petrographically identified, classified, and measured spherule diameters and textures. A 20g sample from the PSL was acidified in a 10% HCl solution to remove carbonate matrix and isolate spherules. Size distribution of the spherules was obtained with a CAMSIZER®.

Results and Discussion: Previous research has shown a large range in the diameters of spherules with different textures [3]. The PSL spherules, however, display relative uniformity of spherule sizes. The six spherule types all show peaks near the diameter range of 0.6mm and predominantly range from 0.2mm to 1mm (Fig 1). These sizes represent minimum values as 2D thin sections rarely transect the exact center of a spherule. CAMSIZER® results show a tight peak centered at 0.8mm, though this represents the long axis of the spherules. The second broad hump in the CAMSIZER® results represents joined spherules. In contrast, Barberton greenstone belt (BGB) S3 layer spherules have diameters (defined petrographically) ranging from 0.25mm to 4mm with values peaking from 0.5mm to 1.5mm for different types [3]. This suggests that the PSL spherules have a cumulatively smaller size population and do not show as much differentiation by spherule types.

The PSL is a fallout layer deposited in a deep water setting; it has a bed thickness of 2cm [1]. The BGB S3 layer is also likely a fallout layer in some sections, but has a bed thickness of 30cm. The smaller size distribution of the PSL spherules is likely indicative of a smaller impact. Unlike the BGB, which displays a distinct difference between sizes of different lithologic types, there is a relatively uniform size within the PSL despite clear variation in texture and composition.

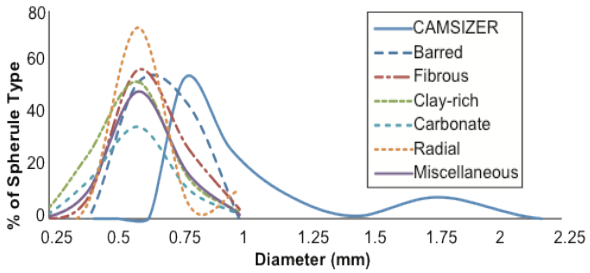

Figure 1: CAMSIZER® distribution and petrographic distribution of spherule sizes by textural type.

References: [1] Hassler, S. W., Simonson, B. M., Sumner, D. Y., Bodin, L. (2011) *Geology* 39, 307-310. [2] Johnson, B.C., Melosh, H.J. (2012) *Icarus* 217, 416-430. [3] Davatzes, A. E. (2011) *42nd LPSC Conference*.

Acknowledgments: Funding for fieldwork was provided by the Temple University Provost Summer Research Award to AEKD.

METER- TO DECAMETER-SCALE MORPHOLOGY OF MELT ROCKS, BRECCIAS, BEDROCK AND STRUCTURES IN CENTRAL UPLIFTS REVEALED BY THE MARS RECONNAISSANCE ORBITER.

L. L. Tornabene[1,2] , G. R. Osinski[1,3], and A. S. McEwen[4]. [1]Dept. of Earth Sciences & Centre for Planetary Science and Exploration, University of Western Ontario, London, ON, N6A 5B7, Canada (livio@cpsx.uwo.ca), [2]SETI Institute, Mountain View, CA 94043, USA, [3]Dept. Physics & Astronomy, Western University, London, ON, N6A 5B7, Canada, [4]Lunar and Planetary Laboratory, University of Arizona, Tucson, AZ 85721, USA.

Introduction: High-resolution sub-meter (~25 cm/pixel) images from the High Resolution Imaging Science Experiment (HiRISE), the Context Camera (CTX; ~5-6 m/pixel) and other data from the Mars Reconnaisance Orbiter (MRO) are providing unprecedented and remarkable geologic detail of surface features [e.g., 1]. Observations elucidating various aspects of the impact process, particularly with respect to impact melt deposits and various impactites associated with central uplifts (CUs) in complex craters are summarized and presented here.

Crater-related pitted materials: Crater-related pitted materials have been observed within 205 fresh and well-preserved impact craters [1-4] on Mars (also associated with fresh craters on Vesta [5]). These craters span ~1–150 km in diameter and 53°S to 62°N with the majority occurring ~10–30° N and S, and fewer to a complete lack of these craters at or near the equator and high latitude, respectively. The pits are distinctive depressions with circular to polygonal shapes. Pits possess subtle topographic rims with no signs of apparent proximal ejecta materials. Pit size shows a relationships with their host deposits and host crater, particularly a strong relationship with crater diameter ($n = 9$; $r^2 = 0.985$) [3].

Pitted matertais occur in similar settings as melt-rich flows and deposits associated with well-preserved lunar craters. This includes within crater-fill and as ponds and flows on CUs, terraces and crater ejecta. Non-dusty and well-exposed sections of the pits show that they consist of lighter-toned decameter-sized clasts enclosed in a darker-toned matrix. These and other PM observations (see [3-5]) are generally consistent with an impactite interpretation, likely consisting of a mixture of impact melt, and mineral and lithic fragments. The pits are specifically thought to be the result of interactions between hot, highly shocked materials with volatile-rich phases or water-ice derived directly from the target materials. Volatilization of water within the deposit leads to rapid, and perhaps explosive, degassing of the deposit, with pits corresponding to locations of degassing pipes (see [4]).

Martian central uplifts: We are compiling a database of crater-exposed bedrock from CUs on Mars using visible images, thermophysical and spectral data primarily derived from instruments on MRO with a focus on HiRISE-scale morphology [6].

Allochthonous units. All Martain CUs in our database exhibit the wide-spread occurrence of a dark-toned, smooth, rigid unit that ranges from clast-poor to clast-rich. This dark-toned unit is often observed as a contiguous mapable unit that extends from the summit of the CU to the crater floor. This unit is most consistent with being impact melt deposits based on their occurrence as a coating, or a flow that varies in clast content. We also interpret a variety of cross-cutting tabular bodies ranging from several meters to as much as a km or so across as allochthonous dikes and sills.

Parautochthonous units. Three types of bedrock are exposed within Martian CUs that conformably underlie, are embayed by, and cross-cut by fractures, faults and dikes. We classify these based on their HiRISE-scale textures (from most obvious to least) [6]: 1) Layered Bedrock (LB) (see [7-10]), 2) Fractured-Massive Bedrock (FB) (see [11-13) and 3) Megabreciated Bedrock (MB) (see [6, 11]). Our preliminary results, based on spectral/petrogenetic interpretations and the global distribution of these three textural types, suggests that CU bedrock correlates well with the local, regional and global Martian geologic history as interpreted from surface mapping.

Structures. Different types of deformation features are observed to occur within Martian CUs. LB-type CUs are the most informative as the layers provide a frame of reference that enables the easy identification of structures such as faults and what appear to be folds [7, 10]. Fractures, joints, faults, dykes and sills are readily recognized at the scale of HiRISE and are currently being mapped in detail by our companion studies by Nuhn et al. [11] and Ding et al. [13] presented at this conference.

References: [1] McEwen et al. (2007) *Science*, doi: 10.1126/science.1143987. [2] Mouginis-Mark et al. (2007) *MAPS*, 1615–1625. [3] Tornabene L. L. et al. (2012) *Icarus,* 348–368. [4] Boyce et al. (2012) *Icarus*, 262-275. [5] Denevi et al. (2012) *Science*, doi: 10.1126/science.1225374. [6] Tornabene L. L. et al. (2012) *3rd Early Mars Conf.*, 7069. [7] Caudill et al. (2012) *Icarus*, 710-720 [8] Wulf et al. (2012) *Icarus*, 194-204. [9] Quantin et al. (2012) *Icarus*, 436-452. [10] Nuhn et al. (2013) abstract present at this conf. [11] Marzo et al. (2010) Icarus, 667-683. [12] Skok et al. (2012) JGR, doi:10.1029/2012JE004148. [13] Ding et al. (2013) abstract present at this conf.

INVERTED STRUCTURE OF MELT-RICH IMPACT BRECCIAS AT BOSUMTWI CRATER: IMPLICATIONS TO MIXING AND COOLING HISTORY OF FALLOUT SUEVITES. R. Välja[1], K. Kirsimäe[2], D. K. Boamah[3], P. Somelar[4], [1]Department of Geology, University of Tartu, Ravila 14a, 50411, Tartu, Estonia, e-mail: rvalja@ut.ee, [2]Department of Geology, University of Tartu, Ravila 14a, 50411, Tartu, Estonia, e-mail: kalle.kirsimae@ut.ee, [3]Geological Survey Department, P.O. Box M80, Accra, Ghana, [4]Department of Geology, University of Tartu, Ravila 14a, 50411, Tartu, Estonia, e-mail: peeter.somelar@ut.ee.

Introduction: The 10.5 km diameter 1.07 Myr old Bosumtwi impact crater in Ghana is one of the world best-preserved large impact structures [1]. Impactite lithologies at Bosumtwi include fallout suevite deposits that are found outside the crater inner rim. According to Boamah & Koeberl [2] the Bosumtwi suevite is found as either large displaced blocks that measure up to several meters or as patches of suevitic material found in the north and southwest of the crater [2].

In this contribution we study mineral and chemical composition of a suevite bed exposed at Sarpong Nkwanta, located north of inner crater rim at 01°23´56.05´´W, 06°33´49.55´´N. The motivation of the study was to characterize the variation of the suevite composition in a nearly 4.5 m thick section with emphasis on devirification/alteration mineralogy.

Results and discussion: Mineralogical analyses reveal gradual changes in lower part of the suevite deposit from a kaolinite-rich composition characteristic to clastic breccia below the suevite bed to a glass-rich suevite material largely devitrified to spinel (hercynite)-plagioclase and secondary cristobalite-smectite mineral phases (Fig. 1). Kaolinite phase in studied samples is detritic, originating from the weathering crust of the target-rock and its content decreases upwards in the outcrop section. In contrast, the content of plagioclase, Mg-hercynite and impact glass alteration products – smectite and cristobalite – increases. Similar trends are in major oxide composition, which show decrease in Al_2O_3 and Fe_2O_3, and contemporary increase in SiO_2 and CaO (Fig. 2).

The partly devitrified glass fragments containing abundant hercynite spinel and plagioclase (Fig. 3) suggest that cooling of the suevite occurred rather slowly to allow mineral crystallization. This also indicates that the initial thickness of the suevite deposit must have been considerably thicker than it appears in present erosional level to allow slow cooling of the suevite.

Compositional trends at the lower boundary of the suevite bed imply to a contact-zone that in our opinion refers to mixing of underlying clastic breccia and overlying suevite deposits due to the horizontal movement of the suevite complex during its formation.

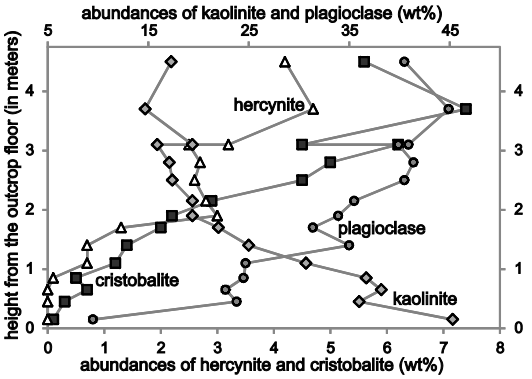

Figure 1. Abundances of hercynite, cristobalite, kaolinite and plagioclase mineral phases in relation to the sample material height in the outcrop.

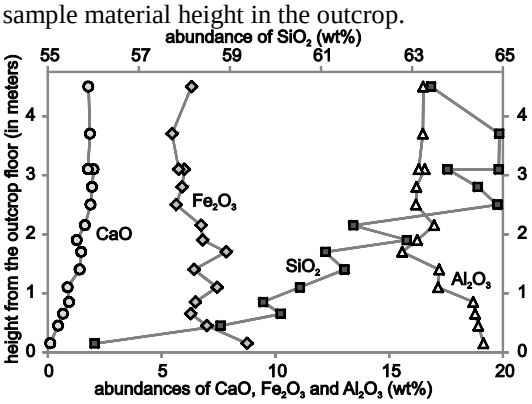

Figure 2. Abundances of SiO_2, CaO, Fe_2O_3 and Al_2O_3 in relation to the sample height from the outcrop floor.

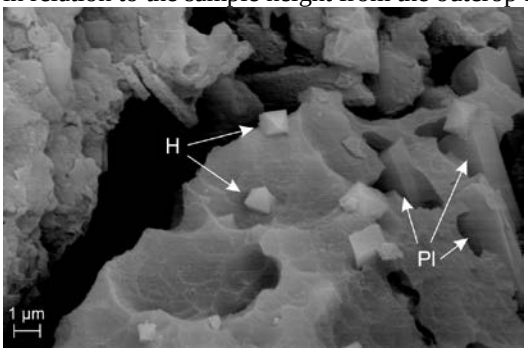

Figure 3. SEM image of a fractured sample from fallout suevite: hercynite (H) octahedrons and plagioclase (Pl) laths in a partly dissolved glass matrix.

References: [1] Koeberl C. et al. (2007) *Meteoritics & Planet. Sci., 42,* 483-511. [2] Boamah D. and Koeberl C. (2006) *Meteoritics & Planet. Sci., 41*, 1761-1774.

NUMERICAL MODELLING OF THE VARGEÃO IMPACT STRUCTURE, SOUTHERN BRAZIL M. A. R. Vasconcelos[1], K. Wünnemann[2], W. U. Reimold[2,3], D. Elbeshausen[2] and A. P. Crósta[1], Institute of Geosciences, University of Campinas, Campinas, SP, Brazil (vasconcelos@ige.unicamp.br,), [2]Museum für Naturkunde, Leibniz Institute for Evolution and Biodiversity Research, Berlin, Germany; [3]Humboldt-Universität zu Berlin, Berlin, Germany.

Introduction: Vargeão impact crater, located in Southern Brazil, is a circular feature of ~12 km diameter, formed in lava flows of the Lower Cretaceous Serra Geral Formation and in sandstones of the Paraná Basin. Although the presence of a central peak is not clear, an uplift is suggested by the occurrence of deformed sandstone strata of the Botucatu/ Pirambóia formations, which stratigrafically are beneath the basalts. The atypical occurrence of these rocks lead us towards numerical modeling in order to understand the genetic process of the formation of this structure. Furthermore, the comprehension of the arrangement of these formations allows to understand more about impact crater formation in lava flows on Mars. Of particular interest is the unusual target configuration of strong consolidated rocks (basalts) over softer and porous strata (sandstone) underneath that may cause deviations from our classical understanding of crater formation mechanics. Here, we review the results of numerical simulations of Vargão, carried out with the iSALE code.

Geological setting In portions of the rim of Vargeão that are somewhat protected from erosion, such as in the Southern section, four different lava flows can be recognized. The topographic gradient between the external plateau outside the rim and the lower part in the area of the town of Vargeão is approximately 180 m, indicating an average thickness of approximately 45 m for individual lava flows. In addition, in several places around the rim, in the inner part of the structure, large blocks of undeformed to tilted rocks from the volcanic formations can be seen. Tilting, suggests that they collapsed from the rim into the interior of the structure [1]. Sandstones crop out at the the central part of the structure as blocks of up to several hundred meters size; they are arranged in a circular ring around the center of the structure. These sandstones have been attributed by [2] and [3] to the Botucatú or Pirambóia formations, which in this portion of the Paraná Basin lie normally at a depth of approximately 1000 m. The rocks found in the interiort of Vargeão comprise slightly to moderately fractured basalt and rhyodacite in a collar-like ridge near the crater rim.

Modeling constraints: As the lithological packages at Vargeão are comprised essentialy of basalts and sandstones, we used only two different layers in the model (granitic basement was not considered, implying that it was not affected by the impact). The first layer comprises a basaltic package about 1.3 km thick (considering ~300 m of erosion) , and the second is a sedimentary layer below the basalts. We assumed the same rheological properties for the whole basaltic package and used the ANEOS [4] to calculate the thermodynamic behavior of the material upon impact. The second layer was matched with the equation-of-state for quartzite [5] coupled with the porosity compaction model [6]. The relative ease of the rocks to succumb to plastic deformation was modeled by the strength model [7]. We assumed also a temporary weakening of the target rocks during crater formation and applied the acoustic fluidization model [8,9,10].

Results: The model that best matches the final morphology of the crater, shows a transient crater that reaches ~2.5 km depth and is ~8 km diameter. The projectile in this model is ~900 m in diameter and an impact velocity of 12 km/s was applied. The final crater size is ~14 km diameter, and considering ~0.3 km of erosion should result in a crater of ~12 km, as observed by remote sensing. The model shows that the sandstone layer below the basalt should have flowed towards the center where it came to the surface. It also shows that there is no uplift of the basalt layer, which is a reasonable explanation for the non-occurrence of a proper central uplift. According to the model rocks of the innermost area have undergone ~1000 m uplift. Models are still running and additional conclusions will be presented at the conference.

References:

[1] Crósta et al. (2012). MAPS 47, 51-71. [2] Paiva Filho et al. (1978). 30º.Congresso Brasileiro de Geologia, Recife, Brazil: 408–412. [3] Crósta et al. (2006). Sítios Geológicos e Paleontológicos do Brasil 2, 1–12. [4] Thompson S.L., Lauson H.S. (1972). Report SC-RR-710714. Sandia Labs., Albuquerque, NM, 119 p. [5] Melosh H. J. (2007) MAPS, 42: 2035–2182; [6] Wünnemann K. et al. (2006) Icarus, 180, 514–527. [7]Collins G.S. et al. (2004). MAPS 39, 217-231. [8] Wünnemann K., Ivanov B.A. (2003) Planetary and Space Science, 51, 831-845. [9] Melosh, H.J. (1979) J. Geophys. Res. 84, 7513–7520. [10] Melosh, H.J., Ivanov, B.A.

Aknowledgments: M.A.R.Vasconcelos aknowledges FAPESP for his post-doctoral grants (#2012/ 04191-2 and 2012/ 19726-9).

IMPACT MELT DIFFERENTIATION IN SOUTH POLE-AITKEN BASIN. W. M. Vaughan[1] and J. W. Head[1].
[1]Department of Geological Sciences, Brown University, Providence, RI 02912, USA, Will_Vaughan@brown.edu.

Introduction: Impact melt sheets associated with the terrestrial Sudbury and Manicouagan impact structures have evidently undergone igneous differentiation [1-2]. Since basin-forming impacts on the Moon are thought to have generated voluminous impact melt sheets [3], a natural question (posed also by [1]) is: Did impact melt sheets on the Moon also differentiate, and, if so, how did the process of impact melt differentiation control lunar crustal evolution?

The process of impact melt differentiation is probably less efficient on the Moon than on Earth (see [4]), as: (1) impact melt sheets on the Moon are generally thinner than on Earth, since a given impactor excavates a larger crater in lunar gravity than in terrestrial gravity; (2) impact melt sheets on the Moon cool more quickly than equally thick impact melt sheets on Earth, mainly because anorthosite clasts predominant in lunar impact melt are less readily fusible than basaltic or granitic clasts in terrestrial impact melt; and (3) if crystal settling is the mechanism by which impact melt sheets differentiate (see [5] for a contrary perspective), crystals settle more slowly through impact melt sheets in lunar gravity than in terrestrial gravity. Considering the magnitude of these effects, we conclude that only the largest lunar basins (Orientale-size and larger) host impact melt sheets that have undergone igneous differentiation. We consider in this abstract the implications of impact melt differentiation in the largest and oldest lunar basin (excepting the dubious Procellarum basin), the South Pole-Aitken basin (SPA).

We ground our discussion of the implications of impact melt differentiation in SPA by modeling the igneous stratigraphy of SPA impact melt differentiates. We will demonstrate that this stratigraphy is consistent with the likely stratigraphy of the SPA interior (Figure 1).

Implications of impact melt differentiation in SPA: (1) The noritic floor of SPA [11-13], though more mafic than typical lunar highlands crust, is anomalously feldspathic for the floor of a basin formed by an impact which is modeled to have excavated nearly 100 km into the Moon [14], completely through the lunar crust. Moreover, geophysical measurements [9] suggest that the noritic floor of SPA is >10 km thick. We suggest that the thick noritic floor of SPA is better understood as an impact melt differentiate than as lunar primary crust. (2) Since the SPA floor is not necessarily primary crust, the noritic composition of the SPA floor need not represent the composition of the lunar primary lower crust. (3) If the noritic SPA floor is an impact melt differentiate, then samples from nearly any nonmare location in the SPA interior can be used to date the SPA-forming impact. (4) An SPA-forming impact that melts pre-cumulate overturn mantle gives rise to a different set of impact melt differentiates than a similar impact that melts post-cumulate overturn mantle [15]. The composition of SPA impact melt differentiates constrains the date of the SPA-forming impact. For additional information about the implications of impact melt differentiation on the Moon, consult [16].

References: [1] Grieve R. A. F. et al. (1991) *JGR*, 96. [2] Spray J. G. and L. M. Thompson (1998), *MAPS*, 43. [3] Cintala M. J. and R. A. F. Grieve (1998) *MAPS*, 33. [4] Warren P. H. et al. (1996) *GSA Spec. Paper,* 307. [5] Zieg M. J. and B. D. Marsh (2005), *GSA Bull.*, 117. [6] Tompkins S. and C. M. Pieters (1999) *MAPS*, 34. [7] Nakamura R. et al. (2009) *GRL*, 36. [8] Yamamoto S. et al. (2012) *Icarus*, 218. [9] Wieczorek M. A. et al. (2013) *Science*, 339. [10] Garrick–Bethell I. and M. T. Zuber (2009) *Icarus*, 204. [11] Head J. W. et al. (1993) *JGR*, 98. [12] Pieters C. M. et al. (2001) *JGR*, 106. [13] Moriarty D. P. et al. (2013) *JGR*, submitted. [14] Potter R. K. et al. (2012) *Icarus*, 220. [15] Hurwitz D. H. and D. A. Kring (2013) *LPS,* 44, #2444. [16] Vaughan W. M. et al. (2013) *Icarus*, 223.

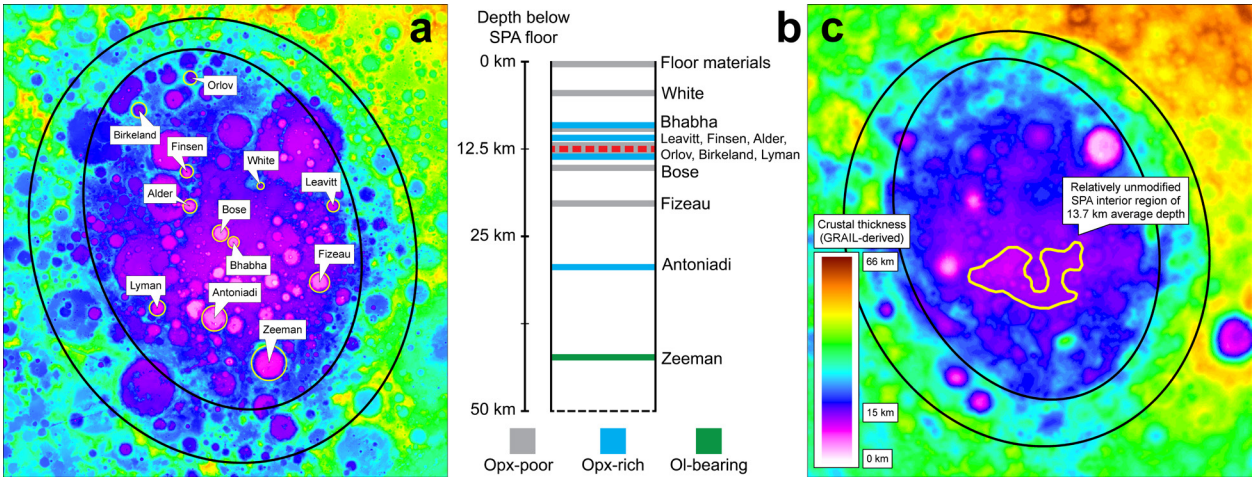

Figure 1. Spectroscopic and geophysical constraints on SPA subsurface stratigraphy: (a) twelve complex craters with previously characterized central peaks [6-8]; (b) constraints on subsurface stratigraphy from central peak mineralogy; the dashed red line at 12.5 km depth corresponds to (c) the average (GRAIL-derived) crustal thickness [9]. Rim outlines from [10].

THE POPIGAI: UNUSUAL FEATURES OF LARGE SCALE IMPACT CRATERING. S. A. Vishnevsky[1], Inst. of Geology & Mineralogy, 3 Koptug prospect, Novosibirsk-90, 630090, RUSSIA, svish@igm.nsc.ru

Introduction: The unique 100-km in diameter and young (35.7 Ma) Popigai astrobleme is described in details both in English and Russian papers [1–3 and refs. therein]. Its two-stage target included the supracrustal cover (a number of Protherozoic to Mesozoic lithologies up to 1700 m in thickness) and the Archean crystalline basement. The astrobleme exhibits a diversity of unusual impact structures, formations, and features, which are still unknown in other terrestrial impact sites. Some of these unusual properties and interpretation of their origin are presented below being of the interest for the current large-scale cratering models.

Impact diatremes and horsts [1–3]: Impact diatremes (IDs) are the pipe-like explosion structures in sedimentary terrains out of the tectonic rim of the crater **(Fig. 1).** They are filled up by klippen+megabreccia mixtures of target rocks. Impact horsts (IHs), of 0.3 to 2 km in length, are also present here, being the blocks of deep-seated target rocks tectonically-intruded into the upper members of non-shocked sedimentary cover. Both IDs and IHs target rocks bear traces of a weak shock metamorphism only ("gries breccia" and shatter cones).

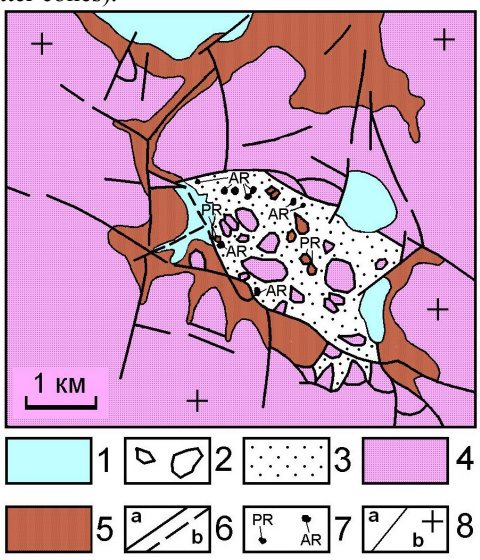

Fig. 1. An example of the Pastakh impact diatreme ~3 km off the west border of the Popigai astrobleme. *Legend:* 1 – Quarternary; 2 – klippen blocks; 3 – megabreccia; 4 – Cambrian; 5 – Protherozoic; 6 – traced (a) and supposed (b) faults; 7 – small klippen's lithology: Protherozoic (PR) and Archean (AR); 8 – geologic boundaries (a) and subhorizontal bedding (b).

Suevite megarbeccia: Suevite megabreccia (SMb) [1–3] is made up of large lumps, up to 80 m in size, of Mesozoic, mainly Cretaceous, rocks, which exhibit traces of weak shock metamorphism only. SMb occupies the top of the suevite column and is present within the annular trough around the inner ring of the crater.

On the origin of IDs, IHs and SMb: IDs and IHs are the evidence of deep sub-vertical impulses of the shock wave which was propagated here in a "buried" state already. As for the SMb, its spatial position and lithology also indicate the subvertical ejection of the subsurface part of the target and does not satisfy to any Z–models of cratering which suppose the monotonous centrifugal rizing-up excavation of ejecta and the "reversal stratigraphy" in the ejecta blanket. We can cite here the opinion by [4] and others that the geology of well-studied complex craters shows that neither excavation flow nor the shape of the excavation cavities are well-approximated by the Z–models. In order to explain the subvertical ejection for IDs, IHs and SMb, we proposed the hypothesis of the dynamic barrier **(Fig. 2),** based upon the vector interpretation of the cratering by [5]. Other unusual features of the Popigai cratering are presented in the papers [1–3 and refs. therein].

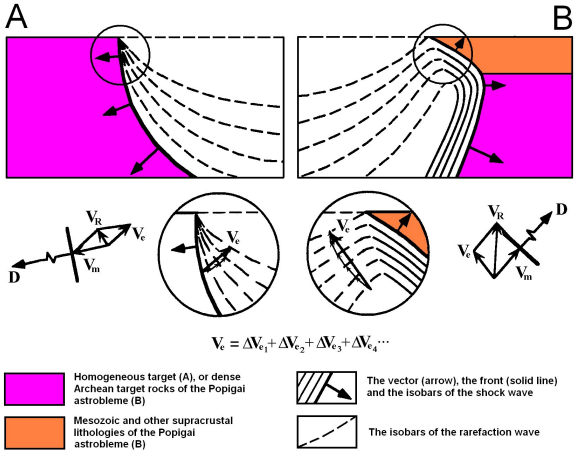

Fig. 2. Simple cratering ejection after [5] (A) and subvertical ejection of Popigai supracrustal lithologies due to subsurface delay of the shock wave after [1–3] (B).

References: [1] Vishnevsky S., Montanari A. (1999) *Geological Society of America Special Paper 339,* 19–59. [2] Vishnevsky S. (2007) *Astroblemes.* Novosibirsk, 288 pp. (in Russian). [3] Vishnevsky S. (2013) *Ural'sky Geologichesky Zhurnal, 93 (3),* 23–45 (in Russian). [4] Sharpton V. L., Dressler B. O. (2003) *Workshop on Impact Cratering*. LPI Contr. #1155. Abstract #8059. [5] Gault D. E., Quaide W. L., Oberbeck V. R. (1968) *Shock Metamorphism of Natural Materials*. Baltimore: Mono Book Corp., p. 87–99.

Miller Range 05029: Evidence for a Large Impact on the L Chondrite Parent Body >4.5 Ga. J. R. Weirich[1], A. Wittmann[2], C. E. Isachsen[3], D. Rumble[4], T. D. Swindle[3], and D. A. Kring[5]. [1]School of Earth and Space Exploration, Arizona State University, 781 E. Terrace Rd., Tempe, AZ 85287, USA (weirichjohn@gmail.com), [2]Department of Earth & Planetary Sciences, Washington University, One Brookings Dr., St. Louis, MO 63130, USA, [3]Department of Planetary Sciences and Lunar and Planetary Laboratory, 1629 E. University Blvd., Tucson, AZ 85721, USA, [4]Geophysical Laboratory, Carnegie Institution of Washington, 5251 Broad Branch Rd. NW, Washington, District of Columbia 20015, USA, [5]Lunar and Planetary Institute, 3600 Bay Area Blvd., Houston, TX 77058, USA.

Introduction: ^{40}Ar-^{39}Ar dating (a variant of K-Ar dating) is a widely used chronometer to study impact heating because the low closure temperature means mild shock events do not affect the K-Ar system, but strong shock events (i.e. large impacts) reset the K-Ar system. Most ^{40}Ar-^{39}Ar ages of highly shocked ordinary chondrites are 50 Ma to 1.5 Ga, or 3 to 4 Ga, with very few other ages [1]. Miller Range (MIL) 05029 is interesting because it is a complete melt with no shock features, and has an unusually old ^{40}Ar-^{39}Ar age.

Brief Description: MIL 05029 is a 132.7 g meteorite, and is paired with MIL 05136. It is classified as an L impact melt [2], and consists of large orthopyroxene grains with interstitial feldspar, both of which are poikilitically enclosing olivine grains.

Procedures: Chemical analyses were obtained with the NASA-Johnson Space Center's Cameca SX-100 microprobe. Modal abundances were calculated using reflected light, BSE maps, and elemental X-ray dot maps. Oxygen isotopes were determined on a Thermo Fisher Scientific MAT 252 mass spectrometer at the Carnegie Institution of Washington. Three splits of MIL 05029,5 were analyzed using a VG5400 noble gas mass spectrometer at the University of Arizona. Further details on all procedures can be found in [3].

Results: Oxygen isotopes and chemical compositions of major minerals for MIL 05029 are consistent with L chondrites. Modal abundances of major minerals in MIL 05029 are mostly consistent with L chondrites, but there is obvious metal depletion (~75%) and plagioclase enrichment (~40%).

A Widmanstätten-like pattern has developed in one of the metal grains, indicative of slow cooling. The lamellae of this grain were too small for analysis, but the metallographic cooling rate (corrected for P abundance) was calculated to be 14 ± 7 °C/Ma from kamacite-taenite paired metal grains.

Combining the ^{40}Ar-^{39}Ar ages of three different splits together gives an age of 4517 ± 11 Ma. The presence of Cl-derived Ar prevents identification of trapped Ar, but if we make the extremely unlikely assumption that all the ^{36}Ar is terrestrial atmosphere an absolute lower age limit of 4.48 to 4.50 Ga is obtained.

Discussion: While the ^{40}Ar-^{39}Ar age of MIL 05029 is 4517 ± 11 Ma, slow cooling indicates the impact occurred earlier. A metallographic cooling rate of ~14 °C/Ma, which records the average rate between 700 and 400 °C, indicates the impact occurred at least ~20 Ma before the ^{40}Ar-^{39}Ar age. Steady cooling down to the measured ^{40}Ar-^{39}Ar closure temperature of MIL 05029 (~40 °C) would indicate an age older than the solar system. More likely, the cooling rate was not steady below 400 °C due to excavation by a second impact, the closure temperature is not 40 °C, or the metallographic cooling rate (which is only accurate to an order of magnitude) was closer to 100 °C/Ma.

Endogenous magmatism is ruled out by oxygen isotope, mineral composition, and mineral abundances, which suggest an L chondrite origin. Since the L chondrite parent body did not melt, MIL 05029 must have formed as a deeply buried impact melt. Slow cooling, metal/sulfide depletion, and the clast-free nature of MIL 05029 all suggest formation in a melt sheet instead of a melt dike.

A cooling rate of ~14 °C/Ma would place MIL 05029 in the thermal regime of the L5-L6 boundary of an onion shell model. [4] calculated this depth to be 5-12 km on the 100-200 km diameter L chondrite parent body. Using scaling laws [5], excavation to this depth would require a 25-60 km diameter crater. A crater of this size on a 100-200 km diameter asteroid would cause rheological weakening or shattering [6,7]. Given the old age of this meteorite, the parent body would have been undergoing thermal metamorphism. Hence, MIL 05029 may provide evidence as to why the onion shell model of thermal metamorphism does not work on the L chondrite parent body [8], because shattering would disrupt the otherwise steady cooling.

References: [1] Swindle T. D. et al. (2013) *^{40}Ar-^{39}Ar Dating,* In Press. [2] Connolly H. C. et al. (2007) *Meteoritics & Planet. Sci., 42,* 1647-1694. [3] Weirich J. R. et al. (2010) *Meteoritics & Planet. Sci., 45,* 1868-1888. [4] Bennett M. E. and McSween H. Y. (1996) *Meteoritics & Planet. Sci., 31,* 783-792. [5] Sullivan R. et al. (1996) *Icarus, 120,* 119-139. [6] Housen K. (2009) *Planet. and Space Sci., 57,* 142-153. [7] Holsapple K. et al. (2002) *Asteroids III*, 443-462. [8] Taylor G. J. et al. (1987) *Icarus, 69,* 1-13.

TERRESTRIAL IMPACT ZIRCON TEXTURES: IMPLICATIONS TO IMPACT GEOCHRONOLOGY. M. M. Wielicki[1,2] and T. M. Harrison[1,2], [1]Department of Earth and Space Sciences, [2]Institue for Planets and Exoplanets, University of California, Los Angeles, 595 Charles Young Drive East, Los Angeles, CA 90095. (correspondence: mwielicki@gmail.com)

Introduction: The bombardment history of our planet has major implications for Earth's atmosphere, habitability, near surface conditions, and the delivery of the building blocks of life over its four and a half billion years. Constraining the impact flux to the Earth-Moon system was highlighted by the National Research Council's 2007 report "The Scientific Context for the Exploration of the Moon" as the top priority goal for lunar research. Evidence of the early impact flux has largely been based on interpretations of ^{40}Ar-^{39}Ar ages of lunar samples which can be problematic due to the presence of relic clasts, incomplete Ar outgassing, diffusive modification during shock and heating, and exposure to solar wind and cosmic rays [1]. Recent studies [2, 3] have utilized zircon from Apollo samples as well as lunar meteorites to better constrain the impact history of the Moon. Sieve textures found in zircon within lunar meteorite SaU 169 have been identified as "poikilitic impact melt zircon formed during equilibrium crystallization of the impact melt" and used to better constrain the age of the Imbrium impact [3]. Such textures had previously not been observed in terrestrial zircon and have been suggested as the best candidate grains with which to identify an impact age [4]. We report SIMS U-Pb analysis on the first terrestrial sieve textured zircons isolated from Vredefort impactites to investigate the use of such grains as probes of planetary impact history.

Results: Zircon grains were isolated from a sample of granophyre dike collected near the Kommandonek Game Reserve of the ~2 Ga Vredefort impact structure in South Africa. Separated grains show an intimate relationship with Mg-rich pyroxene, similar to that seen in the lunar samples (inset Fig. 1). Multiple grains show fractures and embayment's infiltrated with pyroxene in what appears to be resorption of the zircon rather than equilibrium crystallization during the impact. Similar textures have been observed in plagioclase during rapid decompression and could be indicative of the swift unroofing during an impact event [5]. However, U-Pb analysis of such grains (Fig. 1) clearly shows that the zircons have been inherited from the target and are not neo-formed zircon that crystallized from the impact melt and thus should not be used to identify impact ages. Pb-loss is highly variable in these samples and the lower intercept age of ~1985±150 Ma agrees well with that previously reported for the Vredefort impact [6, 7].

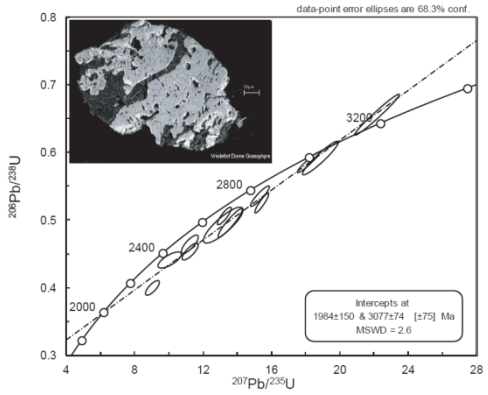

Figure 1. U-Pb concordia diagram of 12 zircons with sieve textures (see inset of BSE of single zircon; scale bar is 20μm) showing that the grains are inherited from the Archean basement and thus should not be used to identify an impact age. Lower intercept age within error of the impact suggests the grains did experience Pb-loss during the impact event.

Discussion: Although zircon geochronology offers an exciting new tool with which to constrain planetary impact histories the effects of impacts on zircon remain poorly understood and need to be explored terrestrially prior to making interpretations on extraterrestrial samples. Sieve-like textures found in terrestrial and extraterrestrial zircon are the result of resorption of pre-existing grains into new melts possibly due to rapid decompression during an impact. U-Pb ages of such grains isolated from the ~2 Ga Vredefort impact structure show clear inheritance from the Archean target and thus should not be used to date impact events in terrestrial or extraterrestrial samples. Pb-loss within these zircons appears to have been affected by the impact however no grains show complete resetting and such age resetting appears to be very rare within terrestrial impact events.

References: [1] Fernandes et al. (2013) *MAPS 48*, 241-269. [2] Nemchin et al. (2008) *GCA 72*, 668-689. [3] Liu et al. (2013) *EPSL 319-320*, 277-286. [4] Grange et al. (2013) *GCA 101*, 112-132. [5] Nelson et al. (1992) American Mineralogist 77, 1242-1249. [6] Kamo et al. (1996) *EPSL 144*, 369-387. [7] Wielicki et al. (2012) *EPSL 321-322*, 20-31.

DECOMPRESSION CRACKS IN ALTERED BASALT UNDER SOLID-STATE SHOCK PRESSURES: A NEW MACROSCOPIC SHOCK TEXTURE S.P. Wright, Department of Geology and Geography, Auburn University, Auburn, AL, shawn.wright@auburn.edu

Summary: Solid-state transformation of labradorite plagioclase feldspar to maskelynite occurs at a specific range of shock pressure [1] referred to as "Class 2" [2] for shocked basalt. A new texture labeled as "decompression cracks" (see scans of cut sides below) forms where the protolith prior to shock was an altered basalt, which likely indicates the importance of volatiles while not melting. At higher shock pressures, glass is formed and it flows, which does not permit decompression cracks. Although only a small range of shocked basalt allows for decompression cracks to form, this can be used as a macroscopic texture in the field to locate shocked basalt and the impact melt-bearing breccia unit. Currently, shatter cones, at lower pressures, are the only macroscopic indicator of shock metamorphism.

Introduction: With three processes analogous to Mars (basaltic volcanism, aqueous alteration, and shock), Lonar Crater shocked basalts are excellent analogs for analyzing results from instrumentation sent to Mars. ~80 kg of "intermediately" (20-80 GPa) shocked basalt, which exist as clasts in the uppermost, impact-melt-bearing breccia (formerly, "suevite" [3]) layer at Lonar Crater, India [2], along with float that were former breccia clasts, were collected during a 2-month field season. These add to a large collection [4] of unshocked basalts and impact melts/glasses (aka Class 5 [1,2]). Petrographic and electron microprobe images reveal of range of shock pressures (deduced by phases and mineralogies of labradorite and augite); various protoliths such as fresh Deccan basalt, altered basalt (altered before shock) showing hematite, calcite, silica veins/pockets, and clays [4]; and what is interpreted as a consolidated soil or a sample from weathering horizons in-between individual basalt flows [4].

Decompression Cracks: Whereas thinly-bedded sedimentary rocks have layers or beds, and regional metamorphic rocks are foliated due to directed stress over long periods of time, typical Deccan basalt shows no such bedding or foliation. However, a subset (~25) of the collection of intermediately-shocked basalt have quasi-parallel "cracks" ~1 cm apart throughout the sample (Figures 1 & 2). These features are apparent in natural samples found in the Lonar ejecta both in-situ and as float, and cut sides display the feature. Petrography of these 25 samples showed all of them to be Class 2 shocked basalt [2], with solid-state maskelynite and no melted plagioclase glass ("Classes 3 to 4") [2], which provides constraints on the approximate shock pressure.

Interpreted Formation: For microseconds, the altered Deccan basalt was held under a shock pressure to compress labradorite into maskelynite; augites are fractured at this pressure. The lack of flowing or vesiculated glass, along with no decompression cracks found in Class 1/3/4/5 shocked basalts, suggest that these features form when the sample decompresses after being held at Class 2 shock pressures. At higher shock pressures, when plagioclase melts to a *flowing* glass, the near-instantaneous change in volume results in the glass flowing to account for the slight change in volume from ambient to compression to decompression. In Class 2 basalts, with no melted, flowing glass, the sample "cracks" to account for decompression, and hence "decompression cracks" are formed. These are only a feature of Class 2 shocked basalts with altered protoliths, and thus volatiles likely play a role. Fresh basalts subject to Class 2 pressures do not contain decompression cracks.

Implications for field geology: Decompression cracks are not a feature of all shocked basalts and are limited to a small subset: Class 2 solid-state shock pressures of altered protoliths. However, this feature is beneficial to locating such samples and thus identifying 1.) outcrops of impact melt-bearing breccia that may be 2.) altered basalts ejected from depth. Both of these are of interest for field geology at Lonar and on Mars.

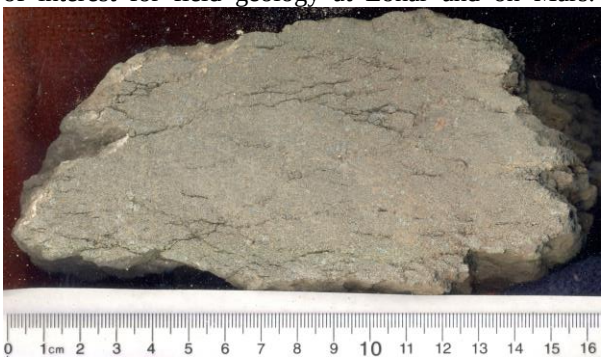

References: [1] Stöffler & Hornemann (1972) *MaPS, 7*, 371-394 [2] Kieffer et al. (1976) *7th LPSC*, 1391-1412 [3] Osinski and Pierrazzo (2012) *Impact Cratering: Processes and Products* [4] Newsom et al. (2011) *LPSC 42*, #1298; Wright and Newsom (2011) *LPSC 42*, #1619; Wright (2012) *LPSC 43*, #2765

SPECTRAL, CHEMICAL, AND PETROGRAPHIC COMPARISONS OF HYDROVOLCANIC TEPHRAS WITH BASALTIC IMPACTITES: RELEVANCE FOR MARS S.P. Wright[1], W.H. Farrand[2], [1]Auburn University, Auburn, AL, shawn.wright@auburn.edu; [2]Space Science Institute, Boulder, CO, farrand@spacescience.org

Introduction: Both pyroclastic volcanism and impact processes have shaped the morphology and geologic history of the martian surface. Distinguishing between the products of these two processes is difficult to determine with rover-based instrumentation. In its exploration of the Columbia Hills, the Mars Exploration Rover Spirit encountered a variety of clastic rocks [1,2]. Mini-TES observations of layered rocks on Home Plate and the Clovis class on Husband Hill indicated a high abundance of basaltic glass [3,4]. That glass could be interpreted as resulting from either impact or volcanic activity.

On Earth, basaltic glass can be produced in association with fire fountaining or hydrovolcanic eruptions. The most well-preserved impact site emplaced into basalt is Lonar Crater in India [5]. In the present investigation, we have begun to characterize a set of hyalotuffs from hydrovolcanic vents as well as basaltic impact glass and alteration products from Lonar Crater using measurement tools available to current and planned rovers.

Alteration Processes: Basaltic glass can alter via several pathways. Palagonitic vs. pedogenic alteration of tephras from the summits of Kilauea and Mauna Kea was examined [6]. [6] determined that pedogenic alteration resulted in disaggregated material, generally lacking in smectite, but with more abundant poorly crystalline materials: ferrihydrite, allophane, and imogolite. In contrast, palagonitically altered materials were indurated with abundant smectites along with other secondary minerals (zeolites, serpentines, carbonates). An important environmental difference between these two pathways is that pedogenic alteration involves ambient conditions while palagonitic alteration involves some level and duration of heating of wet tephra. The mineralogic differences between the two pathways are detectable through remote sensing techniques: reflectance and thermal emission spectroscopy [6,7]. A primary objective of this work has been to better characterize the minerals associated with the alteration pathways of basaltic glass to determine possible analogies with martian surface materials [7]

Field Sites and Samples: Hydrovolcanic tuff samples from maars, tuff rings, tuff cones, and tuyas are being examined [7] in addition to impact melts and glasses from Lonar Crater [5,8, abstract #3049 in this LMI volume]. Further sampling and field work was conducted in 2012 at multiple hydrovolcanic eruption sites throughout the Snake River plains of Idaho: Sinker Butte [9], Split Butte [10] and North Menan Butte [11].

Analyses and Results: Thin sections were prepared and examined using standard petrography (Figure 1) [7]. Reflectance spectra (0.3–2.5 μm) of relatively unaltered and more palagonitized hyalotuffs were examined using a non-linear approach [12] and have reflectance spectra consistent with earlier studies [7,13,14]. Unaltered samples have hydration absorptions at 1.4 and 1.9 μm along with a Si-OH feature at ~2.24 μm, whereas with increasing palagonitization, iron oxidation (orange color) increases and a Fe/Mg-OH absorption near 2.3 μm develops [7]. Mössbauer results indicate a broad Fe^{2+} doublet in glassy samples and a narrower Fe^{3+} doublet attributable to nanophase Fe^{3+} in palagonitized samples [7]. Thermal emission spectra of the most glass-rich samples [5,7] display a deeper 9.56 μm and shallower subsidiary 10.9 μm band. Palagonitized samples have a more symmetric 9.7 μm band and, in some samples, a narrow band at 11 μm [7] that indicates carbonate. Linear deconvolution of the emissivity data [15] and non-linear unmixing of the reflectance data produced contradictory results: more phyllosilicates than glass in unaltered samples and the reverse in highly palagonitized samples [7]. This confusion was resolved with μFTIR microscopy which allowed for distinction of palagonite rinds from glass cores and identification of smectites in interstices. This analysis will lead to improved TIR end-members of both glass-rich and altered materials.

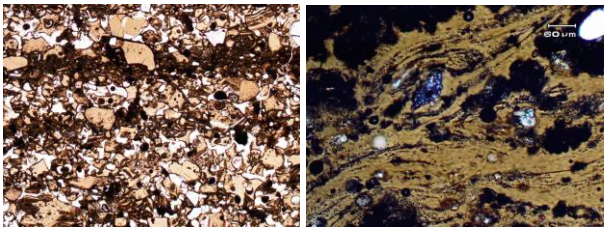

Figure 1. Petrography in plain polarized light of layered palagonite (left) compared to Class 5 impact melt glass from Lonar Crater (right).

References: [1] Squyres et al. (2005) *JGR 111*, 10.1029/2005JE002562 [2] Squyres et al. (2007) *Science, 316*, 738-742 [3] Ruff et al. (2006) *JGR 111*, 10.1029/2006JE002747 [4] Schmidt et al. (2009) *EPSL, 281*, 258-266 [5] Wright et al. (2011) *JGR 116*, 10.1029/2010JE003785 [6] Schiffman et al. (2000) *G^3*, 2000GC000068 [7] Farrand et al. (2013) *LPSC*, #2249 [8] Wright & Newsom (2011) *LPSC 42*, #1619; Wright (2012) *LPSC 43*, #2765 [9] Brand & White (2007) *JVGR, 160*, 319-339 [10] Womer (1977) in *Volcanism of the Eastern Snake River Plain, Idaho*, 189-202 [11] Creighton (1987) *GSA Centennial Field Guide*, 109-111 [12] Shkuratov et al. (1999) Icarus, 137, 235-246 [13] Poulet & Erard (2004) JGR, 109, 10.1029/2003JE002179 [14] Farrand & Singer (1992) *JGR* 97, 17393-17408 [14] Bishop et al. (2002) GS London spec pub 202, 371-392 [15] Ramsey & Christensen (1998) *JGR 103*, 577-596

ADVANCED CRATER SIZE SCALING LAWS THROUGH HYDROCODE SIMULATIONS. K. Wünnemann[1] and B. A. Ivanov[2], Erik Streb del Toro[1], [1]Museum für Naturkunde, Leibniz Institute for Research on Evolution and Biodiversity, D-10115 Berlin, Germany (kai.wuennemann@mfn-berlin.de), [2]Institute for Dynamics of Geospheres, RAS, 119334, Moscow, Russia (baivanov@idg.chph.ras.ru,boris.ivanov@univie.ac.at)

Introduction: To relate the size of a given crater with the kinetic energy of the impactor is a fundamental question that is been addressed primarily by laboratory cratering experiments [e.g. 1]. The resulting crater size after the impact of the projectile of given mass and velocity strongly depends on the gravity and the properties of the target. So-called π-group scaling [e.g. 2] is probably the most successful approach to relate small-scale laboratory cratering experiments with natural craters on different planetary targets in different gravity conditions. The well-established set of equations is calibrated by laboratory experiments in dry and wet sand [1,3] for gravity dominated craters and in cohesive rocks [1,4] for strength dominated craters. In order to investigate a much broader range of target properties, impact velocities, and gravity conditions we use hydrocode simulations of impact cratering. Recent advances in material models [5,6] now allow for studying crater formation in competent rocks in the gravity regime, systematic analysis of the effect of porosity, dry friction, and cohesion on crater size [7], and the investigation of how the impact angle [8] and velocity [9] affect crater size.

Numerical Experiments: We conducted a suite of numerical experiments of crater formation over a large range of impact diameters L in different target configurations of competent rock and granular materials including also layered targets. We use two slightly different variants of the SALE code, SALEB [10] and iSALE [6 and reference in there]. To model the material behavior during crater formation we use ANEOS and Tillotson EOS coupled with a porosity compaction model [6,11,12] and a brittle-ductile failure and damage model [5]. Note we model only the transient crater formation. Subsequent collapse resulting in complex final crater morphologies is not covered by this study.

Results: Fig. 1 shows an example of a series of numerical cratering experiments in three different target lithologies. The gravity-scaled size π_2 is plotted vs. scaled crater diameter π_D. The brown triangles represent crater formation in a granular material (e.g. dry sand, regolith) characterized by the coefficient of friction and porosity. As expected all points plot along a line (power-law) in a double-logarithmic diagram. The blue squares represent numerical cratering experiments in competent rock. For impactors smaller than L=5 m (π_2=1E-7) crater size becomes independent of gravity and crater size scales with the cohesion. The turquoise circles represent numerical cratering experiments in a layered target consisting of (1) a 50m granular material layer, (2) a 1000m transition layer, where porosity decreases and cohesion increases, and (3) competent rock. For very large impactors the data points approach the scaling line for competent rock (blue) as the upper two layers are too thin in comparison to the impactor diameter L to have a significant effect on crater formation. For smaller impactors the data points fall exactly on the brown line as the crater are only formed in the upper layer.

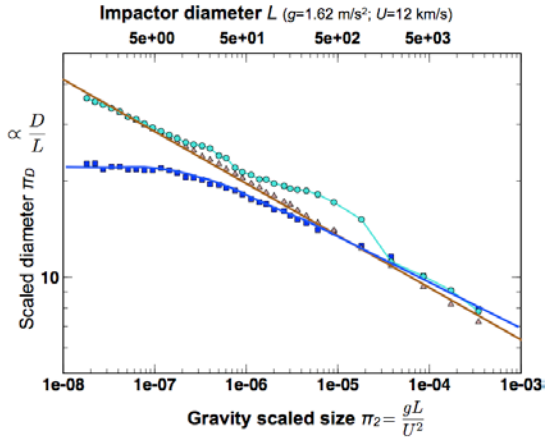

Fig. 1 Gravity-scaled size p2 vs. scaled crater diameter for three different target configurations (see text).

Concussion: Crater scaling is significantly affected by target properties. Layers of different lithologies cause deviations from classical power-law scaling. Surprisingly, crater diameter increases when crater depth reaches down to the boundary between softer and stronger material and/or porous to nonporous lithologies (see bumps in turquoise line).

Acknowledgements: This work was funded by the Helmholtz-Alliance WP3200.

References: [1] Schmidt, R. M. and Housen, K. R. (1987) IJIE, 5, 543-560; [2] Holsapple K.A. (1993), Annu. Rev. Planet. Sci. 12:333-73; [3] Holsapple, K. A., Housen, K. R. (2007) Icarus, 187: 345–356; [4] Poelchau, M. H. et al., (2013) M&PS, 47:8-22; [5] Collins G.S. et al. (2004), M&PS, 39: 217-231; [6] Wünnemann K. et al. (2006), Icarus, 514-527; [7] Wünnemann et al. (2011), Proc. 11th HVIS 2010, 1-14; [8] Elbeshausen et al. (2009), Icarus 204: 716-731; [9] Ivanov B. A. and Kamyshenkov D. (2012), 43rd LPSC Abstract #1407; [10] Ivanov, B.A. et al. (1997) IJIE 17: 375–386; [11] Güldemeister N. et al. (2013) M&PS, 47: 115-133; [12] Collins et al. (2011) IJIE 38: 434-440.

Airburst impact origin hypothesis of Taihu lake basin in Southeast of China in around 7000 years ago. Zhidong Xie, Shuhao Zuo. State Key laboratory for Mineral Deposits Research, School of Earth Sciences and Engineering, Nanjing University, Nanjing, P. R. China, zhidongx@nju.edu.cn.

Introduction

Taihu lake is the third largest freshwater lake in Southeast of China. The diameter of Taihu lake is about 65 km; the water depth is very shallow and its deepest part is only 3 meters. The bottom of the lake is pretty flat with a very gentle slope, and very young with a hard loess layer which extended to vicinity area, which are dated to only 11k to 12k years ago. Several origin hypothesizes of the Taihu lake formation were proposed in recent 60 years, including the origins of tectonic, lagoon, volcano, etc., but none was seriously studied in detail.

The rounded arc shape of southwest of Taihu lake led some geologists to doubt that it was created by a meteorite impact. In the early 1990s, an impact origin was proposed on the basis of fractured quartz, wavy extinction of quartz grains, and claimed shatter cones [1,2]. However, deformation of quartz and the circular structure can have multiple interpretations. There are no clue when the impact were happened in these proposals. The impact origin hypothesis is very difficult to explain the unique features of Taihu lake, such as wide-shallow-flat-young lake bottom. The impact origin hypothesis has fallen into disfavor, and gradually died out.

Recently, some unique rod-shaped and irregular shaped siderite-quartz-rich materials were found in specific mud layer in vicinity of Taihu lake. The discovery of these materials combining with previous claimed impact evidences revived the impact hypothesis in 2009 [3]. The irregular shaped siderite concretions were regarded as an ejecta materials of impact. However, many questions still remain.

Results

The term "concretion" is used in this paper to indicate the texture of these siderite-quartz rich materials, not infer the sedimentary origin. These concretions consist of aggregates of μm-sized siderite spheroids or siderite crystals as concretion matrix and μm-sized angular quartz grains as matrix debris. Quartz grains are angular with sharp edges and corners. The ration of siderite to the quartz ranges from 80% to 10%.

The sizes of concretions range from μm to cm. Micron-spherule, lapilli, rod and irregular concretions were found widely dispersed in a specific mud layer in the vicinity of Tai lake, while rod concretions were found vertically in the mud layer in Shi Lake. Regular ripples and furrows are common in the surfaces of the rod-shaped and irregular-shaped concretions. In addition, some concretions are sporadically found in higher ground, such as piedmont, hills top or hill slope, not in lower lake bottom.

The age of mud layer contained siderite concretions were constrained by peat woods and shell by using C14 dating, indicating a non-calibrated age of ~ 7000 years ago, indicating the concretions formed later than 7000 years ago.

Discussion:

The vertical occurrence of rod concretions and the widely distribution features suggest the siderite concretions either grow from bottom or come down from air. Based on the observation and preliminary results of siderite concretions, the origin of the siderite concretions could be explained by three distinct mechanisms: aqueous deposition within the mud, volcanic lapilli formation and lapilli formed in the ejecta plum of an impact. The round shape of Tai lake has been use as evidence of an impact, but the large size and shallow depth of the lake are inconsistent with a young impact structure.

In addition, the recent work on deformation features of quartz grain of sandstone of Taihu lake area does not provide strong and confirmed evidence of impact origin [4]. The conclusion suggest the impact related evidences by quartz done in twenty years ago need to be re-evaluated and the strong support evidences for the 2009 paper [3] are negative, and the conclusion of confirmation of impact crater of Taihu lake needed be caution.

An alternative impact model that could produce a shallow crater without major crustal disruption is an aerial burst of an impact. The airburst impact hypothesis may explain the features of huge, shallow, flat, young of Tai Lake basin, and the deformation features caused by relatively lower pressure. The strange and unique siderite concretions containing abundant angular quartz debris may provides evidences for the airburst impact hypothesis. The unique morphology, occurrence, distribution, and mineralogy of these concretions indicate a unique origin, more likely formed by airburst rather than aqueous deposition. It is rewarded and valuable to intensively study the formation origin of Tai Lake by multiple approaches.

References: [1] Y. He, D. Xu, D. Lu et al., 1990. *Chinese Science Bulletin*, 36 (10): 847-850. (in Chinese). [2] E. Wang, Y. Wan, Y. Shi, et al. 1993. *Chinese Science Bulletin*, 39 (5): 149-423 (in Chinese). [3] H. Wang, Z. Xie, and H. Qian, 2009. *Geological Journal of China Universities*: 15: 437-444. (in Chinese). [4] Y. Dong, Z. Xie, and S. Zuo, 2012. *Geological Journal of China Universities*: 18: 395-403. (in Chinese).

Mapping Aristarchus Crater: Geology, Geomorphology, and Pre-Impact Stratigraphy. M. Zanetti[1,2], H. Hiesinger[2], B. L. Jolliff[1]. [1]Washington University in St. Louis, Earth and Planetary Science Dept., 1 Brookings Drive, Campus Box 1169, St Louis, MO 63130. [2] Westfälische Wilhelms-Universität Münster, Institut für Planetologie, Wilhelm-Klemm Str. 10, 48149 Münster, Germany. Michael.Zanetti@wustl.edu

Introduction: The lunar crater Aristarchus is a complex impact crater 40 km in diameter and ~3.5 km deep [1,2], and is located in northern Oceanus Procellarum, on the edge of the Aristarchus Plateau. The crater impacted into both the pyroclastic rich deposits of plateau material and the surrounding mare flood basalt deposits, and the region has been extensively studies for decades with many different datasets [1-11]. Recent remote sensing data sets have provided increased detail and sharper focus on the characteristics of these materials. Here we report on efforts to compositionally and geomorphologically map crater ejecta and interior deposits in order to investigate the distribution of ejecta and melt at the crater, and to attempt to reconstruct the pre-impact target stratigraphy.

Geologic Mapping and Pre-Impact Stratigraphy: During the formation of Aristarchus Crater an unusual suite of rocks were exhumed. In addition to basaltic components from the surrounding mare, the crater excavated very high albedo material, especially in areas of the proximal ejecta to the east and southwest, and the central peak. Olivine-rich rocks have been observed [5, 10] and are concentrated in ejecta along a narrow radial deposit east – southeast of the crater. Lunar Prospector Gamma Ray Spectrometer (LP-GRS) results show that Aristarchus Crater lies at the center of one of the strongest Th hot spots on the Moon [3,8,12,13]. Recently, using spectral bands that are sensitive to silicate mineralogy and bulk SiO2 content (i.e. the Christiansen feature at 7.8, 8.25, and 8.55 μm) LRO Diviner radiometer data suggest that bright ejecta rays in the southwest of the ejecta might indicate the presence of abundant quartz (or related phases) and alkali feldspar (i.e. granite or alkali feldspar) [8].

From the integration of various remote sensing data sets, we infer that the Aristarchus target section features a petrogenetically diverse suite of rocks including materials of the Aristarchus Plateau, young and relatively Th-rich basalts of Oceanus Procellarum, a differentiated, KREEP-rich igneous intrusive body, and diverse ejecta deposits from the Imbrium basin including olivine-rich materials [14,15] and KREEP-rich impact-melt deposits. This diversity of lithologic materials associated with the crater and located in the target area reflect the diversity of the target rock formations that exist in the upper few km in this region, and the specific target rocks may be highly localized. Furthermore, some of the components are not easily relatable to specific morphologic units [10,14] and cannot be explained by any simple petrogenetic scenario. For example, compositionally evolved KREEP-rich rocks and olivine-rich rocks [14] are not expected together petrologically, and we infer that these may simply reflect juxtaposition of Imbrium ejecta deposits with evolved intrusive rocks of the PKT. The high albedo materials, including those within the crater and the SW ejecta unit are most likely low-FeO, alkali-rich differentiates of a KREEP-rich, near-surface intrusive body and not primary anorthosite of the Moon's early primary crust. Given the extensive volcanic activity that occurred in this region of the Moon, basaltic underplating, as suggested by Hagerty et al. [23], of KREEP rich rocks, may have caused partial melting and intrusion of silicic magma (with a small degree of melting) or melting and injection of an evolved KREEP-rich magma such as quartz monzogabbro to a shallow level in the Aristarchus target section [15].

Geomorphologic Mapping: A detailed geomorphologic sketch map of the crater interior and proximal ejecta blanket has been created using high resolution Lunar Reconnaissance Orbiter Camera (LROC) Narrow Angle Camera (NAC) images [3]. Major units of focused mapping are impact melt ponds, flows, melt veneer deposits, crater floor deposits, and ejecta materials, which we attempt to correlate to distinct spectral units. Other interesting features such as stratified boulders of ejecta and enormous individual impact melt flows (up to ~16.5 km² in area) are well-characterized through mapping and subsequent analysis. Mapping of melt veneer has been aided by crater counting statistics and morphologically diagnostic crater morphologies on impact melts and allows for preliminary volume estimates of melt production.

References: [1] Guest (1973) GSA Bulletin 84. [2] Zisk et al. (1977) Moon 17. [3] Etchegaray-Ramirez et al. (1983). JGR 88 supplement p A529-A543 [4] Guest & Spudis (1985) Geol. Magazine 144. [5] Lucey et al. (1986) JGR 91. [6] McEwen et al. (1994) Science 266. [7] Le Mouélic et al. (1999) GRL 26. [8] Hagerty et al. (2009) JGR 114. [9] Chevrel et al. (2009) Icarus 199. [10] Mustard et al. (2011) JGR 116. [11] Glotch et al. (2010) Science 329. [12] Lawrence, D. et al. (2003) JGR 108. [13] Lawrence, D. et al. (2007) GRL 34. [14] Wiseman et al. (2012) LPSC 43, Abs #2515. [15] Zhang and Jolliff (2008) LPS 39, #2534. [16] Hagerty et al., 2006 JGR 111. [17] Robinson et al. (2010) Space Science Reviews, 150. [18] Zanetti et al. (2011) LPSC 42, Abs #2330.

GRAVITY RECOVERY AND INTERIOR LABORATORY (GRAIL): ANALYSIS STATUS AND IMPLICATIONS FOR UNDERSTANDING THE ROLE OF IMPACTS IN LUNAR AND PLANETARY EVOLUTION. Maria T. Zuber[1] and the GRAIL Science Team. [1]Dept. of Earth, Atmospheric and Planetary Sciences, Massachusetts Institute of Technology, Cambridge, MA 02129, USA (zuber@mit.edu).

Introduction: The Gravity Recovery and Interior Laboratory (GRAIL) [1], NASA's eleventh Discovery mission, successfully executed its Primary Mission (PM) in lunar orbit between March 1, 2012, and May 29, 2012. GRAIL's Extended Mission (XM) initiated on August 30, 2012, and its endgame was successfully completed on December 14, 2012. High-resolution models of the lunar gravity field, combined with topography from the Lunar Orbiter Laser Altimeter [2], are enabling geophysical analyses that elucidate the role of large impacts on the evolution of the Moon, and by extension, other terrestrial planets.

Primary and Extended Missions: GRAIL launched on September 10, 2012, and the dual spacecraft executed independent low-energy trajectories to the Moon via the EL-1 Lagrange point, inserting into lunar orbit on December 31, 2011, and January 1, 2012. After a series of maneuvers to decrease orbital periods and align the spacecraft into ranging configuration, the PM initiated on March 1, 2012. Initial analysis led to a spherical harmonic model of the gravitational field to degree and order 420 (spatial block size = 13 km), named GL0420A [3], that is improved in spatial resolution by a factor of 3-4 and in quality by three to more than five orders of magnitude in comparison with previous lunar gravity models from the Lunar Prospector (LP) [4] and Kaguya [5] missions. Subsequent analysis of the PM observations has enabled the production of independent spherical harmonic models by science team members at the Jet Propulsion Laboratory (JPL) [6] and Goddard Space Flight Center (GSFC) [7], both to degree and order 660 (spatial block size = 8.3 km).

GRAIL's XM average altitude was 23 km, less than half the average altitude of the PM. Because of the low orbital altitude, XM operations were far more complex than in the PM [8]. Unlike the PM, which featured only one thrust maneuver to change the mutual drift rate of the spacecraft over three months of mapping, the XM required three maneuvers a week to maintain the mapping altitude [9]. The quality of the data coupled with the low mapping altitude in the XM dictated that much higher resolution gravitational fields were possible in comparison to that originally envisioned. Current gravity fields produced at JPL and GSFC are to degree and order 780 (spatial block size = 7 km) and 900 (spatial block size = 6 km), the latter a factor of two improved spatial resolution compared to GL0420A [3].

At spherical harmonic degrees <60 (spatial block size = 91 km) corresponding to spatial scales of major lunar basins, the GRAIL models are now improved by as much as 10^6 over LP and Kaguya. Gravity and topography are highly coherent at degrees >100 (spatial block size = 55 km), interpreted to be a consequence of significant impact-related fracturing of the upper lunar crust and regolith re-distribution [3]. High coherence extends to increasingly small spatial scales as the lunar gravity field resolution is increased.

Additional aspects of GRAIL modeling bear directly on the role of impacts. Results show that the Moon's crustal density is less than previously thought and porosity is higher [10]. As for the high coherence, these observations are also interpreted to be a consequence of impact-related brecciation of the lunar crust. The lowest densities and highest porosities occur in association with ejecta blankets of major impact basins [10]. Modeling of basin formation and subsequent relaxation, compared to present-day gravitational signatures of mare and non-mare basins, have revealed the processes that contribute to the formation of lunar mascons [11].

These and other ongoing studies of GRAIL, LOLA and other remote sensing data sets in concert with laboratory analyses of lunar samples are collectively providing quantitative insight into the effect of impacts on the lunar crust and upper mantle and their contribution to lunar evolution.

References: [1] Zuber M. T. et al. (2013) *Space Sci. Rev.,* doi:10.1007/s11214-012-9952-7. [2] Smith D. E. et al. (2010) *GRL 37,* doi:10.1029/2010GL043751. [3] Zuber M. T. et al. (2013) *Science 339,* doi:10.1126/science.1231507. [4] Konopliv A. S. et al. (2001) *Icarus 150,* 1-18. [5] Matsumoto K. et al. (2010) *JGR. 115,* doi:10.1029/2009JE003499. [6] Konopliv A. S. et al. (2013) *JGR,* in press. [7] Lemoine F. G. et al. (2013) submitted to *JGR.* [8] Wallace M. S. et al. (2012) *AIAA Astrodyn. Specialist Conf.,* AIAA-2012-4748, Minneapolis, MN. [9] Sweetser T. H. et al. (2012) *AIAA Astrodyn. Specialist Conf.,* AIAA-2012-4429, Minneapolis, MN. [10] Wieczorek M. A. (2013) *Science, 339,* doi: 10.1126/science.1231530. [11] Melosh H. J. et al. (2013) *Science,* in press.